The investigation into the potential of ceramic waste powder as a pozzolanic material and inert cement filler in concrete

A thesis submitted to the Faculty of Engineering and Built Environment, Durban University of Technology, in fulfilment of the requirement for the degree of Master of Engineering

Author

Peace Opeyemi Adedeji
(Student No: 22173780)

Supervisor: Dr Jacob Olumuyiwa Ikotun

Co-supervisor: Prof Adewumi John Babafemi

Date: 4 November 2025

Declaration

I, Peace Opeyemi Adedeji declare that:

i. The research reported in this thesis, except where otherwise indicated, is my original work.
ii. This thesis has not been submitted for any degree or examination at any other university.
iii. This thesis does not contain other persons' data, pictures, graphs, or other information, unless specifically acknowledged as being sourced from other persons.
iv. This thesis does not contain other persons' writing, unless specifically acknowledged as being sourced from other researchers. Where other written sources have been quoted, then:

(a) their words have been re-written, but the general information attributed to them has been referenced.

(b) where their exact words have been used, their writing has been placed inside quotation and referenced.

v. This thesis does not contain text, graphics, or tables copied and pasted from the Internet, unless specifically acknowledged, and the source being detailed in the thesis and in the References sections.

Signed: Date: 04/04/2025

Jacob Ikotun

As the candidate's supervisor, I _____,
approve this thesis for submission.

03-11-2025

Signed Date: _____

As the candidate's co-supervisor, I Prof Adewumi J Babafemi,
approve this thesis for submission.

Signed: _ Date: 04-11-2025

Dedication

This thesis is dedicated to the Almighty God.

Acknowledgment

First and foremost, I express my deepest gratitude to God Almighty for His unwavering protection, provision, strength, and wisdom throughout this research journey. His grace has been my sustaining force, and without His guidance, this work would not have been possible.

I extend my heartfelt appreciation to my main supervisor, Dr. Jacob Ikotun, for his invaluable mentorship, patience, and continuous support throughout my research. His expertise, encouragement, and constructive feedback played a crucial role in shaping the direction of this work. I am equally grateful to my co-supervisor, Prof. Adewumi John Babafemi, for his insightful guidance and technical support, which greatly enriched the quality of this research. Their unwavering commitment to my academic growth is deeply appreciated.

I would like to acknowledge the Durban University of Technology (DUT) Research Grant Assistant for funding this research and providing the necessary financial support that enabled me to complete my studies successfully. My sincere gratitude also goes to my academic institution, the DUT, Civil Engineering Department, Midlands Campus, for their unwavering support and for providing the necessary resources to facilitate my research.

I extend my sincere appreciation to the dedicated staff at DUT, who played significant roles in my academic journey. I especially acknowledge Dr. Zesizwe Ngubane, the Head of Department, for her invaluable support and encouragement. I am also grateful to Dr. Jacob Adedayo Adedeji, as well as Ms. Nonkululeko Sthabile Mkhize, and Ms. Samukelisiwe Thusi, the departmental secretaries, whose consistent assistance and support greatly eased my administrative processes. Their kindness and willingness to help did not go unnoticed, and I truly appreciate their efforts.

A special acknowledgement goes to the University of the Witwatersrand (WITS), School of Civil and Environmental Engineering, Johannesburg, where I conducted all my experiments. My profound gratitude goes to Prof. Mike Otieno, who was the Head of School at the time, for hosting me and ensuring I had access to the necessary laboratory facilities. I also appreciate the support of the lab assistant, Mr. Masindi Lambani, whose dedication and assistance made my experimental work much smoother.

I extend my appreciation to Dr. Isaac Sanusi of the University of KwaZulu-Natal for his valuable advice, which contributed significantly to my academic journey. I am also deeply

grateful to Dr. Gabriel Aruwajowe and his family for their moral support, encouragement, and hospitality throughout my studies.

My academic journey would not have been as fulfilling without the camaraderie of my student colleagues. I sincerely appreciate Miss Rhoda Adeyeye, Mr. Gbenga Aderinto, and Mr. David Sithole for their team support, collaboration, and constructive discussions. Their companionship made the research process more manageable and enjoyable.

I extend my heartfelt gratitude to my beloved parents, Mr. and Mrs. Adedeji, for their unconditional love, prayers, and encouragement. As the fourth of eight children, I also acknowledge my seven wonderful siblings, who have been my constant source of motivation and support. Their belief in me has been instrumental in my journey.

I am also grateful to my spiritual family, the Deeper Life Campus Fellowship, both in Pietermaritzburg and Johannesburg. Their prayers and spiritual encouragement uplifted me during challenging times. I sincerely appreciate Pastor (Dr.) Ola, Pastor (Dr.) Peter, Brother Patrick, and all other brethren for their unwavering spiritual and moral support.

I would also like to acknowledge my wonderful friends, Omowumi Sakiru, Bankole Falade and Dipolelo Radebe, for their support, encouragement, and companionship throughout this journey. Their presence has been a source of great motivation and joy.

Finally, I appreciate everyone who contributed in one way or another to the success of this research but whose names are not mentioned here. Your support and encouragement mean the world to me. Thank you all.

Abstract

The construction industry is increasingly seeking sustainable alternatives to Portland cement (PC) due to its high carbon footprint. Ceramic waste powder (CWP) offers potential as either a supplementary cementitious material or an inert filler. However, its role in cement hydration is uncertain due to conflicting reports on its pozzolanic reactivity. This study investigates the potential of CWP as a partial replacement for both pozzolanic material (Ground Granulated Blast Furnace Slag, GGBS) and inert filler (limestone powder, LSP) in concrete. The CWP was incorporated into Portland-slag and Portland-limestone cement blends at varying levels. Its chemical compositions were analysed using X-ray fluorescence (XRF). Scanning electron microscopy with energy dispersive spectroscopy (SEM-EDS), and X-ray diffraction (XRD) were use to better understand its microstructure. Workability (slump), strength, and durability were evaluated at water-binder ratios of 0.45, 0.50, and 0.55. Compressive and splitting tensile strength tests were conducted at 7, 28, 56, and 90 days. Durability performance was determined using the Oxygen Permeability Index (OPI), Water Sorptivity Index (WSI), and Chloride Conductivity Index (CCI). Additionally, SEM analysis was used to examine hydration products, pore distribution, and interfacial transition zones (ITZ) in concrete microstructures.

Results indicated that CWP has limited pozzolanic reactivity, leading to lower early-age (7 days) strength compared to GGBS. However, it outperformed LSP in both early-age and long-term strength, as well as in durability. CWP reduced the slump in GGBS mixes, requiring more superplasticizers, but improved the slump in LSP-based mixes. Durability tests confirmed that CWP enhances resistance to permeability, moisture ingress, and chloride penetration. Microstructural analysis revealed improved densification, reduced porosity, and better hydration over time. Compared to LSP, CWP demonstrated similar filler effects but also generated minor secondary hydration products, suggesting partial pozzolanic activity. However, its hydration rate, as indicated by strength development over time, was lower than that of GGBS. Overall, CWP primarily acts as an inert filler with limited pozzolanic reactivity.

Table of Contents

List of Figures

List of Tables

List of Abbreviations/Acronyms

Abbreviation	Full Meaning
ANOVA	Analysis of Variance
ASTM	American Society for Testing and Materials
Adj.	Adjusted
Al_2O_3	Aluminium Oxide
C & Cl	Cement and Concrete Institute
C-A-S-H	Calcium Aluminosilicate Hydrate
C-S-H	Calcium Silicate Hydrate
CCI	Chloride Conductivity Index
CH	Calcium Hydroxide
CWP	Ceramic Waste Powder
CaO	Calcium Oxide
DF	Degree of Freedom
DUT	Durban University of Technology
EDX	Energy Dispersive X-ray
FA	Fly Ash
FM	Fineness Modulus
Fe_2O_3	Iron (III) Oxide
GGBS	Ground Granulated Blast Furnace Slag
GJ	Giga Joule
ITZ	Interfacial Transition Zone
K_2O	Potassium Oxide
KV	Kilo Volt
LEED	Leadership in Energy and Environmental Design

MPa	MegaPascal
MPa/s	MegaPascal per Seconds
MS	Mean Square
MgO	Magnesium Oxide
Ml	Millilitre
N	Porosity
Na_2O	Sodium Oxide
OPI	Oxygen Permeability Index
PC	Portland Cement
SAI	Strength Activity Index
SCC	Self-Consolidating Concrete
SCM	Supplementary Cementitious Material
SEM	Scanning Electron Microscopy
SO_3	Sulphide
SiO_2	Silicon Dioxide
STS	Splitting Tensile strength
SP	Superplasticiser
TGA	Thermogravimetric Analysis
w/b ratio	Water/binder ratio
WSI	Water Sorptivity Index
XRD	X-ray Diffraction
XRF	X-ray Fluorescence
F_c	Compressive Strength
F_{sp}	Splitting Tensile Strength
kPa	KiloPascal
Kg	Kilogram

kg/cm^3	Kilogram per Centimetre Cube
kg/m^3	Kilogram per Meter Cube
Pa	Pico Ampere
WITS	University of the Witwatersrand

CHAPTER ONE
INTRODUCTION

1.1 Background of the Research

Concrete production is fundamental to the construction industry, serving as the basis for countless infrastructure projects worldwide. Concrete is the second most consumed material on Earth after water, with approximately 30 billion tonnes used annually worldwide (Li, Lin, Bao & Min Xie 2022). Traditional concrete is a composite mixture of aggregates, binder, and water (Li et al. 2022). The characteristics of concrete are influenced by mix design (proportion of cement, aggregates, water, and other concrete materials), aggregates properties, and cement types (Zhang, Qian, Zhang & Li 2022). Cement is an important constituent of a concrete mixture as it provides the binding properties that keep it together (Jamal, Mohammed & Ali 2025; Barbhuiya, Das, Qureshi & Adak 2024). Figure 1.1 shows that cement constitutes about 20% of an average concrete mix (Zhang et al. 2022). However, cement is also the concrete material associated with the highest environmental concern, accounting for 8% of global CO_2 emissions (Ige, Olanrewaju, Duffy & Collins 2022; Fayomi, Mini, Fayomi & Ayoola 2019). Therefore, sustainable practices recommend reducing the quantity of cement used in concrete production while maintaining or improving the quality of the concrete.

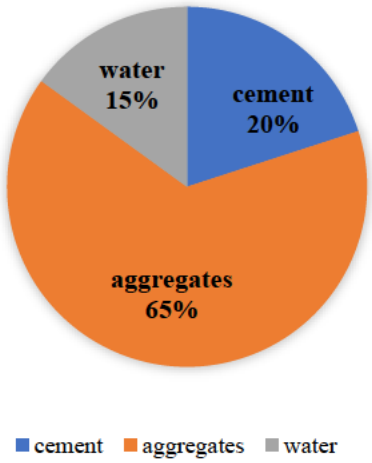

Figure 1.1: Percentage composition of average concrete mix (Zhang et al. 2022)

Portland cement (PC) is the most common type of cement (Ige et al. 2022). It is divided into different types based on the material constituents and their proportions. The type of cement used in a concrete mixture affects the properties of the concrete, such as strength development, workability, plasticity, setting time and durability (Kulovaná et al. 2016a).

According to SANS 50197-1, common cements are divided into five major types: CEM I, CEM II, CEM III, CEM IV and CEM V (SANS 2013). As shown in Table 1.1, each cement type is composed of two or more of the following materials at a specific range of proportion: clinker, ground granulated blast-furnace slag (GGBS), silica fume, fly ash, burnt shale, limestone, and gypsum.

Apart from PC clinker (K), the constant constituent of all types of cement in South Africa, other cement materials can be classified as either supplementary cementitious material (SCM) or inert filler materials according to SANS 50197-2013 (SANS 2013). Chemically active materials like GGBS are classified as SCMs, while inert materials like limestone are considered fillers. According to John et al., (2018), fillers are fine particles that produce little or no pozzolanic reactions in cement hydration when added to cement or other SCM. Fine fillers are used in cement to occupy spaces that would otherwise be filled with water, allowing for a lower water-cement ratio and reducing the permeability of concrete (Moosberg-Bustnes, Lagerblad & Forssberg 2004). Fine fillers are valuable ingredients in modern construction practices because they enhance concrete performance without inducing any reaction. In addition to the filler effect (optimization of particle packing by reducing voids between larger particles in concrete), fine fillers also mitigate drying shrinkage, reduce cracking, and increase the long-term durability of the concrete. In contrast, SCMs contribute to producing more cementitious compounds due to their pozzolanic reactivity, which increases the strength and durability of concrete. SCMs are usually used to replace PC clinker at a higher percentage when compared to fillers as in SANS 50197-1 (SANS 2013).

Table 1.1: Common cement: SANS 50197-1 (SANS 2013)

Main Types	Notation of Products (Types of common cement)		Composition, percentage by mass[a]										
			Clinker	Blast-furnace slag	Silica fume	Pozzolana		Fly ash		Burnt shale	Limestone		Minor additional constituents.
						Natural	Natural calcined	Siliceous	Calcareous				
			K	S	D[b]	P	Q	V	W	T	L	LL	
CEM I	PC	CEM I	95-100	-	-	-	-	-	-	-	-	-	0 – 5
CEM II	Portland- slag cement	CEM II/A-S	80-94	6-20	-	-	-	-	-	-	-	-	0 – 5
		CEM II/B-S	65-79	21-35	-	-	-	-	-	-	-	-	0 – 5
	Portland -silica fume cement	CEM II/A-D	90-94	-	6-10	-	-	-	-	-	-	-	0 – 5
	Portland pozzolana cement	CEM II/A-P	80-94	-	-	6-20	-	-	-	-	-	-	0 – 5
		CEM II/B-P	65-79	-	-	21-35	-	-	-	-	-	-	0 – 5
		CEM II/A-Q	80-94	-	-	-	6-20	-	-	-	-	-	0 – 5
		CEM II/B-Q	65-79	-	-	-	21-35	-	-	-	-	-	0 – 5
	Portland-fly ash cement	CEM II/A-V	80-94	-	-	-	-	6-20	-	-	-	-	0 – 5
		CEM II/B-V	65-79	-	-	-	-	21-35	-	-	-	-	0 – 5
		CEM II/A-W	80-94	-	-	-	-	-	6-20	-	-	-	0 – 5
		CEM II/B-W	65-79	-	-	-	-	-	21-35	-	-	-	0 – 5
	Portland- burnt shale cement	CEM II/A-T	80-94	-	-	-	-	-	-	6-20	-	-	0 – 5
		CEM II/B-T	65-79	-	-	-	-	-	-	21-35	-	-	0 – 5
	Portland-limestone cement	CEM II/A-L	80-94	-	-	-	-	-	-	-	6-20	-	0 – 5
		CEM II/B-L	65-79	-	-	-	-	-	-	-	21-35	-	0 – 5
		CEMII/A -LL	80-94	-	-	-	-	-	-	-	-	6-20	0 – 5
		CEMII/B-LL	65-79	-	-	-	-	-	-	-	-	21-35	0 – 5
	Portland-composite cement	CEM II/A-M	80-94	←	———	———	———	6 – 20	———	———	———	→	0 – 5
		CEM II/B-M	65-79	←	———	———	———	21 – 35	———	———	———	→	0 – 5
CEM III	Blast furnace cement	CEM III/A	35-64	36-65	-	-	-	-	-	-	-	-	0 – 5
		CEM III/B	20-34	66-80	-	-	-	-	-	-	-	-	0 – 5
		CEM III/C	5 -19	81-95	-	-	-	-	-	-	-	-	0 – 5
CEM IV	Pozzolanic cement	CEM IV/A	65-89	-	← ———	———	11 – 35	———	→	-	-	-	0 – 5
		CEM IV/B	45-64	-	← ———	———	36 – 55	———	→	-	-	-	0 – 5
CEM V	Composite cement	CEM V/A	40-64	-	← ———	18 – 30	———	→		-	-	-	0 – 5
		CEM V/B	20-39	-	← ———	31 – 50	———	→		-	-	-	0 – 5

Waste materials are usually introduced as SCMs and fillers in cement compositions to reduce the negative environmental impacts of cement. Meanwhile, a significant amount of ceramic waste is generated in South Africa. They can be obtained from construction and demolition activities, tiles, pottery and sanitary ware manufacturing, and consumer discards. It was estimated that over 2 million tons of ceramic waste are generated yearly in South Africa (Department: Environmental Affairs 2018; Department of Enviromental Affairs 2011). About 85% of ceramic wastes end up in landfills, degrading the environment (Department: Environmental Affairs 2018; Department: Mineral Resources 2010). Therefore, it becomes very important to design a system that utilises ceramic wastes to limit the amounts being discharged into the environment. Many studies have also used ceramic powder in concrete. However, some researchers argued that ceramic waste powder (CWP) acts as a SCM due to its chemical reactivity, while other researchers suggested that CWP will only act as an inert filler in cement because of its poor reactivity (Chen et al. 2022; Salvi, Gupta & Sharma 2021; Li, Liu, You, Chen & Zeng 2020; Patel, Arora & Vaniya 2015). Therefore, this study examines its role as both SCM and inert filer. The research experimented with CEM II (CEM II/A-LL and CEM II/B-S) cement. According to Table 1.1, Portland-limestone cement consisting of 80–94% clinker, 6–20% limestone and 0–5% gypsum (additional constituents) is classified as CEM II/A-LL cement type. Also, Portland-slag cement consisting of 65–79% clinker, 21–35% blast-furnace slag and 0–5% gypsum is classified as CEM II/B-S.

1.2 Problem Statement

Despite the numerous studies on CWP, researchers are yet to make a conclusion on the pozzolanic reactivity of the material. Thus, it remains difficult to explicitly state the role of this material in concrete. Some researchers observed that when CWP is used in concrete production, a substantial amount of it is usually unreactive (Chen et al. 2022a; Alsaif 2021). This is probably because the raw materials have undergone high temperatures during calcination (Lee et al. 2014; Nikodemski, Tong & O'Hayre 2013). This causes phase transitions that alter the crystal structure with less reactive and more stable phases (Lee et al. 2014). It also justifies why most researchers observed a decrease in the permeability of concrete containing CWP despite a lesser or insignificant improvement in the concrete's strength (especially early age strength) (Heidari and

Tavakoli, 2013; Zimbili, Salim and Ndambuki, 2014; Patel, Arora and Vaniya, 2015; Hussain et al., 2019; Salvi, Gupta and Sharma, 2021). Such researchers tend to admit that CWP acts as an inert filler (like limestone powder, LSP) in concrete. However, other researchers argued that CWP reacts with the alkali in cement to form a calcium silicate hydrate (C-S-H)–like gel in the concrete microstructure. For instance, Li *et al.* (2020) observed the formation of complex calcium-silicate-alumina hydrates with a Ca/Si ratio of around 1 from the pozzolanic reaction between ceramic grains and calcium hydroxides. This is also possible because CWP contains a high percentage of silicate (SiO_2) and aluminate (Al_2O_3) (Magbool 2022). Pozzolanic reactivities are significantly influenced by silicate and aluminate (Madadi & Wei 2022). The C-S-H gel, which is the main binding component in concrete, is produced when silicate combines with calcium hydroxide (in a pozzolanic reaction). Aluminates, primarily present in cement as tricalcium aluminate (C_3A), also react with alkali to form calcium aluminate hydrate (CAH), which contributes to the early strength development in concrete. Hence, many researchers assumed that CWP is best used as a SCM for the partial replacement of PC. Therefore, the conflicting reports in the literature necessitate a further investigation into the behaviour of CWP in fresh and hardened concrete. This study investigates the performance of blended cement systems where CWP is used as a partial replacement for both pozzolanic material (GGBS) and inert filler (LSP), focusing on its impact on the fresh and hardened properties of concrete. The research examined the physical and chemical characteristics of the binders as well as the slump and the mechanical properties of concrete. The microstructure of the concretes was also examined for meaningful conclusions.

1.3 Research Significance

This study has several substantial implications; thus, this section lists and justifies the areas in which the research will significantly impact.

- The study provides scientific evidence on the feasibility of CWP as a SCM, contributing to the development of sustainable concrete. By utilizing waste ceramics, this research promotes the reduction of cement consumption, thereby lowering carbon emissions associated with cement production. The findings will support the adoption of CWP in eco-friendly construction practices, aligning with global sustainability goals.

- Understanding CWP's impact on microstructural, mechanical, and durability properties helps improve concrete mix designs for long-term performance. The study demonstrates that CWP enhances densification and reduces permeability at optimal replacement levels, making it a viable option for durable concrete applications, particularly in structural and non-structural elements.
- The research establishes optimal replacement levels of CWP in GGBS- and LSP-based concrete, providing practical recommendations for engineers, material scientists, and construction professionals. These findings will help optimize workability, strength, and durability while maintaining sustainability in construction projects.
- The study promotes waste valorisation by repurposing ceramic waste in concrete production, addressing solid waste management challenges. By reducing the environmental footprint of ceramic waste disposal, the research aligns with the principles of a circular economy, where waste materials are reintegrated into production cycles.
- The findings serve as a foundation for future studies exploring methods to enhance the pozzolanic reactivity of CWP, such as thermal or chemical activation techniques. Additionally, the study provides insights for researchers investigating the synergistic effects of CWP with other SCMs in self-compacting concrete.

1.4 Research Aim and Objectives

This research aims to investigate the role of CWP in concrete, either as a pozzolan or an inert filler.

The aim is achieved through the following objectives:

i. To analyse the physical and chemical characteristics of CWP in comparison to other binder materials – PC, GGBS and LSP.

ii. To analyse the workability of concrete mixes with CWP and compare them with those of concrete made with GGBS and LSP.

iii. To analyse the compressive strength and splitting tensile strength of CWP concrete.

iv. To analyse the durability of CWP concrete.

v. To examine the microstructure of CWP concrete in order to understand the hydration products, bonding mechanisms, and their influence on strength and durability.

1.5 Scope and Limitations of the Study

This study examines the role of CWP as a binder material in concrete, focusing on its potential pozzolanic activity or inert filler behaviour. The investigation is limited to assessing the effects of CWP in comparison to two reference binders: Portland-slag cement (CEM II/A-LL) and Portland-limestone cement (CEM II/B-S). The study explores the influence of CWP on the properties of concrete by replacing the GGBS in Portland-slag by 10% and 20% of CWP and LSP in Portland-limestone at 5% and 7% levels. Concrete mixes are designed with w/b ratios of 0.45, 0.50, and 0.55 to evaluate the effects across different mix proportions.

1.6 Delimitations of the Study

This research is limited to the assessment of fresh and hardened concrete properties—specifically workability, compressive strength, and splitting tensile strength—because these parameters are the most fundamental indicators of concrete performance and are directly influenced by the inclusion of supplementary materials such as CWP. Evaluating these properties provides essential insights into the immediate behaviours and mechanical integrity of the material.

The durability performance is examined through the OPI, WSI, and CCI, as these standardized indices are reliable predictors of the long-term resistance of concrete to ingress of harmful agents. Focusing on these indices allows for a comprehensive understanding of how CWP affects the pore structure and permeability-related durability without requiring extended field exposure testing, which is beyond the available timeframe and resources of this study.

Microstructural characterization is confined to SEM analysis to observe the interfacial transition zone (ITZ) and pore morphology. SEM provides adequate resolution and detail for evaluating microstructural changes resulting from CWP incorporation, making it suitable for correlating microscopic observations with macro-level performance.

The study does not cover large-scale structural performance, long-term field exposure tests, or alternative curing conditions beyond standard laboratory procedures. These exclusions are deliberate to maintain experimental control, ensure reproducibility of results, and keep the scope aligned with the available facilities and duration of the research project. Moreover, focusing on controlled laboratory conditions allows for isolating the effects of CWP without the interference of environmental and operational variables that could obscure the primary research objectives.

1.7 Structure of the Dissertation

The thesis consists of five chapters. The description of each chapter is given below.

- **Chapter One** gives a general overview of the research, which includes the background of the research, problem statement and research significance, aim and objectives, research scope, and thesis outline.
- **Chapter Two** provides a literature review that focuses on previous studies on CWP.
- **Chapter Three** describes the experimental investigation showing the test procedure for obtaining data that defines the properties of CWP concrete.
- **Chapter Four** presents the results, analyses, and discussion of the experimental investigations that were carried out in Chapter Three.
- **Chapter Five** gives the general conclusion of the chapters and recommendations for further studies.

CHAPTER TWO
LITERATURE REVIEW

2.1 Preamble

This chapter presents a systematic literature review that evaluates the potential of ceramic waste powder (CWP) as a cement material in concrete, focusing on its effects on workability, mechanical, durability and microstructural properties. A structured and rigorous methodology was adopted in sourcing articles to ensure relevance, transparency and reproducibility. The scope included studies published between 2010 and 2024, emphasising peer-reviewed journal articles, conference proceedings, and credible industry reports that examined the impact of CWP on concrete performance.

A comprehensive search was conducted using Scopus, Web of Science, ScienceDirect, SpringerLink, and Google Scholar. Search terms included “Ceramic Powder Concrete”, “ceramic wastes concrete powder cement”, “ceramic AND wastes AND concrete AND powder AND cement (Figure 2.1)”, “sustainable concrete materials”, and “durability and mechanical properties of concrete containing ceramic powder”. Filters were applied to limit results to English-language publications. Studies were selected based on specific inclusion criteria, such as focusing on CWP concrete made from tiles and sanitary wares, providing quantitative data on concrete properties, and employing experimental or analytical methods. Articles lacking empirical data or addressing other ceramic waste materials were excluded.

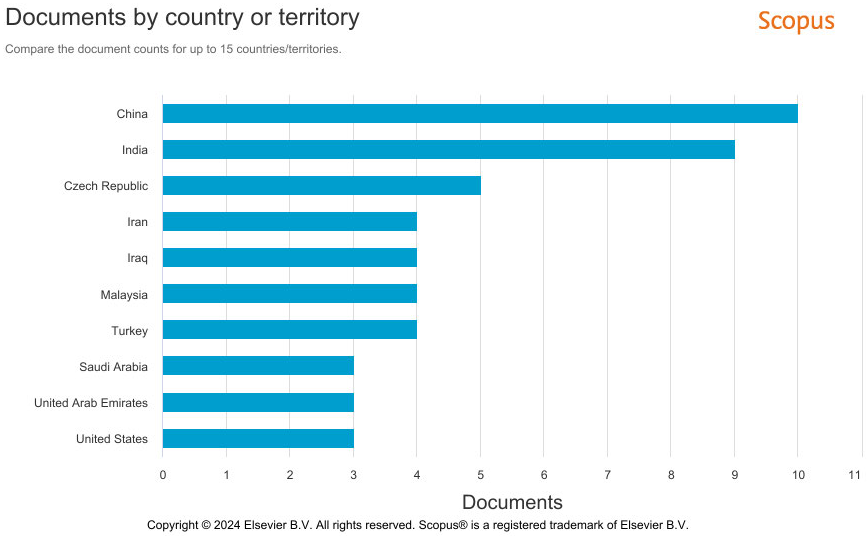

Figure 2.1: Analysis of 51 documents found on Scopus for KEY (ceramic AND wastes AND concrete AND powder AND cement)

Data were extracted systematically, capturing details such as concrete mix proportions, replacement levels, measured properties, and experimental conditions. Findings were categorized into thematic groups to identify trends, patterns, and inconsistencies. A critical quality assessment of each study ensured that only methodologically sound research with complete and reliable data was included in the synthesis. Quantitative findings were summarized and compared, while qualitative analysis identified mechanisms such as pozzolanic reactions and microstructural changes contributing to the performance.

2.2 Use of CWP as a Sustainable Cement Material in Concrete

Portland cement (PC) is increasingly considered unsustainable due to its significant negative environmental impact, accounting for approximately 8% of global CO_2 emissions (Scrivener, John & Gartner 2018). To mitigate this issue, waste materials such as CWP have gained recognition as a promising alternative to reduce the environmental hazards associated with PC (Ikotun, Adedeji, Babafemi & Otieno 2025). Using ceramic waste in concrete is generally considered environmentally beneficial, though concerns such as boron leaching require careful examination (Medina, Sánchez De Rojas, Thomas, Polanco & Frías 2016; Ling & Poon 2014; Siddique 2014). Ceramic waste, especially from tile production, often contains small amounts of boron compounds such as boron oxide (B_2O_3) (Silva, De Brito & Dhir 2014). Large quantity of boron can be toxic to the ecosystems if it leaches into the environment (Howe 1998). However, research indicates that the boron content in ceramic wastes often used in concrete is generally low, typically ranging from 0% to 1.3% B_2O_3, posing minimal environmental risk at these concentrations (Gol et al. 2023). Studies have also shown that ceramic waste derived from tiles and sanitary wares exhibits negligible leaching properties, making it a safe material for construction applications (Govindarajalu & Ganapathy 2024; Medina, Frías & Sánchez de Rojas 2014). Therefore, the use of ceramic waste benefits the environment without posing any major risk of toxicity (Medina et al. 2014).

In addition to its environmental benefits, the incorporation of CWP in cement has been shown to improve concrete properties, such as long-term mechanical properties and durability (Ikotun et al. 2025; Salvi, Gupta & Sharma 2021). Researchers have also established that CWP can lower the cost of concrete production. For instance, a study by

Raval *et al.* found that replacing 30% of PC with CWP reduced cement costs by 12.7% in Iran (Raval, Patel & Pitroda 2013).

Some researchers obtain CWP from the final cutting and polishing stages of ceramic manufacturing. Others produce it by crushing and milling ceramic wastes (tiles, sanitary wares, and table wares) into powder. A detailed analysis of studies on CWP as a cement replacement material is presented later in this chapter. Despite the different sources, the chemical compositions of CWP are consistent (Ikotun et al. 2025; Mezidi, Merabti, Benyamina & Sadouki 2023; Mohit, Haftbaradaran & Riahi 2023; El-Dieb, Taha, Kanaan & Aly 2018; Subaşı, Öztürk & Emiroğlu 2017a; Pacheco-Torgal & Jalali 2010). Figure 2.2 shows the image of CWP obtained from ceramic cutting and polishing, while Figure 2.3 shows CWP obtained by crushing and milling ceramic wastes.

Figure 2.2: CWP obtained from final cutting and polishing stages of ceramic production (Attaelmanan, Elhaj Mahgoub Kambal & Mansour 2021)

Figure 2.3: CWP obtained by crushing and milling ceramic tiles into powder (Taher, Abed & Hashim 2023)

Researchers often use CWP as a pozzolanic material, like ground granulated blast-furnace slag (GGBS), fly ash or silica fume, or as an inert filler, like limestone powder (LSP) in concrete. When CWP is used in high quantities, such as replacing up to 50% of PC, researchers aim to observe whether it behaves like a pozzolanic material (Ikotun et al. 2025). This expectation is reasonable given that microstructural analyses frequently report that ceramic powder contains high levels of silica, up to 65%. Silica is crucial for pozzolanic reactions, where it combines with calcium hydroxide (CH) to form calcium silicate hydrate (C-S-H) gel, the main binding component in cement, contributing to its strength and durability (Mohit et al. 2023a; El-Dieb et al. 2018). This reaction also helps mitigate alkali-silica reaction in concrete. On the other hand, researchers use smaller amounts of CWP, typically 10% of PC replacement or less, expecting it to act more like an inert filler, which improves concrete durability by densifying the concrete matrix (El-Hawary & Nouh 2018; Moosberg-Bustnes, Lagerblad & Forssberg 2004b).

The production processes that ceramic waste undergoes significantly affect the reactivity of the silica in its composition (Mohamed N Rahaman 2007). Due to this process, the silica possibly loses its pozzolanic reactivity, making CWP behave more like an inert filler than a reactive material. This raises a valid argument over the role of CWP in concrete—whether as a pozzolan that contributes to hydration products and improves mechanical properties or as an inert filler that enhances the concrete durability simply by filling the pores in the concrete microstructure. Meanwhile, it is also important to note that other properties, such as the specific surface area of the powder, also play an important role in the reactivity of CWP in concrete (Mehta & Monteiro 2001).

While many studies show consistent results regarding the performances of CWP concrete, there are still some contradictions in the literature. Several studies suggest that CWP exhibits lower strength at early ages but eventually gains comparable strength to PC concrete at later ages (Mohit et al. 2023a; El-Dieb et al. 2018). These Researchers precisely observe that CWP concrete shows lower strength at 7 days but achieves higher strength at 28 to 90 days, like pozzolanic concrete (Mezidi et al. 2023; Mohit et al. 2023a; El-Dieb et al. 2018; Subaşı et al. 2017). Pozzolans like fly ash, GGBS and silica fume are known for their slower hydration rates, which initially result in lower compressive strength but lead to stronger and more durable concrete over time as additional C-S-H forms (Mehta & Monteiro 2001). This delayed strength development is a basic characteristic of pozzolanic materials, as highlighted by Mehta & Monteiro (Mehta &

Monteiro 2001). However, some researchers have reported little or an invariable rate of strength development (compared to PC concrete) with no long-term strength improvement. Such studies also observe improved durability at later curing ages. This suggests that CWP behave similarly to inert materials like LSP.

2.2.1 Manufacturing of ceramics

Ceramics are inorganic, non-metallic materials made from metallic oxides (Richerson & Lee 2018; *Ceramic Materials* 2007). Sanitary wares and table wares are classified as oxides ceramics (Hampshire & Pomeroy 2021). The raw materials include kaolin, ball clay, silica, sand, and feldspar (Richerson & Lee 2018). The manufacturing of oxide ceramics follows a series of well-defined steps to transform raw materials into finished products.

Sintering (firing) is the most crucial process in converting ceramic raw materials into a dense, connected microstructure (Rahaman 2017; Mohamed N Rahaman 2007). Sintering is performed at temperatures from 1,000 °C to 1,400 °C. (Rahaman 2017). These high temperatures facilitate chemical reactions and phase transformations. (Wang, Zhu, Zhou & Zhang 2022). Some oxides undergo various reactions at elevated temperatures, enhancing their bonding and densification (Hampshire & Pomeroy 2021). This can decrease the reactivity of the ceramics. During the rehydration of recycled ceramic powder in concrete, the densified structure may slow down reactions between the ceramic material and calcium hydroxide ($Ca(OH)_2$) from the cement paste. This may cause CWP to behave like an inert cement filler when used in concrete despite its high silica content.

2.2.2 Characteristics of CWP

According to the literature, CWP is typically cream or brownish in colour, with a fine and granular texture (Mohit et al. 2023; El-Dieb et al. 2018; Subaşı et al. 2017). Table 2.1 provides a detailed comparison of the physical characteristics of CWP and PC from different studies. CWP, with specific gravities ranging from 2.53–2.97, tends to have lower densities than PC, which typically ranges from 3.10–3.15. This indicates that the CWP is lighter in weight compared to conventional cement. Bulk density for CWP ranged from 2.56–2.97g/m^3, while PC typically falls within the range of 1.44–1.60 g/cm^3. The specific surface area of CWP used in the literature varies widely, from as low as 365 m^2/kg to as high as 34100 m^2/kg. This shows the high variations in the sizes of powder

used by different researchers. In comparison, PC usually has a specific surface area between 300–400 m²/kg. Water absorption of CWP was found to be 0.1% by Heidari *et al.* (2013), which is an advantage in construction applications, as it suggests lower porosity. In contrast, PC has a slightly higher water absorption range of 0.25–0.30%. Finally, an autoclave expansion of 0.08% was observed for CWP by Heidari *et al.* (2013), while PC typically shows an expansion of 0.80% (Afrisam 2018).

Microstructural analyses also establish similarities between the chemical composition of fired ceramic products and their raw materials, with differences primarily in mineral composition post-heating (Pacheco-Torgal & Jalali 2010). CWP exhibits a distinct chemical composition compared to PC, primarily due to its high silica (SiO_2) and alumina (Al_2O_3) content and low calcium oxide (CaO) levels (Li, Joseph, Zhang & Zhang 2024). Silica concentration in CWP ranges from 57–66%, significantly higher than the 17–25% typically found in PC (Mohit et al. 2023a; El-Dieb et al. 2018; Subaşı et al. 2017a; Rani 2016; Patel, Arora & Vaniya 2015b). This high silica content suggests CWP could serve as a pozzolanic material in cement blends, enhancing long-term strength through secondary hydration reactions. According to el-Dieb *et al.* (2018), this composition meets the ASTM C618 2019 requirements for natural pozzolana, indicating its potential as a supplementary cementitious material (SCM). However, the low CaO content (2.5–7.4%) in CWP means it lacks the necessary calcium for primary cementitious reactions, limiting its use as an independent binder. Additionally, CWP contains 18%–22% Al_2O_3, much higher than the 3%–8% usually observed in PC, potentially benefiting early strength. Minor oxides, such as iron oxide (Fe_2O_3) and sulfur trioxide (SO_3), vary across CWP samples but generally fall within ranges found in PC. Table 2.2 shows the chemical composition of CWP against PC.

Table 2.1: Physical characteristics of CWP against cement

Reference	Specific gravity	Bulk density (g/cm^3)	Specific surface area (m2/kg)	Autoclave expansion (%)	Water absorption
(Heidari & Tavakoli 2013)		2.57	34100	0.08	
(Mohit, Haftbaradaran & Riahi 2023b)		2.78	887		0.1
(Li et al. 2020)		2.56	458		
(Chen et al. 2022)		2.97			
(Abou Rachied, Dbouk, Hamad & Assaad 2023)	2.65		365		
(Zhang, Ahn, Lin & Wang 2021)		2.61			
(Abou Rachied et al. 2023)	2.65				
(Mohammadhosseini et al. 2020)	2.53				
(Taher et al. 2023)		2.56			
PC (Neville 2011; Mindess, Young & Darwin 2003; Mehta & Monteiro 2001)	3.10 - 3.15	1.44 – 1.60	300 – 2 400	0.80	0.25 – 0.30

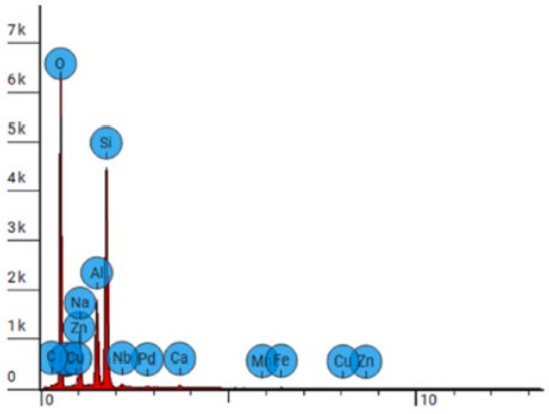

Element Symbol	Element Name	Weight Conc.
C	Carbon	1.399
O	Oxygen	47.353
Na	Sodium	8.192
Al	**Aluminium**	**12.787**
Si	**Silicon**	**26.573**
Ca	Calcium	0.699
Mn	Manganese	0.200
Fe	Iron	0.500
Cu	Copper	0.400
Nb	Niobium	1.199

Figure 2.4: Energy Dispersive Spectroscopy (EDS)

analysis of CWP (Li et al. 2024)

Table 2.2: Chemical composition of CWP versus PC

Reference	Al_2O_3 (%)	CaO (%)	SiO_2 (%)	Fe_2O_3 (%)	SO_3 (%)	Na_2O (%)	K_2O (%)	TiO_2 (%)	P_2O_5 (%)	MnO (%)	MgO (%)	L.O.I. (%)
Heidari and Tavakoli (2013)	21.8	5.1	64.8	3.9	2.0	-	-	-	-	-	1.7	1.3
Mohit, Haftbaradaran and Riahi (2023b)	22	4	65	5	1.5	0.25	1	-	-	-	1	-
(Li et al. 2020a)	20.47	5.90	59.64	4.80	2.08	0.80	-	-	-	-	2.74	1.97
(Sondarva, Pitroda, Gujar & Soni 2022a)	21.77	2.59	57.01	0.65	2.41	-	-	-	-	-	2.71	1
(Chen et al. 2022a)	20.64	6.30	58.47	3.40	2.04	0.74	-	-	-	-	2.45	1.88
(Abou Rachied et al. 2023)	21.5	4.6	66.6	2.8	2.7	-	-	-	-	-	1.2	3
(Najm & Ahmad 2022)	22.18	7.35	63.71	3.83	-	0.28	0.11	0.13	-	0.04	0.95	1.6
(Hussain Ali et al., 2019)	20.91	6.32	65.06	2.8	2.06	-	-	-	-	-	2.75	1.56
(Ahmad & Alhayani 2022)	21.33	5.43	60.3	3.88	0.183	-	-	-	-	-	-	-
(Kulovaná et al. 2016b)	18.89	4.24	62.37	3.83	2.31	0.12	1.14	0.31	0.12	0.07	0.99	1.52
(Subaşı, Öztürk & Emiroğlu 2017b)	18.37	4.26	64.04	3.89	3.01	0.12	-	-	-	-	1.52	4.23
(Taher et al. 2023)	22.31	6.67	61.62	1.24	0.07	0.96	1.55	-	-	-	0.65	3.96
Portland cement	4.77	62.5	19.1	2.74	2.74	-	0.30	0.37	0.08	-	2.67	3.93

2.3 Effects of CWP on Concrete Properties

This section discusses existing studies on CWP as a partial cement replacement in concrete, focusing on its workability, mechanical properties, durability, and microstructural influence. Research indicates that moderate CWP replacement (5–20%) enhances strength and durability through pozzolanic activity, while higher levels may reduce performance. Microstructural analyses, scanning electron Microscopy (SEM), X-ray Diffraction (XRD), Thermogravimetric Analysis (TGA) highlight the role of CWP in refining pore structure and improving long-term concrete properties. However, inconsistencies in findings emphasize the need for further research on its long-term behaviour, optimal dosage, and pozzolanic reactivity.

2.3.1 Effects of CWP on concrete workability

The workability of concrete is the ease of mixing, placing, and compacting without segregation or excessive bleeding (Rawarkar & Ambadkar 2018). This property significantly impacts the quality and performance of hardened concrete. Numerous factors influence workability, with the water-binder ratio being the most critical (Rawarkar & Ambadkar 2018). The type of cementitious materials used also plays a vital role. Finer cementitious materials enhance workability while reducing bleeding and segregation (Rawarkar & Ambadkar 2018). Various supplementary materials are employed to improve the workability of fresh concrete. For example, fly ash enhances workability, whereas materials like steel or synthetic fibres tend to reduce it (Rawarkar & Ambadkar 2018). The most common method for assessing concrete workability is the slump test. Table 2.3 provides an overview of the workability of CWP concrete. Most findings indicate a decrease in slump and workability with increased CWP content, often due to higher particle friction and density. For example, Daniel *et al.* (2018) observed a slump reduction from 110 mm to 95 mm at 30% CWP, while Li *et al.* (2024) reported a 52.4% slump decrease at 20% CWP. However, some studies, such as Sondarva *et al.* (2022) and Abubakr *et al.* (2019), noted improved workability with finer CWP particles and chemical additives.

Table 2.3: Overview of studies on workability of CWP concrete

Reference	Average particle size	Type of additive	Percentage replacement	Water/binder ratios	Source of CWP	Effect of CWP on concrete workability
(Daniel & Raju 2018)	Not specified	Ceraplast-300 (naphthalene-based superplasticiser, 0.2%)	0%, 5%, 10%, 15%, 20%, 25%, 30%	Not specified	CWP from dressing and polishing of ceramics	Slump decreased from 110 mm (0% CWP) to 95 mm (30% CWP). Compaction factors also decreased from 0.92 (0% CWP) to 0.87 (30% CWP)
(Tahir & Kumar Poloju 2017)	Not specified	Na_2SiO_3	0%, 10%, 20%, 30%, 40%, 50%, 60%	Not specified	Ceramic wall tiles waste	Slump decreased generally; however, slump increases at 10 and 40% replacement in Mix 1. The inclusion of Na_2SiO_3 in Mix 2 further reduces slump
(Attaelmanan et al. 2021)	Below 1 mm	None	0%, 10%, 15%, 20%	Not specified	CWP was obtained from a ceramic factory	Slump decreased as CWP content increased, starting at 135 mm (0% CWP) and decreasing to 65 mm (20% CWP)
(Kannan, Aboubakr, EL-Dieb & Reda Taha 2017)	Not specified	None	0%, 10%, 30% 40%	Not specified	CWP was obtained from the final polishing process of ceramic products	Slump decreased initially with increased CWP; improved slump at 20% and 30% CWP. Higher CWP levels (40%) exhibit significant slump loss
(Sondarva, Pitroda, Gujar & Soni 2022b)	Not specified	Bacillus megaterium (bacterial additive)	0%, 5%, 10%, 15%, 20%	Not specified	Ceramic tile waste powder	Slump increased from 80 mm (0% CWP) to 105 mm (20%)
(Abubakr et al. 2019)	Finer particles passing through ASTM sieve #200	None specified	0%, 10%, 20%	0.38	CWP from a local ceramic factory	Workability increased significantly with CWP content; doubled that of control mixes at 20%
(Li et al. 2024).	Majority of particles fall between 5–10 μm	Superplasticizer added. (Type not specified)	0%, 10%, 20%	0.40	CWP was obtained from ceramic tiles manufacturer	Control mix slump is 105 mm; slump decreased by 33.3% at 10% CWP and 52.4% at 20% CWP due to increased friction between particles
(Huseien, Sam, Shah & Mirza 2020)	Median particles of 35 μm	None	0–80%	Not specified	Not specified	Increased slump flow and workability with higher CWP content (50–80% CWP meets EFNARC SCC criteria)

Daniel *et al.* (2019) tested the slump of concrete containing CWP at 0%–30% in steps of 5%. The researchers reveal that as the proportion of CWP increases, there is a noticeable decrease in the workability of the concrete mixture. The researchers suggest that the workability of CWP concrete is only enhanced with superplasticisers. This agrees with Attaelmanan *et al.* (2021), who found that mixtures with CWP have a relatively lower slump compared to the reference mix without CWP. The addition of CWP to the cement decreases the concrete slump, as shown in Figure 2.5.

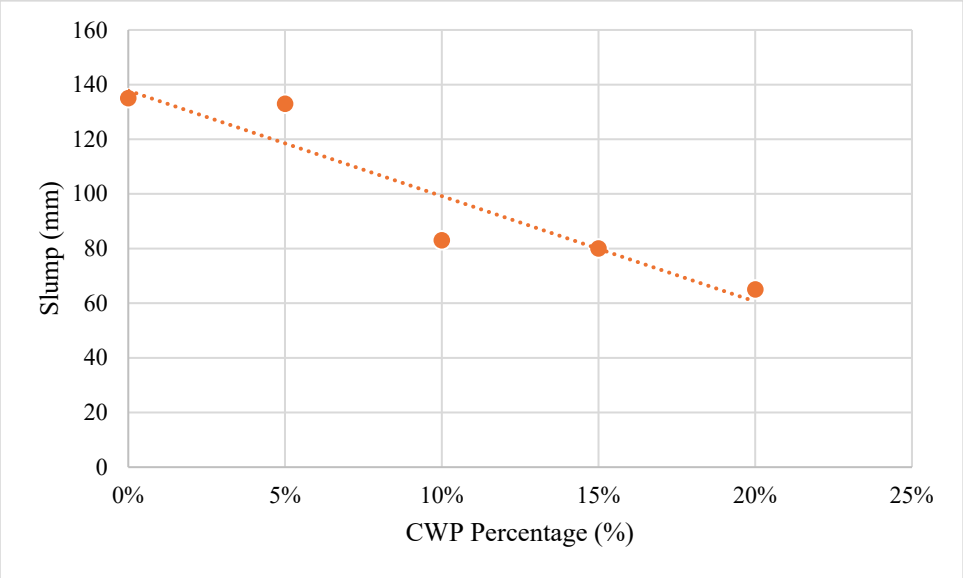

Figure 2.5: Slump test results (Attaelmanan et al. 2021)

Tahir *et al.* (2017) investigated concrete containing CWP at 0% to 60% in steps of 10%. The study comprised the formulation of three distinct concrete mixtures: one without silicate (Na_2SiO_3), the second and third mix containing 1% and 2% Na_2SiO_3 of the binder. The researcher's findings show that in Mix 1, the slump value decreased compared to conventional concrete. However, when 10% and 40% of CWP were used as a replacement, the slump value increased by 3.03% and 6.06%, respectively. In Mix 2, which contained 1% Na_2SiO_3 in the binder, the slump value decreased generally, except at 10% and 40% CWP. The research indicates that the addition of CWP can have varying effects on the workability of CWP concrete. Including Na_2SiO_3 in Mix 2 led to a further reduction in slump, underscoring the importance of precise mix proportions for achieving the desired workability in CWP concrete.

Kannan *et al.* (2017) investigated high-performance concrete containing CWP at 0% to 40% cement replacements. The researchers' findings indicate that as the replacement level of CWP in concrete increased, the initial slump value decreased, except for the 20% and 30% replacement levels. This decrease was attributed to the higher specific surface area of CWP, which is 1.5 times greater than that of cement. Furthermore, slump values decreased with time due to cement hydration, with the control mixture losing all slump within 60 minutes. However, the mixtures containing CWP demonstrated improved slump retention, with slump values reaching zero only around 120 minutes for the 20% replacement level. This improved slump retention was also attributed to the limited immediate hydraulic reaction of CWP due to its low CaO content. Notably, the 40% CWP mixture exhibited a slump loss trend like the control mixture, possibly due to the very high surface area of CWP, especially at higher replacement ratios.

Li *et al.* (2024) found that the slump value of concrete decreases significantly when cement is partially replaced with CWP. Replacing 10% and 20% of cement with CWP results in a slump decrease of 33.3% and 52.4%, respectively. The researchers stated that the irregular, angular shape and higher specific surface area of CWP increase friction between particles, leading to reduced slump values. The researchers also recommended the use of superplasticisers for CWP concrete to increase the slump value and workability by reducing internal friction among concrete particles. Comparatively, a similar study by Patel *et al.* (2015) reported smaller changes in slump values with CWP increment, likely due to higher water/binder ratios and differences in aggregate properties used in their experiments (Li et al. 2024). These factors can also affect concrete workability.

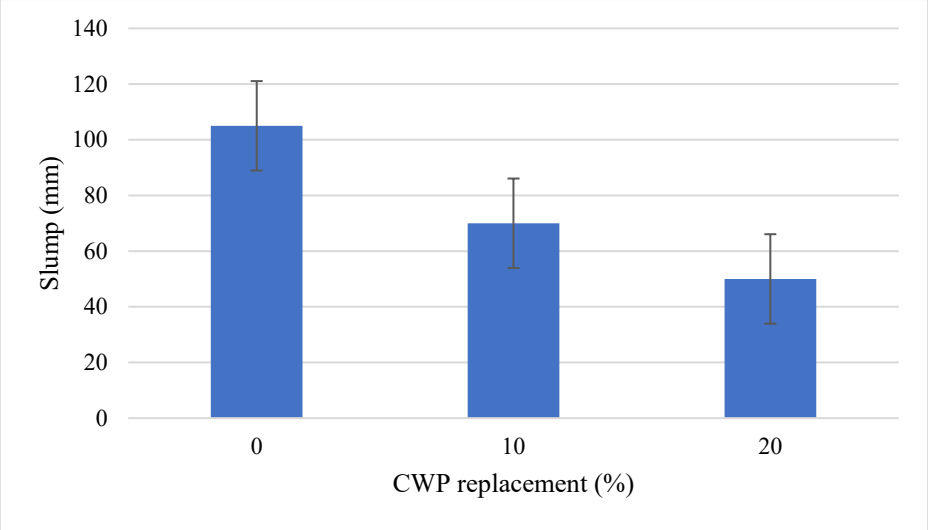

Figure 2.6: Slump test values of concrete specimens at different CWP replacement ratios of cement (Li et al. 2024)

Huseien *et al.* (2020) conducted three tests—slump flow, T50, and L-box to evaluate the impact of CWP on the filling ability of self-compacting concrete (SCC). In contrast to conventionally compacted concrete, the slump flow test showed a significant increase in concrete workability with higher CWP content replacing GGBS. As CWP content increased from 0% to 80%, the flow diameter expanded from 560 to 780 mm, indicating enhanced flowability. The researchers stated that concrete mixes with 50% to 80% CWP met the European Federation of National Associations Representing producers and applicators of specialist building products for Concrete (EFNARC) criteria for SCC (EFNARC 2002). The T50 test results also mirrored these findings. According to the study, concrete specimens demonstrated improved workability as the T50 time decreased from 6 seconds to 2.5 seconds with increasing CWP levels. Mixes with 40% or more CWP replacement also met the EFNARC standards for SCC (EFNARC 2002). The L-box test further confirmed these results, showing that all samples except those with 0% and 10% CWP passed the SCC requirements (EFNARC 2002). The increased flowability was attributed to the larger particle size distribution and lower specific surface area of CWP compared to GGBS, as well as the lower water demand of CWP, which enhances plasticity and workability by affecting the chemical reaction rate.

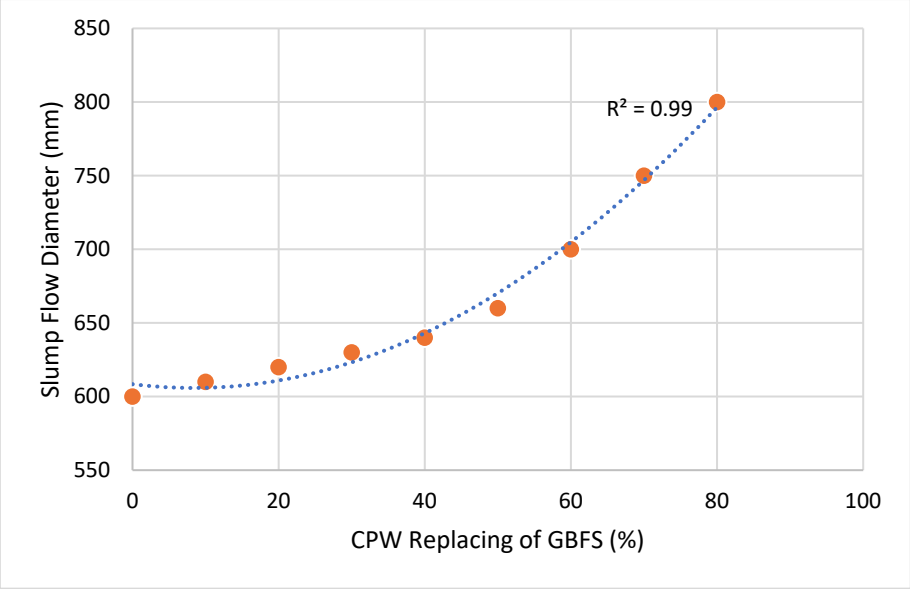

Figure 2.7: Slump flow of SCC containing different ratios of CWP replacing GGBS (Huseien et al. 2020).

2.3.2 Effects of CWP on concrete mechanical properties

Table 2.4 provides a detailed overview of studies on the effects of CWP on the mechanical properties of concrete. Compressive strength— the critical parameter in concrete load-bearing application, varies notably depending on the percentage replacement of CWP and particle size (Figure 2.7 - 2.8). Most studies identified optimal replacement levels between 10% and 30% to achieve enhanced or comparable performance to PC concrete.

The enhanced performance of CWP concrete is usually attributed to the pozzolanic reactivity of CWP. Pozzolanic reactivity is the material's ability to chemically interact with calcium hydroxide (CH), a by-product of cement hydration, in the presence of moisture (Mehta & Monteiro 2001). Cement hydration is an exothermic chemical process that produces compounds such as C-S-H (the primary contributor to concrete strength), ettringite, monosulphate, and CH (also known as portlandite) (Lasseuguette et al. 2019; *Ceramic Materials* 2007; Taylor 1997). The silica in CWP supposedly reacts with CH in a secondary pozzolanic reaction to form additional C-S-H, which acts as a glue that binds the aggregates and other cementitious materials together (Hilal 2016). This cohesion increases the overall load-bearing capacity of the concrete. However, this pozzolanic reaction occurs slowly, which is why pozzolanic concretes typically exhibit lower early-age strength, but higher long-term strength compared to conventional PC concrete (Hilal 2016; Mehta & Monteiro 2001).

Although pozzolanic reactivity is most accurately analysed using microstructural techniques like SEM to observe hydration products, the Strength Activity Index (SAI) is also a practical method (Diamond 2004). The SAI measures the compressive strength of cement-CWP blends relative to PC concrete. Studies show that CWP concrete achieves comparable performance at optimal replacement levels due to a combination of pozzolanic activity and enhanced particle packing.

The fine particles of CWP improve the particle distribution of concrete and strengthen the interfacial transition zone (ITZ) between aggregates and the cement paste (Lai, Hanzic & Ho 2019; Moosberg-Bustnes et al. 2004b). This refined microstructure also enhances the mechanical properties of the concrete (Moosberg-Bustnes et al. 2004b). However, determining whether the improved strength or durability of CWP-based concrete is due to the pozzolanic reaction or merely the result of CWP filling voids in the concrete microstructure can be challenging. Therefore, the mechanical behaviour of CWP-based concrete is often clarified by analysing the composition of its microstructure.

Daniel *et al.* (2018) and Tahir *et al.* (2017) found that moderate (30% or below) CWP replacement levels produced enhanced mechanical properties. Daniel *et al.* observed that 15% replacement yielded the highest compressive, tensile, and flexural strengths in M30 grade concrete, with compressive strength rising from 34.1 MPa for conventional concrete to 38.56 MPa at 28 days (Figure 2.8). Beyond 15%, properties declined rapidly, possibly due to dilution effects (Figure 2.9). Similarly, Tahir *et al.* identified 30% CWP combined with 2% sodium silicate as optimal in M25 grade concrete, significantly improved compressive strength while maintaining tensile strength and slightly reducing flexural strength. The study suggests that sodium silicate enhances pozzolanic activity at higher CWP levels. Both studies highlight that moderate CWP levels optimise particle packing and pozzolanic activity, resulting in improved strength.

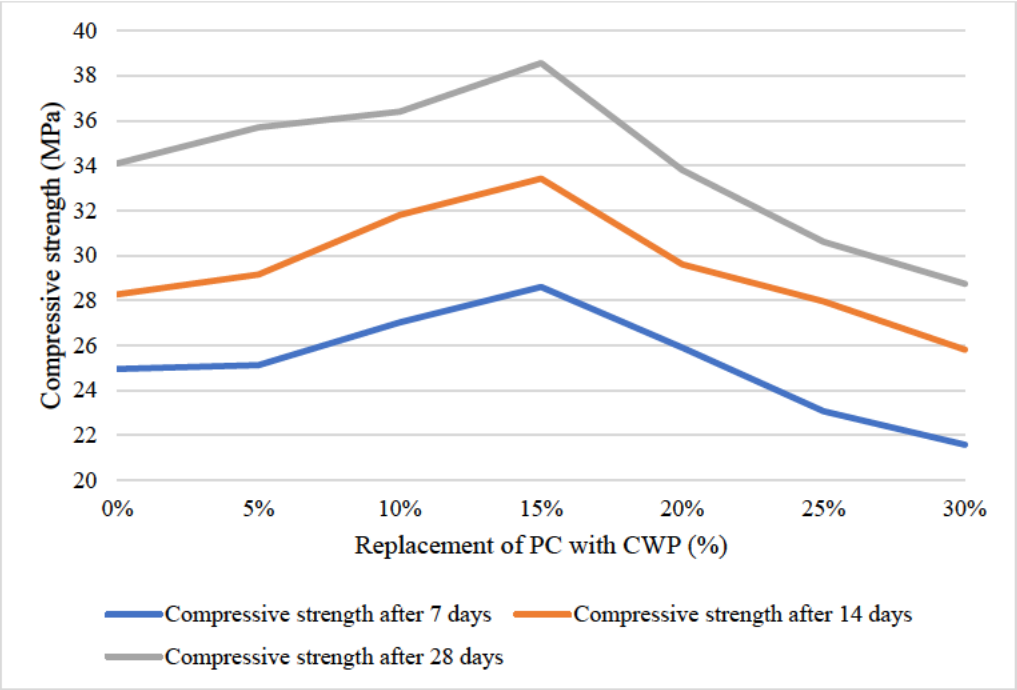

Figure 2.8: Compressive strength of CWP concrete at 7, 14 and 28 days (Daniel & Raju 2018)

Sondarva *et al.* (2022), Li *et al.* (2024), and Huseien *et al.* (2020) reported that lower CWP replacement levels (5%–10%) offered peak mechanical properties. Sondarva *et al.* (2022) observed a 15% increase in compressive strength at 5% replacement in bacterial concrete. The researchers attribute this performance to improved early strength development due to CWP. This is reasonable because, besides SiO_2, CWP contains approximately 20% Al_2O_3, which significantly contributes to the early strength of concrete. Similarly, Li *et al.* (2024) noted an 8.75% increase in compressive strength at 10% CWP but a significant reduction in strength afterwards (Figure 2.10). Huseien *et al.* (2020) also found maximum strength at 5% replacement, with extended curing periods allowing mixes to meet or exceed characteristic strength.

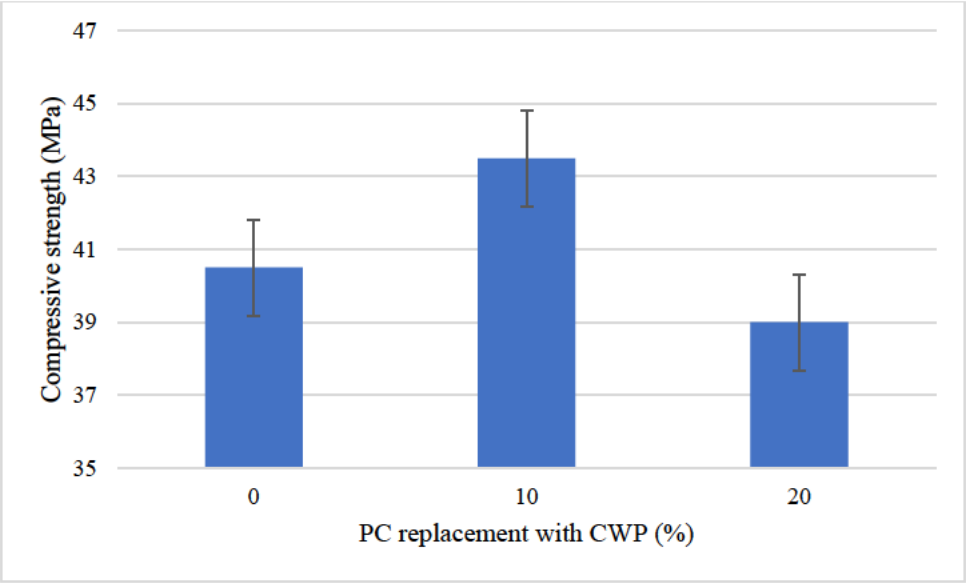

Figure 2.9: Compressive strength of CWP concrete (Li et al. 2024)

Studies by Abubakr *et al.* (2019), Kumar *et al.* (2017), and Rani (2016) also observed diminishing returns with higher CWP levels. Abubakr *et al.* reported significant reductions in compressive strength at 10%–20% replacements. Similarly, Kumar *et al.* observed peak strength at 10% replacement, with progressive declines up to 80%. The decline was linked to reduced CWP CaO content and slowed pozzolanic reactions. Rani (2016) noted that strength peaked at 10% replacement but significantly declined beyond this level, with the steepest reduction at 50%.

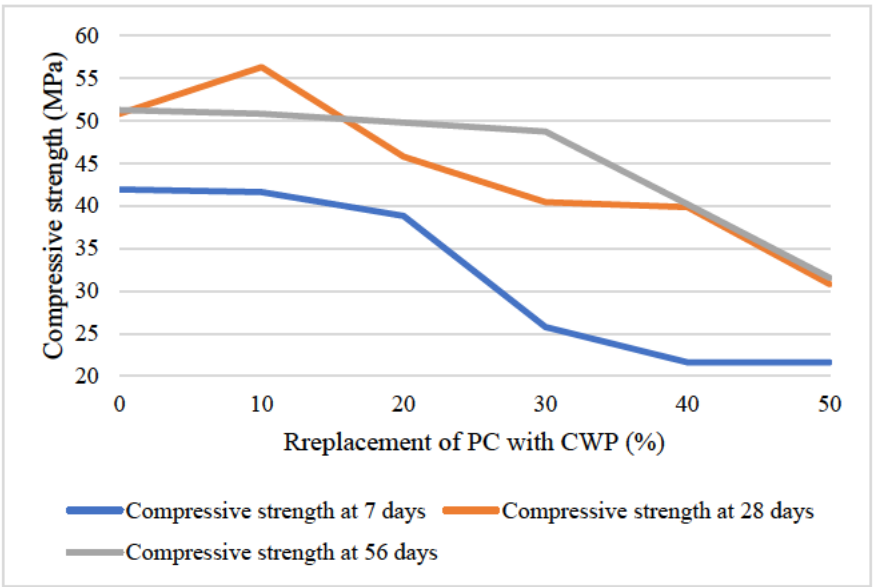

Figure 2.10: Compressive strength of CWP concrete at 7, 28 and 58 days (Rani 2016)

Heidari *et al.* (2013) and Umar *et al.* (2021) also agree that moderate CWP levels benefit long-term performance. Heidari *et al.* (2013) found minimal strength losses at 10% – 20% replacement after 91 days, demonstrating negligible long-term durability impact on CWP. Umar *et al.* (2021) confirmed that 30% replacement produced satisfactory strength at 7 and 28 days but warned of reductions at higher levels. These studies underscore the importance of maintaining replacement ratios within optimal thresholds to balance immediate performance and long-term durability.

Table 2.4: Overview of mechanical properties of CWP concrete

Author(s)	Source of CWP	Strength class	Percentage replacement	Average particle size	Curing days	Effect of CWP on compressive strength	Effect of CWP on flexural strength
(Daniel & Raju 2018)	Ceramic Industry Waste Powder	M30	5%, 10%, 15%, 20%, 25%, 30%	Not specified	7, 14, 28	Increases up to 15% replacement, with optimal strength at 15% after 28 days; decreases with higher replacements	Increases up to 15% replacement, with the highest tensile strength at 15%; decreases with higher replacements
(Tahir & Kumar Poloju 2017)	Ceramic Wall Tile Waste Powder	M25	0%, 10%, 20%, 30%, 40%, 50%	Not specified	28	Increases up to 30% replacement, optimal strength at 30%; decreases with higher replacements	Minor loss in tensile strength compared to conventional concrete
(Sondarva et al. 2022b)	Ceramic Tile Waste Powder with Bacillus megaterium	M25	0%, 5%, 10%, 15%, 20%	Not specified	7, 28	Compressive strength increases with bacterial concrete: peak strength at 5% CWP, 15% higher than control	Splitting tensile strength increases up to 13.52% with 5% CWP at 7 days
(Abubakr et al. 2019)	Local Ceramic Factory Waste Powder	M25	10%, 20%	Passed through ASTM #100 sieve	14, 28	Compressive strength decreases by 11% at 10% CWP and 23% at 20% CWP at 28 days due to coarser particle size	Flexural strength matches or slightly increases with CWP addition (recommended applications where flexural strength is critical)
(Li et al. 2024)	CWP from Polishing of ceramic tiles	M40	0%, 10%, 20%	5–10 μm (50% of particles)	28	Compressive strength increases by 8.75% at 10% CWP replacement (43.5 MPa vs. 40.5 MPa in control) due to pozzolanic reaction; decreases by 10.3% at 20% replacement	Predicted flexural strength (using an empirical model based on compressive strength) matches control
(Heidari & Tavakoli 2013b)	Recycled Ceramic Tile Waste	M40	10%, 15%, 20%, 25%, 30%, 40%	≤75 μm (200 mesh)	7, 28, 56, 91	Minor strength loss for 10-20% CWP replacement at 91 days, with only a 0.4 MPa reduction for 20% CWP compared to control	Not tested

Author(s)	Source of CWP	Strength class	Percentage replacement	Average particle size	Curing days	Effect of CWP on compressive strength	Effect of CWP on flexural strength
(Rani 2016)	Ceramic Industry Waste Powder	M40	0%, 10%, 20%, 30%, 40%, 50%	Not specified	7, 28, 56	Increases up to 10% replacement, with peak compressive strength at 10% CWP at all curing ages; decreases significantly beyond 10%, with maximum reduction at 50% CWP replacement	Not tested
(Kumar & Reddy 2017)	Industrial CWP	M25	0%, 10%, 20%, 30%	≤45 microns	7, 14, 28	Increases at 10% replacement, reaching maximum strength at 10% after 14 days; decreases beyond 10%, with 30% showing reduced strength compared to control	Flexural strength reduces progressively with higher CWP, highest at 10% CWP; further decreases with higher replacements
(Umar et al. 2021)	Ceramic Waste	M25	0%, 10%, 20%, 30%, 40%, 50%	Not specified	7, 28	Maximum compressive strength achieved at 30% CWP replacement; compressive strength reduces at replacements above 30%	Not tested
(Attaelmanan et al. 2021)	CWP from Ceramics Factory	M30	0%, 5%, 10%, 15%, 20%	Below 1mm	7, 28	Maximum compressive strength at 5% CWP at both 7 and 28 days; all CWP mixes showed good 28-day strength development, with 20% CWP slightly below 30 N/mm² (29.72 N/mm²). CWP slowed early strength development but achieved higher control mix strength at 28 days for all mixes except 20% CWP	Maximum tensile strength achieved at 5% CWP

Author(s)	Source of CWP	Strength class	Percentage replacement	Average particle size	Curing days	Effect of CWP on compressive strength	Effect of CWP on flexural strength
(Huseien et al. 2020)	Ceramic Tile Powder Waste (CWP)	Not specified	10%, 20%, 30%, 40%, 50%, 60%, 70%, 80%	Not specified	3, 28, 56	Compressive strength decreases with increasing CWP, with the lowest value at 80% CWP (18.6 MPa at 3 days) Strength improves with age but remains lower compared to control mix	Not tested
(Parashar, Sharma & Sharma 2022)	Waste Nano Ceramic Powder and Nano-SiO_2	Not specified	Nano ceramic powder: 0%, 2%, 4%, 6%, 8%, 10%; Nano-SiO_2: 0% to 4%	Nano particles scale.	7, 28	Compressive strength increased significantly with the addition of nano ceramic powder. Maximum compressive strength achieved with 6% nano ceramic powder and 3% nano-SiO_2 replacement. Strength gains are minimal beyond this level	Not tested

2.3.3 Effects of curing age on the mechanical properties of CWP concrete

Beyond replacement percentage and particle size, curing age is also a critical factor. The compressive strength of concrete, measured at different day intervals, provides insights into the hydration rate of the binder materials. Pozzolanic materials such as GGBS, fly ash, and silica fume tend to hydrate more slowly, leading to a gradual increase in compressive strength over time compared to PC (Lasseuguette et al. 2019; Taylor 1997). This explains why pozzolanic cement concretes exhibit lower early-age strength than those made with PC (Paiva, Silva, Velosa, Cachim & Ferreira 2017; Malhotra & Mehta 2004). Figure 2.11 and Figure 2.12 show the percentage change in compressive strength of CWP concrete at 7 and 28 days. The figures show that the compressive strength of CWP concrete improves significantly with curing age. At 7 days, there are variations in strength change across different replacement levels, with some studies reporting increases while others show reductions in strength. The strength changes range broadly from around +40% to -50% at this early age. However, at 28 days, the range of compressive strength changes narrows, and the data points trend towards neutral or slightly negative changes. This suggests that CWP concrete benefits from extended curing time; this is likely due to pozzolanic reactions contributing to strength development over time.

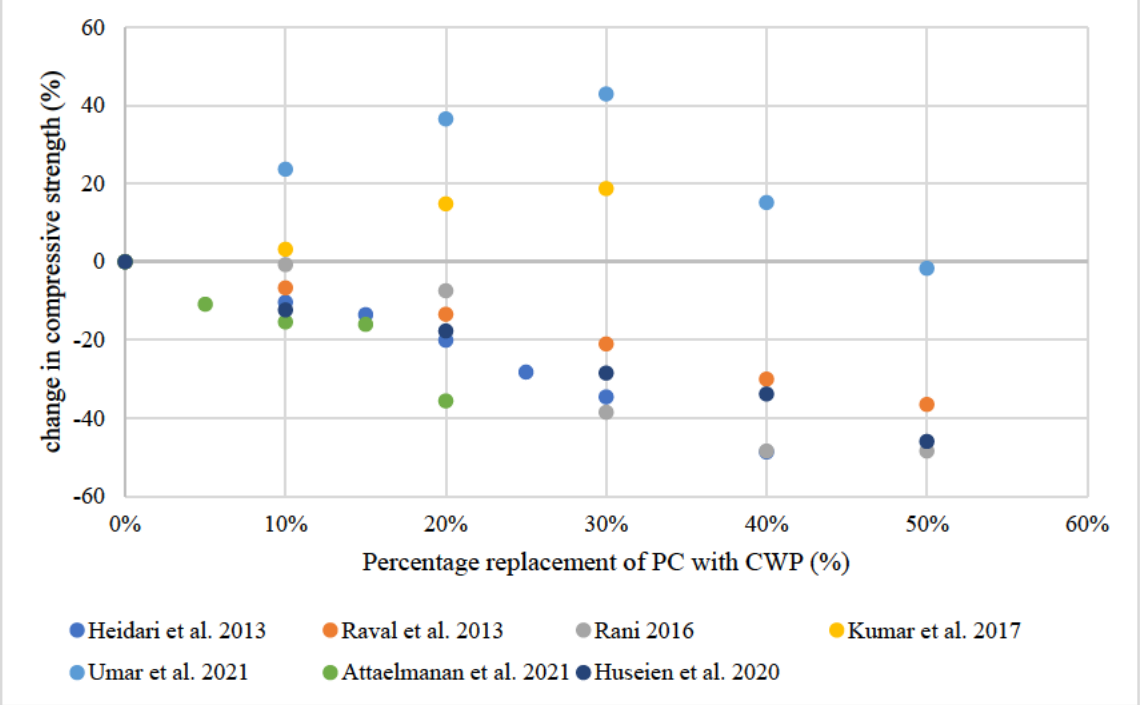

Figure 2.11: Percentage change in strength of CWP concrete at 7 days

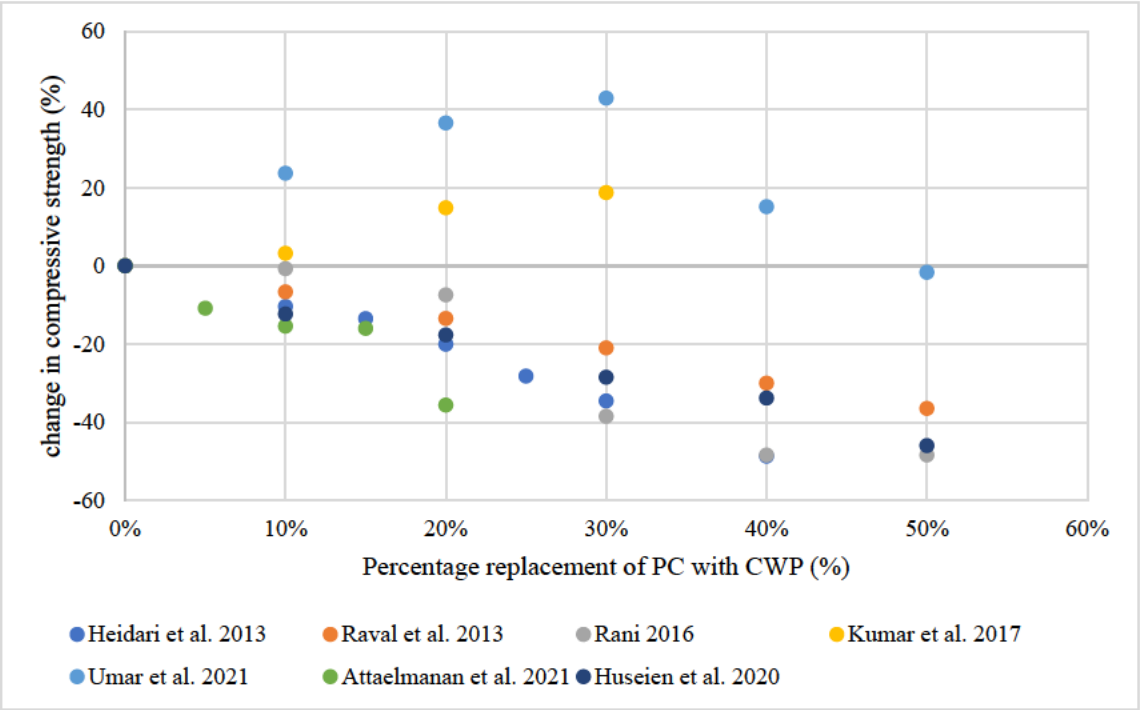

Figure 2.12: Percentage change in strength of CWP concrete at 28 days

Most of the studies highlighted in Table 2.4 show that compressive strength in CWP concrete generally improves over time, particularly when the replacement level of CWP is typically less than 30%. Huseien *et al.* (2020) report that CWP concrete mixes achieve satisfactory 28 and 56-day compressive strengths even at higher replacement levels of 20%, though strength development may be slower. This trend suggests that while CWP can initially inhibit early strength gain due to slower pozzolanic activity but continues to contribute to strength development as curing progresses, ultimately meeting or exceeding the PC concrete.

In contrast, Kumar and Reddy (2017) observe that compressive strength for concrete with 10% CWP peaks at all curing ages up to 28 days. However, at 28 days, strength declines significantly for mixes with higher CWP replacements (50%), indicating that very high CWP content may negatively affect long-term strength. In studies where the compressive strength is measured at extended curing durations such as 56 and 91 days (Heidari & Tavakoli 2013b). find only minor strength losses for mixes with 10%–20% CWP, with a 0.4 MPa decrease compared to the control at 91 days. This suggests that CWP concrete maintains satisfactory long-term durability and compressive performance, especially with low replacement levels and fine particle sizes.

Although the direct testing of flexural strength is limited, the available studies indicate similar trends as observed in compressive strength. For instance, Sondarva *et al.* (2022) highlight that flexural strength tends to improve at an early curing age, with CWP replacements around 5%.

Daniel and Raju (2018) also observe enhanced flexural strength up to 15% CWP replacement, beyond which performance declines. This pattern suggests a limit for effective flexural performance, beyond which CWP negatively impacts the concrete matrix. Studies such as those by Kumar and Reddy (2017) and Li *et al.* (2024) also support this, noting that CWP inclusion is suitable for applications where flexural strength is critical, provided the replacement level is carefully controlled. This improvement is consistent with findings in compressive strength, suggesting that pozzolanic activity in CWP concrete supports both compressive and tensile strength over time.

Overall, it can be deduced from most of the studies in the literature that curing age positively influences the mechanical properties of CWP concrete, especially when moderate levels of CWP are used. The pozzolanic reaction of CWP, though slower initially, becomes increasingly effective with extended curing, particularly after 28 days, resulting in concrete with satisfactory or even improved mechanical performance over conventional concrete in long-term applications.

2.3.4 Effects of CWP on concrete durability properties

Table 2.5 summarises the key research findings on the durability properties of concrete incorporating CWP as a partial cement replacement. Most of the studies evaluated the effects of CWP on water absorption, permeability, chemical resistance, and thermal stability. The findings indicate that optimal CWP replacement levels, typically around 10%–30%, can improve concrete's durability by reducing water absorption and enhancing resistance to chloride and chemical attacks (Umar et al. 2021; Tahir & Kumar Poloju 2017). Additionally, combinations such as CWP with nano-SiO_2 or microbial agents show further improvements in durability, making CWP-modified concrete a promising material for aggressive environmental conditions (Parashar et al. 2022).

Table 2.5: Overview of durability properties of CWP concrete

Author(s)	Key findings on durability properties of CWP concrete
(Kumar & Reddy 2017)	Concrete with 10% CWP replacement shows the best durability in NaCl solution, with minimal mass loss. However, 30% CWP results in higher mass loss, indicating reduced durability at higher replacements.
(Parashar et al. 2022)	Waste nano ceramic pozzolan and nano-SiO_2 at 4% reduce water absorption by refining pore structure, enhancing durability through improved water resistance.
(Tahir & Kumar Poloju 2017)	Concrete with 30% CWP and 2% sodium silicate demonstrates resilience under acidic conditions, particularly in HCl and H_2SO_4, with improved durability in aggressive environments
(Li et al. 2024)	At 20% CWP replacement, concrete shows improved thermal insulation, reduced thermal conductivity by 11.2%, and no spalling or cracks under fire exposure, enhancing durability in high-temperature environments
(El-Dieb & Kanaan 2018)	CWP replacement (10–40%) in concrete reduces chloride ion penetration and enhances resistance to chloride-induced corrosion across different concrete strengths (25 MPa, 50 MPa, 75 MPa) due to a denser microstructure and refined pore system
(Al-Ruqaishi, Ali Allamki & Poloju 2019)	Sorptivity tests show that concrete with up to 30% CWP replacement exhibits lower sorptivity and better durability than conventional concrete, suggesting that CWP is a favourable alternative for enhancing concrete durability
(Kannan et al. 2017)	CWP addition (up to 30%) reduces permeable pores in concrete cured for 90 days; however, beyond 30% replacement, permeable pores increase, often due to dilution effects, which impacts durability negatively at high replacement levels

2.3.4.1 Water absorption and permeability

Water absorption is a key durability indicator for concrete durability. It reflects its ability to resist environmental degradation caused by moisture ingress. Studies generally show that CWP enhances the moisture resistance of concrete. Kannan *et al.* (2017) and Al-Ruqaishi *et al.* (2019) reported reductions in permeability with increasing CWP content. Kannan *et al.* (2017) observed that concrete with up to 30% CWP replacement exhibited reduced permeable pores at 90 days of curing, although permeability increased beyond 30% replacement due to dilution effects. Similarly, Al-Ruqaishi *et al.* (2019) found lower sorptivity in concrete containing up to 30% CWP replacement, enhancing resistance to moisture ingress.

El-Dieb *et al.* (2018) demonstrated variability in permeability reduction based on concrete strength. For concrete with a compressive strength of 50 MPa, permeability decreased significantly at 20% CWP replacement but rose at higher levels. In contrast, concrete with strengths of 25 MPa and 75 MPa exhibited different trends, with 25 MPa concrete experiencing

rapid permeability reduction beyond 20% CWP, while 75 MPa concrete showed a more gradual but consistent decrease. The reduction in water absorption and permeability is primarily attributed to the pozzolanic activity of CWP. CWP reacts with calcium hydroxide during cement hydration to form additional C-S-H gel, which strengthens the microstructure by reducing capillary pores. Moreover, the fine and dense particles of CWP fill voids in the concrete matrix, further limiting water ingress and enhancing durability.

Parashar *et al.* (2022) investigated the water absorption of concrete incorporating nano CWP at 7 and 28 days. Results showed a range of water absorption capacities decreasing from 7.2% at 7 days to 6.42% at 28 days, indicating improved density and reduced porosity over time. As the percentage of nano CWP in the concrete mix increased, water absorption also increased. The study also highlights the delayed pozzolanic activity of CWP, as significant reactions do not occur during the early curing stages, as indicated by water absorption. This suggests that CWP may act primarily as an inert filler initially, with its pozzolanic properties developing over time.

2.3.4.2 Chemical resistance

The use of CWP in concrete significantly improves resistance to chemical degradation, particularly in acidic environments. This property is critical for concrete structures exposed to aggressive conditions, such as industrial zones or wastewater treatment plants. Tahir *et al.* (2017) demonstrated that concrete with a 30% CWP replacement combined with 2% sodium silicate admixture exhibited remarkable durability under exposure to hydrochloric acid (HCl) and sulfuric acid (H_2SO_4). Their study showed that sulfuric acid caused more severe durability loss compared to hydrochloric acid, but the concrete mix retained strength longer due to the denser microstructure created by CWP's pozzolanic activity, which limits aggressive ion penetration.

El-Dieb *et al.* (2018) highlighted that CWP reduces chloride ion penetration in concrete, enhancing resistance to chloride-induced corrosion across various compressive strengths (25 MPa, 50 MPa, 75 MPa). This improvement is attributed to a denser microstructure and refined pore system provided by CWP. Kannan *et al.* (2017) also noted the impact of CWP in reducing permeable pores, further aiding the resistance of concrete to chemical attacks. However, they cautioned that higher replacement levels beyond 30% may increase porosity and reduce durability due to dilution effects.

These findings underscore the importance of optimal CWP replacement levels in achieving chemical resistance in concrete. The improved resilience to chemical attack, whether from acids

or chloride ions, highlights the potential of CWP for use in aggressive environmental conditions where long-term durability and structural integrity are critical.

2.3.4.3 Thermal insulation and fire resistance

The inclusion of CWP in concrete enhances its thermal insulation and fire resistance properties, critical factors for improving structural durability in high-temperature environments. Li *et al.* (2024) found that concrete with up to 20% CWP replacement demonstrated a reduction in thermal conductivity by 11.2% and thermal diffusivity by 13.6%. (Thermal diffusivity is a material property that describes how quickly heat spreads through a material when there is a temperature gradient (Luhar et al. 2019)). This improved thermal insulation is particularly advantageous for buildings exposed to high temperatures or those requiring energy efficiency, as it reduces heat transfer through the structure, maintaining a stable internal environment.

Additionally, the study reported that CWP-based concrete exhibited superior fire resistance. It did not undergo spalling or develop major cracks during fire exposure, showcasing its ability to maintain structural integrity under extreme heat. The improved fire resistance is due to the dense microstructure formed by CWP in the concrete mix. When CWP is used, it refines the pore structure by reducing the number and size of capillary pores (Li et al. 2024). These small pores are where moisture can accumulate in conventional concrete. Under high temperatures, trapped moisture rapidly turns into steam, creating internal pressure that can cause concrete to crack or explosively spall. Since CWP reduces permeability and limits moisture retention, the risk of this explosive spalling is significantly lowered.

El-Dieb *et al.* (2018) support these findings, stating that the denser microstructure achieved with CWP reduces not only moisture penetration but also the ingress of harmful ions. This lower permeability indirectly enhances the fire resistance of the concrete by limiting internal pressure buildup and maintaining material stability under thermal stress. The combination of enhanced thermal insulation and fire resistance underscores the value of CWP in modern concrete formulations. CWP not only contributes to structural safety in fire-prone environments but also aligns with sustainability goals by reducing energy requirements for climate control in buildings. These benefits position CWP as a sustainable and efficient material for concrete construction, emphasising its role in achieving durability and environmental resilience.

2.3.5 Microstructural analysis of CWP concrete

Table 2.6 summarises research findings on the effects of CWP on concrete microstructure using various testing methods. Researchers have used SEM-EDS, XRD, TGA, and the Frattini test to

explored how CWP enhances microstructure of concrete. Key observations include reduced CH content due to pozzolanic activity, increased C-S-H gel formation, and improved densification of the ITZ. The findings demonstrate the potential of CWP to refine pore structure and contribute to stronger, more durable concrete.

Table 2.6: Overview of the key findings on microstructural properties of CWP concrete

Author(s)	Testing method	Summary of key findings on microstructure
(Li et al. 2024)	SEM and EDS	Observed well-dispersed CWP particles within cement matrix, reducing microcracks; 10% CWP replacement showed no significant alkali-silica reaction, indicating stable integration in microstructure
(Chen et al. 2022b)	XRD, TGA and SEM	XRD and TGA indicated reduced portlandite (CH) levels, enhancing C–S–H gel formation through pozzolanic reaction; 10% CWP produced a denser microstructure with fewer pores after 28 days
(Li, Liu, You, Chen & Zeng 2020b)	XRD, TGA, SEM and EDS	Identified pozzolanic interactions between CWP and cement hydrates, with reduced CH content over time and a denser ITZ in recycled aggregate concrete; EDS confirmed Ca, Si, Al variations indicating calcium-silicate-aluminate hydrate formation
(Kannan et al. 2017)	Frattini Test and XRD	Frattini test at 28 days confirmed pozzolanic activity with a reduction in CH levels and formation of complex calcium-silicate-aluminate hydrates at 20-40% CWP replacement levels

2.3.5.1 Scanning electron microscopy (SEM) of CWP concrete

Li *et al.* (2014), using SEM at 5000x magnification, observed that CWP particles, identified as white dots, were well-dispersed within the cement matrix. At a 10% CWP replacement, the researchers' SEM images displayed minimal microcracks, suggesting the compatibility of CWP with cement and aggregate bonding, with no significant alkali-silica reaction noted at this replacement level. Chen *et al.* (20122) conducted SEM imaging on CWP-cement pastes. The researchers observed a denser microstructure at 10% replacement, particularly after 28 days of curing. This compactness was attributed to CWP's pozzolanic reaction, which forms additional hydration products, reducing pore size and improving microstructure.

Tawfik *et al.* (2024) examined the effects of substituting PC0 with CWP on the microstructure and performance of high-strength concrete. SEM analysis of samples after 28 days of curing revealed that concrete with 10% CWP had a less homogeneous and compact microstructure compared to the reference sample (Figure 2.13). The researcher observed that the roughness of CWP particles led to stress concentrations at sharp edges, causing increased cracking and reduced strength characteristics. However, blending CWP with waste brick powder improved

the compactness and reduced crack formation due to better packing of particles with different sizes and shapes.

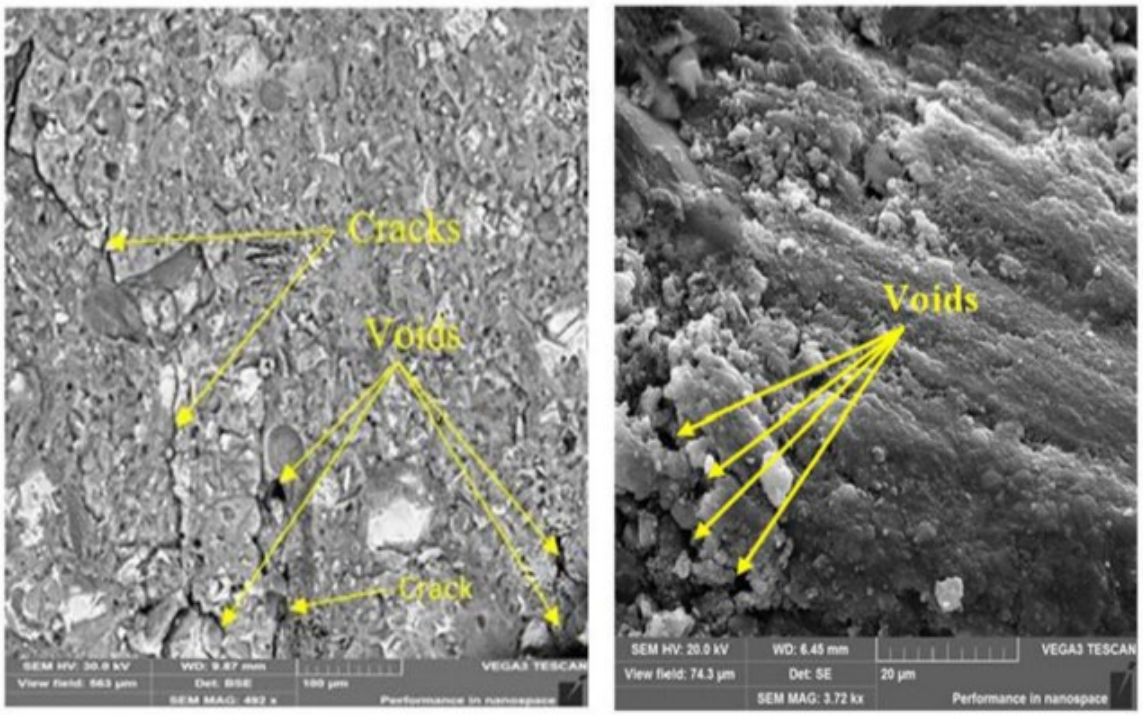

Figure 2.13: SEM image of concrete with 10% CWP at 28 days (Tawfik et al. 2024)

Li *et al.* (2022) reported that SEM-EDS suggests pozzolanic reactions on CWP surfaces, particularly between the ceramic grains and hydration products. The SEM images also showed a more compact ITZ, improving overall durability by reducing the porosity within the concrete structure.

2.3.5.2 X-ray diffraction (XRD) of CWP concrete

The XRD analysis by Chen *et al.* (2022) as presented in Figure 2.15, Figure 2.16 and Figure 2.17 show that CWP in cement paste reduced CH content due to its pozzolanic reaction, forming additional C–S-H gel. Peaks for portlandite diminished with increased curing days of concrete, indicating that CWP consumed CH and contributed to pozzolanic reaction.

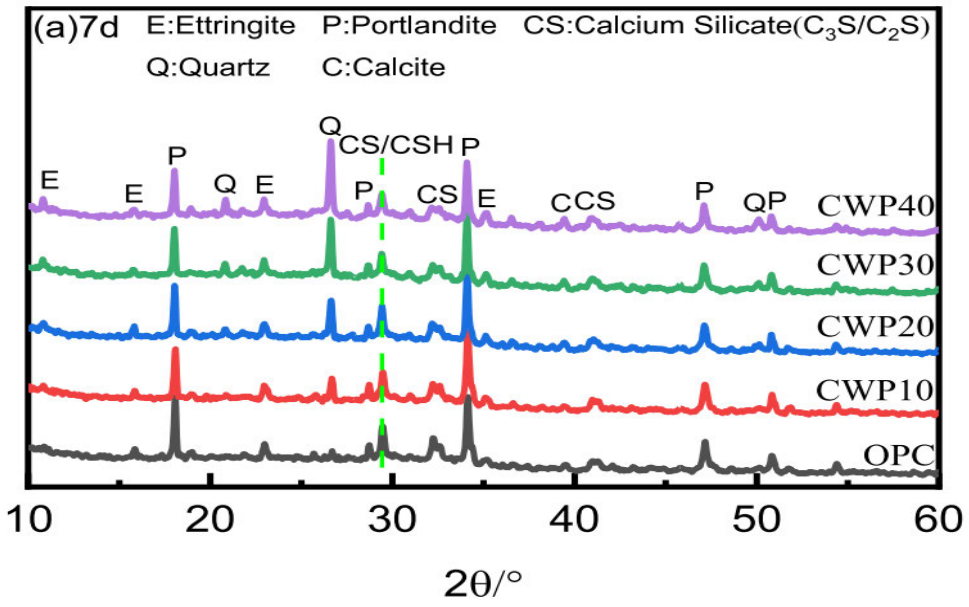

Figure 2.14: XRD patterns of CWP-cement pastes at 7 days (Chen et al. 2022b)

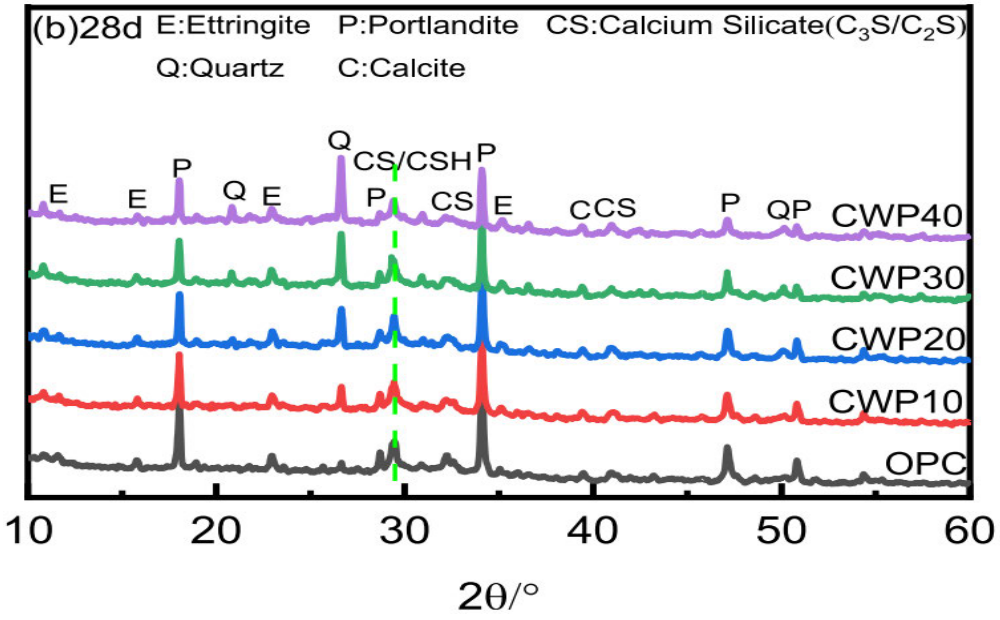

Figure 2.15: XRD patterns of CWP-cement pastes at 28 days (Chen et al. 2022b)

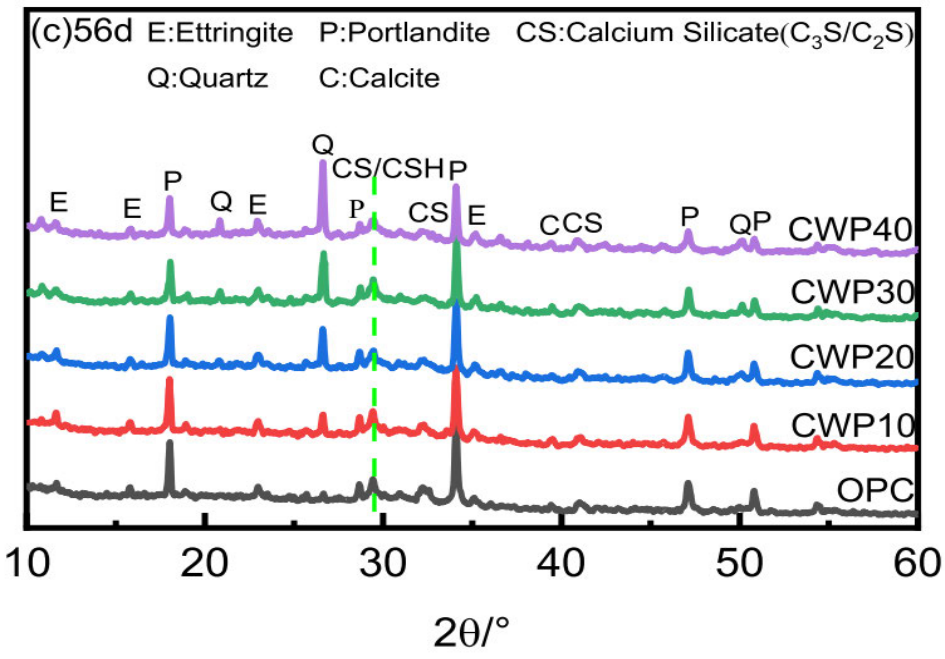

Figure 2.16: XRD patterns of CWP-cement pastes at 56 days (Li et al., 2020b)

Li *et al.* (2020) observed that the XRD spectra of hardened cement paste (HCP), in which PC was replaced with CWP, exhibited increased quartz peaks, particularly at 20% and 40% CWP substitution. These higher quartz levels, originating from CWP, accompanied reduced CH peaks over time, signifying that CWP enhanced the hydration process and aided in creating a denser microstructure.

Tawfik *et al.* (2024) also conducted XRD analysis on CWP concrete HCP, the results showed that CWP promoted the formation of crystalline phases like quartz and calcite, while reducing portlandite levels due to pozzolanic reactions. Despite its finer particle size, CWP exhibited slower pozzolanic activity compared to waste brick powder, attributed to potential recrystallization during production and the dilution effect from cement substitution. This initially led to reduced hydration products with strong mechanical properties. However, over time, CWP concrete demonstrated significant improvements in mechanical properties, likely due to delayed pozzolanic activity and the gradual release of water from its structure. Kannan *et al.* (2017) also confirmed the formation of calcium-alumino-silicate-hydrate (C-A-S-H) in CWP-blended samples, where a reduction in CH was noted at 20-40% CWP replacement. The complex hydrates contributed to microstructural enhancement and reduced porosity.

2.3.5.3 Thermogravimetric analysis (TGA) of CWP concrete

Chen *et al.* (2022) used TGA to track mass loss stages, linking them to hydration products like C-S-H, CH, and ettringite. The results are presented in Figure 2.17, Figure 2.18 and Figure 2.19.

The TGA confirmed a progressive reduction in CH content with increased curing days, supporting XRD findings that the pozzolanic activity of CWP refines the microstructure by consuming CH and producing additional C-S-H formation.

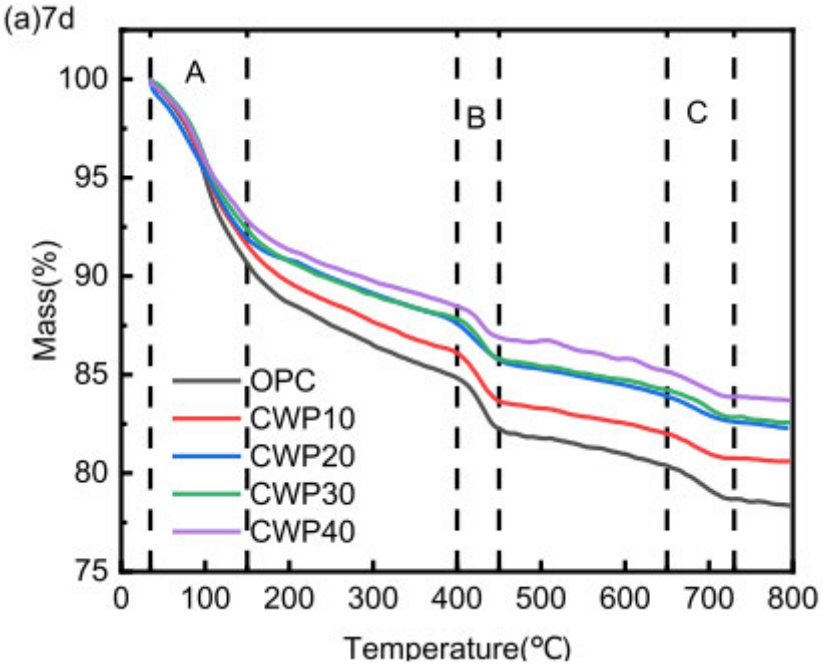

Figure 2.17: TGA curve of CWP-cement pastes at 7 days (Chen et al. 2022b)

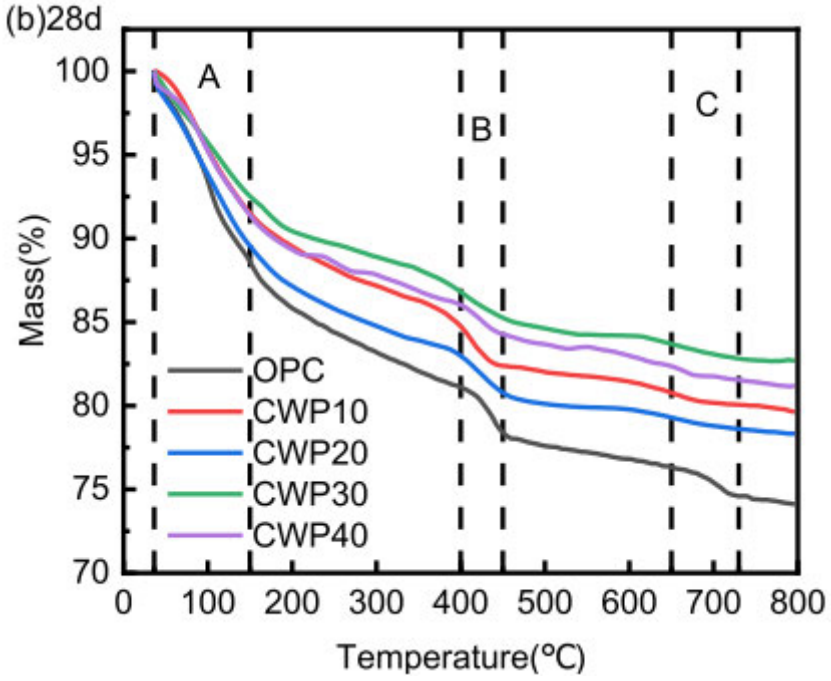

Figure 2.18: TGA curve of CWP-cement pastes at 28 days (Chen et al., 2022)

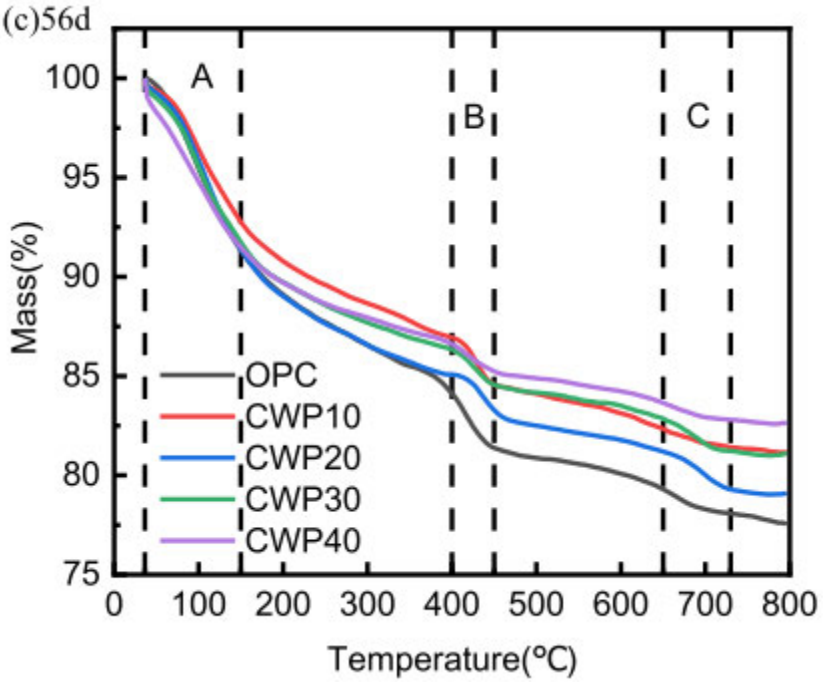

Figure 2.19: TGA curve of CWP-cement pastes at 56 days (Chen et al., 2022)

Li *et al.* (2022) indicated through TGA analysis, distinct mass loss phases: bound water evaporation and CH decomposition. The largest mass loss corresponded to bound water release, affirming hydration activity of CWP. With higher CWP content, more CH was consumed at later stages, highlighting ability of TGA to measure the pozzolanic reactivity of CWP in concrete microstructure.

2.3.6 Summary

Replacing PC with CWP in concrete has numerous effects on the fresh, mechanical, and microstructural properties of concrete, including its durability. However, there are still gaps in the understanding of the performance of CWP in concrete, particularly regarding the mechanical properties and reactivity of concrete containing above 20% PC replacement with CWP. This discussion covers the observed effects of CWP on concrete properties while also highlighting some contradictions found in existing studies.

The effect of CWP on the workability of concrete is inconsistent across studies. However, an increase in CWP content generally leads to a reduction in slump. For instance, a decrease in slump was observed from 110 mm (0% CWP) to 95 mm (30% CWP) by Daniel *et al.* (2018), and a more significant reduction was noted from 135 mm to 65 mm at 20% CWP replacement by Tahir *et al.* (2017). This is usually attributed to the finer particles in CWP, which increase surface area and water demand, thus reducing the concrete's flowability. However, other studies

have reported increased workability with CWP, especially when relatively coarser particles of CWP are used (Sondarva et al. 2022b). This indicates that the workability of CWP concrete depends on the particle size and the type of CWP used.

CWP generally improves compressive and flexural strength at low to moderate replacement levels, typically up to 5% to 20%. For instance, Compressive strength increases up to 8.75% within 28 days at 10% CWP replacement, according to Abubakr *et al.* (2019), and flexural strength also increases with up to 10% CWP according to Sondarva *et al.* (2022). These improvements are attributed to the pozzolanic reactions between CWP and cement hydrates, which enhance the formation of C-S-H gel, thereby strengthening the concrete matrix. However, higher CWP contents beyond 20% to 30% generally lead to a decrease in strength. For example, at 30% of CWP replacement, compressive strength decreases by up to 11% Abubakr *et al.* (2019), and flexural strength declines progressively beyond 10% CWP contents, according to Tahir *et al.* (2017). These findings highlight the importance of optimizing the replacement level to achieve the best balance between workability and strength. The observed reduction in strength at higher replacements is often attributed to the coarser particle size and reduced pozzolanic activity at elevated CWP levels.

Interestingly, some studies contradict these findings. For example, some researchers report that CWP can enhance compressive strength by up to 30% replacement of PC (Li et al. 2024). This discrepancy indicates a need for further research to better understand the factors influencing CWP's contribution to compressive and flexural strength.

The incorporation of CWP into cement also shows promising effects on concrete durability. It enhances various durability properties such as water absorption, permeability, chemical resistance, thermal insulation, and fire resistance (Mezidi et al. 2023; Mohit et al. 2023a; El-Dieb et al. 2018; Chen, Fang, Xu & Xie 2017; Subaşı et al. 2017a; Patel, Arora & Vaniya 2015c). The ability of CWP to refine the concrete matrix through its supposed pozzolanic activity is essential to its durability performance. By reacting with CH in a pozzolanic reaction, CWP forms additional C-S-H gel, which densifies the concrete structure and reduces capillary pores. The improved durability is also attributed to the filler effects of finer CWP particles. This process directly improves water absorption and permeability, as highlighted by Kannan *et al.* (2017) and Al-Ruqaishi *et al.* (2019). Lower water absorption reduces the ingress of harmful chemicals and moisture, thereby enhancing chemical resistance (Li et al. 2024). Chemical resistance, particularly in acidic and chloride-laden environments, further highlights CWP's role in improving durability. Study by Tahir *et al.* (2017) demonstrated that CWP concrete

performs well in aggressive environments due to its dense matrix, which limits ion penetration and structural degradation.

The SEM, XRD, and TGA provide valuable insights into the effects of CWP on the concrete matrix. Li *et al.* (2024) observed well-dispersed CWP particles within the cement matrix, which reduced microcracks in the CWP concrete microstructure. XRD and TGA results from Chen *et al.* (2022) confirmed a reduction in CH levels and enhanced C–S–H gel formation, suggesting a pozzolanic reaction.

However, the extent of pozzolanic reactivity of CWP in concrete remains uncertain, particularly at higher replacement levels. Some studies report that CWP exhibits insignificant pozzolanic reactivity beyond 10% replacement, as evidenced by invariable CH content and slower strength development at higher replacement levels (Kannan et al. 2017). Contradictory findings have been reported by other authors who found CWP exhibiting significant pozzolanic activity even at higher replacement levels (Li et al. 2024). These variations may be due to differences in the particle size, source of CWP or testing method.

There is also limited data on the long-term microstructural behaviour of CWP-concrete mixes, as majority of the studies tested at 28 days of curing. While short-term results suggest positive pozzolanic interactions, further studies are required to assess the microstructure of CWP-based concrete over extended periods, particularly under aggressive environmental conditions like sulphate or chloride exposure.

2.3.7 Methodological limitations of literature

One of the primary challenges identified in the literature is the variability in the sourcing and processing of CWP. Although many studies indicate the origin of the CWP used, a significant number lack comprehensive characterization of the material or fail to detail the processing methods employed in making the wastes CWP. This complicates meaningful comparisons of CWP from different sources.

Another critical limitation is the inconsistent durability testing procedures. While most researchers follow recognized standards like ASTM or EN, some adopt modified or undefined procedures without sufficient explanation. These methodological inconsistencies reduce the reliability of comparative analyses and obscure a clear understanding of the durability performance of CWP. Furthermore, although short-term performance indicators such as compressive strength results at 28 days are commonly reported, there is a notable lack of long-

term assessments. Given the importance of long-term performance in evaluating the durability and viability of CWP as a SCM, comprehensive long-term durability testing is essential.

Additionally, the highest concrete strength level assessed in current literature is generally limited to 40 MPa. High-strength concrete (above 40 MPa) has not been adequately investigated. Further research is therefore recommended to evaluate the performance of CWP in high-strength concrete applications.

Lastly, most studies compare the performance of CWP solely with Portland cement. To better assess its effectiveness, it is advisable to also compare CWP with conventional SCMs such as GGBS and fly ash.

CHAPTER THREE
MATERIALS AND RESEARCH METHODS

3.1 Preamble

The use of ceramic waste powder (CWP) as a substitute for ground granulated bast-furnace slag (GGBS) and limestone powder (LSP) is another innovative step in the study of sustainable cement materials. This chapter serves as the compass guiding the investigation of the pozzolanic and filler effects of CWP on concrete. The materials used in this study have been carefully acquired and formulated to ensure their suitability for the research objectives. The materials were also characterised with a focus on obtaining essential properties crucial for their integration into concrete. All the research experiments were conducted at the University of the Witwatersrand unless otherwise specified. Concrete testing was done in adherence to relevant South African standardised procedures, ensuring consistency and reliability in the obtained data. The adherence to proper standards not only upholds the integrity of the research but also allows for meaningful comparisons with established benchmarks.

The experimental program was structured into three phases as follows:

Phase 1 – Characterization of research materials

Phase 2 – Fresh properties of concrete incorporating CWP

Phase 3 – Hardened properties of concrete incorporating CWP

Phase 1: Characterization of research materials

The first phase involved laboratory investigations to characterize the materials used in the study. Tests conducted on the samples included particle size distribution, particle relative density, bulk density, and microstructural analysis. This phase focused on comparing the physical and chemical properties of CWP with other binders—GGBS, LSP, and PC.

Phase 2: Fresh properties of concrete

The second phase assessed the fresh properties of concrete incorporating CWP. The primary test conducted at this stage was the slump test, which evaluated the workability of the concrete mix.

Phase 3: Hardened properties of concrete

The third phase investigated the hardened properties of CWP concrete, focusing on strength performance (compressive strength and splitting tensile strength), durability indicators (water

sorptivity index (WSI), oxygen permeability index (OPI), and chloride conductivity index (CCI)), and microstructural analysis using scanning electron microscopy (SEM).

The properties of CWP concrete were analysed in comparison to concrete incorporating the two reference binders separately—LSP and GGBS. A comprehensive comparison was then made between the different mixes to evaluate their performance. Figure 3.1 provides an overview of the research procedures.

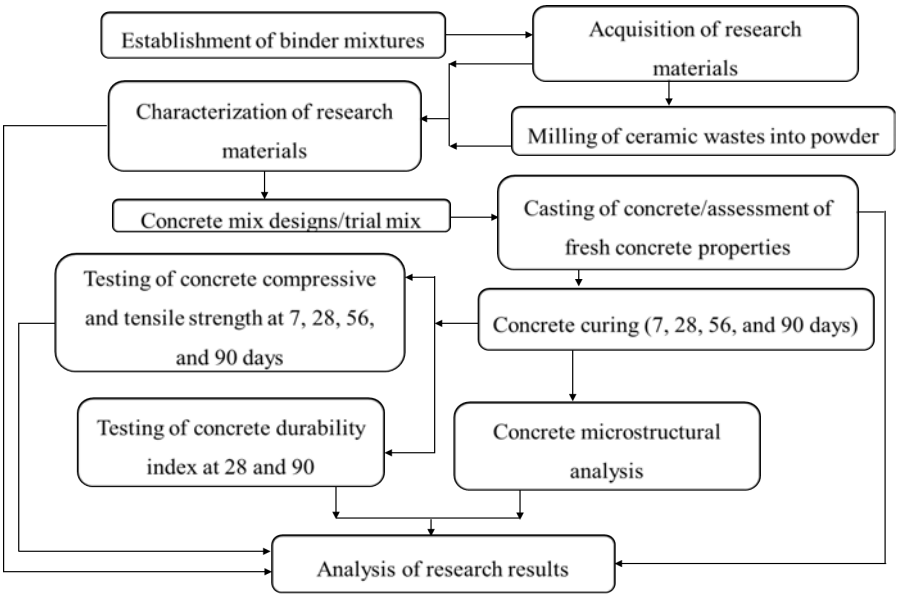

Figure 3.1: Overview of the research procedures

3.2 Materials

The materials used were carefully selected to investigate the role of CWP in concrete in comparison to GGBS and LSP. Each material plays a specific role in the concrete mix, contributing to its properties. As shown in the Table 3.1, PC, GGBS, LSP, and CWP act as binders, varying by mix design, while crusher sand and crushed stone remain constant across all water-binder (w/b) ratios. Potable water is used for mixing, while a superplasticizer (SP) is added as needed to enhance the workability of the concrete.

The selection of GGBS and LSP as reference materials in this research stems from the deliberate attempt to investigate the fitness of CWP to either of the two contrasting behaviours of cementitious materials – pozzolanic reactivity and inertness. GGBS, known for its high pozzolanic activity, represents the peak of reactivity among pozzolanic materials.

Table 3.1: Overview of research materials

S/N	Materials	Purpose	Type	Usage
1	PC	Binder	CEM I 52,5 R	Variable
2	GGBS	Binder	Afrisam GGBS	Variable
3	LSP	Binder	Finely ground $CaCO_3$	Variable
4	CWP	Binder	Tiles and sanitary wares	Variable
5	Crusher sand	Fine aggregate	Andesite	Constant (for each w/b)
6	Crushed stone	Coarse aggregate	14mm andesite	Constant
7	Water	Mixing	Potable water	Constant
8	SP	Additive	Sika	As required

3.2.1 Binder materials

The following materials were used to form different binders: PC, GGBS, LSP and CWP.

3.2.1.1 Portland cement (PC)

Portland cement, CEM I 52,5 R was used. The cement was manufactured by Afrisam. Figure 3.2 shows the image of the cement used.

Figure 3.2: Portland cement CEM I 52,5 R

3.2.1.2 Ground granulated blast furnace slag (GGBS)

The GGBS was obtained from Afrisam. Figure 3.3 shows the image of the GGBS used in the research.

Figure 3.3: Image of GGBS obtained from Afrisam (Photo by Peace Adedeji, taken at WITS concrete laboratory, 2024)

3.2.1.3 Limestone powder (LSP)

Figure 3.4 presents the LSP used in this research. The LSP complies with the requirements of SANS 50197-1. This ensures its suitability as a cement filler in concrete mixes without contributing chemically reactive components such as $Ca(OH)_2$ or CaO. It is a white powder obtained from Reflecta Laboratory Supplies, Germiston, Johannesburg, South Africa.

Figure 3.4: Image of LSP (Photo by Peace Adedeji, taken at WITS concrete laboratory, 2024)

3.2.1.4 Ceramic waste powder (CWP)

The CWP used in this research originates from discarded ceramics, mostly tiles and sanitary wares as shown in Figure 3.5. The collected waste undergoes rigorous cleaning to eliminate impurities, then it was finely crushed and milled, with a laboratory pulveriser transforming it into powder. Figure 3.9 summarize the transformation process.

Figure 3.5: Ceramic wastes dumped on a site in Pietermaritzburg (Photo by Peace Adedeji, taken at Pietermaritzburg, 2023)

Renovation sites proved to be the ideal source of ceramic waste due to the removal of outdated fixtures and surfaces during the renovation process. Discarded floor and wall tiles and sanitary wares, including broken toilets and washing hand ceramics, were collected from these sites. Ceramic wastes were also collected from construction sites, mostly from errors in installation processes or damages incurred during construction. These wastes have a variety of colours and designs.

Figure 3.6: Crushing of ceramic wastes with a jar crusher (Photo by Peace Adedeji, taken at WITS concrete laboratory, 2024)

The ceramic materials were originally used for various purposes, such as wall coverings and flooring. Different processes were employed to detach ceramic tiles from any mortar or

adhesive used during installation. The ceramic surfaces were thoroughly cleaned of any remaining gums or adhesive materials. Solvents and mechanical methods were employed to achieve a clean and residue-free finish.

Figure 3.7: Laboratory pulveriser used to milled ceramic wastes into powder (Photo by Peace Adedeji, taken at WITS Geotechnic laboratory, 2024)

Processing ceramic waste into fine powder was challenging due to its brittleness. To address this, the waste was sun-dried to reduce moisture, then crushed with a jar crusher for easier milling as shown in Figure 3.6. Finally, a laboratory pulveriser (Figure 3.7) refined the material into fine powder as shown in Figure 3.8.

Figure 3.8: Ceramic waste powder

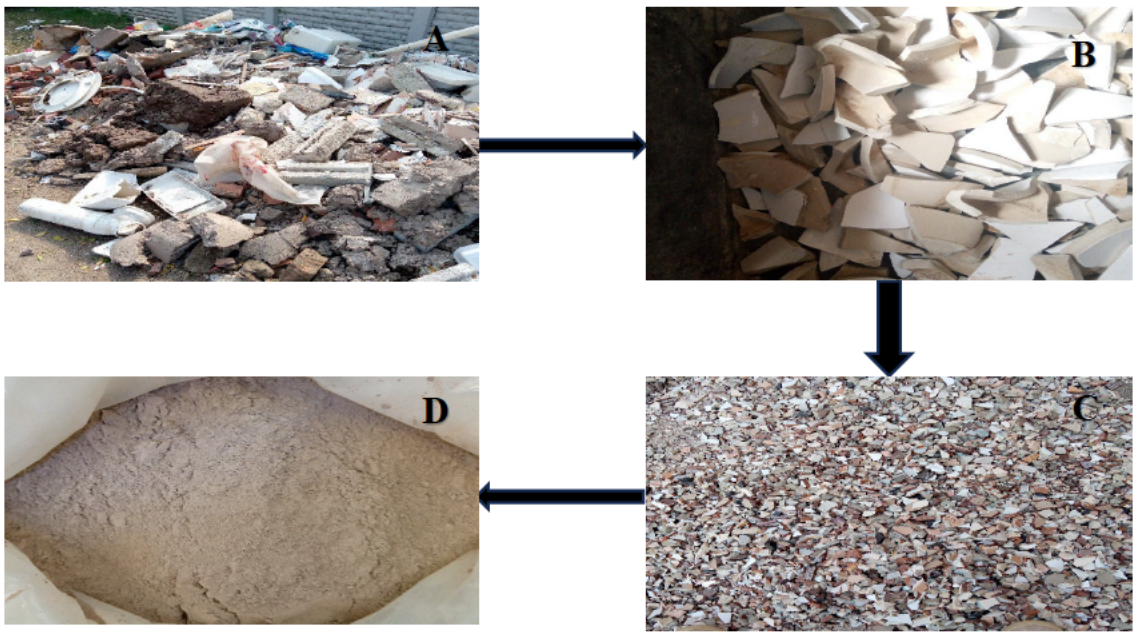

Figure 3.9: Transformation of ceramic wastes into CWP (Photo by Peace Adedeji, taken at WITS Geotechnic laboratory, 2024)

3.2.2 Characterization of binder materials

This section outlines the characterization of PC, GGBS, LSP, and CWP. Various tests were conducted to assess their physical and chemical properties, ensuring a comprehensive understanding of their influence on concrete performance.

3.2.2.1 Particle size distribution

The particle size analysis of the binders was conducted using the Anton Paar PSA 1090, using the dry dispersion method. The instrument was prepared by ensuring it was clean, calibrated, and free of any residual materials. Any clumps in the sample were removed by sieving to ensure consistency and flowability. The dry dispersion method was selected, and key parameters were configured, including air pressure for dispersion, refractive index, and obscuration limits, based on the manufacturer's recommendations.

The binder sample (0.5–2 grams) was placed in the sample hopper. The feed rate was adjusted to ensure a uniform flow of particles into the measurement cell without clumping or excessive scatter. The measurement process was initiated, with the PSA 1090 dispersing the sample using a controlled air stream. The particle size distribution was determined using laser diffraction technology, producing a particle size distribution curve and associated parameters, including

D_{10}, D_{50}, and D_{90} values. Upon completion, the data was reviewed, saved, and exported for further analysis.

Figure 3.10: Anton Paar particle size analyser (PSA 1090) (Photo by Peace Adedeji, taken at WITS concrete lab, 2024)

3.2.2.2 Relative density

The relative densities of the binders were determined using a gas pycnometer (Anton Paar ultrapyc 3000 gas pycnometer density analyser) to ensure precise and reliable measurements. Before testing, the gas pycnometer was calibrated using a reference standard material to confirm its accuracy. A known mass of the binder sample was then placed into the sample chamber of the pycnometer, and the chamber was tightly sealed. The pycnometer purged the chamber with inert gas, typically helium, to displace any air or contaminants. By detecting the gas displacement, the instrument measured the volume of the binder sample. The relative density was then calculated automatically by the pycnometer software as the ratio of the sample's mass to its measured volume, expressed in g/cm³. To ensure repeatability and minimize experimental errors, the measurements were performed in triplicate for each binder sample, and the average value was recorded.

Figure 3.11: Anton Paar ultrapyc 3000 gas pycnometer density analyzer (Photo by Peace Adedeji, taken at WITS Geotechnic laboratory, 2024)

3.2.2.3 Bulk density

The compacted bulk densities of PC, LSP, GGBS and CWP were determined by SANS 5845:2006 (SANS, 2006)**.** The procedure involved the use of a cylindrical metal container and a tamping rod for compaction. First, the empty cylindrical container was thoroughly cleaned, dried, weighed, and the mass was recorded. The container was then filled with the binder in three approximately equal layers. Each layer was compacted 20 times using a tamping rod to ensure uniform packing and eliminate voids. Care was taken to distribute the compaction evenly across the surface of each layer. After compacting the third layer, the surface of the binder was carefully levelled off using a straight edge, and any excess material was scraped away to ensure a flat and even surface.

Once the container was filled and levelled, it was weighed again, and the mass was recorded. The bulk density (D) was calculated using equation 3-1 from SANS 5845:2006 (SANS 2006a), which is defined as the mass of the binder divided by the volume of the container. The procedure was repeated to ensure accuracy, and the average bulk density was reported.

$$D = \frac{m_2 - m_1}{V} \qquad 3\text{-}1$$

where:

- D (kg/m^3) denotes the density of the andesite crushed stone,
- m_2 (kg) denotes the mass of the empty container,

- m_1 (kg) denotes the mass of the container with andesite crusher sand,
- V (m^3) denotes the volume of the container.

3.2.2.4 Microstructural analysis of binders

The microstructural analyses of CWP, LSP, GGBS, and PC were performed using a combination of SEM-EDS, XRD, and XRF techniques to thoroughly evaluate their composition and morphology.

1. **SEM-EDS Analysis**: SEM combined with EDS was carried out specifically for the CWP. The analysis was performed using a ZEISS MERLIN high-resolution field emission scanning electron microscope (FE-SEM) at the Central Analytical Facility (CAF) Microscopy Unit, Stellenbosch University, South Africa. The operating parameters included an accelerating voltage of 20 kV, a probe current of 1.1 nA, a specimen current of 19 nA, and a working distance of 8.5 mm. The spectrum was recorded three times, and high-resolution electron images were captured to study the microstructure and chemical composition of the CWP.
2. **XRD Analysis**: XRD analysis was performed for both CWP and LSP using a Bruker D2 Phaser XRD instrument. The analysis was conducted at the Microscopy and Microanalysis Unit (MMU) at the University of the Witwatersrand in Johannesburg, South Africa, to identify the crystalline phases present in the samples.
3. **XRF Analysis**: This analysis was conducted for all binders (CWP, LSP, GGBS, and PC) at the Pretoria Portland Cement (PPC) Quality Advisory Services (QAS). The oxide components were analysed using XRF fused beads. The samples were ignited for 60 minutes in a furnace at 1000 °C. The fused beads were prepared by combining the sample with a flux mixture (66% $Li_2B_4O_7$: 34% $LiBO_2$) and heating to 1050 °C.

3.2.3 Aggregates

3.2.3.1 Fine aggregates

Andesite crusher sand was used as a fine aggregate in this experiment. It was obtained from the Afrisam Plant, Johannesburg, South Africa, with manufacturer specifications conforming to SANS 1083: 2014 (South African Bureau of Standards, 2014). The particle size distribution, particle relative density, and bulk density of andesite crusher sand were important in determining the mixture proportioning of concrete.

3.2.3.2 Coarse aggregates

Andesite crushed stone of size 14 mm was used as a coarse aggregate in this experiment. It was obtained from the Afrisam Plant, Johannesburg, South Africa, with manufacturer specifications conforming to SANS 1083: 2014 (South African Bureau of Standards, 2014).

3.2.4 Water and admixture

Tap water was used to mix and cure concrete in this experiment, which meets the suitable criteria outlined in SANS 10100-22014 and SANS 51008:2014 (South African Bureau of Standards, 2014, 2014)

A water-reducing admixture was used to reduce the high-water content required in concrete. A superplasticizer, Sika ViscoCrete 3088, composing an aqueous solution of modified polycarboxylate, was used as a high-range water reducer admixture to attain a target slump of range 75 to 150 mm. The performance of the SP specified by the manufacturer is required to conform to BS EN 934-2: 2009 (British Standards Institution 2009)

3.3 Concrete Mix Design

Two primary reference binder compositions were established for the mix design: CEM II/B-S (CR1) and CEM II/A-LL (CR2)**,** derived from PC, CEM I 52.5 R. CR1 comprised 70% PC and 30% GGBS, while CR2 contained 90% PC and 10% LSP. Subsequent binder variants were developed by partially replacing GGBS and LSP with CWP. For CR1, 10% (CR1-C1) and 20% (CR1-C2) of GGBS were replaced with CWP. Similarly, for CR2, 5% (CR2-C1) and 7% (CR2-C2) of LSP were substituted with CWP. These variations are detailed in Table 3.3. Subsequently, the six binder compositions were tested at three different w/b ratios: 0.45, 0.5, and 0.55. These ratios were chosen to target concrete strength classes C60/65, C50/55, and C40/45 per SANS 10100-2:2014 (South African Bureau of Standards, 2014a). However, the quantity of water was kept constant while the quantity of binders was varied to achieve the desired water binder ratio. This ensures that the research focus remains on the binder and achieves meaningful comparison across different w/b ratios.

Table 3.2: Binder formulations

S/No	Binder label	Binder formation	Percentage composition of CWP (%)
		Replacement of GGBS with CWP	
1	CR1 (CEM II/BS)	70% PC+ 30% GGBS	0
2	CRI-C1	70% PC + 20% GGBS + 10 % CWP	10
3	CR1-C2	70% PC + 10% GGBS + 20% CWP	20
		Replacement of LSP with CWP	
4	CR2 (CEM II/A-LL)	90% PC + 10% LSP	0
5	CR2-C1	90% PC + 5% Limestone + 5% CWP	5
6	CR2-C2	90% PC + 3% Limestone + 7% CWP	7

The Cement and Concrete Institute (C & CI) mix design method was employed to determine the proportions of the concrete mixtures. The mix constituents were calculated by weight per cubic meter of concrete. The mix design table, Table 3.3 presents a total of 18 concrete mix variations derived from the six binder formations and three w/b ratios.

A trial mixture of each reference concrete was prepared to verify the design mix, achieving a target slump class S2 of 50 mm – 150 mm as per BS EN 206:2013 (British Standards Institution 2013). Consistency was further assessed by measuring the slump as per SANS 5862-1:2006 (SANS 2006b). The SP doses were added as necessary to achieve the required workability in compliance with BS EN 934-2:2009 (British Standards Institution 2009).

Each concrete mix is expressed with a compact mix label that is used throughout this study. For example, M3B. The mix conveys two crucial pieces of information: the binder composition and the w/b ratio. The numeral (1 – 6) at the start of the label refers to the binder formulation, while the trailing letter (A, B, or C) represents the w/b ratio as indicated below.

- "A" → w/b = 0.45
- "B" → w/b = 0.50
- "C" → w/b = 0.55

The number (1 – 6) identifies the binder formulation as indicated below.

For the GGBS based concrete:

- M1 is the reference mix for the GGBS-based concrete, containing CR1: 70% PC + 30% GGBS.

- M2 contains CR1-C1: 70% PC + 20% GGBS + 10% CWP.
- M3 contains CR1-C2: 70% PC + 10% GGBS + 20% CWP.

For the LSP-based concrete:

- M4 is the reference mix for the LSP-based concrete, it contains CR2: 90% PC + 10% LSP.
- M5 contains CR2-C1: 90% PC + 5% LSP + 5% CWP.
- M6 contains CR2-C2: 90% PC + 3% LSP + 7% CWP.

Thus, a label like M3B refers to concrete with a binder containing 70% PC + 10% GGBS + 20 % CWP (binder set "3") and that the w/b ratio is 0.50 (series "B").

Table 3.3: Concrete mix design table

Mix Label	Binder Type	w/b ratio	Binder Quantity					Aggregates		Water (l)	SP (l/m^3)
			Total binder	PC (kg/m^3)	Limestone (kg/m^3)	GGBS (kg/m^3)	CWP (kg/m^3)	Sand (kg/m^3)	Stone (kg/m^3)		
M1A	CR1	0.45	478	334.4	-	143.3	-	785	1065	215	0.6
M2A	CR1-C1		478	334.4	-	95.5	47.8	785	1065	215	0.6
M3A	CR1-C2		478	334.4	-	47.8	95.5	785	1065	215	0
M4A	CR2		478	430.0	47.8	-	-	785	1065	215	0.5
M5A	CR2-C1		478	430.0	23.9	-	23.9	785	1065	215	1.0
M6A	CR2-C2		478	430.0	14.3	-	33.4	785	1065	215	0.8
M1B	CR1	0.50	430	301	-	129	-	832	1065	215	0.2
M2B	CR1-C1		430	301	-	86	43	832	1065	215	0.2
M3B	CR1-C2		430	301	-	43	86	832	1065	215	0.2
M4B	CR2		430	387	43	-	-	832	1065	215	0.6
M5B	CR2-C1		430	387	21.5	-	21.5	832	1065	215	0
M6B	CR2-C2		430	387	12.9	-	30.1	832	1065	215	0.8
M1C	CR1	0.55	391	273.9	-	143.3	-	867	1065	215	0.2
M2C	CR1-C1		391	273.9	-	78.3	39.1	867	1065	215	0.2
M3C	CR1-C2		391	273.9	-	39.1	78.3	867	1065	215	0
M4C	CR2		391	352.2	39.1	-	-	867	1065	215	0.6
M5C	CR2-C1		391	352.2	19.6	-	19.6	867	1065	215	0
M6C	CR2-C2		391	352.2	11.7	-	27.4	867	1065	215	0

3.3.1 Mixing procedure

The cement formulations were thoroughly mixed in separate large containers. Following this, 18 batches of concrete were prepared, each corresponding to its specific binder formulation and w/b ratio. The batching and mixing took place in a concrete laboratory, where the temperature

ranged from 22 °C to 25 °C**.** The mixing procedures followed SANS 5861-1:2006 (SANS 2006c).

Prior to mixing, the aggregates for each batch were air-dried under laboratory temperature conditions. All experimental materials for each mix were weighed to an accuracy of 0.5%**.** The SP was batched by volume using a measuring cylinder graduated in 10 ml intervals. The dry materials were added into a 0.06 m³ pan mixer in the following sequence: aggregates, binders, and remaining aggregates. These materials were mixed for 3 minutes**.** Afterwards, water and SP were added to the mixture, and the mixing continued for an additional 1-3 minutes**.**

Slump tests were conducted both before and after adding the SP. The SP was only incorporated if the initial slump did not meet the target slump value.

Figure 3.12: Concrete mixing (Photo by Peace Adedeji, taken at WITS concrete laboratory, 2024)

3.4 Test Procedures

3.4.1 Slump test

The slump test was conducted following SANS 5862-1:2006 (SANS 2006b)**,** which outlines the procedure for determining the slump of freshly mixed concrete. This method applies to plastic and cohesive concrete with a slump range between 5 mm and 175 mm. The test utilized a frustum-shaped metal mould with nominal dimensions: a base diameter of 200 mm ± 2 mm, a top diameter of 100 mm ± 2 mm, and a height of 300 mm ± 2 mm. The mould, made from corrosion-resistant metal with a smooth internal surface, was cleaned and dampened before the test, ensuring it was free of superfluous moisture.

Figure 3.13: Slump test apparatus (Photo by Peace Adedeji, taken at WITS concrete laboratory, 2024)

The mould was placed on a clean, rigid, horizontal, and non-absorbent surface and held firmly in place using foot-pieces. It was filled with freshly mixed concrete in three equal layers. Each layer was compacted with 25 strokes of a 16 mm diameter, 600 mm long steel tamping rod with a hemispherical end. Care was taken to ensure that the strokes penetrated the underlying layers during tamping. After tamping the top layer, the excess concrete was struck off using a rolling and sawing motion to level the surface.

The mould was then carefully removed by raising it vertically for 5 to 10 seconds without disturbing the concrete. The height difference between the mould and the highest point of the slumped concrete was measured to the nearest 5 mm. This value, referred to as the slump, was calculated and recorded. If the initial slump value did not fall within the target range, a predetermined quantity of SP was added to the mix. The concrete was thoroughly remixed to ensure uniform distribution of the SP. The slump test was then repeated following the same procedure to measure the modified slump value. The final slump is also measured. This step ensured that the final mix achieved the desired workability without compromising the mix proportions.

Figure 3.14: Concrete slump measurement (Photo by Peace Adedeji, taken at WITS concrete laboratory, 2024)

3.4.2 Casting and curing of the concrete specimens

The casting and curing of concrete specimens were carried out in the concrete laboratory. Plastic cube moulds of 100 mm were used for casting, and their preparation was done in compliance with SANS 5860:2006 (SANS 2006d). The moulds were cleaned and thinly coated with oil for easy removal of hardened concrete. Then, the moulds were placed and secured to the mechanical vibrating table. The freshly mixed concrete was poured into the moulds and vibrated for 10 seconds. The mould was topped up with adequate concrete and further vibrated for another 10 seconds. Afterwards, the mould with compacted concrete was arranged in a secured place and immediately covered with polypolyethene sheets for 24±2 hours to prevent moisture loss in fresh concrete. After 24 hours, the hardened samples were demoulded. The hardened samples were removed from the moulds using an air compressor and properly labelled.

The concrete specimens were systematically labelled to indicate the binder type and w/b ratio used in each mix. Figure 3.15 and 3.16 show typically labelled concrete samples. The labels combine numbers and letters, where the numbers (1 to 6) correspond to different binder types, and the letters (A, B, C) represent the w/b ratio. For instance, M1 concrete is made with the CR1 (CEM II/BS) binder, consisting of 70% PC and 30% GGBS. M2 concrete uses the CRI-C1 binder, composed of 70% PC, 20% GGBS, and 10% CWP. M4 concrete is produced with the CR2 (CEM II/A-LL) binder, containing 90% PC and 10% LSP. Additionally, the w/b ratio is specified using letter designations. For example, M1A represents concrete made with the CR1 binder at a 0.45 w/b ratio, M2B corresponds to concrete with the CR1 binder at a 0.50 w/b ratio,

and M1C refers to concrete with the CR1 binder at a 0.55 w/b ratio. This labelling is shown in Table 3.2. Casting and curing were performed per SANS 5861-3:2006 (SANS 2006c).

Figure 3.15: Concrete cubes label (Photo by Peace Adedeji, taken at WITS concrete laboratory, 2024)

Figure 3.16: Concrete cube (Photo by Peace Adedeji, taken at WITS concrete laboratory, 2024)

3.4.3 Mechanical properties tests

3.4.3.1 Compressive strength test

The compressive strength test was conducted on the hardened concrete in accordance with SANS 5863:2006 (SANS 2006e). The cube samples were tested at 7, 28, 56, and 90 days of curing age. These four moist curing periods were chosen to evaluate the strength development of the concrete at both early age and later age. At each testing age, three cube samples were removed from the curing tank, weighed, and recorded after the water had been wiped off the

surface. Each sample was centrally placed in the Cube Press-Foote test machine, model CTE 56-1216 FTP, for compression testing. Then the uniaxial load at a rate of 0.3 MPa/s was applied to the sample in a perpendicular direction of casting. Failure loading of the samples occurred so that all four exposed faces were cracked approximately equally with little damage to faces in contact with the platens. Then, the failure was recorded. Figure 3.17 shows the compressive strength testing machine. The average compressive strength of the three cubes in MPa was determined as the compressive strength of each concrete sample using equation 3-2.

$$f_c = \frac{F}{A_c} \qquad 3\text{-}2$$

where:

- f_c (MPa) denotes compressive strength,
- F (N) denotes maximum load at failure,
- A_c (mm^2) denotes the cross-sectional area of the specimen on which the compressive force acts.

Figure 3.17: Compressive strength testing setup (Photo by Peace Adedeji, taken at WITS concrete laboratory, 2024)

3.4.3.2 Splitting tensile strength test

This test aims to determine the tensile strength of concrete containing CWP. This test was carried out in compliance with SANS 6253:2006 (SANS 2006f). The cube samples were tested at 7, 28, 56, and 90 days of curing age, at each testing age, three cube samples were removed from the curing tank, weighed, and recorded after excess water had been wiped off the surface. A centre line was drawn on the opposite sides of the cube samples. Each sample was loaded

into the Amsler compressive strength testing machine. Then, the steel bars sealed on the steel plates were placed on the centre line drawn on the opposite sides of the cube samples. Compressive forces were applied along the two opposite centre lines, causing the distribution of the compressive stress across the contact surface. The compressive force was applied at the rate of 0.03 MPa/s until the fracture and the splitting along the centre line occurred. Figure 3.18 shows the splitting tensile strength test setup. The average splitting strength of the three cubes in MPa was determined as the tensile strength of each sample using equation 3-3.

$$f_{sp} = \frac{2P}{\pi A} \qquad 3\text{-}3$$

where:

- f_{sp} (MPa) denotes split tensile strength,
- P (N) denotes failure load,
- A (mm^2) denotes the area of the splitting surface.

Figure 3.18: Splitting tensile strength test setup (Photo by Peace Adedeji, taken at WITS structures laboratory, 2024)

3.5 Durability Tests

South African durability index tests, namely oxygen permeability index (OPI), water sorptivity index (WSI) and chloride conductivity index (CCI) tests, were used to characterize the quality of the concrete samples concerning the transportation of gas, moisture, and chloride in the concretes. Each durability index test is linked to a specific transport mechanism pertinent to a particular deterioration process in hardened concrete. The concrete specimens were tested to

assess the influence of the replacement of PC sand with CWP on the transport properties. The tests were conducted on the hardened concrete samples after curing periods of 28 and 90 days. The preparation of the test specimens and the procedures of the tests were performed in accordance with the SANS 3001-CO3-1, 2 & 3:2015 (SANS 2015).

3.5.1 Preparation of concrete samples for durability index tests

Concrete samples for the three durability index tests were prepared in the same way. Concrete was cast into a mould of 100 mm cubes and cured for 28 and 90 days. The coring of concrete cubes took place immediately after curing. Concrete cubes were clamped firmly with a G-clamp into the core drilling machine. The core drilling machine was connected to tap water to reduce the dust level. The concrete cubes were cored through a core barrel machine of 70±2 mm diameter. The cutting of the cored samples was done the same day with coring using a diamond cutter machine. The cutting machine was connected to the tap water to reduce the dust level. The cored samples were fixed one after the other into the cutting machine, and a 5 mm thickness was cut away from the exterior faces of the cored samples. This is important to have near-surface properties of concrete which is very sensitive to durability indexes. The required thickness of 30±2 mm concrete discs was cut from the cored sample. After assigning mix labels, the concrete disc specimens for durability tests were further labelled numerically from 1 to 4 to differentiate between the four specimens prepared for each test.

Figure 3.19: Cutting of concrete samples (Photo by Peace Adedeji, taken at WITS durability laboratory, 2024)

Figure 3.20: Typical disc for durability test (Photo by Peace Adedeji, taken at WITS durability laboratory, 2024)

3.5.2 Oxygen permeability index (OPI) test

The OPI test was used to assess the overall micro- and macrostructure of the cast concrete and is particularly sensitive to macro-voids and cracks which act as short-circuits for the permeating gas. The test was conducted on four concrete discs of diameter 70±2 mm and thickness 30±2 mm. The concrete discs were placed in the oven at 50±2ºC for 7 days. The concrete discs were removed from the oven and immediately cooled in the desiccator for a minimum of 2 hours to 23±2 ºC. The thickness and diameter of each concrete disc were measured with a Vernier calliper placed at the four points around the perimeter of the concrete discs. The average of each set of four readings was calculated and recorded.

Each concrete disc was placed in the compressible collar within the rigid sleeve, ensuring the interior faces rested against the lips of the collar and the exterior face at the bottom of the rigid sleeve. The rigid sleeve containing the concrete disc was then placed on top of the permeability cell. The solid ring, collar, and covered plate were connected. The connection was fitted into the rigid sleeve in the permeability cell, ensuring no gas leakage. The other gases apart from oxygen in the test chamber were eliminated by opening the oxygen inlet and outlet valves of the permeability cell. Afterward, the valve of the oxygen supply tank was opened, permitting 100 kPa of oxygen to flow through the permeability cell for 5 seconds. The outlet valve was closed while the inlet valve was closed after the pressure in the permeability cell was increased to 100±5 kPa. After 5 minutes of the valve closure, the initial time and pressure denoted as t_o

and P_o, respectively, were recorded. A minimum of eight readings were taken and recorded automatically by the data logging devices at an interval of 15 minutes until the pressure dropped to 50±2.5 kPa or after 6 hours±15 minutes. The testing was then terminated. The oxygen permeability cell setup is presented in Figure 3.21. The OPI was determined from the coefficient of permeability. The coefficient of permeability was calculated using Equation 3-4 (Alexander, Mackechnie & Ballim 1999; Alexander, Ballim & Stanish 2008).

$$k = \frac{wVgdz}{RAT} \qquad 3\text{-}4$$

where:

- k (m/s) denotes the coefficient of permeability of the test specimen in meters per second,
- w (kg/mol) denotes the molecular mass of oxygen,
- g (m/s^2) denotes acceleration due to gravity,
- V (m^3) denotes the volume of the permeability cell,
- R (Nm/Kmol) denotes the universal gas constant,
- A (m^2) denotes the cross-sectional area of the specimen,
- T (K) denotes temperature in Kelvin,
- d (m) denotes average specimen thickness,
- z (s^{-1}) denotes the slope of the linear regression. It can be calculated using Equation 3-5 obtained from SANS 3001-CO3-1:2015 (SANS 2015).

$$z = \frac{\sum[ln\frac{P_0}{P_t}]^2}{\sum[ln\frac{P_0}{P_t}t]} \qquad 3\text{-}5$$

where:

- t (s) denotes time since the start of the test,
- P_o (kPa) denotes initial oxygen pressure,
- P_t (kPa) denotes oxygen pressure reading at time t.

Figure 3.21: Oxygen permeability cell setup (Photo by Peace Adedeji, taken at WITS durability laboratory, 2024)

The coefficient of permeability k was calculated for each specimen. The negative logarithm of each concrete disc coefficient of permeability given in Equation 3-6 is the OPI in accordance with SANS 3001-CO3-1:2015 (SANS 2015).

$$OPI = -\log_{10} k \qquad 3\text{-}6$$

The OPI is the average of the individual OPI values of the four concrete discs for each curing age and is given in Equation 3-7.

$$OPI = [\frac{1}{4}(OPI_1 + OPI_2 + OPI_3 + OPI_4)] \qquad 3\text{-}7$$

3.5.3 Water sorptivity index (WSI) test

The WSI test was used to measure the porosity and the rate of water absorption in the concrete. The calcium hydroxide solution for this test was prepared by dissolving 30 g of calcium hydroxide in 10L of potable water in a sealed container and stored for a minimum of 1 day at a temperature of 23±2 ºC. Four concrete discs of diameter 70±2 mm and thickness 30±2 mm was used for this test. The same concrete discs that were used in the oxygen permeability tests were also used in the water sorptivity test. A water sorptivity test was not carried out on the concrete discs immediately after they were removed from the OPI test. Therefore, the concrete discs

were placed back in the oven for a night at 50 ºC. The concrete discs were cooled for a minimum of 2 hours to 23±2 ºC in the desiccator before testing. Then, the curved sides of the concrete discs were sealed with a sealant. The concrete discs were weighed and recorded as dry mass. Then, the calcium hydroxide solution maintained at 23±2 ºC was poured on the 10 layers of paper towel in the tray, ensuring the saturation and surface covering of the paper towel. The water level in the tray was maintained somewhat above the bottom edge of the concrete discs and not beyond 2 mm up the sides of the concrete discs.

The sealed concrete discs were placed in the tray ensuring the test face (outer face) rested on the wet paper, and the stopwatch was started immediately. The concrete discs were weighed at 3, 5, 7, 9, 12, 16, 20, and 25 mins after patting them once on the moistened absorbent paper towel. The unsealed faces of the concrete discs were saturated and surface dry at the time the mass was determined within 10 seconds of their removal from the tray. The stopwatch was not stopped during the weighing procedure. The concrete discs were the kept in the sealed vacuum saturation tank of – 75 kPa for 3 hrs±15 minutes and arranged by standing each concrete disc upon its curved edges maximizing the exposed surface area. Afterwards, calcium-saturated water was released into the chamber with no entering of air until the water level reached 40 mm above the top of the concrete discs. The vacuum was reinstated to – 75 kPa for 1 hr±15 mins, allowing air to enter and then soaking the concrete discs for another 18±1 hours. The concrete discs were removed from the solution and dried with a paper towel. Then, the concrete discs were immediately weighed and recorded as the vacuum-saturated mass of the concrete discs. Figure 3.22 shows water sorptivity and porosity testing of concrete discs.

Figure 3.22: Water sorptivity and porosity testing of concrete samples (Photo by Peace Adedeji, taken at WITS durability laboratory, 2024)

The porosity of each concrete disc was determined using Equation 3-8 in accordance with SANS 3001-CO3-2:2015 (SANS 2015).

$$n = \frac{M_{sv} - M_{s0}}{Adp_w} \times 100 \qquad 3\text{-}8$$

where:

- M_{vs} (g) denotes the vacuum-saturated mass of the concrete disc,
- M_{v0} (g) mass of the concrete discs at the beginning of the test,
- A (mm^2) cross-sectional area of the concrete disc,
- d (mm) denotes the average concrete disc thickness,
- p_w (g/mm) denotes the density of water.

The water sorptivity of the concrete disc is calculated using Equation 3-9.

$$S = \frac{Fd}{M_{sv} - M_{s0}} \qquad 3\text{-}9$$

where:

- S (mm/√h) denotes the water sorptivity of the specimen,
- F (g/√h) denotes the slope of the best-fit line,
- d (mm) denotes average specimen thickness,
- M_{sv} (g) denotes vacuum saturated mass,
- M_{s0} (g) denotes the mass of the specimen at the initial time.

The WSI is the average of the individual WSI values of the four concrete discs for each curing age and is given in Equation 3-10.

$$\text{WSI} = [\frac{1}{4}(\text{WSI}_1 + \text{WSI}_2 + \text{WSI}_3 + \text{WSI}_4)] \qquad 3\text{-}10$$

3.5.4 Chloride conductivity index (CCI) test

The CCI test was used to measure the coefficient of diffusion of the concrete containing CWP. The chloride solution of 5M for this test was prepared by dissolving 2.93 kg of sodium chloride

in 10L of potable water in a sealed container and stored for a minimum of 1 day at a temperature of 23±2 ° C. Four concrete discs of diameter 70±2 mm and thickness 30±2 mm was used for each test. The concrete discs were placed in the oven at 50±2 ° C for 7 days. Then, the concrete discs were removed from the oven and immediately cooled in the desiccator for a minimum of 2 hours to 23±2 ° C. The thickness and diameter of each concrete disc were measured with a Vernier calliper placed at the four points around the perimeter of the concrete disc. The average of each set of four readings was calculated and recorded. Also, concrete discs were weighed and recorded as dry mass.

The concrete discs were kept in the sealed vacuum saturation tank of -75 kPa for 3 hrs±15 minutes and arranged by standing each concrete disc upon its curved edges maximizing the exposed surface area. The tank was isolated allowing the flow of sodium chloride solution and no entering of air into the chamber until the water level reached 40 mm above the top of the concrete discs. The vacuum was reinstated to -75 kPa for 1 hr±15 minutes, allowing air to enter and soaking the concrete discs in sodium chloride solution for another 18±1 hours. Afterwards, the concrete discs were removed from the solution and dried with a paper towel then immediately weighed and recorded as the vacuum-saturated mass of the concrete discs.

Each concrete disc was removed from the sodium chloride solution and placed within the flexible rubber collar, ensuring the flat face of the concrete disc rested against the plastic lip of the rigid ring. Then the plastic tubes of the chloride cell and both chambers of the cell were filled with 5M of sodium chloride solution. The assembled test rig (anode, cathode, and rubber collar) was positioned standing upright on a horizontal surface, ensuring the cathode section was positioned on the right side and the anode section was positioned on the left side. The ammeter and voltmeter were connected to the assembled test rig with the equation of DC power supplying 10 V across the concrete discs. The current and voltage were measured simultaneously. Afterwards, the circuit was switched off ensuring the completion of the test within 15 minutes of the concrete disc removal from the sodium chloride solution. Figure 3.23 shows the chloride conductivity testing of concrete discs.

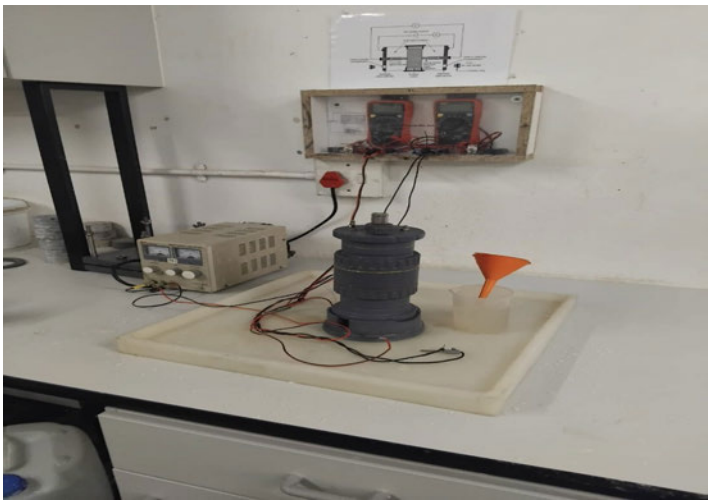

Figure 3.23: Chloride conductivity testing of concrete samples (Photo by Peace Adedeji, taken at WITS durability laboratory, 2024)

The chloride conductivity of each concrete disc was determined using Equation 3-11.

$$\sigma = \frac{id}{VA} \qquad 3\text{-}11$$

where:

- σ (mS/cm) denotes the chloride conductivity of the specimen,
- i (mA) denotes electric current,
- d (cm) denotes the average thickness of the concrete disc,
- V (V) denotes voltage difference,
- A (cm^2) denotes the cross-sectional area of the concrete disc.

The CCI is the average of the individual CCI values of the four concrete discs for each curing age and is given in Equation 3-12 in accordance with SANS 3001-CO3-3:2015 (SANS 2015).

$$CCI = [\frac{1}{4}(\mathrm{CCI}_1 + \mathrm{CCI}_2 + \mathrm{CCI}_3 + \mathrm{CCI}_4)] \qquad 3\text{-}12$$

3.6 Microstructural analysis of concrete

The microstructural analysis of the concrete samples was carried out using a Tescan Vega Scanning electron Microscope at the Microscopy and Microanalysis Unit (MMU) of the University of the Witwatersrand (Figure 3.24). This analysis focused on evaluating the internal

structure of the concrete to better understand the material's durability and performance characteristics.

Before the SEM analysis, the concrete specimens were carefully prepared by cutting them into small, representative sections and ensuring the surfaces were polished to achieve a flat, smooth finish. This preparation minimizes surface irregularities and enhances imaging quality. The samples were then coated with a thin layer of platinum to improve their conductivity during SEM imaging.

The SEM analysis included the examination of pore structures within the concrete, where pore sizes were measured to assess porosity and its influence on durability. Special attention was given to the ITZ, which were examined for the presence and distribution of ceramic grains using SEM-EDS. The EDS analysis provided elemental composition data, aiding in identifying the specific phases within the ITZ.

High-resolution images were captured using Back Scattered electron (BSE) mode to enhance contrast and provide detailed visualization of the microstructural features. Microstructural analysis was conducted exclusively on GGBS-CWP-based concrete. The samples tested were mixed according to the M1A, M2A, and M3A concrete mix designs. Analyses were conducted on concrete samples cured for 7 and 28 days to observe the progression of hydration and microstructural development over time. Multiple images at varying resolutions were taken to capture a comprehensive view of the concrete microstructure.

Different magnifications were used to capture varying levels of microstructural detail in the concrete samples. Lower magnifications (2,000×–4,600×) provide a broad view of the matrix, allowing for the observation of overall density, distribution of ceramic powder grains, and general crack patterns. Higher magnifications (10,000×–46,100×) reveal finer features such as microcracks smaller than 1 μm, detailed morphology of C-S-H, and interactions at the interfacial transition zone (ITZ).

Figure 3.24: Tescan Vega scanning electron microscope at MMU, University of the Witwatersrand

In conclusion, this chapter details the materials, mix formulations, and experimental methods employed to investigate the pozzolanic and filler effects of CWP in concrete. By integrating both physical and chemical analyses of CWP, alongside mechanical and microstructural testing of CWP concrete, this methodology establishes a comprehensive foundation for understanding the role of CWP in concrete. The procedures outlined in this chapter provide the experimental basis upon which the subsequent chapter presents and discusses the results and findings of this research.

CHAPTER FOUR
RESULTS AND DISCUSSION

4.1 Preamble

This chapter presents the results of ceramic waste powder (CWP) as a partial replacement for ground granulated blast-furnace slag (GGBS) and limestone powder (LSP) in concrete. It begins with an analysis of CWP characteristics compared to other binder materials, focusing on particle size distribution, density, and chemical composition. The workability of fresh concrete is assessed through slump tests, highlighting variations in performance based on water-binder (w/b) and binder replacement levels.

The mechanical properties are explored through compressive and splitting tensile strength tests, analysing strength development over different curing periods. Regression analysis evaluates the relationship between CWP concrete mixes and their reference mixes. The durability properties are assessed using South African durability indices; oxygen permeability index (OPI), water sorptivity index (WSI) and chloride conductivity index, examining permeability, water absorption, and chloride resistance. The chapter concludes with a microstructural analysis using the SEM technique to assess the impact of CWP on the cement matrix, porosity, and interfacial transition zones.

4.2 Characteristics of CWP Compared to Other Binder Materials

4.2.1 Particle size distribution

The particle size distribution graph compares the four binder materials, CWP, GGBS, limestone, and CEM I, showing their cumulative volume percentages across different particle sizes (Figure 4.1). The CWP exhibits the broadest distribution, with particle sizes ranging from below 1 μm to over 100 μm, indicating a mix of fine and coarse particles. In contrast, GGBS and LSP have finer, more uniform distributions, with their cumulative volumes reaching 100% at smaller sizes (below 10 μm). Portland cement (CEM I) lies between these extremes, having a moderately narrow range. The steep rise in GGBS and LSP curves reflects their predominance of fine particles, while gradual slope of CWP suggests a wider particle size variation.

The comparison in Table 4.1 focuses on key particle size parameters, including D_{10}, D_{50}, and D_{90} volumes, mean size volume, and span. These parameters provide more insight into the fineness and particle distribution of each material and their potential impact on cementitious performance.

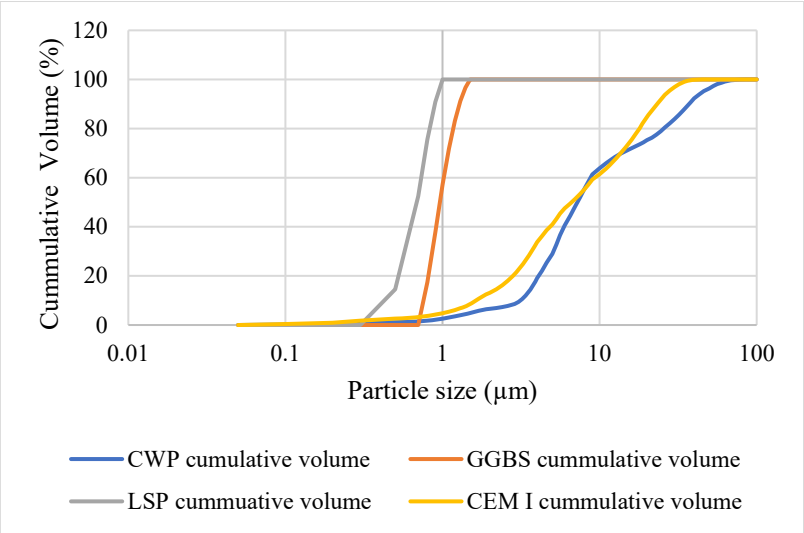

Figure 4.1: Particle size distribution of binders

The CWP exhibits an average particle size distribution characterized by a D_{10} volume of 0.4 µm, a D_{50} volume of 1.3 µm, and a D_{90} volume of 1.8 µm, with a mean size volume of 1.2 µm. The span, which measures the width of the particle size distribution, is 1.1, indicating a moderate spread in particle sizes. These values suggest that CWP is relatively coarse compared to the other binders analysed. The larger D_{50} and D_{90} volumes point to a wider distribution of particle sizes, with a significant proportion of particles being larger than 1 µm. This coarser particle size distribution may influence the reactivity and performance of CWP when used as a binder or filler material in concrete applications. The span value further emphasizes the broad range of particle sizes, indicating a less uniform distribution compared to the other binders.

Table 4.1: Particle size parameter of binders

Material	D_{10} Volume (µm)	D_{50} Volume (µm)	D_{90} Volume (µm)	Mean Size Volume (µm)	Span
CWP	0.4	1.3	1.8	1.2	1.1
PC	0.7	0.9	1.2	1.0	0.5
LSP	0.4	0.6	0.8	0.7	0.8
GGBS	0.7	0.9	1.2	1.0	0.5

In contrast, PC has a finer particle distribution than CWP, with a D_{10} volume of 0.7 µm, a D_{50} volume of 0.9 µm, and a D_{90} volume of 1.2 µm. These values suggest that PC particles are more finely ground and possess a narrower particle size range. The smaller D_{50} value compared to CWP's D_{50} indicates that the median particle size for PC is significantly finer. This finer particle size distribution may contribute to enhanced early strength development and higher reactivity

in concrete mixes. The D_{90} of value of 1.2 µm is also much lower than that of CWP, indicating fewer coarse particles and a more uniform distribution of particle sizes, which could positively impact the strength and workability of concrete mixes.

The LSP exhibits an even finer particle size distribution than both CWP and PC. Its D_{10} volume is 0.4 µm, its D_{50} volume is 0.6 µm, and its D_{90} volume is 0.8 µm. These values reflect a very fine particle size distribution, with most particles being smaller than 1 µm. The D_{50} value of 0.6 µm, which is less than half the D_{50} value of CWP, highlights the significantly finer nature of LSP. This finer particle distribution enhances the filler effect in concrete, improving particle packing and reducing voids in the mix, which can lead to improvements in workability and durability. The significantly lower D_{90} value of LSP at 0.8 µm further indicates the absence of larger particles, ensuring a smooth and uniform distribution.

The GGBS, like PC, also has a finer particle size distribution than CWP. The average particle size values for GGBS are a D_{10} volume of 0.7 µm, a D_{50} volume of 0.9 µm, and a D_{90} volume of 1.2 µm, with a mean size volume of 1 µm. The span for GGBS is 0.5, which is significantly lower than the span for CWP, indicating a narrower particle size distribution with more uniform particle sizes. The finer D_{50} value of 0.9 µm compared to CWP's D_{50} of 1.3 µm suggests that GGBS has a much finer median particle size. This finer distribution can lead to improved pozzolanic activity and better performance in concrete, particularly in terms of long-term strength and durability. The lower D_{90} value of GGBS at 1.2 µm means that GGBS contains fewer coarse particles compared to CWP, which can further enhance its reactivity and its ability to fill voids in concrete mixes.

The particle size distribution analysis reveals that CWP is slightly coarser than PC, LSP, and GGBS. The larger D_{50} and D_{90} values of CWP indicate a broader particle size range, with a higher proportion of coarse particles. According to ISO 13320:2020, a wider distribution suggests reduced packing efficiency, which affects workability and strength development in cementitious systems (ISO 2020). The finer and more uniform particle distributions of PC, LSP, and GGBS align with EN 197-1 (Cement Composition Standard) and ASTM C989 (GGBS Specification), which emphasize the role of fine particles in enhancing reactivity and pozzolanic activity (ASTM 2018; CEN 2011). Although CWP is coarser, it still falls within acceptable particle size specifications for supplementary cementitious materials (SCMs) as per ASTM C618 and EN 197-1, indicating its potential use as a partial cement replacement or filler in concrete applications (ASTM 2019; CEN 2011).

4.2.2 Densities of the binder materials

Table 4.2 presents other physical characteristics of the PC, LSP, GGBS and CWP. The CWP has a relative density of 2.6 g/cm³. The CWP is less dense than PC (2.9 g/cm³) and LSP (2.8 g/cm³) but denser than GGBS (2.5 g/cm³). This moderate density suggests that CWP can replace cement in concrete without significantly increasing weight. However, the compact bulk density of CWP (2021.6 kg/m³) is notably the highest among the binders, significantly surpassing GGBS (1206 kg/m³), LSP (1450 kg/m³), and CEM I (1440.3 kg/m³). This indicates excellent packing potential, which can reduce porosity and improve concrete durability.

Table 4.2: Other physical characteristics of binders

Physical Characteristics	CWP	GGBS	LSP	CEM I 52,5 R
Relative density g/cm^3	2.6	2.5	2.8	2.9
Compact bulk density, kg/m^3	2021.6	1206	1450	1440.3

4.2.3 Chemical compositions of binders using XRF analysis

The chemical composition of CWP, as presented in Table 4.3, is distinct from that of other binders. The predominant constituents of CWP are SiO_2 and Al_2O_3, which aligns with findings reported in the literature (Mezidi et al. 2023; Mohit et al. 2023a; Mouiya et al. 2019; El-Dieb et al. 2018; Subaşı et al. 2017a).

Table 4.3: Chemical composition of the binders

Binder	SiO_2	Al_2O_3	Fe_2O_3	Mn_2O_3	TiO_2	CaO	MgO	P_2O_5	SO_3	K_2O	Na_2O	LOI
CWP	69.0	19.0	3.11	0.09	0.73	1.78	1.03	0.07	0.00	2.60	0.88	0.60
PC	19.1	4.77	2.74	0.10	0.37	62.5	2.67	0.08	2.74	0.30	0.00	3.93
GGBS	36.5	15.7	0.67	1.81	0.69	33.8	8.50	0.00	1.88	1.25	0.13	1.97
LSP	0.78	0.11	0.00	0.02	0.00	54.5	1.45	0.00	0.06	0.02	0.00	42.4

The chemical composition of CWP indicates that it is predominantly composed of SiO_2 (69.0%), Al_2O_3 (19.0%), and Fe_2O_3 (3.1%), resulting in a total oxide content of 91.1%. This exceeds the 70% threshold required for pozzolanic materials according to SANS 50197-1 (SANS 2013), SANS 50450-1 & 2 (SANS 2014d), and ASTM C618 (ASTM 2019). Although CWP meets the total oxide requirement for Class F pozzolans, its SiO_2 content (69.0%) is slightly below the 70% requirement in ASTM C618 for Class F pozzolan (ASTM 2022). Since CWP contains only 1.78% CaO, it does not meet ASTM C618 Class C requirements, which specify a minimum of 10% CaO for self-cementing behaviour. This means CWP behaves

primarily as a Class F pozzolan, requiring external activation from PC to contribute to strength development.

The alkali content in CWP is relatively high, with K_2O (2.60%) and Na_2O (0.88%), resulting in a total alkali content of 3.48%. Despite its high alkali content, CWP has no sulphate content (SO_3 = 0.00%), reducing concerns about sulphate attack, unlike PC (2.74%) and GGBS (1.88%), which contain higher sulphate levels. This suggests that CWP is beneficial in sulphate-resistant cement blends, particularly in aggressive environments where sulphate attack is a concern (ASTM 2020).

CWP qualifies as a Class F pozzolan based on ASTM C618, SANS 50197-1, and SANS 50450-1 & 2, but its high alkali content requires consideration when designing concrete mixtures. Its low CaO content also limits its self-cementing properties, making it dependent on external activators, such as PC. However, its low sulphate content and high silica content indicate its potential for sulphate-resistant and pozzolanic concrete.

4.2.4 Other microstructural analysis of binders

Figure 4.2 presents the SEM-EDS analysis of CWP. The SEM-EDS spectrum highlights the chemical composition of CWP. The dominant peaks indicate that CWP primarily consists of silicates and alumina. Minor elements, such as calcium (Ca), iron (Fe), magnesium (Mg), and potassium (K), are also observed, but in lower quantities. This agrees with the XRD analysis in Figure 4.5. In Figure 4.3, the SEM micrograph of CWP reveals its irregular particle morphology. The particles exhibit a rough texture with sharp edges, which is beneficial for physical interlocking within the cement matrix. The high surface area associated with this texture has the potential to enhance the reactivity of CWP.

Figure 4.4 shows the XRD Analysis of LSP. The XRD pattern for LSP shows a peak corresponding to calcite ($CaCO_3$), indicating its high purity as a carbonate material. Figure 4.5 shows the XRD analysis of CWP**.** The XRD analysis of CWP demonstrates a distinct quartz (SiO_2) peak, confirming the crystalline nature of silicon dioxide. However, quartz is a chemically stable phase.

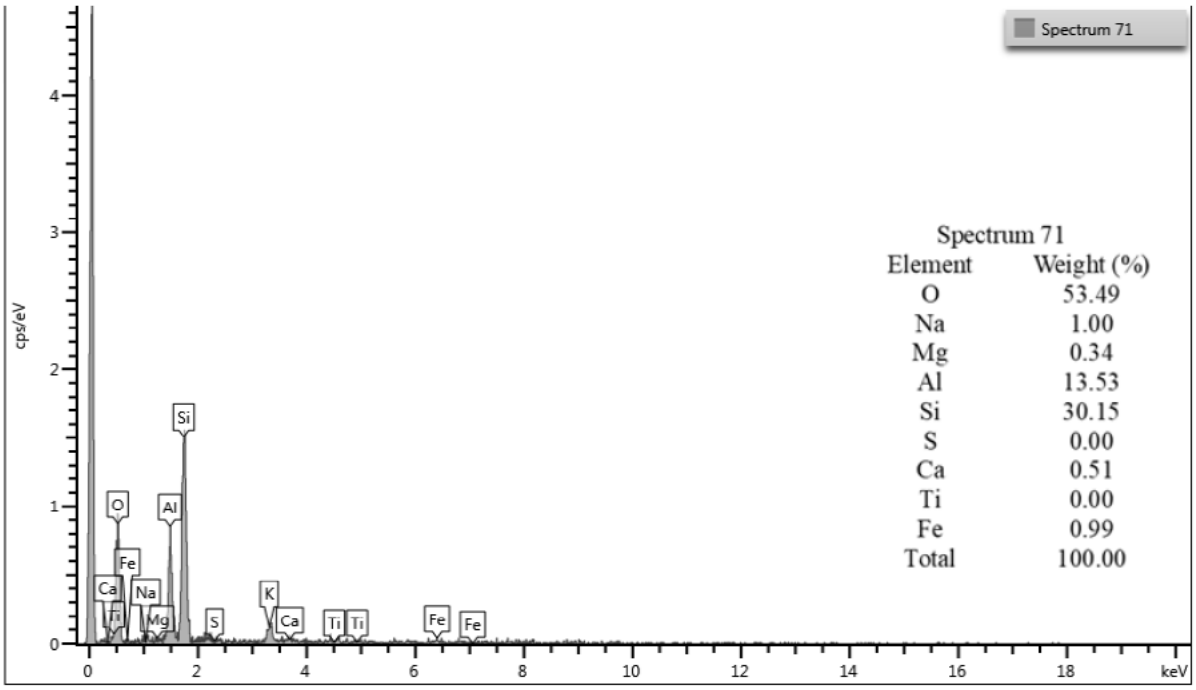

Figure 4.2: Elemental composition of CWP from SEM-EDS *(Spectrum 71)*

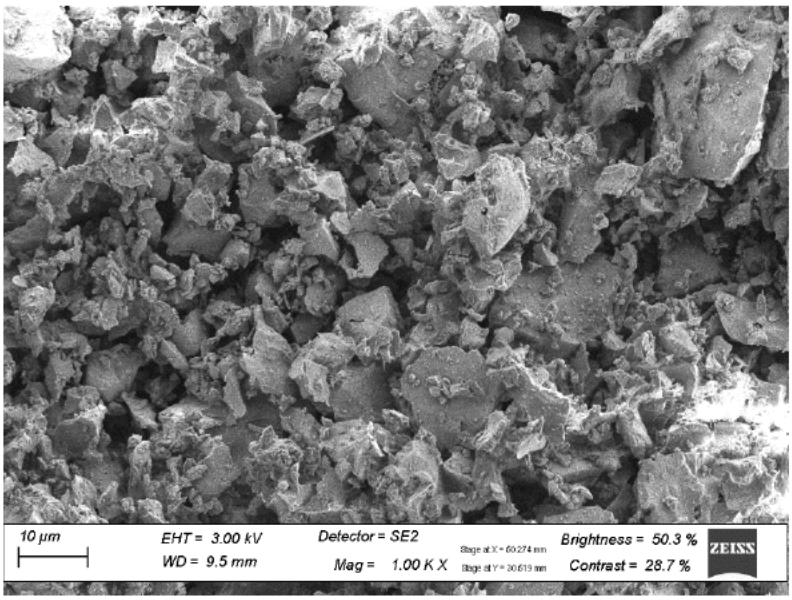

Figure 4.3: SEM image of CWP

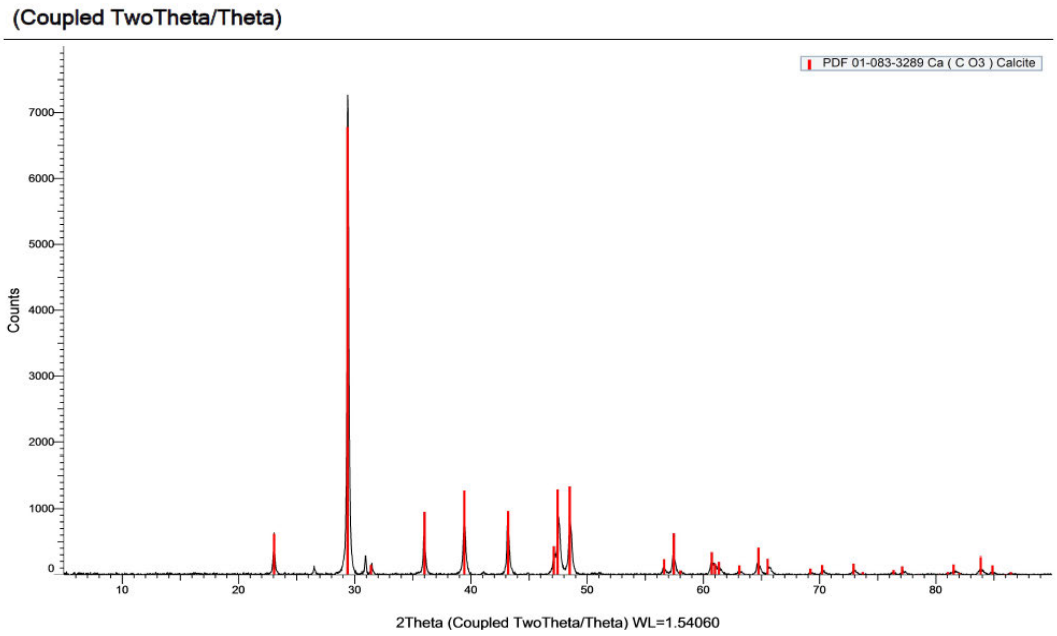

Figure 4.4: XRD analysis of LSP showing calcite peak

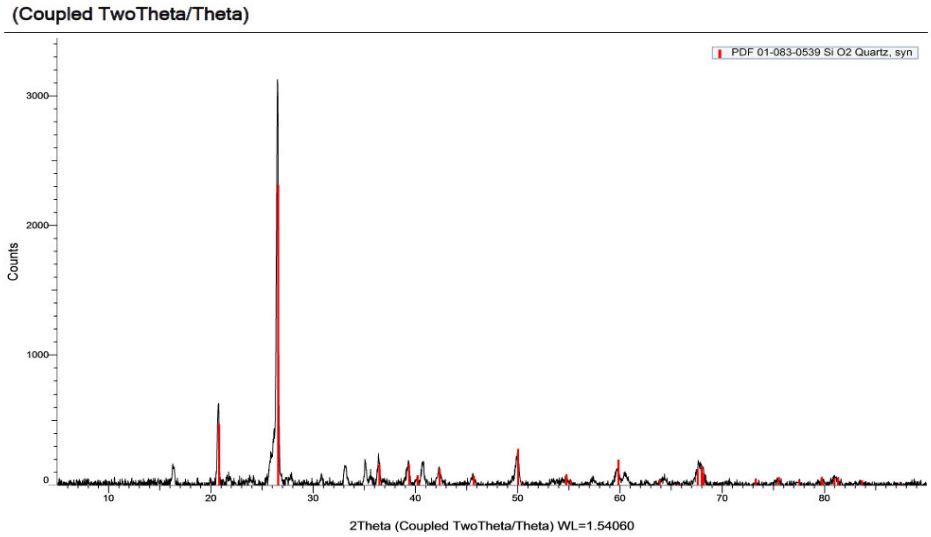

Figure 4.5: XRD analysis of CWP showing quartz peak

4.3 Slump of Fresh Concrete

The slump tests conducted at various w/b ratios (0.45, 0.5, and 0.55) provide important insights into the workability and performance of concrete mixes containing CWP as a partial replacement for GGBS and LSP. The test results demonstrate the influence of CWP on both the initial and final slump values. The initial slump represents the slump before the addition of SP, while the final slump reflects the impact of SP in achieving the target slump of Class S2, as specified in BS EN 206:2013 (BSI 2013). The results are presented in Table 4.4 – 4.6.

Table 4.4: Concrete slump at 0.45 w/b

Concrete mix label	Binder	Percentage replacement (%)	Initial slump (mm)	Final slump (mm)	SP (l/m³)
Replacement of GGBS with CWP					
M1A	CR1	0	35	60	0.6
M2A	CR1-C1	10	43	75	0.6
M3A	CR1-C2	20	72	72	0
Replacement of LSP with CWP					
M4A	CR2	0	30	51	0.5
M5A	CR2-C1	5	23	58	1.2
M6A	CR2-C2	7	31	61	0.8

Table 4.5: Concrete slump of 0.50 w/b

Concrete mix label	Binder	Percentage replacement (%)	Initial slump (mm)	Final slump (mm)	SP (l/m³)
Replacement of GGBS with CWP					
M1B	CR1	0	42	72	0.2
M2B	CR1-C1	10	51	70	0.2
M3B	CR1-C2	20	38	63	0.2
Replacement of LSP with CWP					
M4B	CR2	0	35	59	0.6
M5B	CR2-C1	5	60	60	0
M6B	CR2-C2	7	42	74	0.8

Table 4.6: Slump at 0.55 w/b

Concrete mix label	Binder	Percentage replacement (%)	Initial slump (mm)	Final slump (mm)	SP (l/m³)
Replacement of GGBS with CWP					
M1C	CR1	0	52	54	0.2
M2C	CR1-C1	10	34	58	0.2
M3C	CR1-C2	20	63	63	0
Replacement of LSP with CWP					
M4C	CR2	0	45	72	0.6
M5C	CR2-C1	5	52	52	0
M6C	CR2-C2	7	54	54	0

At a 0.45 w/b ratio, the influence of CWP on workability is particularly noticeable as shown in Figure 4.6 and 4.7. In the GGBS replacement mixes, the initial slump increases as the CWP replacement level rises. For example, the control mix (M1A) with no CWP had an initial slump of 35 mm, while at 20% CWP replacement (M3A), the initial slump reached 72 mm without any need for SP to meet the target slump. This suggests that at higher CWP content, the concrete

becomes more workable, likely due to improved particle packing. In contrast, for the LSP replacement mixes, CWP appears to reduce the initial workability. In mix M5A, a 5% replacement with CWP decreased the initial slump to 23 mm, requiring a higher SP dosage (1.2 l/m³) to bring the final slump to 58 mm. This reduction in workability could be due to the coarser nature of CWP compared to LSP, which may reduce the availability of free water for lubrication.

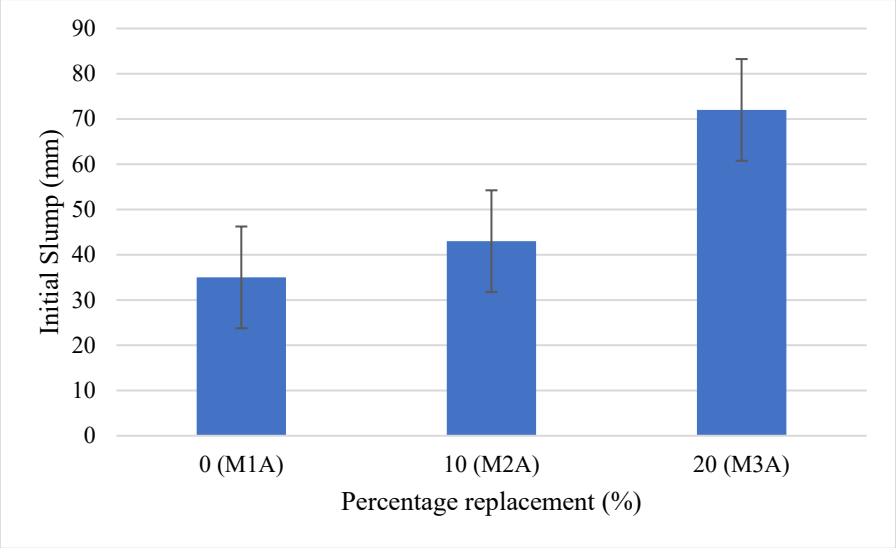

Figure 4.6: Slump of concrete for replacement of GGBS with CWP at 0.45 w/b ratio

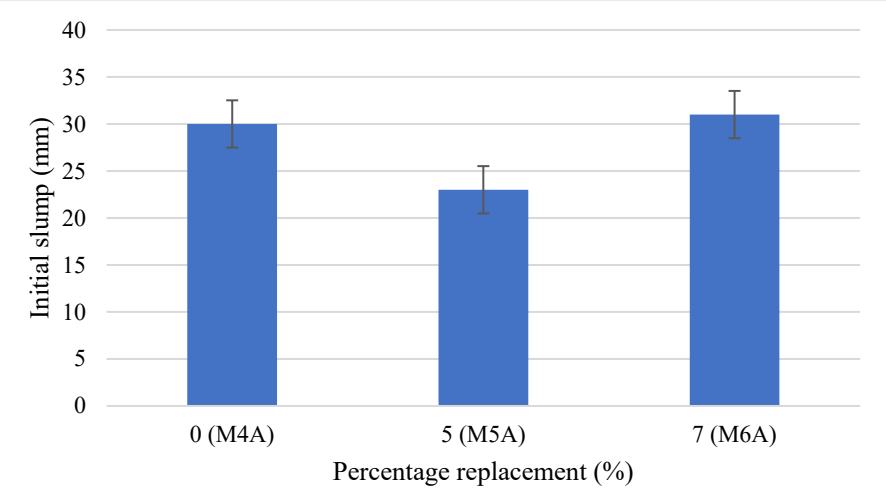

Figure 4.7: Slump of concrete for replacement LSP with CWP at 0.45 w/b ratio

At a 0.5 w/b ratio, the results show some variability in the effect of CWP on workability, as shown in Figure 4.8 and 4.9. For the GGBS replacement mixes, a 10% replacement with CWP (M2B) increased the initial slump to 51 mm, but at 20% replacement (M3B), the initial slump dropped to 38 mm. To meet the desired slump range, M3B required a significant amount of SP (23 l/m³), indicating that while CWP can initially improve workability at lower replacement

levels, higher amounts might stiffen the mix, making it harder to achieve the target slump without additional admixtures. In contrast, CWP had a more positive effect on the LSP replacement mixes. Mixes M5B and M6B, with 5% and 7% CWP replacement, respectively, achieved initial slumps of 60 mm and 42 mm, with minimal or no SP needed to meet the final slump requirement. This suggests that CWP improves workability when replacing LSP, likely due to its interaction with the finer limestone particles, enhancing flow without requiring excessive water or SP.

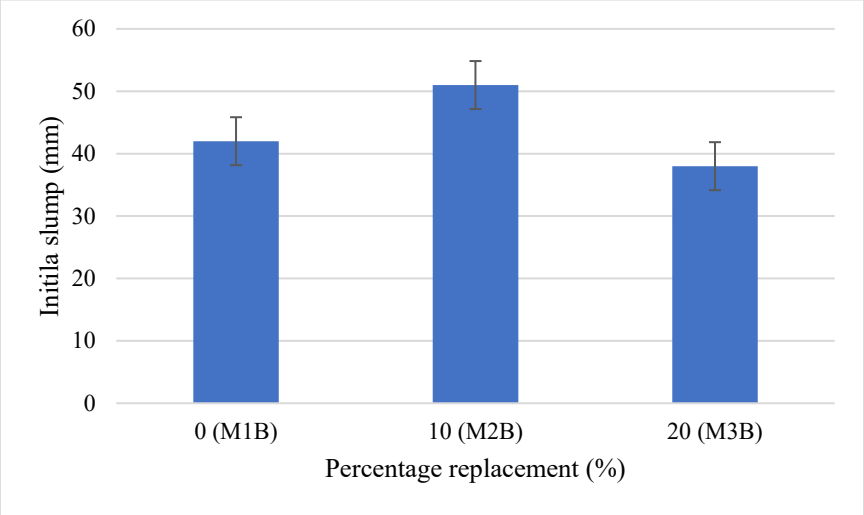

Figure 4.8: Slump of concrete for replacement of GGBS with CWP at 0.50 w/b ratio

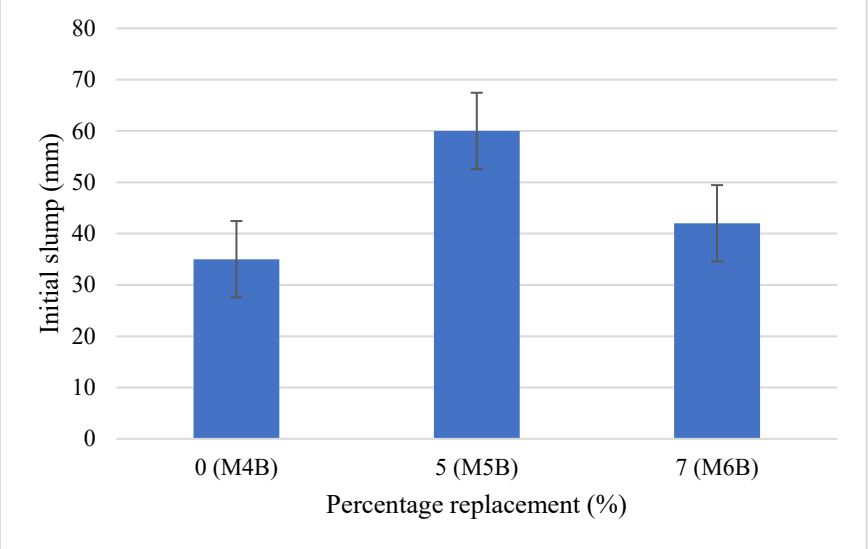

Figure 4.9: Slump of concrete for replacement of LSP with CWP at 0.5 w/b ratio

At a 0.55 w/b ratio, the effect of CWP becomes more stable in GGBS replacement mixes, as shown in Figure 4.10 and Figure 4.11. The 20% CWP replacement mix (M3C) achieved an initial slump of 63 mm without any superplasticizer needed to meet the final slump requirement.

This indicates that at higher water contents, CWP can help stabilize the mix's workability. For the LSP replacement mixes, CWP consistently enhanced workability. Mixes M5C and M6C, with 5% and 7% CWP replacement, both achieved acceptable initial slumps of 52 mm and 54 mm, respectively, without requiring any superplasticizer to meet the target slump range. This reinforces the idea that CWP works well with LSP, providing adequate workability and reducing the need for admixtures to achieve the desired slump.

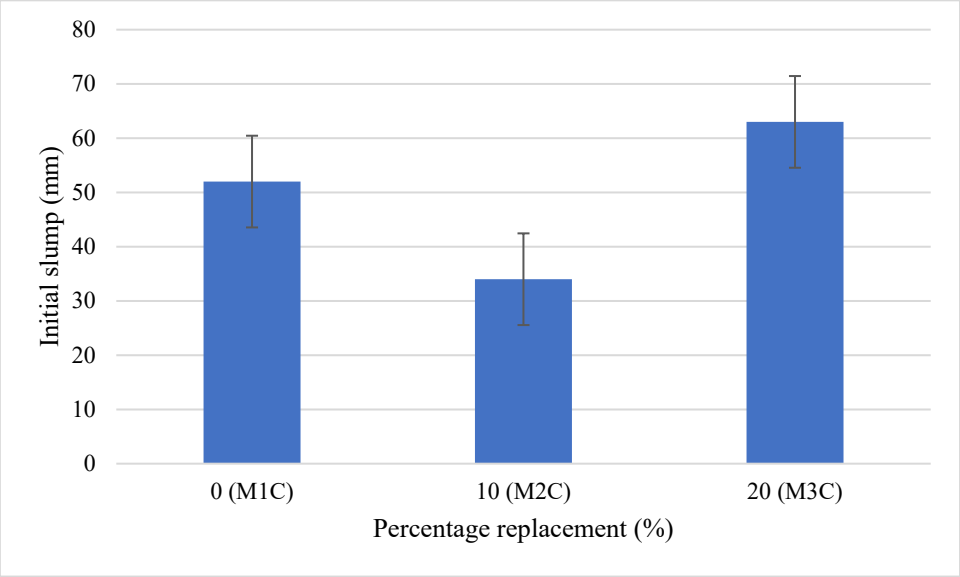

Figure 4.10: Slump of concrete for replacement of GGBS with CWP at 0.55 w/b ratio

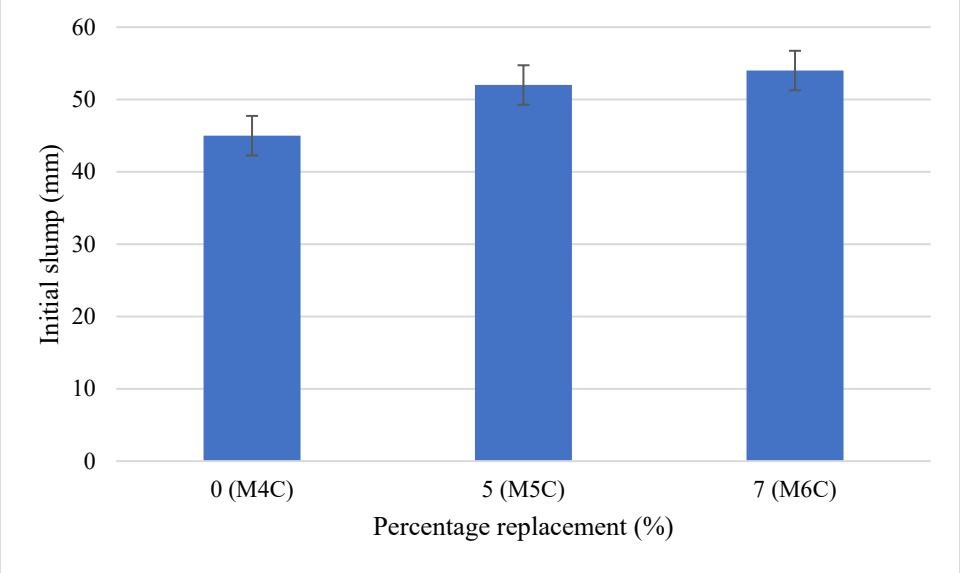

Figure 4.11: Slump of concrete for replacement of limestone power with CWP at 0.55 w/b ratio

In comparison, CWP shows more favourable performance in LSP concrete mixes than in GGBS mixes. This means CWP concrete performs better than LSP in workability but less than GGBS. While CWP in GGBS mixes often requires higher amounts of superplasticizer, particularly at higher replacement levels, it improves workability in LSP mixes with minimal or no superplasticizer needed. The coarser particle size distribution of CWP likely plays a role in this behaviour, as it influences the availability of water for lubrication and the overall particle packing within the mix. In LSP mixes, this particle packing seems to work to the advantage of CWP, enhancing workability without compromising the target slump range.

Overall, the results indicate that CWP can positively impact workability, particularly when used in combination with LSP. However, when used as a replacement for GGBS, higher replacement levels of CWP may stiffen the mix, requiring more superplasticizer to meet the desired slump. The results also highlight that CWP's coarser particle size distribution influences its behaviour, with positive effects on workability in certain contexts and potential drawbacks in others, particularly in terms of superplasticizer demand in GGBS mixes.

4.4 Compressive Strength

This section presents the compressive strength data for various concrete mixes, with emphasis on the development of early-age strength (7 days) and its progression over longer curing periods (28, 56 and 90 days). The study evaluates the effects of replacing GGBS and LSP with CWP at different w/b ratios. The analysis examines trends and variations in strength development across these curing periods to determine whether CWP exhibits pozzolanic behaviour like GGBS or functions as an inert filler like LSP.

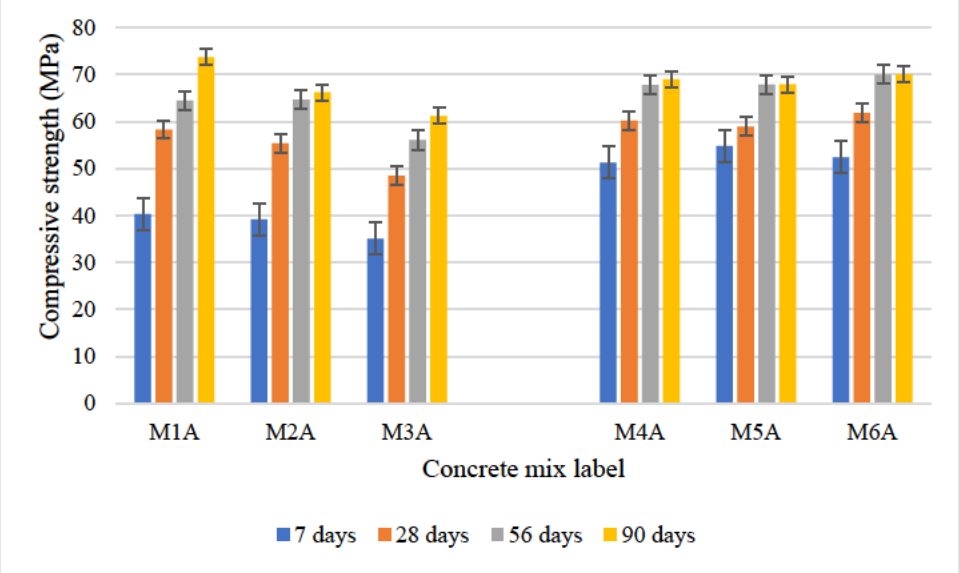

Figure 4.12: Compressive strength of CWP concrete at 0.45 w/b ratio

Figure 4.12 shows the compressive strength of CWP concrete at a 0.45 w/b ratio. For the GGBS-based mixes (M1A, M2A, and M3A), the early-age compressive strength (7 days) decreases with increasing CWP content. The reference mix, M1A (70% PC + 30% GGBS), achieves the highest 7-day strength at 40.3 MPa, while M2A (10% CWP) reaches 39.2 MPa, and M3A (20% CWP) decreases further to 35.1 MPa. This decline suggests that the pozzolanic activity of CWP is slower compared to GGBS, resulting in reduced early-age strength. At 28 days, a similar trend is observed, with M1A achieving 58.3 MPa, outperforming M2A (55.4 MPa) and M3A (48.5 MPa). The strength of M2A (64.6 MPa) slightly exceeds that of M1A (64.5 MPa) at 56 days, indicating that 10% CWP substitution is effective in maintaining long-term strength. However, M3A lags at 56.1 MPa, showing that higher CWP content diminishes strength. At 90 days, the reference mix M1A achieves the highest strength of 73.7 MPa, while M2A and M3A reach 66.3 MPa and 61.2 MPa, respectively. This suggests that higher CWP replacement levels in the GGBS mixes hinder long-term strength development.

For the LSP-based mixes (M4A, M5A, and M6A), the inclusion of CWP enhances compressive strength across all curing ages. At 7 days, the reference mix, M4A (90% PC + 10% LSP), achieves 51.3 MPa, while M5A (5% CWP) and M6A (7% CWP) achieve 54.8 MPa and 52.4 MPa, respectively. This shows that even at early ages, the pozzolanic activity of CWP complements the inert filler effect of LSP, resulting in strength improvements. At 28 days, M6A achieves the highest strength of 61.9 MPa, surpassing M4A (60.2 MPa) and M5A (58.9 MPa). By 56 days, M6A continues to show superior performance at 70 MPa, compared to M4A (67.8 MPa) and M5A (67.9 MPa). At 90 days, M6A achieves the highest strength of 70.1 MPa, demonstrating that CWP enhances long-term strength in LSP-based systems, with higher replacement levels yielding better results.

When comparing the two systems, it is evident that the inclusion of CWP, however, has a more pronounced positive effect on LSP-based mixes, as seen in M6A's consistent improvement across all curing periods. The data suggests that CWP is more effective in LSP-based systems, where it enhances both early and later-age strengths, particularly at higher replacement levels (7% CWP in M6A). However, in GGBS-based systems, 10% CWP substitution (M2A) performs well and matches the long-term strength of the reference mix, but 20% CWP substitution (M3A) results in reduced strength.

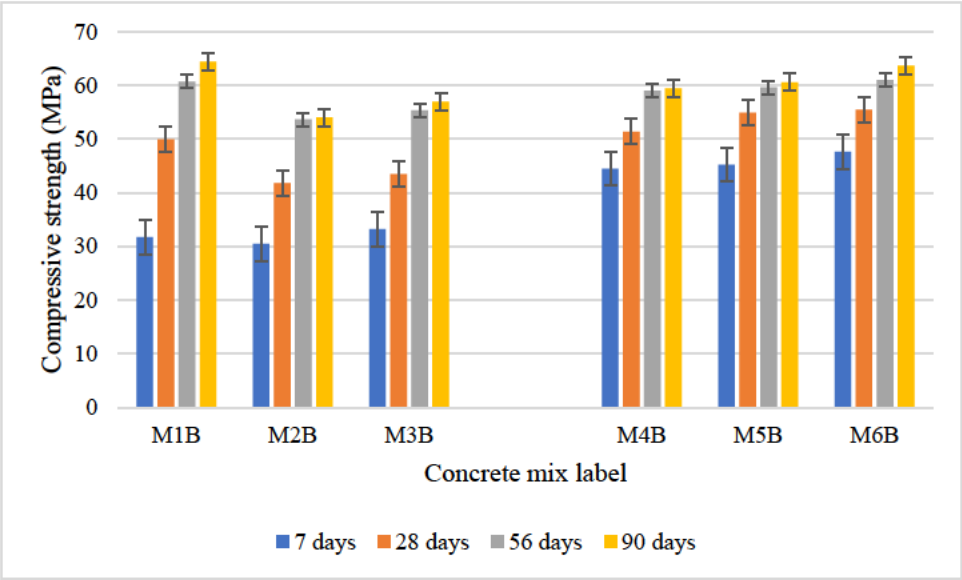

Figure 4.13: Compressive strength of CWP concrete at 0.50 w/b ratio

Figure 4.13 shows the compressive strength of CWP concrete at a 0.5 w/b ratio. For the GGBS replacements (M1B, M2B, and M3B), early-age compressive strength (7 days) decreases as CWP content increases. The reference mix, M1B achieves a 7-day compressive strength of 31.7 MPa, while M2B (10% CWP) and M3B (20% CWP) achieve 30.5 MPa and 33.2 MPa, respectively. Interestingly, M3B slightly outperforms M2B at 7 days, suggesting that a higher CWP content may improve early-age strength to some extent. However, at 28 days, M1B achieves a strength of 49.9 MPa, compared to 41.8 MPa for M2B and 43.5 MPa for M3B. By 90 days, the reference mix reaches 64.4 MPa, significantly outperforming M2B (54 MPa) and M3B (57 MPa). These results indicate that while CWP aids in strength development, it cannot fully match the performance of GGBS at later ages, particularly when used at higher replacement levels.

For the LSP replacements (M4B, M5B, and M6B), the inclusion of CWP consistently enhances compressive strength at all curing ages. At 7 days, the reference mix, M4B (90% PC + 10% limestone), achieves a compressive strength of 44.5 MPa, while M5B (5% CWP) and M6B (7% CWP) achieve 45.2 MPa and 47.6 MPa, respectively. This trend of improvement continues at 28 days, where M4B reaches 51.4 MPa, compared to 54.9 MPa for M5B and 55.5 MPa for M6B. By 90 days, M6B achieves the highest strength of 63.7 MPa, surpassing both M4B (59.4 MPa) and M5B (60.6 MPa). These results demonstrate that the addition of CWP enhances both early and later-age strength in LSP-based mixes, likely due to the combined effects of CWP's pozzolanic activity and improved particle packing. This also shows that CWP has a more pronounced positive impact on LSP-based mixes than GGBS-based mixes. In GGBS-based

mixes, increasing CWP content reduces long-term strength, indicating that higher replacement levels may hinder hydration processes. On the other hand, LSP-based mixes consistently benefit from the inclusion of CWP, with higher replacement levels leading to superior performance at all curing ages.

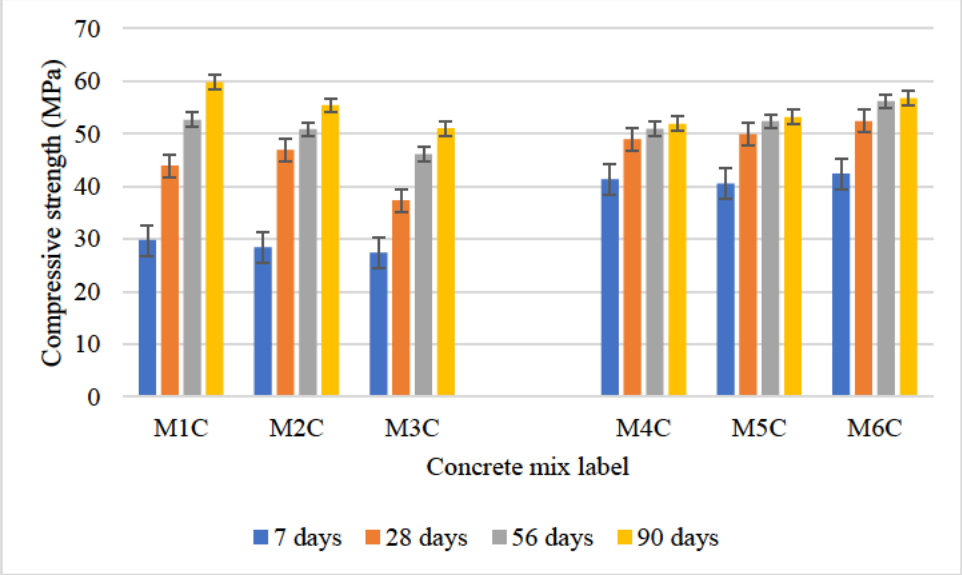

Figure 4.14: Compressive strength of CWP concrete at 0.55 w/b ratio

Figure 4.14 shows the compressive strength of CWP concrete at a 0.55 w/b ratio. For the GGBS-based mixes (M1C, M2C, and M3C), compressive strength decreases with increasing CWP content, particularly at early ages. At 7 days, M1C (70% PC + 30% GGBS) achieves the highest strength of 29.8 MPa, while M2C (10% CWP) and M3C (20% CWP) record 28.4 MPa and 27.41 MPa, respectively. By 28 days, M1C achieves 44 MPa, while M2C slightly surpasses it with 46.9 MPa, showing the beneficial effect of 10% CWP at this age. However, M3C falls behind at 37.3 MPa, indicating that 20% CWP replacement negatively impacts strength. By 90 days, M1C achieves the highest strength of 59.8 MPa, while M2C and M3C reach 55.4 MPa and 51.1 MPa, respectively, showing a clear reduction in long-term strength with higher CWP content.

In contrast, the LSP-based mixes (M4C, M5C, and M6C) show consistent improvements in compressive strength with CWP replacement. At 7 days, M6C (7% CWP) achieves the highest strength of 42.5 MPa, surpassing M4C (41.4 MPa) and M5C (40.6 MPa). By 28 days, M6C continues to outperform with 52.4 MPa, compared to 49.9 MPa for M5C and 49 MPa for M4C. At 56 and 90 days, M6C maintains its superiority, achieving 56.2 MPa and 56.8 MPa, respectively, while M4C lags at 51.9 MPa by 90 days. These results indicate that CWP enhances

both early and later-age strength in LSP-based mixes, particularly at higher replacement levels. This confirms that CWP has a more pronounced positive impact on LSP-based mixes compared to GGBS-based mixes across all w/b ratios. For GGBS systems, 10% CWP replacement provides a slight improvement at 28 days but reduces long-term strength. In limestone systems, higher CWP replacement levels consistently enhance both early and long-term compressive strength. The error bars are relatively larger at early curing days (7 days). This suggests greater uncertainty in early-age strength development due to hydration variability. At later ages (56 and 90 days), the error bars are generally smaller, indicating more stable and predictable strength development over time.

4.4.1 Rate of compressive strength development in CWP concrete

Figure 4.15 and 4.16 in this section show the rate of change of compressive strength with curing age. The equations provided in the graphs highlight the linear relationship between compressive strength and curing days for the various concrete mixes. The slopes of these equations indicate the rate of compressive strength gain, while the R^2 values reflect the strength of the linear correlation.

The reference mix M1A shows the steepest slope (10.6), indicating the highest rate of compressive strength gain per day, with a strong R^2 value of 0.9, reflecting a consistent strength progression. When 10% of GGBS is replaced with CWP (M2A), the slope decreases to 9, suggesting a reduced rate of strength gain due to the slower pozzolanic reaction of CWP. Despite this, the R^2 value of 0.9 indicating that the linear relationship is predictable. In the case of 20% CWP replacement (M3A), the slope further decreases to 8.6, reflecting the slowest strength gain among the GGBS mixes. However, the high R^2 value of 1.0 confirms that the strength development remains consistent over time.

In the LSP-based systems (M4A, M5A, and M6A), the strength gain rates are generally lower than in GGBS systems, as indicated by the flatter slopes. For the reference mix M4A, the slope is 6.1, showing a modest rate of strength gain, with an R^2 value of 0.9, indicating good consistency. When 5% CWP is introduced (M5A), the slope reduces to 4.8, reflecting a slower rate of strength development. However, the inclusion of 7% CWP in M6A increases the slope to 6.1, showing an enhanced strength gain rate due to the synergistic effect of the pozzolanic reaction of CWP with the LSP. The R^2 values for these mixes remain high, suggesting reliable linear trends.

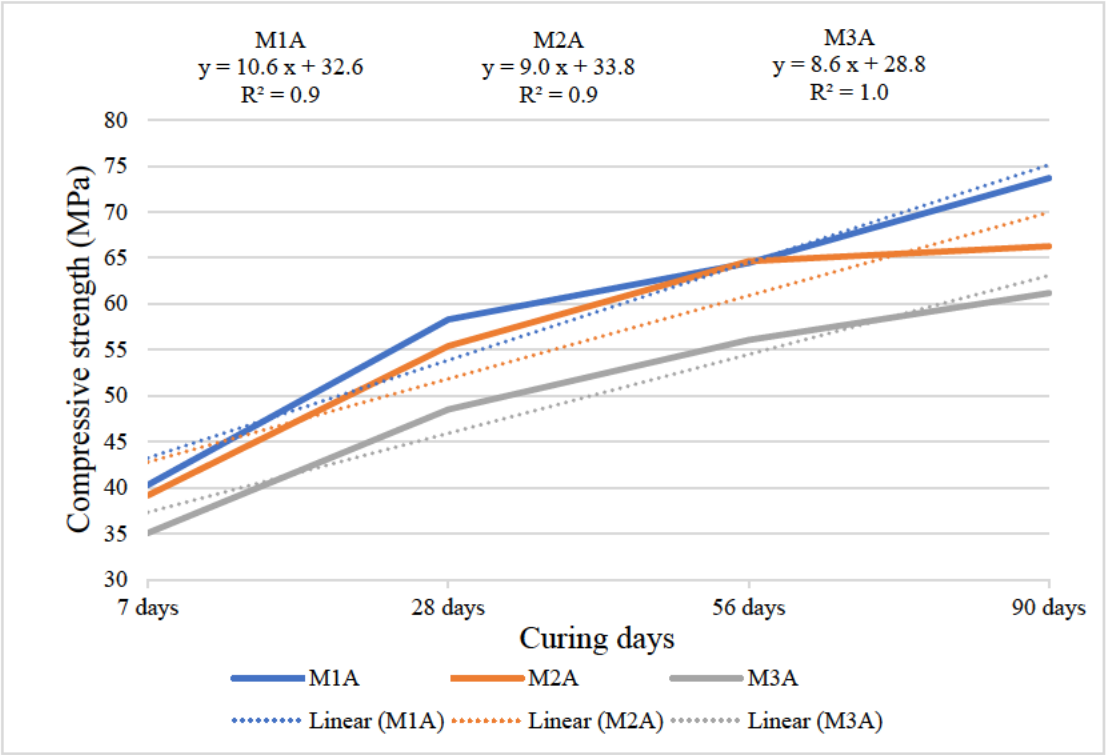

Figure 4.15: Compressive strength of GGBS – CWP base concrete at 0.45 w/b ratio

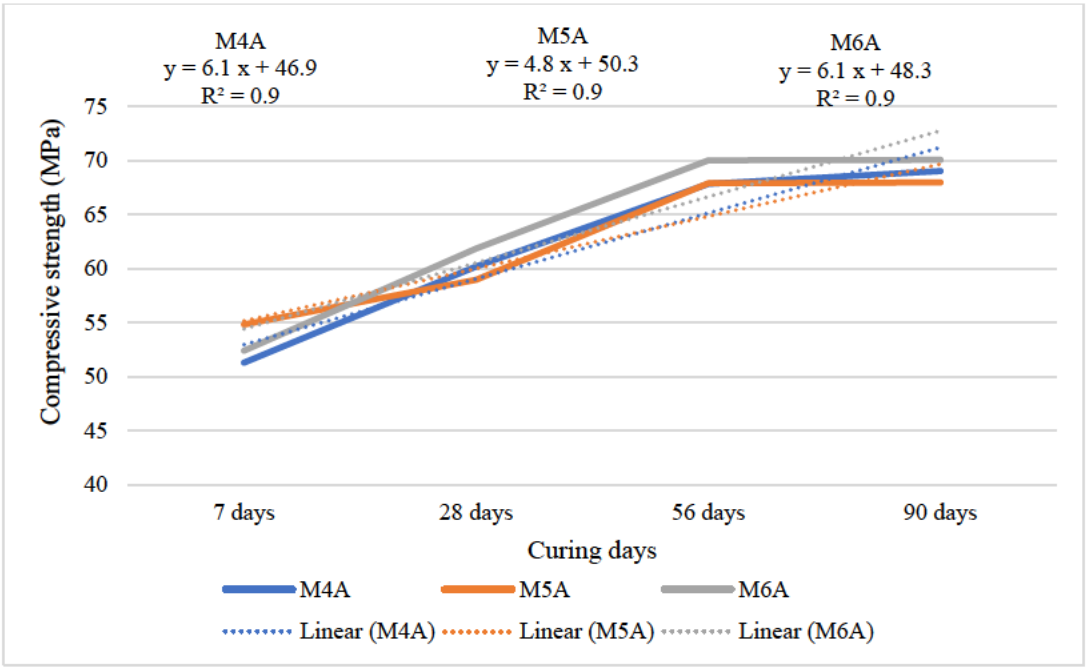

Figure 4.16: Compressive strength of limestone – CWP base concrete at 0.45 w/b ratio

Figure 4.17 and 4.18 illustrate the compressive strength development rate of concrete mixes with curing age at 0.50 w/b ratio. For the GGBS-based mixes (M1B, M2B, and M3B) in Figure 4.17, the reference mix, M1B shows the steepest slope (10.9), indicating the highest rate of strength gain among all the mixes. The high R^2 value (0.9) indicates a strong and consistent

linear progression of strength. For M2B (10% CWP), the slope decreases to 8.3, indicating a reduced rate of strength gain due to partial replacement of GGBS with CWP. However, the intercept (24.3 MPa) is like M1B, showing comparable early-age strength. In M3B (20% CWP), the slope (8.3) reflects the slowest rate of strength gain among the GGBS-based mixes, and while the intercept is slightly higher at 26.5 MPa, the overall strength development remains subdued due to the higher CWP content. These results highlight that while CWP contributes to pozzolanic activity, higher replacement levels negatively impact the rate of strength development in GGBS systems.

For the LSP-based mixes (M4B, M5B, and M6B) in Figure 4.18, the reference mix, M4B, has a slope of 5.2, reflecting a moderate rate of strength gain, with a starting compressive strength of 40.4 MPa. The high R^2 value (0.9) confirms consistent strength development over time. In M5B (5% CWP), the slope decreases slightly to 5.1, indicating a marginally slower rate of strength gain compared to M4B. However, the higher intercept (42.4 MPa) indicates improved early-age performance due to the addition of CWP. M6B (7% CWP) demonstrates the highest slope (5.4) among the LSP-based mixes, indicating the fastest rate of strength gain. The intercept (43.5 MPa) and the high R^2 value (1.0) emphasize the positive impact of higher CWP content in LSP-based mixes, which enhances both early and later-age compressive strength due to its higher pozzolanic reactivity.

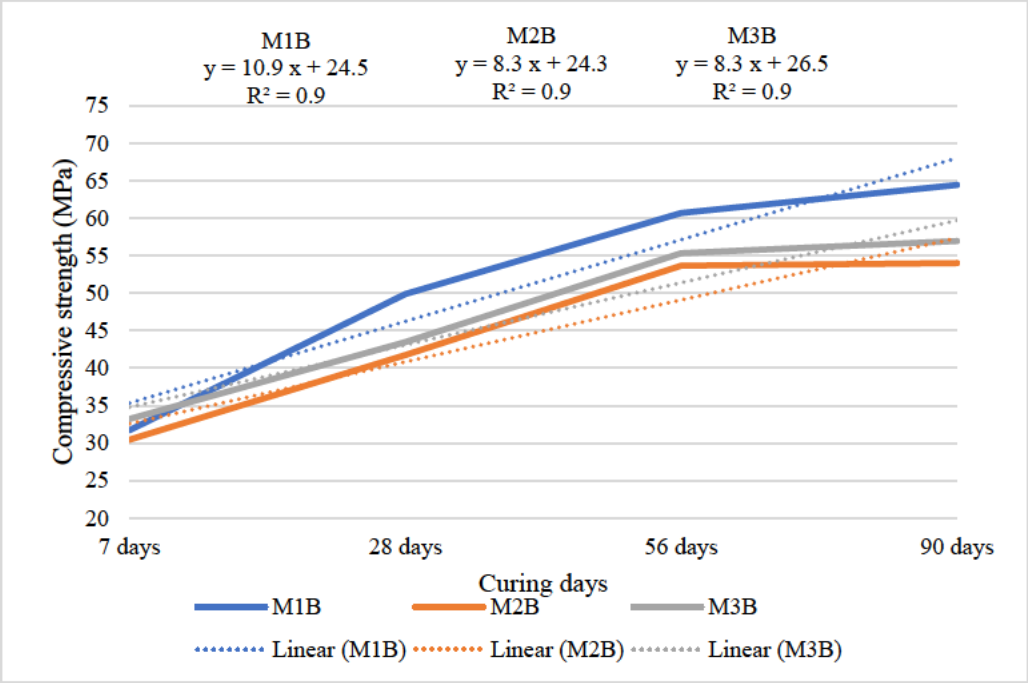

Figure 4.17: Compressive strength of GGBS – CWP base concrete at 0.5 w/b ratio

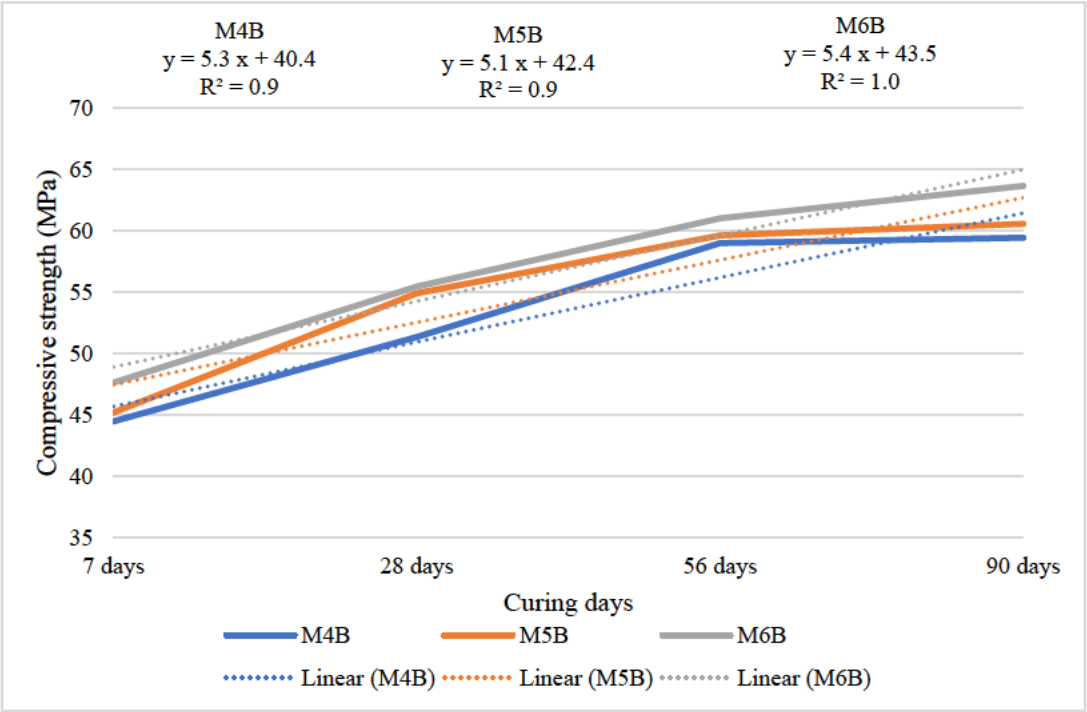

Figure 4.18: Compressive strength of LSP – CWP base concrete at 0.5 w/b ratio

Figure 4.19 and Figure 4.20 present the graphs for the 0.55 w/b ratio. In the GGBS-based mixes (M1C, M2C, and M3C), the reference mix M1C has the steepest slope (9.9), showing the highest rate of strength gain. Its R^2 value (1.0) highlights a highly consistent strength progression with curing days. When 10% of GGBS is replaced with CWP (M2C), the slope decreases to 8.5, indicating a slower rate of strength gain compared to M1C. However, M2C exhibits a higher intercept (24.2 MPa), showing slightly better early-age strength. For M3C, with 20% CWP, the slope further drops to 8.0, reflecting the slowest rate of strength development among the GGBS-based mixes. While the R^2 value remains high (1.0), indicating a reliable trend, the lower intercept (20.6 MPa) and reduced slope suggest that higher CWP content diminishes both early and long-term strength.

In the LSP-based mixes (M4C, M5C, and M6C), the reference mix M4C has the lowest slope (3.4), indicating a much slower rate of strength gain. Strength gain in M4C was heavily influenced by the filler effect of LSP, resulting in gradual strength development. However, the relatively lower R^2 value (0.8) suggests some variability in the strength progression. For M5C, with 5% CWP, the slope increases to 4.0, showing a slight acceleration in strength gain, although the intercept decreases to 39.0 MPa, reflecting a minor reduction in early-age strength. M6C, with 7% CWP, exhibits the highest slope (4.7) among the mixes, indicating the fastest strength development. The higher intercept (40.3 MPa) and improved slope reflect the

beneficial contribution of CWP in enhancing both early and later-age strength. The R^2 value (0.8) indicates a relatively reliable strength trend.

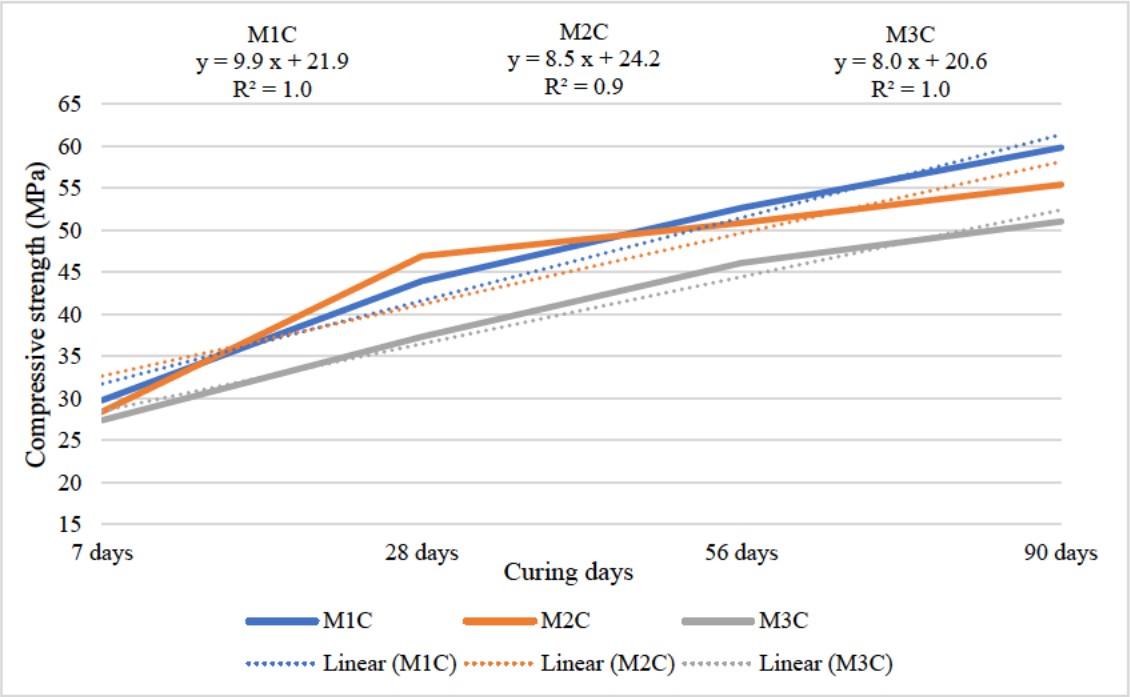

Figure 4.19: Compressive strength of GGBS – CWP base concrete at 0.55 w/b ratio

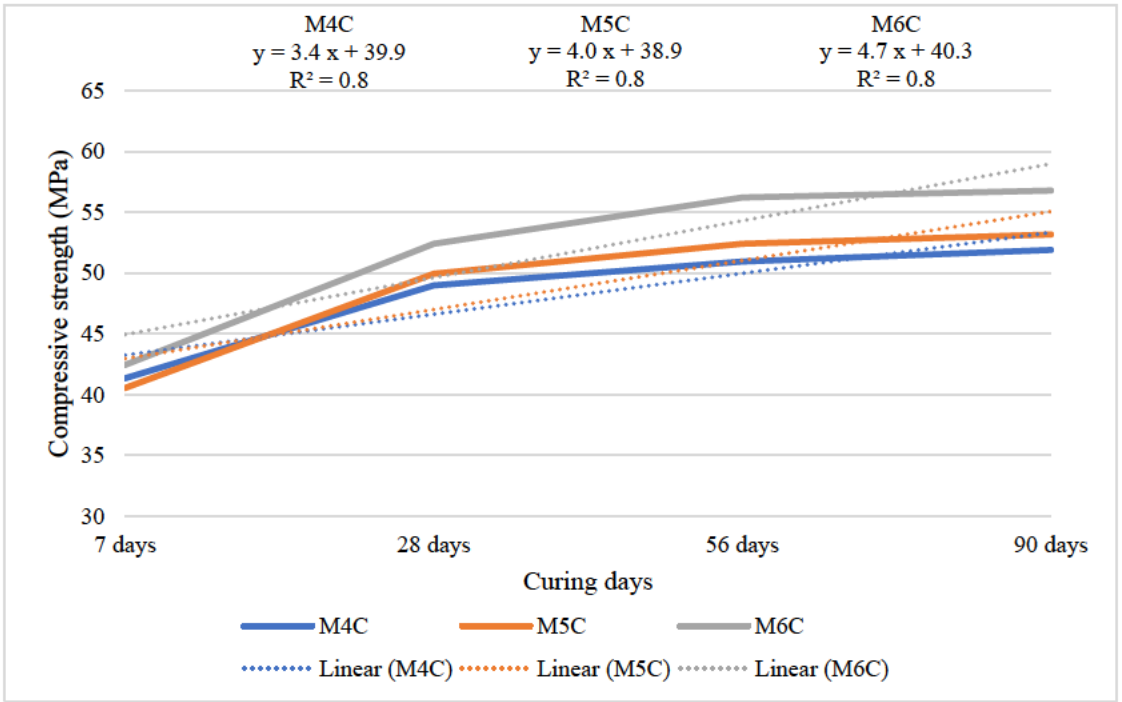

Figure 4.20: Compressive strength of GGBS – LSP base concrete at 0.55 w/b ratio

Overall, the GGBS-based mixes demonstrate a higher rate of strength development compared to the LSP-based mixes, as evidenced by their steeper slopes. This is attributed to GGBS functioning as a reactive binder, whereas LSP acts as an inert filler, which delays hydration. However, the addition of CWP significantly influences the performance of both systems. In GGBS-based mixes, increasing CWP content reduces the rate of strength gain, particularly at higher replacement levels, with 20% CWP (M3C) showing the weakest performance. Conversely, in LSP-based mixes, higher CWP levels enhance the rate of strength gain, with M6C achieving both the highest rate of strength development and the best early-age performance. These results confirm that CWP is a more reactive binder than LSP but less reactive than GGBS. The high R^2 values across all equations validate the reliability of the linear model in predicting strength development trends.

4.4.2 Regression analysis of compressive strength of CWP concrete mixes against their reference mix

The regression statistics in Table 4.7 and 4.8 examine the relationship between the compressive strength of CWP concrete mixes and their respective reference mixes across three w/b ratios. Table 4.7 presents the regression statistics for the compressive strength of CWP concrete in comparison to its reference mixes, while the figures illustrate the regression line fit plots. The equations displayed on these plots serve as predictive models for estimating the compressive strength of CWP concrete based on its reference mix. The linear regression models exhibit strong correlations, as indicated by the high R^2 values across all mixes, confirming their reliability in predicting strength development. Table 4.7 shows the regression statistics of the compressive strength of CWP concrete mixes against their reference mix for GGBS replacement.

Table 4.7: Regression statistics of the compressive strength of CWP concrete mixes against their reference mix for GGBS replacement

Concrete mix	Multiple R	R Square	Adjusted R square	Standard error	Observations
0.45 w/b ratio					
M2A vs M1A	0.99	0.95	0.93	3.27	4
M3A vs M1A	1.00	0.99	0.98	1.43	4
0.50 w/b ratio					
M2B vs M1B	0.99	0.98	0.97	1.96	4
M3B vs M1B	0.99	0.98	0.97	2.06	4
0.55 w/b ratio					
M2C vs M1C	0.97	0.95	0.92	3.33	4
M3C vs M1C	1.00	0.94	0.99	0.95	4

For the 0.45 w/b ratio presented in Figure 4.21 and Figure 4.22, M2A and M3A were compared against the reference mix M1A. The regression equation for M2A shows an R2 value of 0.95, indicating a strong linear relationship. The slope of 0.9 suggests that M2A achieves about 86% of the compressive strength of M1A, with an intercept factor of 5.4 MPa contributing to additional strength. The adjusted R^2 (0.9) and standard error (3.3 MPa) reflect a well-fitted model with minimal variability. Similarly, the regression equation of M3A shows an R^2 value of 0.99. The slope (0.8) indicates that M3A achieves approximately 80% of the strength of M1A, with the model exhibiting very low variability (standard error of 1.4 MPa).

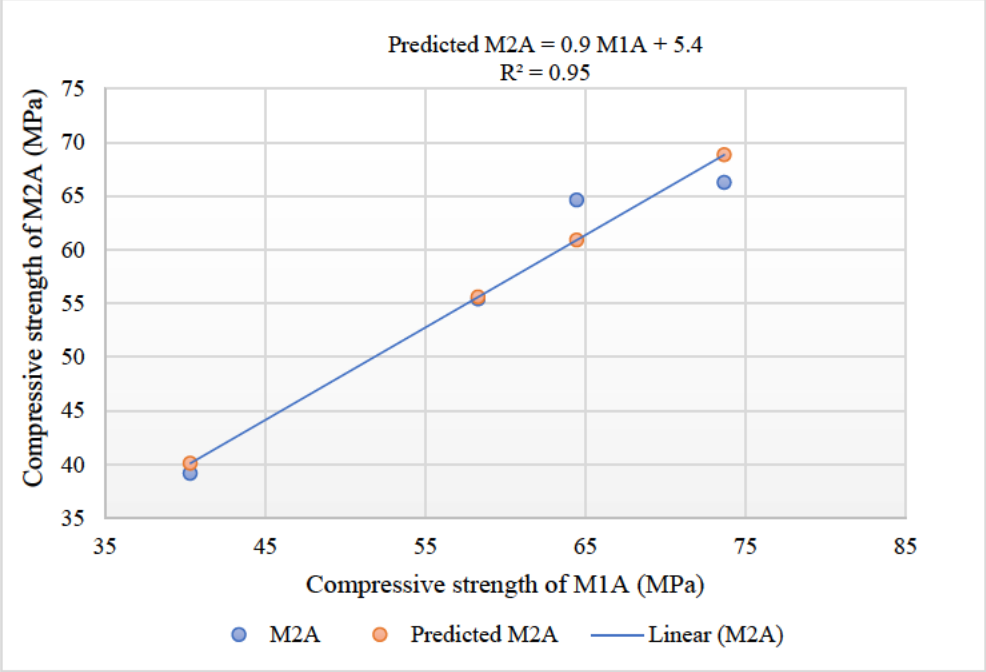

Figure 4.21: Regression line fit plot of M2A against M1A

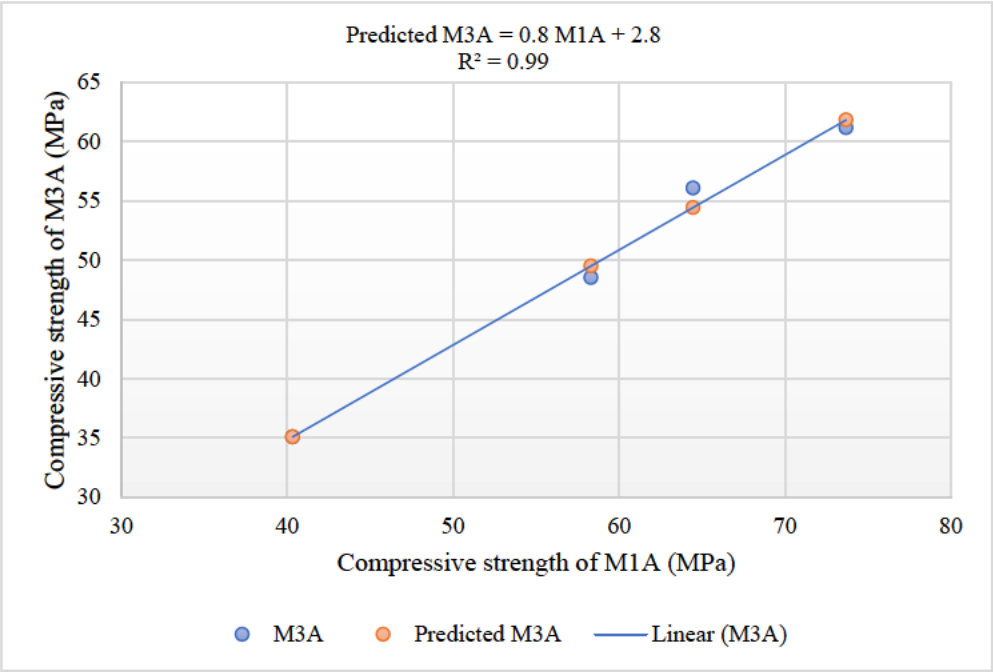

Figure 4.22: Regression line fit plot of M3A against M1A

For the 0.50 w/b ratio presented in Figure 4.23 and 4.24, M2B and M3B were compared against M1B. The regression equation for M2B demonstrates an R^2 value of 0.98, reflecting a highly reliable model. The slope (0.8) indicates that M2B achieves 75.8 % of the strength of M1B, with an intercept of 5.8 MPa. The adjusted R^2 (0.97) and standard error (2.0 MPa) confirm the accuracy of the model and low variability. The equation for M3B shows an R^2 value of 0.98, with M3B achieving 74.9 % of the strength of M1B. The standard error (2.1 MPa) reflects good precision.

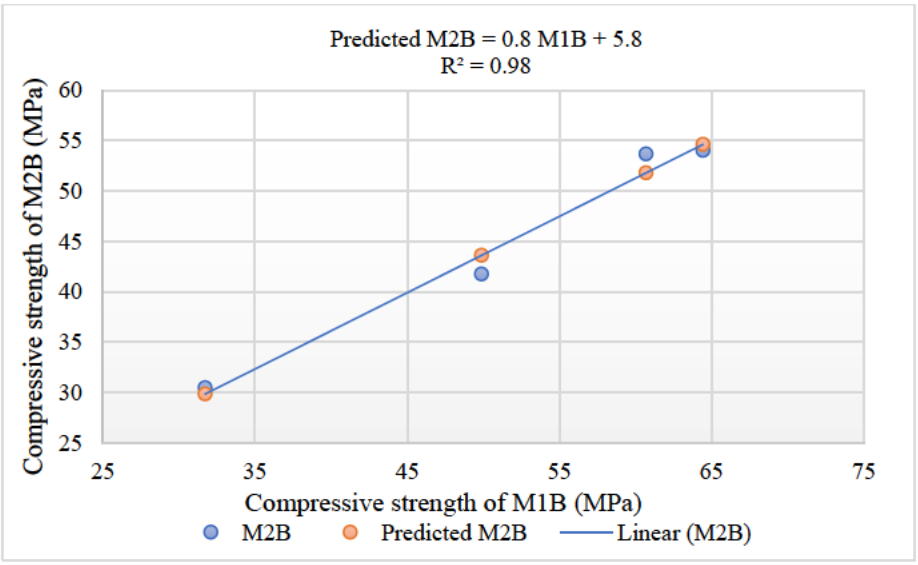

Figure 4.23: Regression line fit plot of M2B against M1B

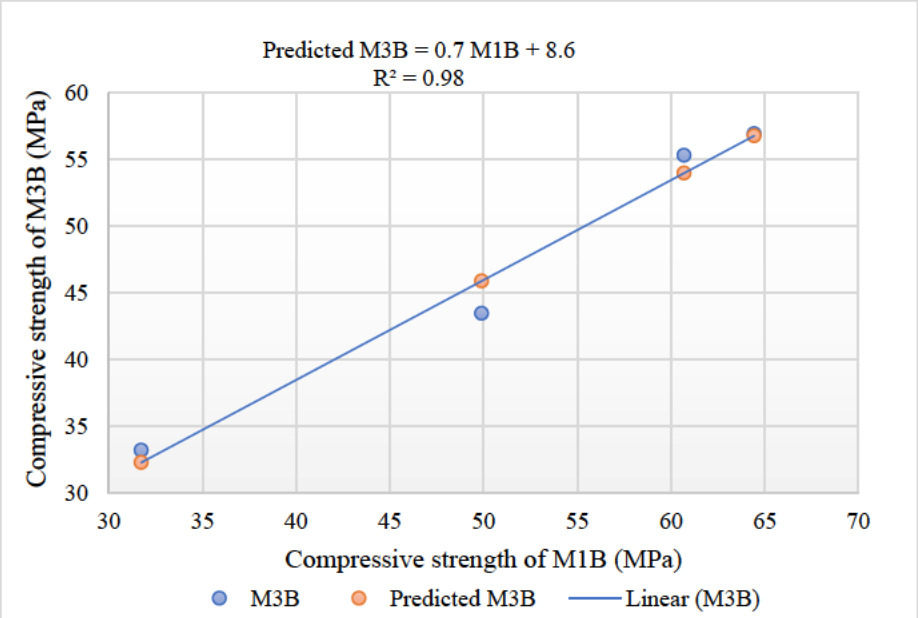

Figure 4.24: Regression line fit plot of M3B against M1B

At the 0.55 w/b ratio shown in Figure 4.25 and 4.26, M2C and M3C were analysed against M1C. The regression equation for M2C has an R^2 value of 0.95, indicating a strong linear relationship. M2C achieves 89.2% of the compressive strength of M1C, with an intercept of 3.9 MPa. However, the standard error (3.3 MPa) suggests slightly higher variability than observed in lower w/b ratios. The equation for M3C yields an exceptional R^2 value of 0.99, indicating an almost perfect correlation. M3C achieves 80.2% of the compressive strength of M1C, with the very low standard error (0.9 MPa) reflecting excellent accuracy.

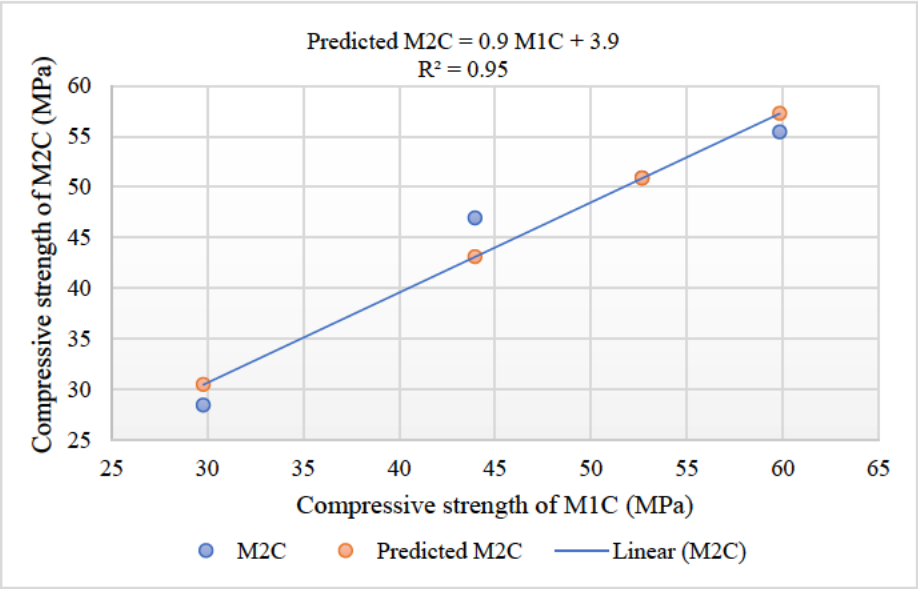

Figure 4.25: Regression line fit plot of M2C against M1C

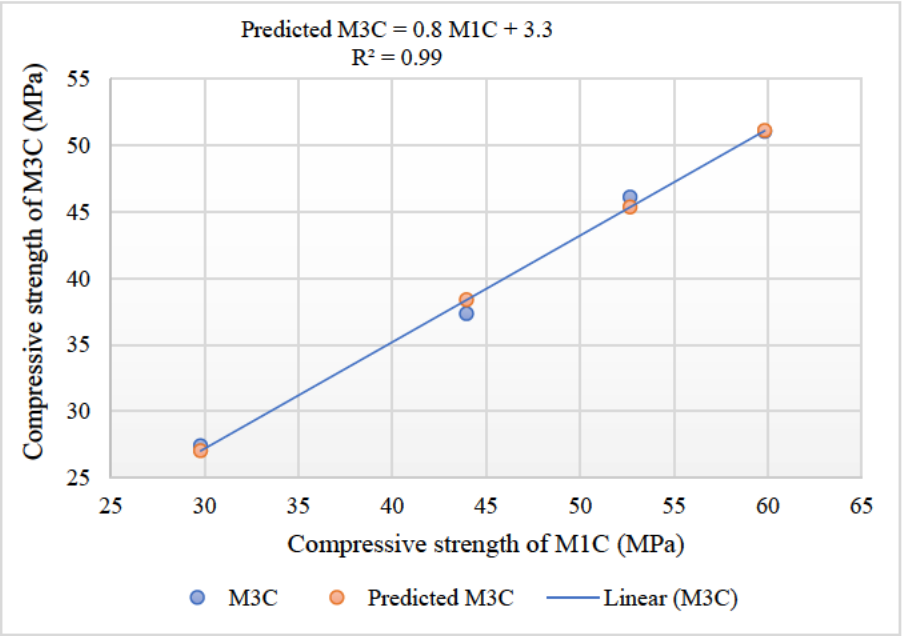

Figure 4.26: Regression line fit plot of M3C against M1C

Table 4.8 shows the Regression statistics of the compressive strength of CWP concrete mixes against their reference mix for LSP replacement. The regression analysis for the compressive strength of CWP concrete mixes against their reference mixes for LSP replacement shows strong linear relationships, as evidenced by high R^2 values across all w/b ratios.

Table 4.8: Regression statistics of the compressive strength of CWP concrete mixes against their reference mix for LSP replacement

Concrete mix	Multiple R	R Square	Adjusted R square	Standard error	Observations
0.45 w/b ratio					
M5A vs M4A	0.98	0.96	0.94	1.68	4
M6A vs M4A	1.00	1.00	1.00	0.61	4
0.50 w/b ratio					
M5B vs M4B	0.98	0.96	0.94	1.68	4
M6B vs M4B	0.99	0.98	0.97	1.25	4
0.55 w/b ratio					
M5C vs M4C	1.00	1.00	1.00	0.21	4
M6C vs M4C	1.00	1.00	0.99	0.56	4

For the 0.45 w/b ratio presented in Figure 4.27 and 4.28, the regression equation for M5A has an R^2 value of 0.96. This indicates a strong correlation between the compressive strengths of M5A and M4A, where M5A achieves about 78.8 % of the strength M4A, with an additional contribution of 13.5 MPa. The adjusted R^2 (0.94) and the standard error (1.7 MPa) reflect high reliability and low variability in the model. For M6A, the regression equation yields an

exceptional R^2 value of 1.00, showing a nearly perfect fit. The slope of 1.02 indicates that M6A slightly surpasses the strength of M4A, with the very low standard error (0.6 MPa) confirming the precision of the model.

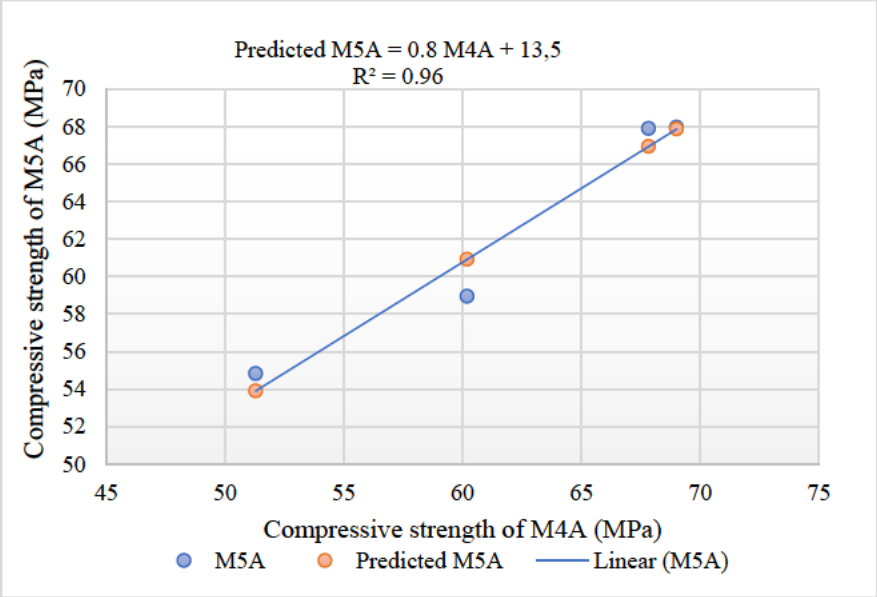

Figure 4.27: Regression line fit plot of M5A against M4A

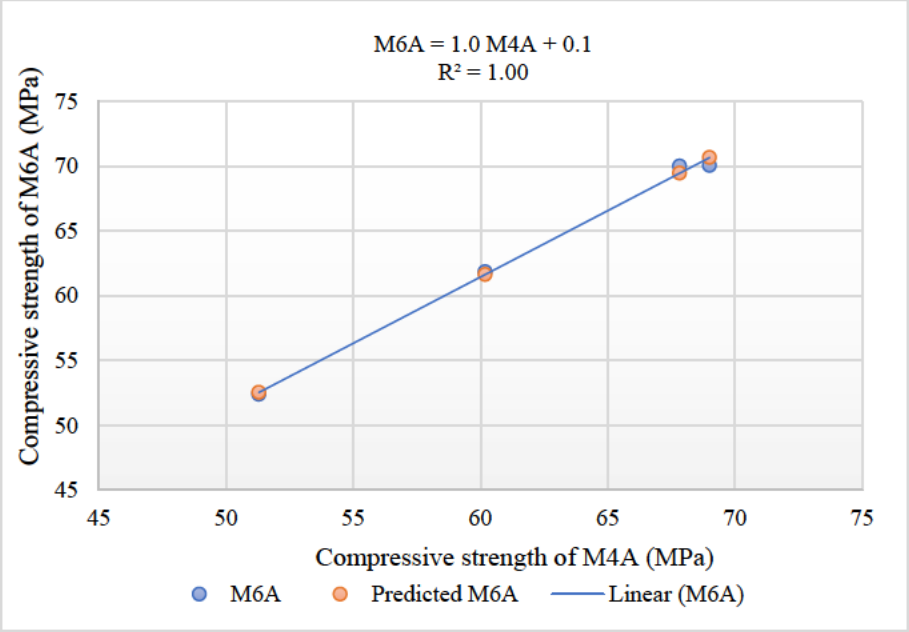

Figure 4.28: Regression line fit plot of M6A against M4A

At the 0.50 w/b ratio shown in Figure 4.29 and 4.30, the regression equation for M5B has an R^2 value of 0.96. This indicates that M5B closely follows the strength progression of M4B, achieving approximately 97.1 % of its strength. The adjusted R^2 (0.94) and the standard error

(1.7 MPa) demonstrate the strong accuracy of the model. For M6B, the regression equation shows an R^2 value of 0.98, suggesting a highly reliable relationship. The slope (0.99) indicates that M6B closely matches the strength progression of M4B, with minimal variability as reflected by the standard error (1.3 MPa).

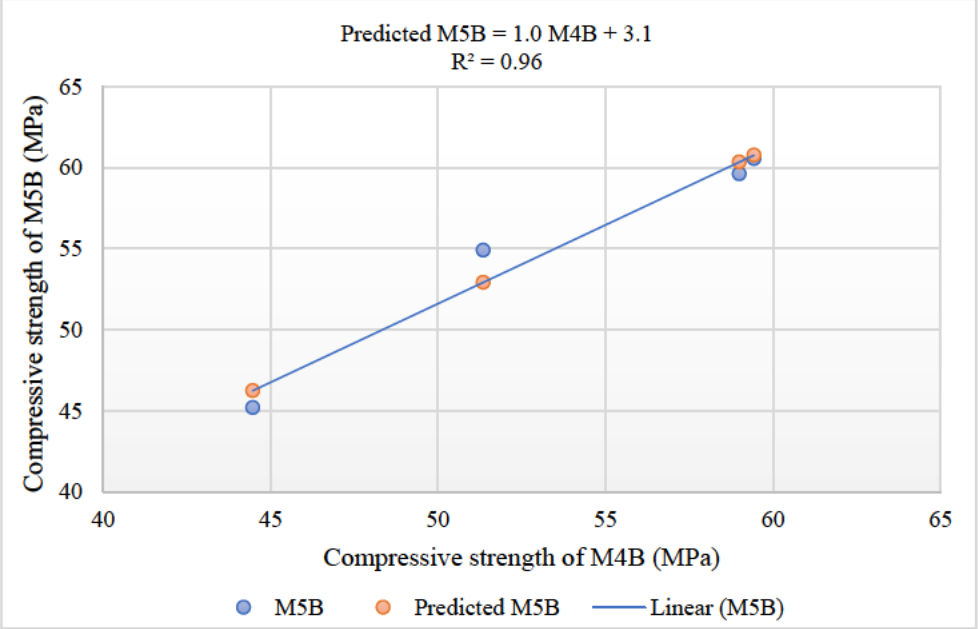

Figure 4.29: Regression line fit plot of M5B against M4B

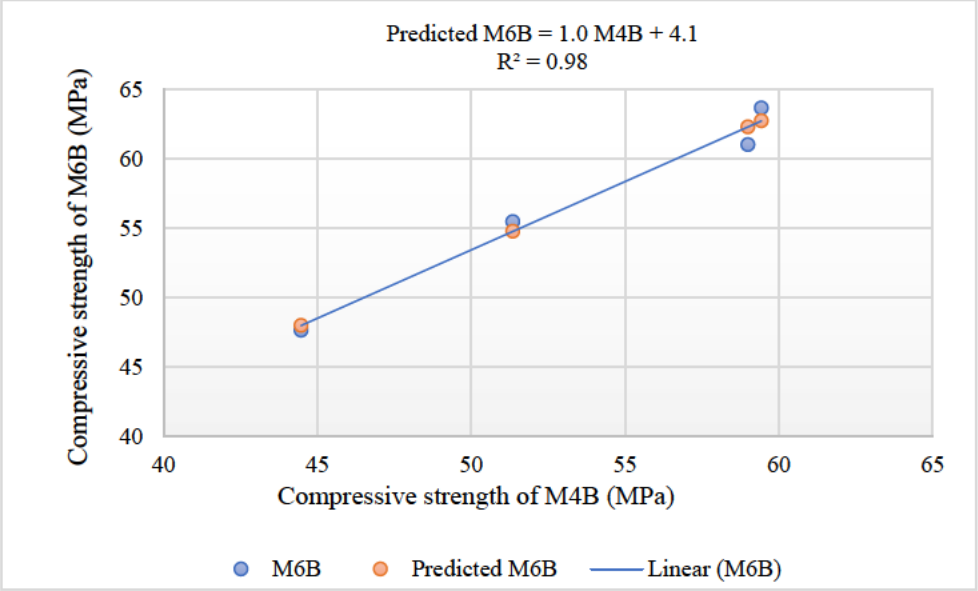

Figure 4.30: Regression line fit plot of M6B against M4B

For the 0.55 w/b ratio presented in Figure 4.31 and 4.32, the regression equation for M5C has an exceptional R^2 value of 1.00. This demonstrates an almost perfect linear relationship, where

M5C slightly exceeds the compressive strength of M4C. The very low standard error (0.2 MPa) indicates excellent model accuracy. For M6C, the regression equation has an R^2 value of 1.00, showing a strong correlation. The slope (1.4) suggests that M6C significantly surpasses the strength of M4C, with the low standard error (0.6 MPa) further validating the reliability of the model.

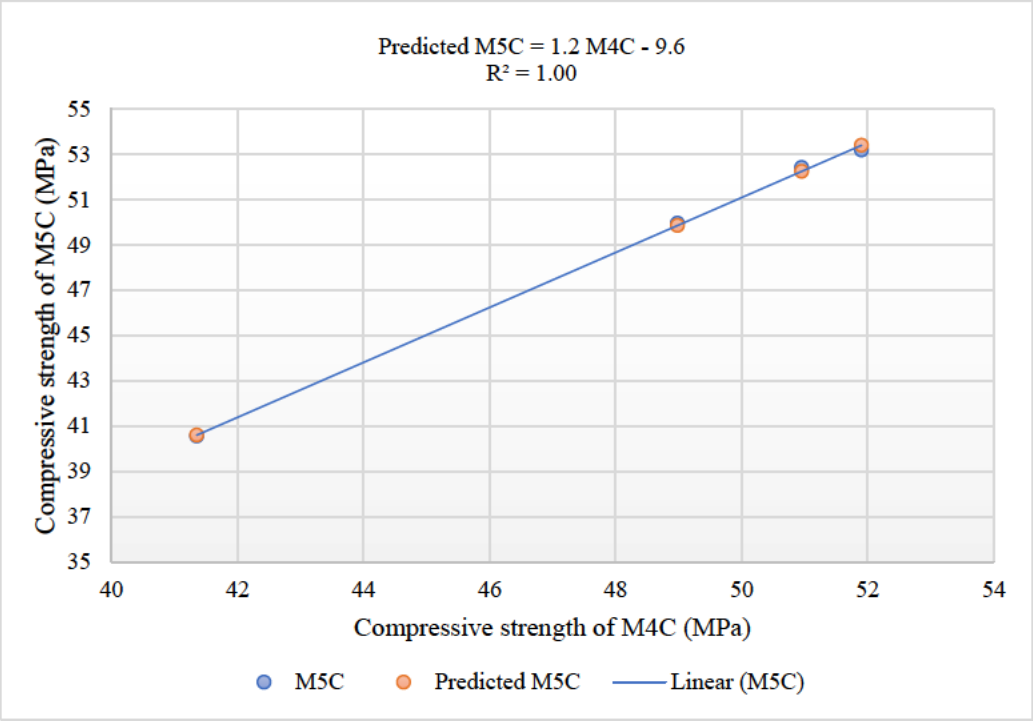

Figure 4.31: Regression line fit plot of M5C against M4C

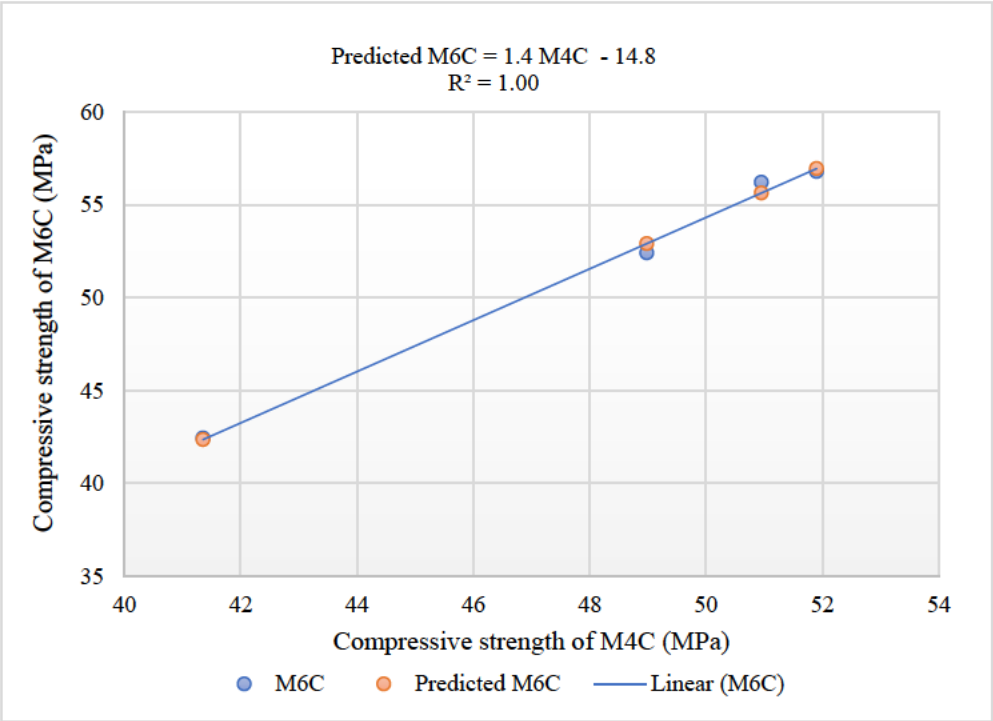

Figure 4.32: Regression line fit plot of M6C against M4C

Overall, the regression analysis confirms strong linear relationships between CWP concrete mixes and their respective reference mixes, as indicated by consistently high R^2 values. In GGBS replacements, the slopes generally decrease with increasing CWP content, signifying a reduction in compressive strength compared to the reference mixes. Conversely, in LSP replacements, the inclusion of CWP either improves or maintains compressive strength relative to the reference mixes, with M5 and M6 exhibiting enhanced performance at higher CWP levels. Additionally, the standard error increases slightly with higher w/b ratios, likely due to the greater variability introduced by increased water content. Notably, the models for the 0.55 w/b ratio demonstrate the highest R^2 values and lowest standard errors, indicating better predictability and reduced variability. These findings establish a reliable basis for predicting the performance of CWP concrete and underscore its potential as an effective substitute for LSP, particularly at higher replacement levels.

4.5 Splitting Tensile Strength of Concrete

This section presents the splitting tensile strength data for various concrete mixes, with particular emphasis on the development of early-age strength (7 days) and its progression over longer curing periods (28 to 90 days). The study evaluates the effects of replacing GGBS and LSP with CWP at different w/b ratios. The analysis examines trends and variations in strength

development across these curing periods to determine whether CWP exhibits pozzolanic behaviour like GGBS or functions as an inert filler like LSP. Figure 4.33 shows the splitting tensile strength of CWP concrete at 0.45 w/b ratio.

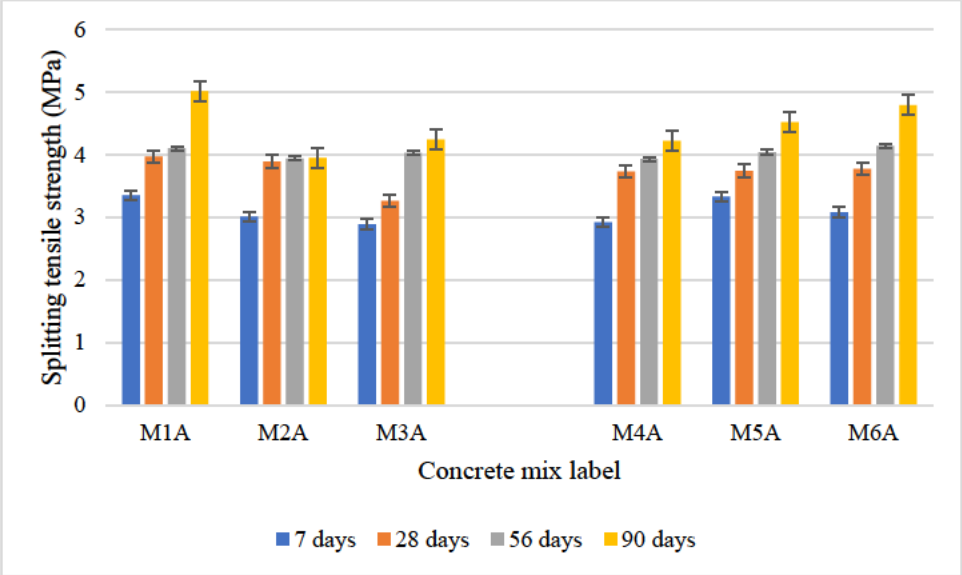

Figure 4.33: Splitting tensile strength of CWP concrete at 0.45 w/b ratio

The replacement of GGBS with CWP results in a decrease in early-age strength as the CWP content increases. For example, M1A achieves a tensile strength of 3.4 MPa at 7 days, while M2A and M3A reach 3.0 MPa and 2.9 MPa, respectively. However, at later ages, the strength progression variably improves. By 90 days, the reference mix M1A achieves the highest tensile strength of 5.0 MPa, while M3A surpasses M2A, reaching 4.24 MPa compared to 4.0 MPa. For LSP replacement, the reference mix M4A exhibits the lowest early-age strength of 2.9 MPa, while M5A and M6A achieve higher strengths of 3.3 MPa and 3.1 MPa, respectively. By 90 days, M6A shows the highest tensile strength of 4.8 MPa, demonstrating the positive effect of higher CWP content in enhancing long-term performance.

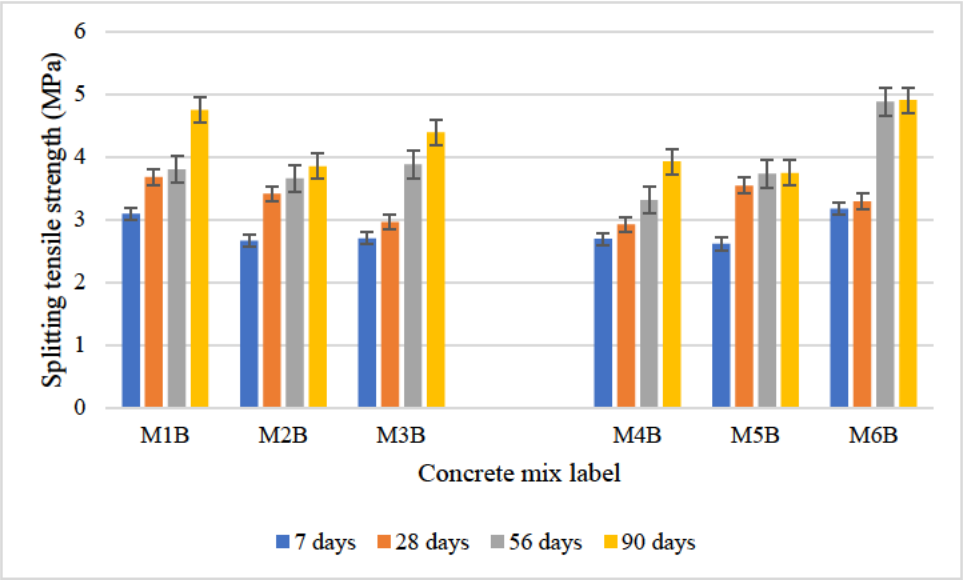

Figure 4.34: Splitting tensile strength of CWP concrete at 0.5 w/b ratio

Similar trends are observed at the 0.50 w/b ratio, as shown in Figure 4.34. For GGBS replacement, M1B records the highest early-age tensile strength of 3.1 MPa, while M2B and M3B achieve 2.7 MPa and 2.7 MPa, respectively. By 90 days, reference mix M1B reaches 4.8 MPa, maintaining its superior performance, while M3B surpasses M2B with 4.4 MPa compared to 3.9 MPa. For LSP replacement, early-age strengths are relatively low for reference mix M4B (2.8 MPa) and 5% CWP, M5B (2.6 MPa), while M6B (7% CWP) achieves a higher tensile strength of 3.2 MPa at 7 days. By 90 days, M6B demonstrates a significant improvement, reaching 4.9 MPa, which is higher than M4B and M5B.

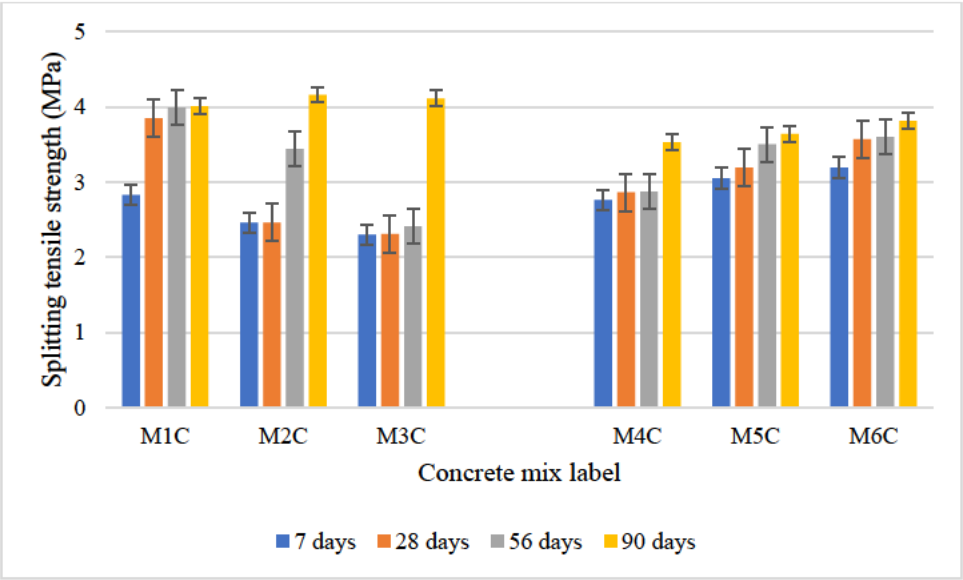

Figure 4.35: Splitting tensile strength of CWP concrete at 0.55 w/b ratio

At the 0.55 w/b ratio presented in Figure 4.35, the splitting tensile strength shows a consistent decline with increasing CWP content for GGBS replacement. M1C records the highest early-age strength of 2.8 MPa, while M2C and M3C achieve 2.5 MPa and 2.3 MPa, respectively. However, by 90 days, the strength progression becomes more uniform, with M2C achieving the highest tensile strength of 4.2 MPa, followed by M1C (4.0 MPa) and M3C (4.1 MPa). For LSP replacement, M4C shows the lowest early-age strength of 2.8 MPa, while M5C and M6C achieve 3.1 MPa and 3.2 MPa, respectively. By 90 days, M6C exhibits the highest tensile strength of 3.8 MPa, followed by M5C (3.6 MPa) and M4C (3.5 MPa).

The splitting tensile strength exhibited a more uniform early-age performance across GGBS, and limestone systems compared to compressive strength, where early-age strength was higher in GGBS mixes. However, long-term tensile strength gains were more pronounced in LSP-based mixes (for instance M6A). Both compressive and tensile strengths showed a decline in early-age performance with increasing CWP content in GGBS mixes. However, LSP-based mixes (especially M6B and M6C) demonstrated improved tensile strength at later curing ages.

Overall, early-age tensile strength was higher in mixes with lower CWP content when replacing GGBS, whereas higher CWP levels enhanced both early age and long-term strength in LSP-based systems. The strength progression from 7 to 90 days highlights the pozzolanic activity of CWP, which significantly contributes to tensile strength development, particularly in limestone replacement systems.

4.5.1 Rate of change of splitting tensile strength in CWP concrete over curing days

The rate of change of splitting tensile strength in CWP concrete over curing days is illustrated by the regression line plots and equations in this section. The slopes of the equations predict the rate of strength development, while the R^2 values indicate the reliability of the linear relationships.

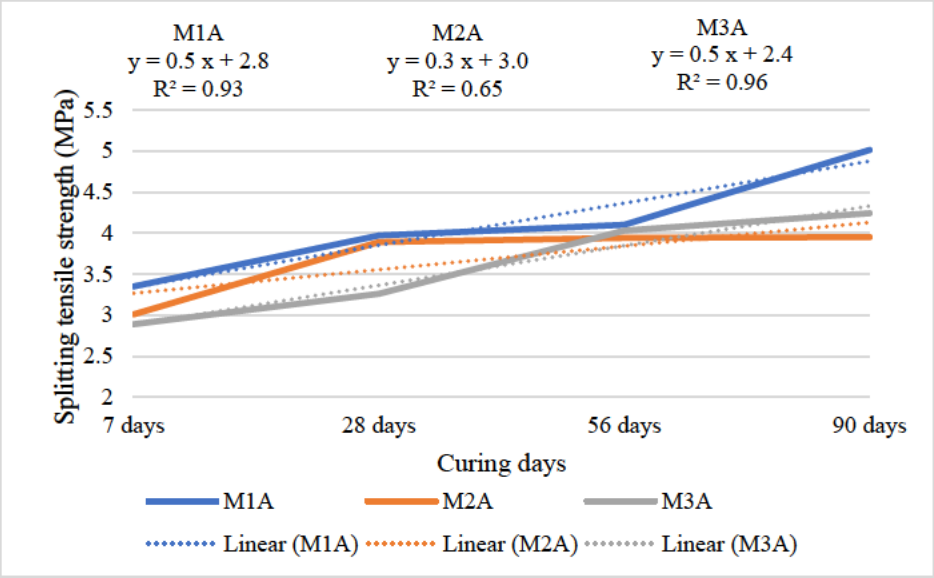

Figure 4.36: Splitting tensile strength of GGBS – CWP base concrete at 0.45 w/b ratio

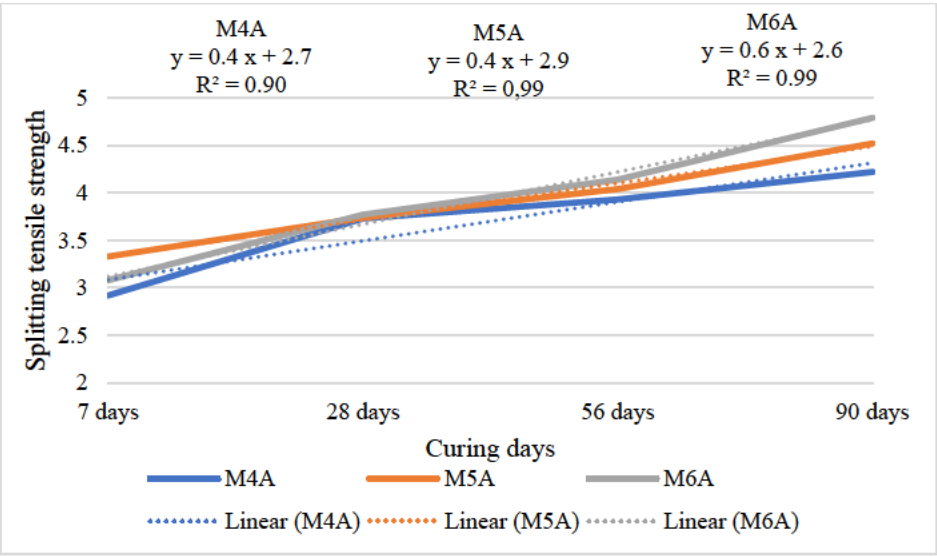

Figure 4.37: Splitting tensile strength of LSP – CWP base concrete at 0.45 w/b ratio

Figure 4.36 and Figure 4.37 show the splitting tensile strength development over time for concrete mixes with a 0.45 w/b ratio. For GGBS replacement with CWP, the reference mix (M1A) shows the highest splitting tensile strength gain, with an R^2 of 0.93 and a steady slope of 0.5, reflecting a relatively efficient hydration rate. However, 10% CWP replacement (M2A) slows strength gain significantly (slope: 0.3, R^2: 0.65), indicating a negative impact on tensile development. At 20% CWP (M3A), strength gain improves (slope: 0.5, R^2: 0.96), suggesting better long-term performance despite lower early-age strength.

For limestone replacement, reference mix, M4A shows moderate strength progression (slope: 0.4, R^2: 0.90), reflecting the filler effect of LSP. M5A (5% CWP) has a slightly lower slope

(0.4) but a higher intercept, indicating better early-age performance. M6A (7% CWP) achieves the highest strength gain rate (slope: 0.6, R^2: 0.99), highlighting the beneficial long-term impact of higher CWP content.

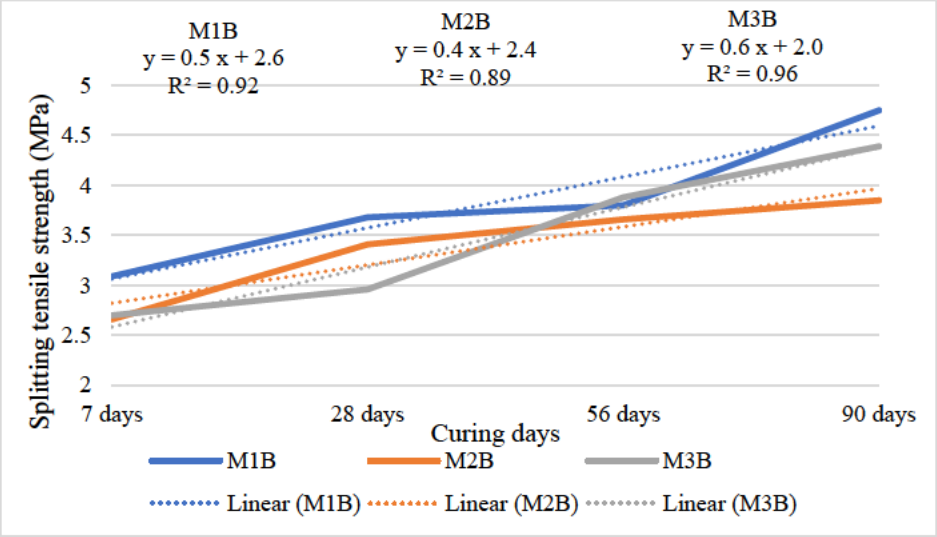

Figure 4.38: Splitting tensile strength of GGBS – CWP base concrete at 0.5 w/b ratio

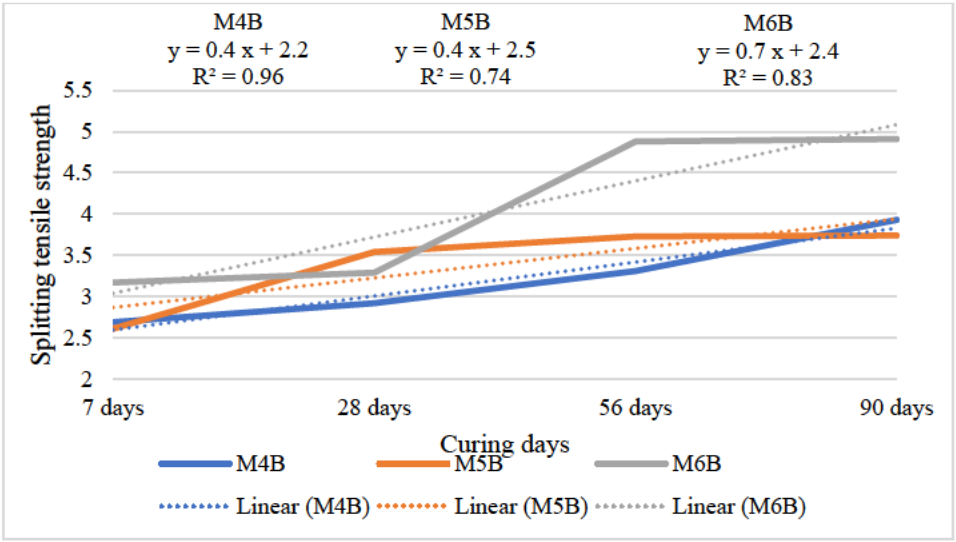

Figure 4.39: Splitting tensile strength of LSP – CWP base concrete at 0.5 w/b ratio

Figure 4.38 and 4.39 show the splitting tensile strength development over time for concrete mixes with a 0.50 w/b ratio. For GGBS replacement with CWP, the reference mix M1B exhibits the highest tensile strength gain, with a slope of 0.5 (R^2: 0.92), demonstrating the effectiveness of GGBS in enhancing strength over time. At 10% CWP replacement (M2B), the rate of strength gains decreases (slope: 0.4, R^2: 0.89), reflecting the negative impact of partial GGBS replacement. However, with 20% CWP (M3B), strength gain improves (slope: 0.6, R^2: 0.96),

suggesting that higher CWP content contributes positively to long-term performance despite lower early-age strength.

For limestone replacement, M4B shows a moderate strength gain (slope: 0.4, R^2: 0.96), driven by the filler effect of LSP. M5B (5% CWP) has a slightly lower slope (0.4, R^2: 0.74) but a higher intercept, indicating better early-age performance due to the combined effects of CWP and limestone. M6B (7% CWP) achieves the highest tensile strength gain among the LSP-based mixes (slope: 0.7, R^2: 0.83), highlighting the enhanced long-term strength contribution of CWP.

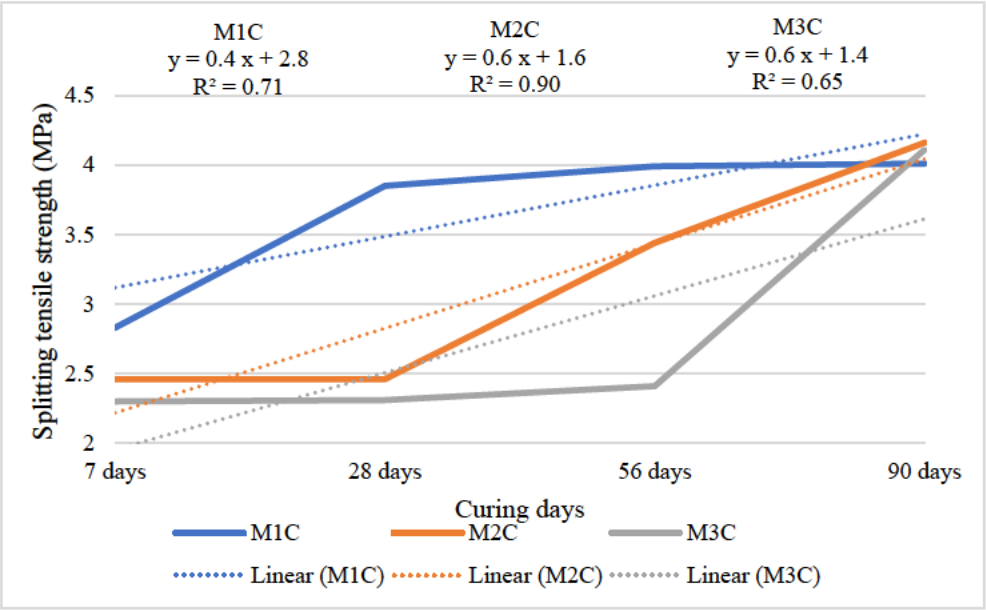

Figure 4.40: Splitting tensile strength of GGBS – CWP base concrete at 0.55 w/b ratio

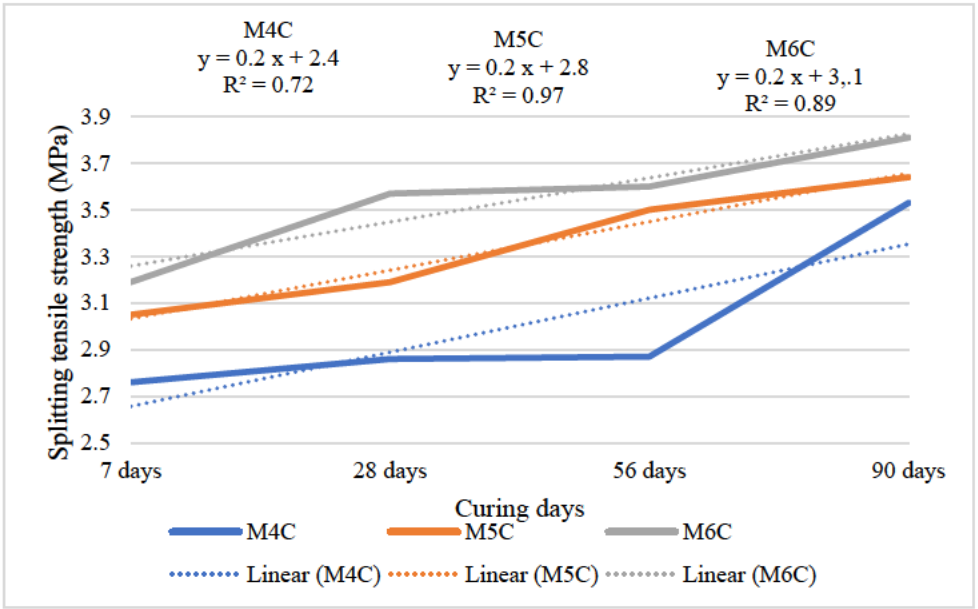

Figure 4.41: Splitting tensile strength of LSP – CWP base concrete at 0.55 w/b ratio

Figure 4.40 and 4.41 show the splitting tensile strength development over time for concrete mixes with a 0.55 w/b ratio. For GGBS replacement with CWP, M1C shows a moderate tensile strength gain (slope: 0.4, R^2: 0.71), indicating steady progression driven by GGBS hydration and pozzolanic activity, though with some variability. M2C, with 10% CWP replacement, achieves the highest strength gain rate (slope: 0.6, $R^2 = 0.90$), highlighting the beneficial effect of partial CWP replacement. However, M3C (20% CWP) shows a lower rate of strength development (slope: 0.6, R^2: 0.65), suggesting that higher CWP content limits early-age strength while contributing to long-term performance with greater variability.

For limestone replacement, M4C has the lowest tensile strength gain rate (slope: 0.2, R^2: 0.72), reflecting the slow progression due to limestone's inert filler effect. M5C (5% CWP) shows a slightly higher rate (slope: 0.2, R^2: 0.97), indicating reliable strength improvement. M6C (7% CWP) achieves the highest rate of strength gain among LSP-based mixes (slope: 0.2, R^2: 0.89), emphasizing the positive influence of higher CWP content, particularly at later curing ages.

Overall, GGBS-based mixes exhibit higher early-age strength, though strength gain slows with increased CWP replacement. Among them, M1B achieves the highest rate of strength gain, M3B shows improved long-term performance, and M2C demonstrates the best overall tensile strength development. In contrast, LSP-based mixes benefit from higher CWP levels, with M6A and M6B exhibiting the most significant strength progression. M1C maintains steady performance, while M3C experiences reduced early-age strength gain. The high R^2 values across all cases confirm the reliability of the regression models in predicting tensile strength trends, highlighting the distinct roles of GGBS and LSP in shaping the tensile strength evolution of CWP concrete.

4.5.2 Regression analysis of splitting tensile strength of CWP concrete mixes against their reference mix

The regression analysis explores the relationship between the splitting tensile strength of CWP concrete mixes and their respective reference mixes across three w/b ratios (0.45, 0.50, and 0.55). The regression statistics presented in Table 4.9 compare the STS development of CWP-modified mixes to baseline mixes for GGBS replacement, while the figures illustrate regression line fit plots. The equations on these plots serve as predictive models for estimating the strength of CWP concrete based on its reference mix. The correlations observed in the linear regression models, as indicated by high R^2 values across all mixes, indicate their reliability in predicting strength development.

Table 4.9: Regression statistics of the splitting tensile strength of CWP concrete mixes against their reference mix for GGBS replacement

Concrete mix	Multiple R	R Square	Adjusted R square	Standard error	Observations
45 w/b ratio					
M2A vs M1A	0.76	0.58	0.38	0.36	4
M3A vs M1A	0.89	0.79	0.68	0.36	4
0.50 w/b ratio					
M2B vs M1B	0.89	0.78	0.67	0.30	4
M3B vs M1B	0.91	0.83	0.74	0.40	4
0.55 w/b ratio					
M2C vs M1C	0.64	0.41	0.11	0.78	4
M3C vs M1C	0.44	0.19	0.22	0.98	4

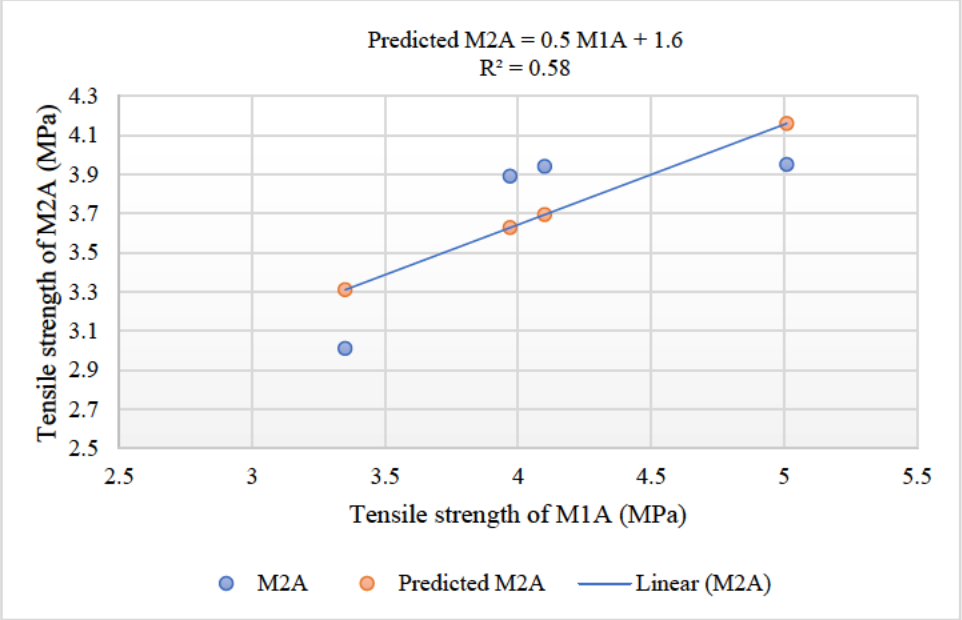

Figure 4.42: Regression line fit plot of M2A against M1A

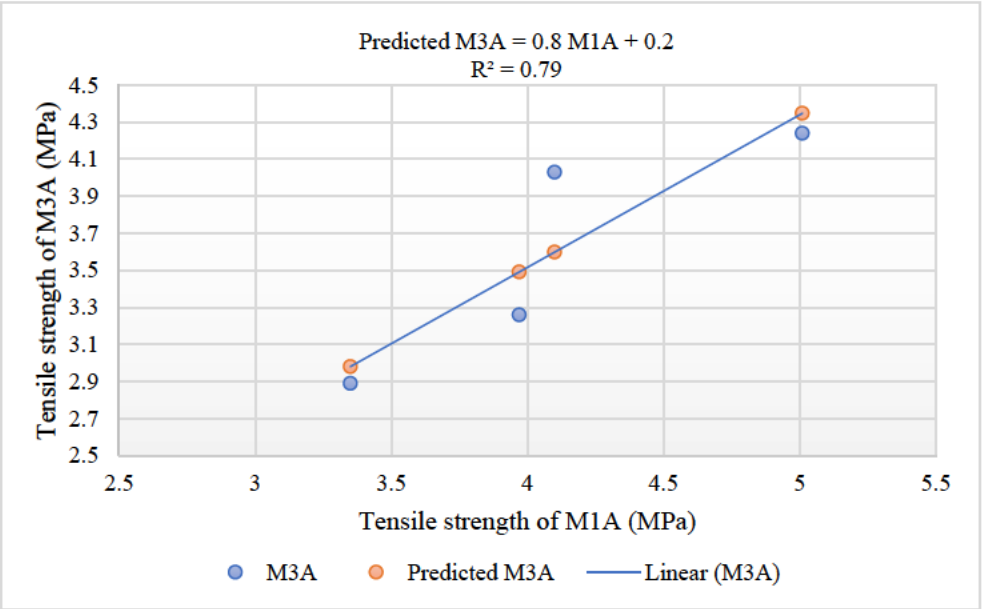

Figure 4.43: Regression line fit plot of M3A against M1A

For the 0.45 w/b ratio, M2A and M3A were compared to M1A as presented in Figure 4.42 and 4.43. The regression line for M2A has an R^2 value of 0.583. This indicates a moderate correlation between M2A and M1A, though the variability is relatively high as reflected by the standard error of 0.363 MPa. For M3A, the regression equation achieves an R^2 value of 0.786, showing a stronger correlation than M2A. The slope of 0.8235 indicates that M3A develops tensile strength at a comparable rate to M1A. The adjusted R^2 values of 0.375 for M2A and 0.679 for M3A further reflect the reliability of these models, with M3A demonstrating better predictability.

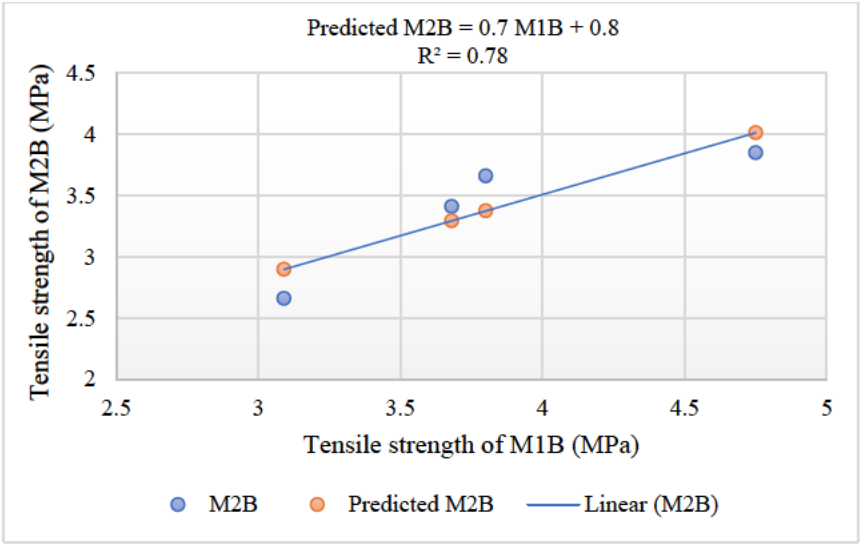

Figure 4.44: Regression line fit plot of M2B against M1B

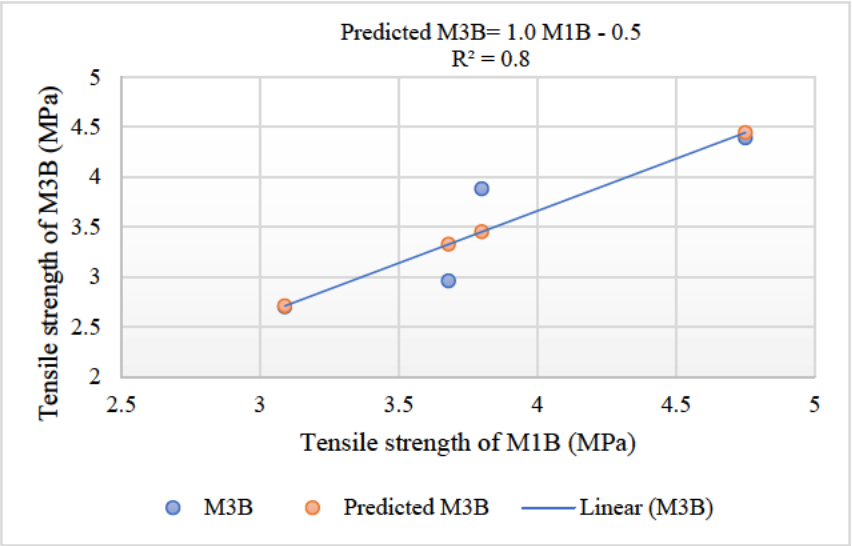

Figure 4.45: Regression line fit plot of M3B against M1B

At the 0.50 w/b ratio, M2B and M3B were compared to M1B as presented in Figure 4.44 and 4.45. M2B exhibits a regression equation of an R^2 value of 0.78, indicating a moderately strong correlation. The slope (0.7) is lower than M1B, suggesting a reduced rate of tensile strength development. For M3B, the regression line yields an R^2 value of 0.83, indicating a stronger relationship than M2B. The slope of 1.0 suggests that M3B slightly surpasses M1B in tensile strength development, although the early-age strength is lower. The adjusted R^2 values (0.67 for M2B and 0.74 for M3B) and the standard errors (0.3 MPa and 0.4 MPa, respectively) confirm the higher reliability of the M3B model.

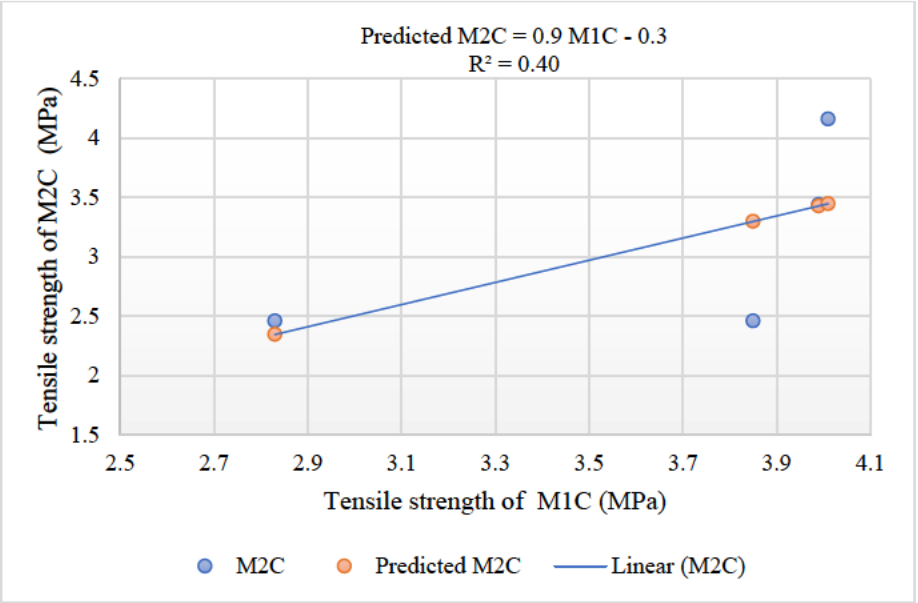

Figure 4.46: Regression line fit plot of M2C against M1C

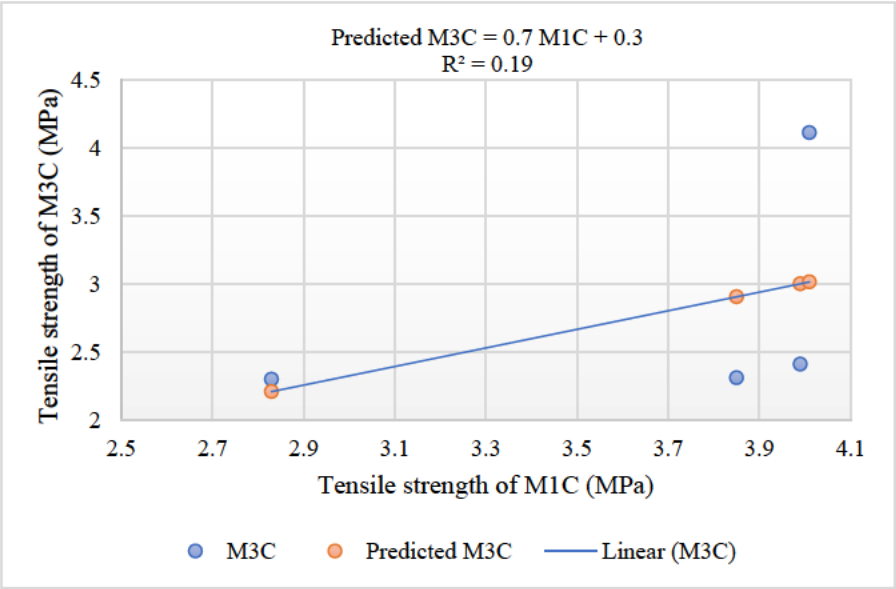

Figure 4.47: Regression line fit plot of M3C against M1C

The regression results for the 0.55 w/b ratio show weaker correlations as presented in Figure 4.46 and 4.47. M2C has an R^2 value of 0.41, reflecting a weak relationship with M1C. The slope of 0.9 suggests a relatively comparable rate of tensile strength development, but the high standard error of 0.8 MPa indicates significant variability. Similarly, M3C demonstrates an even weaker correlation, with R2 of 0.19. The slope (0.68) and high standard error (1.0 MPa) highlight the limited predictability of the model, suggesting that increased CWP content at this w/b ratio introduces substantial variability in tensile strength development.

Table 4.10 shows the regression statistics of the splitting tensile strength of CWP concrete mixes against their reference mix for LSP replacement. The regression analysis of splitting tensile strength for CWP concrete mixes with LSP replacement compares the performance of mixes M5 and M6 against their respective reference mixes (M4) across three w/b ratios: 0.45, 0.50, and 0.55. The results highlight the relationship between tensile strength development in CWP-modified mixes and their reference LSP-based concrete mixes.

Table 4.10: Regression statistics of the splitting tensile of CWP concrete mixes against their reference mix for LSP replacement

Concrete Mix	Multiple R	R Square	Adjusted R Square	Standard Error	Observations
0.45 w/b ratio					
M5A vs M4A	0.95	0.90	0.85	0.20	4
M6A vs M4A	0.97	0.93	0.90	0.23	4
0.50 w/b ratio					
M5B vs M4B	0.74	0.55	0.32	0.44	4
M6B vs M4B	0.88	0.78	0.66	0.56	4
0.55 w/b ratio					
M5C vs M4C	0.79	0.63	0.44	0.20	4
M6C vs M4C	0.79	0.62	0.43	0.20	4

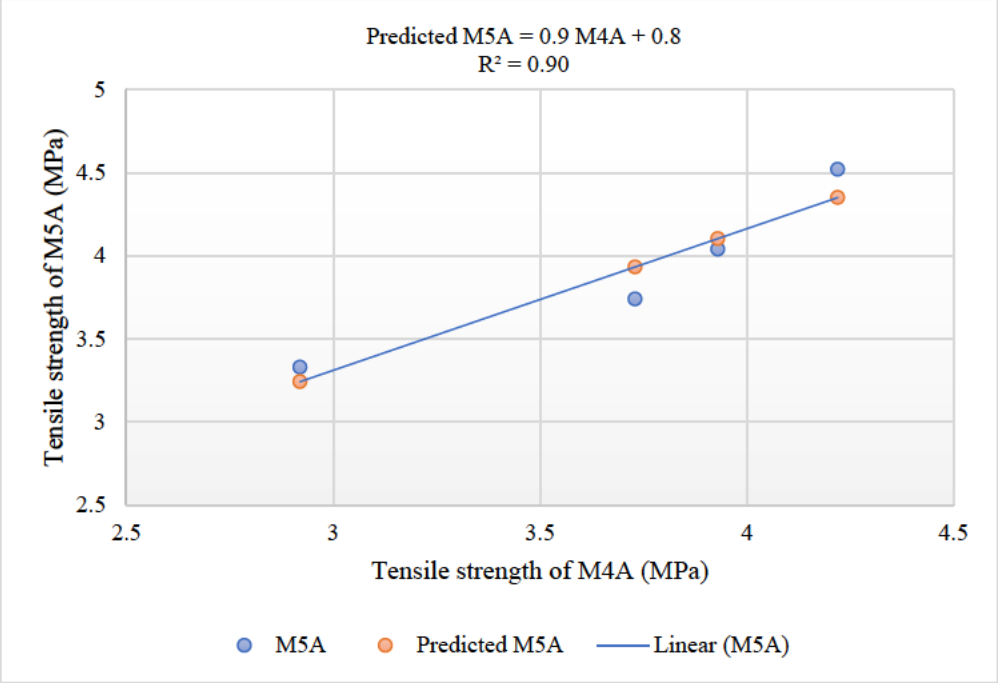

Figure 4.48: Regression line fit plot of M5A against M4A

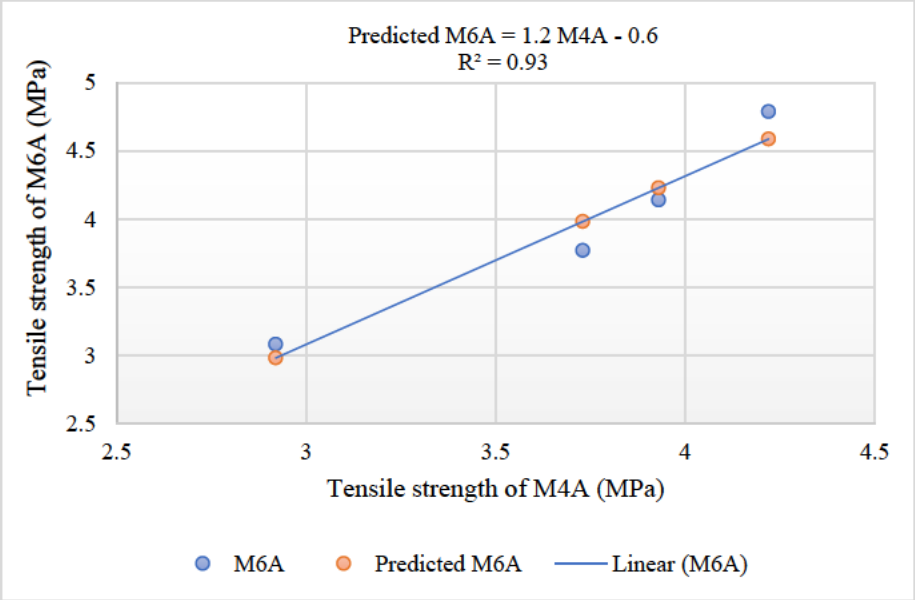

Figure 4.49: Regression line fit plot of M6A against M4A

For the 0.45 w/b ratio in Figure 4.48 and 4.49, the regression model for M5A vs. M4A has an R^2 value of 0.89, indicating a strong correlation between the two mixes. The slope of 0.85 reflects a high rate of strength gain in M5A relative to M4A, supported by a low standard error of 0.2 MPa. For M6A against M4A, the regression line has an R^2 value of 0.93. The higher slope of 1.2 suggests that M6A develops tensile strength more rapidly than M4A, despite the slightly higher standard error of 0.2 MPa. These results emphasize the positive impact of increased CWP content on tensile strength in mixes with a 0.45 w/b ratio.

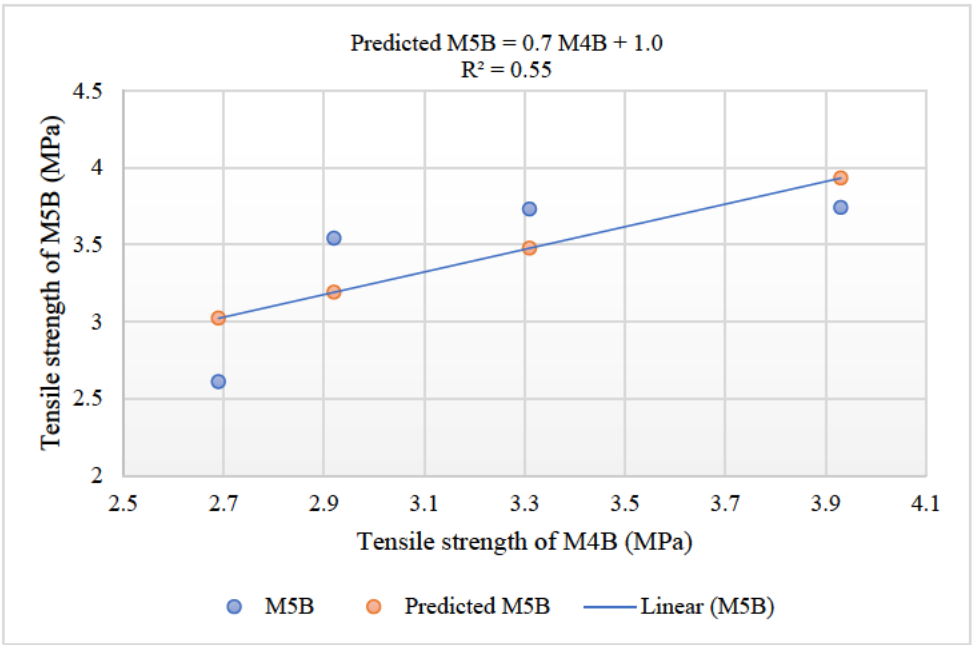

Figure 4.50: Regression line fit plot of M5B against M4B

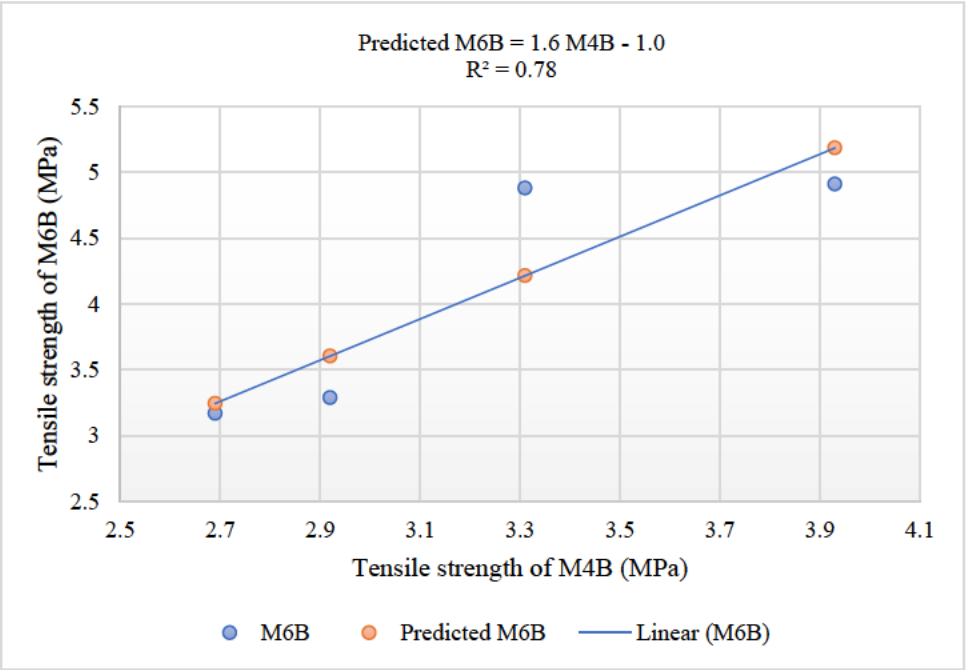

Figure 4.51: Regression line fit plot of M6B against M4B

At the 0.50 w/b ratio presented in Figure 4.50 and 4.51, the correlation between M5B and M4B is moderate, with an R^2 value of 0.55. The slope (0.7) reflects a slower rate of tensile strength gain, while the standard error of 0.4 MPa indicates greater variability. In contrast, M6B demonstrates a stronger relationship with M4B, as indicated by an R^2 value of 0.78. The slope (1.6) suggests a significantly faster rate of strength development, though the standard error of 0.6 MPa highlights some variability in the data.

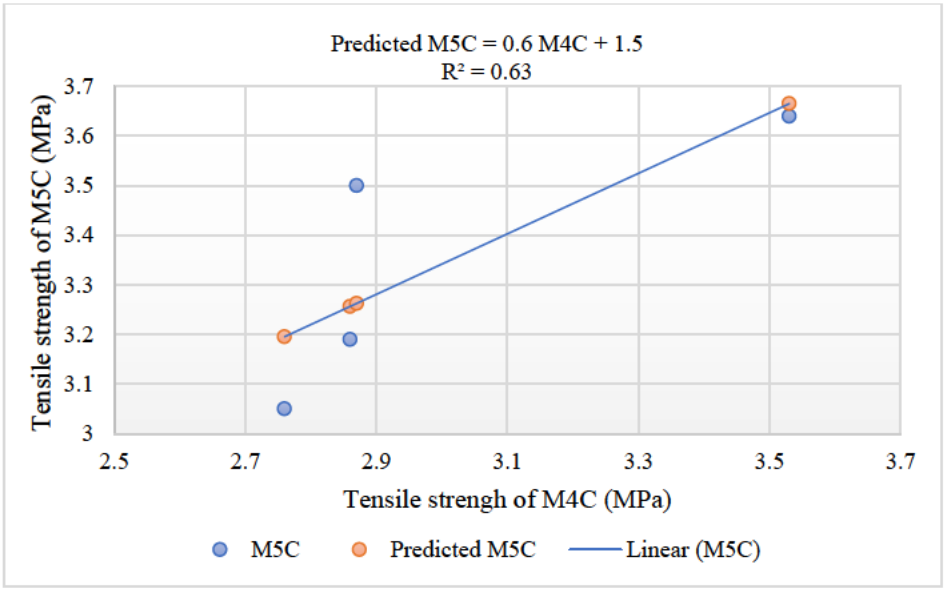

Figure 4.52: Regression line fit plot of M5C against M4C

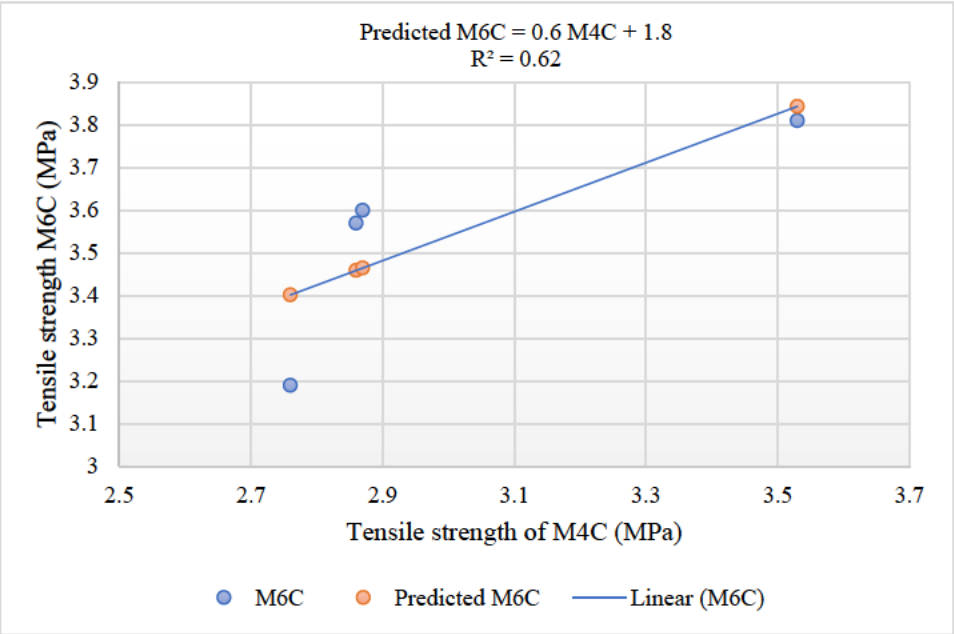

Figure 4.53: Regression line fit plot of M6C against M4C

For the 0.55 w/b ratio presented in Figure 4.52 and 4.53, the regression analysis for M5C vs. M4C results in an R^2 value of 0.63, indicating a moderate correlation. The slope of 0.61 reflects a reduced rate of strength development compared to the reference mix, M4C. The standard error of 0.2 MPa suggests moderate variability. Similarly, M6C vs M4C demonstrates an R^2 value of 0.62. The slope (0.57) is lower than M5C vs M4C, indicating a slower rate of tensile strength gain. The standard error of 0.2 MPa indicates slightly improved consistency compared to M5C.

The regression analysis reveals that the relationship between CWP concrete mixes and their reference mixes weakens as the w/b ratio increases. Models for the 0.45 and 0.50 w/b ratios exhibit stronger correlations and better predictability, with M3 and M6 mixes consistently outperforming M2 and M5 mixes, respectively, particularly at lower w/b ratios. This superior performance is attributed to higher CWP content, which enhances tensile strength development. However, at a 0.55 w/b ratio, the models become less reliable, likely due to increased variability introduced by higher water content and CWP levels. These findings emphasize the need to optimize CWP replacement levels and curing conditions to ensure consistent tensile strength development.

4.5.3 The relationship between splitting tensile strength and compressive strength

The correlation between compressive strength (f_c) and splitting tensile strength (f_{sp}) was evaluated using the empirical expression from ACI 318-19 (ACI 2019) in Equation 4-1.

$$f_{sp} = 0.56\sqrt{f_c} \quad 4\text{-}1$$

The $f_{sp}/\sqrt{f_c}$ ratio was calculated for the 7, 28, 56, and 90-days strengths of each mix. The $f_{sp}/\sqrt{f_c}$ ratio for the four ages was then averaged to obtain a single representative ratio per mix. These averages were compared with the ACI 318-19 reference value of 0.56, as presented in Table 4.11 to 4.13.

Table 4.11: Comparison of experimental $f_{sp}/\sqrt{f_c}$ with the ACI 318 model for 0.45 w/b ratio

Mix	Average Measured ($f_{sp}/\sqrt{f_c}$)	ACI Coefficient	Deviation
GGBS replacements			
M1A	0.54	0.56	Near ACI
M2A	0.50	0.56	Slightly below ACI
M3A	0.51	0.56	Slightly below ACI
LSP replacements			
M4A	0.47	0.56	Below ACI
M5A	0.49	0.56	Below ACI
M6A	0.49	0.56	Below ACI

Table 4.11 evaluates how the experimental $f_{sp}/\sqrt{f_c}$ ratios for 0.45 w/b concretes compare with the ACI-318 coefficient of 0.56, distinguishing between GGBS-based mixes (M1A–M3A) and LSP-based mixes (M4A–M6A). The GGBS reference mix M1A records 0.54, only 4% below 0.56. This indicates that pure GGBS substitution maintains the tensile–compressive strength relationship. As CWP replaces part of the GGBS (M2A, M3A), the ratio reduces to 0.50–0.51, suggesting that every 10% increment of CWP in a GGBS system reduces tensile efficiency by ~6 %. However, the LSP reference mix M4A shows 0.47, already 16 % beneath ACI, and mixes with CWP (M5A, M6A) hover around 0.49. These figures suggests that LSP mixes performs poorly in splitting tensile strength compared to CWP.

Table 4.12: Comparison of experimental fsp /√fc with the ACI 318 model for 0.50 w/b ratio

Mix	Average Measured ($f_{sp}/\sqrt{f_c}$)	ACI Coefficient	Deviation
GGBS replacements			
M1B	0.54	0.56	Near ACI
M2B	0.51	0.56	Slightly below ACI
M3B	0.51	0.56	Slightly below ACI
LSP replacements			
M4B	0.44	0.56	Below ACI
M5B	0.46	0.56	Below ACI
M6B	0.54	0.56	Near ACI

For the 0.50 w/b ratio (Table 4.13), the measured $f_{sp}/\sqrt{f_c}$ ratios again diverge by binder type. In the GGBS group, the reference mix M1B matches its 0.45 w/b counterpart at 0.54, also within 4% of the ACI-318 value, confirming that w/b increase from 0.45 to 0.50 does not diminish tensile efficiency when only GGBS is present. Introducing CWP lowers the ratio to 0.51 in both M2B and M3B, similar to the ∼6–8 % reduction observed at 0.45 w/b ratio and showing that the influence of CWP is largely independent of w/b in GGBS-based mixes. The LSP mixes behave differently. The reference mix M4B drops to 0.44, a 21 % drop relative to ACI. This is also similar to what is observed at 0.45 w/b. The 5% replacement (M5B) increases the ratio to 0.46, but only the mix with 7 % CWP and 3 % LSP (M6B) recovers to 0.54, almost equalling the GGBS reference. These results suggest that CWP can partly offset LSP-induced tensile deficits at 0.50 w/b.

Table 4.13: Comparison of experimental $f_{sp}/\sqrt{f_c}$ with the ACI 318 model for 0.55 w/b ratio

Mix	Average Measured ($f_{sp}/\sqrt{f_c}$)	ACI Coefficient	Deviation
GGBS replacements			
M1C	0.54	0.56	Slightly below ACI
M2C	0.47	0.56	Below ACI
M3C	0.44	0.56	Below ACI
LSP replacements			
M4C	0.43	0.56	Below ACI
M5C	0.48	0.56	Below ACI
M6C	0.49	0.56	Below ACI

At the 0.55 w/b ratio in Table 4.13, the GGBS-based reference mix M1C still attains 0.54 as in previous w/b ratios. Furthermore, 10 % CWP drops the number sharply to 0.47 in M2C and 0.44 in M3C. This shows that CWP consistently reduces the splitting tensile strength on GGBS-based concrete. This is likely due to the inferior pozzolanic reactivity of CWP compared to GGBS. The LSP-based mixes also behave

The LSP-based mixes at 0.55 w/b also mirror the trends seen at lower w/b ratios. The reference blend M4C gives the lowest $f_{sp}/\sqrt{f_c}$ ratio (0.43), deviating most from the ACI benchmark of 0.56. Replacing part of the LSP with CWP raises the ratio to 0.48 in M5C and 0.49 in M6C, indicating that CWP improves tensile efficiency in LSP concretes. This gain supports the higher compressive and splitting tensile strengths observed for CWP mixes relative to the LSP reference. This confirms the superior pozzolanic reactivity of CWP and its greater contribution to overall strength compared to LSP alone.

4.6 Density of Hardened Concrete

Figure 4.57 to 4.59 illustrate the hardened concrete density for the three sets of mixes prepared with w/b ratios of 0.45 (M1A–M6A), 0.50 (M1B–M6B), and 0.55 (M1C–M6C) over different curing periods (7, 28, 56, and 90 days). Across all the mixes, the concrete density shows minimal variation regardless of the curing age or w/b ratio. This consistency indicates that the replacement of a certain percentage of the binder with CWP does not significantly affect the density of the concrete.

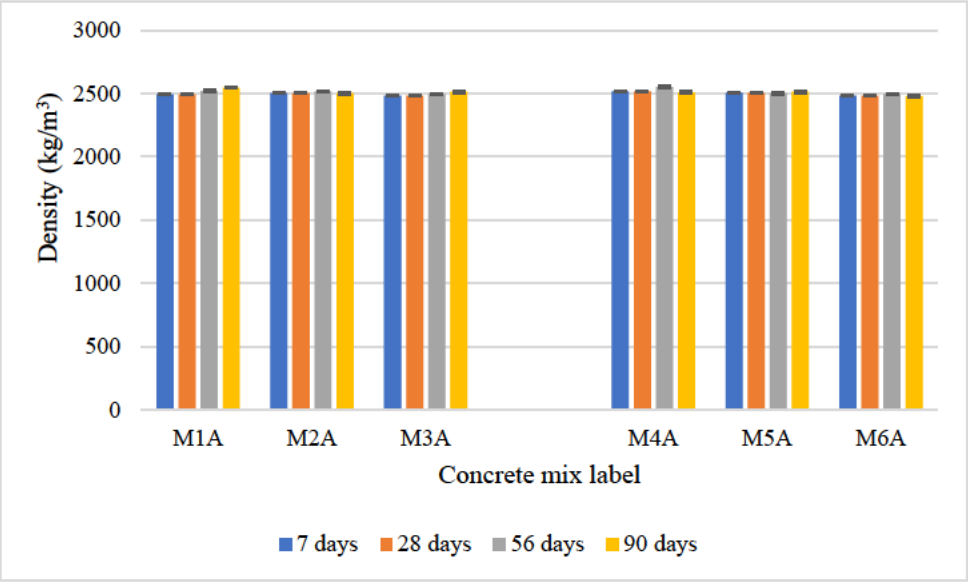

Figure 4.54: Density of hardened concrete at 0.45 w/b ratio

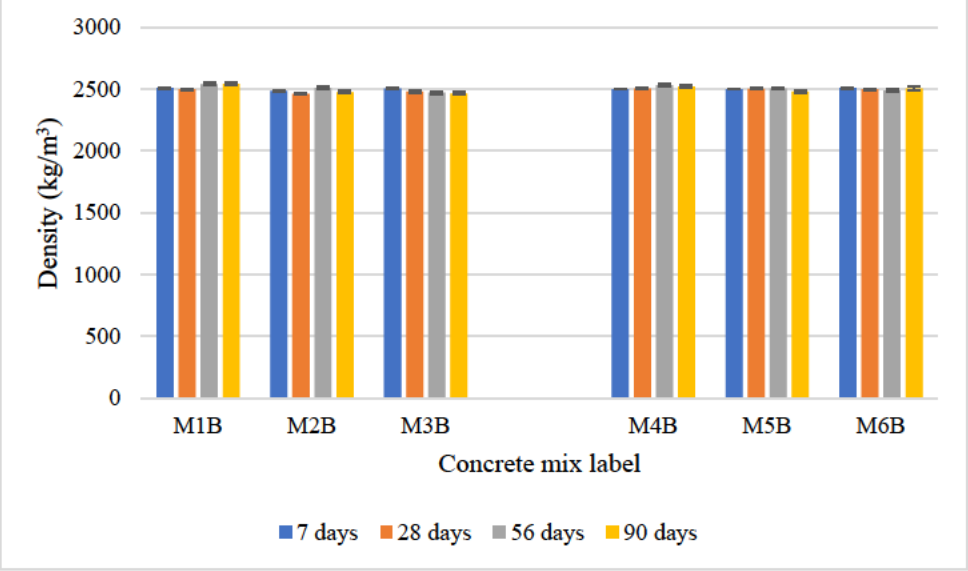

Figure 4.55: Density of hardened concrete at 0.5 w/b ratio

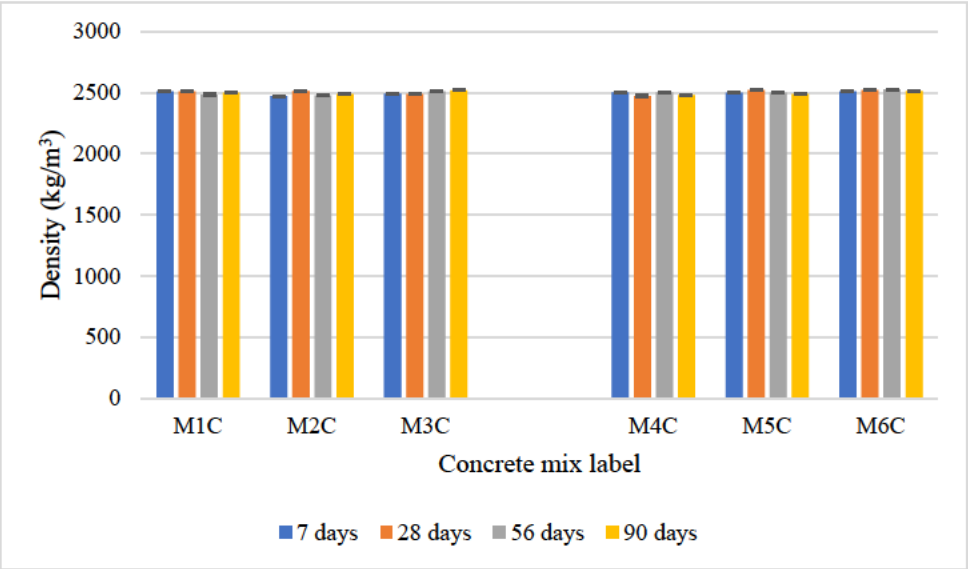

Figure 4.56: Density of hardened concrete at 0.55 w/b ratio

The CWP has a relatively low density compared to PC, GGBS and LSP. However, its proportion in the mix is insufficient to produce a noticeable impact on the overall concrete density. Additionally, the substitution of CWP does not introduce substantial changes in the mix composition that would influence density, as the other mix components (aggregates, water, and remaining cement) dominate the bulk density of the concrete.

The small variations observed in the graphs can be attributed to experimental or environmental factors during curing rather than the material properties of CWP. Across all curing periods, the densities of the mixes remain close to 2500 kg/m³, consistent with the typical density of normal-weight concrete.

The use of CWP as a partial binder replacement does not significantly influence the hard concrete density. This result highlights that CWP can be incorporated into concrete mixes without compromising the material's density, making it a viable sustainable option for reducing cement content in concrete while maintaining key physical properties.

4.7 Durability of Concrete

This section presents the durability of CWP concrete in comparison with their reference mixes. The South African durability indices were used. South Africa employs a performance-based design approach incorporating durability indices such as the Oxygen Permeability Index (OPI), Water Sorptivity Index (WSI), and Chloride Conductivity Index (CCI). These indices, as proposed by Alexander *et al.* (2008), and Alexander *et al.* (1999), provide a systematic method for assessing the resistance of the concrete to deterioration mechanisms like permeability,

sorption, and chloride ingress. These indices provide quantitative measures of the resistance of concrete to the ingress of aggressive agents and reflect both material characteristics and construction quality as shown in the Table 4.11. The OPI measured as the negative logarithm of the D'Arcy permeability coefficient, typically ranges from 8 to 11. Higher values indicate lower permeability and enhanced durability. For example, an OPI of 11 corresponds to highly impermeable concrete, suitable for exposure to aggressive environments, whereas values closer to 8 indicate higher permeability and reduced durability. The WSI quantifies the rate of water absorption normalized by porosity, typically ranging from 5 mm/h$^{0.5}$ to 20 mm/h$^{0.5}$. Lower values (such as 5 mm/h$^{0.5}$) suggest well-cured concrete with superior resistance to water ingress, while higher values (such as 20 mm/h$^{0.5}$) are indicative of low-quality concrete with increased vulnerability to water penetration. The CCI measures the electrical conductivity of concrete saturated with a chloride solution, reflecting its resistance to chloride ingress. The CCI values range from less than 0.5 mS/cm for highly chloride-resistant concrete such as slag to over 2.5 mS/cm for ordinary PC concretes with lower resistance to chloride penetration. Lower CCI values denote better durability in chloride-laden environments, such as marine conditions. Porosity, a key structural parameter, influences all these indices. Lower porosity corresponds to denser concrete, which inherently exhibits lower permeability, sorptivity, and conductivity, contributing to improved durability. In this discussion, the experimental results of these indices are interpreted within their respective ranges to evaluate the performance of concrete. This analysis highlights the relationship between these indices, the concrete's microstructure, and its durability in various environmental conditions.

Table 4.14: Concrete quality grading for durability classification using index values (Alexander, Mackechnie, and Ballim, 1999)

Concrete quality	OPI	WSI	CCI
Excellent	> 10	< 6	< 0.75
Good	9.5 – 10	6 – 10	0.75 – 1.5
Poor	9 – 9.5	10 – 15	1.5 – 2.5
Very poor	< 9	> 15	> 2.5

4.7.1 Oxygen permeability index (OPI)

Figure 4.60 presents the graph of OPI at a 0.45 w/b. It illustrates the OPI for replacement of GGBS and LSP with varying percentages of CWP assessed at 28 and 90 days. Mix M1A, the reference GGBS based mix, shows an OPI value of approximately 9.99 at 28 days, and increases to 10.18 at 90 days. When 10% and 20% of GGBS are replaced with CWP in M2A and M3A, the OPI values slightly increase at 28 days to 10.66 and 10.55, respectively. However, at 90

days, these values reduce slightly to 10.36 and 10.48, remaining close to the reference mix. These results indicate that replacing GGBS with CWP has a marginal impact on permeability, with OPI values staying within the "good" to "excellent" range, signifying low permeability and enhanced durability. Mix M4A, reference LSP mix demonstrates an OPI of 10.65 at 28 days, decreasing slightly to 10.35 at 90 days. When 5% and 7% CWP are added (M5A and M6A), the OPI values at 28 days range from 9.67 to 10.26, and at 90 days, they range from 10.38 to 10.40. These results indicate a notable improvement in permeability when CWP is incorporated, reducing capillary porosity and enhancing durability compared to LSP alone. The higher OPI values for M5A and M6A suggest that CWP provides some pozzolanic activity, unlike LSP, leading to better densification of the concrete matrix.

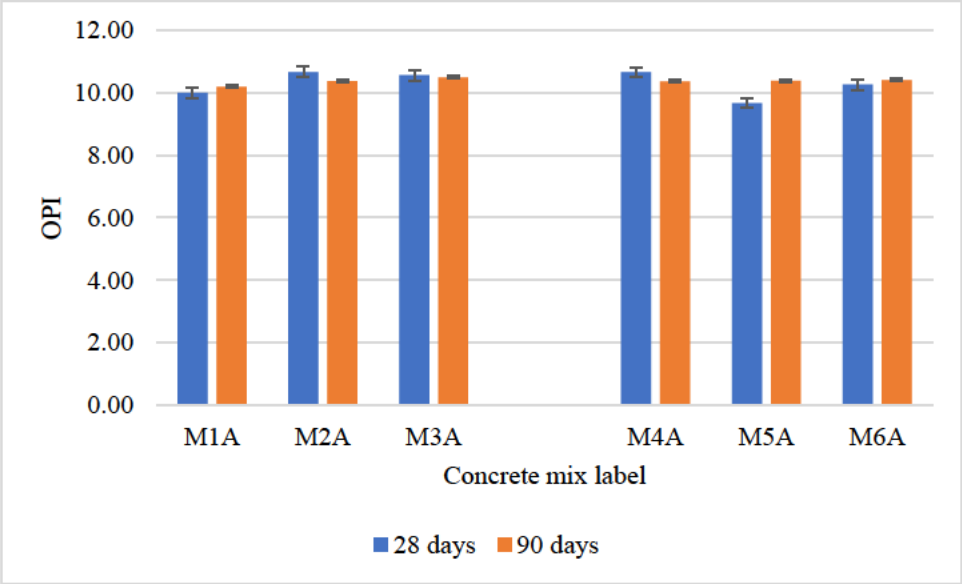

Figure 4.57: OPI of concrete at 0.45 w/b ratio

The OPI of concrete at 0.50 w/b ratio is presented in Figure 4.61. Mix M1B, the reference GGBS-based mix achieves an OPI of 10.47 at 28 days and 10.46 at 90 days. When 10% and 20% of GGBS are replaced with CWP in M2B and M3B, the OPI values demonstrate a slight decrease in permeability. At 28 days, M2B records an OPI of 10.08, and M3B achieves the highest OPI among the GGBS-CWP blends at 10.85. By 90 days, the OPI values for M2B and M3B are 10.42 and 10.68, respectively, reflecting continued hydration and pozzolanic reactions. These results confirm that replacing GGBS with up to 20% CWP enhances concrete's durability, maintaining OPI values well within the "good" to "excellent" range (Table 4.11).

Mix M4B, the LSP reference mix, achieves an OPI of 10.12 at 28 days, increasing slightly to 10.35 at 90 days. However, replacing a portion of LSP with CWP significantly improves OPI

values. Mix M5B (5% CWP) achieves an OPI of 10.68 at 28 days, increasing slightly to 10.38 at 90 days. Mix M6B (7% CWP) shows further improvement, with an OPI of 10.24 at 28 days, increasing to 10.53 at 90 days. These results indicate that CWP contributes to reduced permeability and improved microstructural refinement, surpassing the performance of LSP alone.

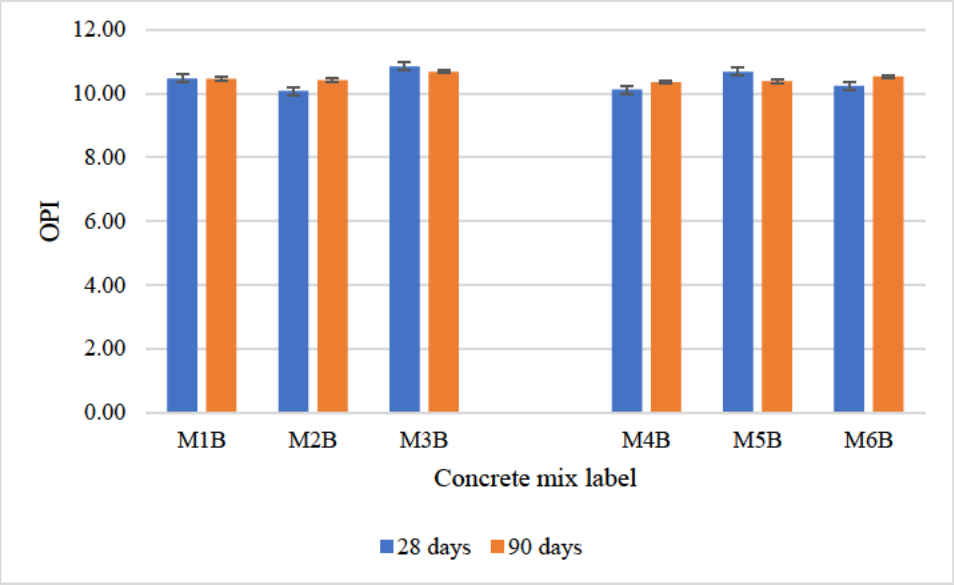

Figure 4.58: OPI of concrete at 0.50 w/b ratio

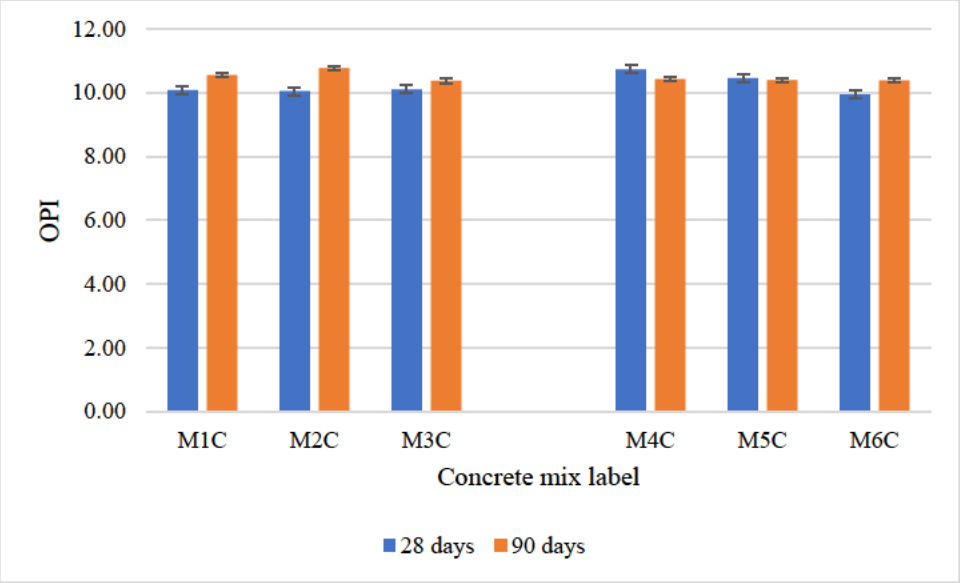

Figure 4.59: OPI of concrete at 0.55 w/b ratio

Figure 4.62 illustrates the effects of replacing GGBS and LSP with CWP on concrete OPI at 0.55 w/b. Mix M1C shows an OPI of 10.08 at 28 days, increasing significantly to 10.55 at 90 days. When 10% and 20% of GGBS are replaced with CWP in M2C and M3C, the OPI values

remain relatively stable, with only little variations. At 28 days, M2C records an OPI of 10.05, while M3C achieves 10.10. By 90 days, these values increase to 10.77 for M2C and 10.37 for M3C. These results demonstrate that replacing up to 20% of GGBS with CWP maintains or slightly enhances durability, with OPI values firmly within the "good" to "excellent" range. The higher OPI of M2C at 90 days suggests an optimal balance between GGBS and CWP in improving microstructural densification. Mix M4C, LSP reference mix achieves an OPI of 10.73 at 28 days, decreasing slightly to 10.42 at 90 days. This indicates a moderate improvement in permeability due to the filler effect of LSP, although the lack of pozzolanic activity limits long-term performance. When LSP is partially replaced with CWP, as in M5C (5% CWP) and M6C (7% CWP), the OPI values show varying effects. At 28 days, M5C achieves an OPI of 10.46, while M6C records a lower value of 9.94. By 90 days, the OPI for M5C decreases marginally to 10.39, and for M6C, it increases slightly to 10.39. These results suggest that incorporating CWP into LSP mixes provides some improvement in durability, particularly for M5C, which exhibits a balanced blend of limestone and CWP. However, higher percentages of CWP (as in M6C) may reduce the effectiveness due to its particle size or reactivity limitations.

Across all mixes, OPI values generally increase from 28 to 90 days, reflecting the continued hydration and secondary reactions that improve concrete's microstructure. The GGBS mixes consistently demonstrate higher OPI values than the LSP mixes, showcasing the superior pozzolanic properties of GGBS. The addition of CWP maintains or slightly enhances durability in both replacement scenarios, with M2C and M5C showing optimal performance at 90 days.

4.7.2 Water sorptivity index (WSI)

Figure 4.63 presents the WSI of CWP concrete at 0.45 w/b. Mix M1A, reference GGBS mix achieves a WSI of 6.73 mm/hr$^{0.5}$ at 28 days, increasing slightly to 7.70 mm/hr$^{0.5}$ at 90 days. When 10% and 20% of GGBS are replaced with CWP in M2A and M3A, the WSI values vary significantly. At 28 days, M2A records a higher WSI of 7.80 mm/hr$^{0.5}$, while M3A achieves 7.65 mm/hr$^{0.5}$. However, by 90 days, M2A shows a notable reduction in WSI to 6.23 mm/hr$^{0.5}$, reflecting significant improvement in water resistance over time. Conversely, M3A experiences an increase in WSI to 8.84 mm/hr$^{0.5}$ at 90 days, suggesting that replacing 20% of GGBS with CWP may not be as effective in reducing water absorption. These results suggest that a 10% replacement of GGBS with CWP improves water resistance in concrete. Mix M4A, reference LSP-based mix, achieves a WSI of 7.95 mm/hr$^{0.5}$ at 28 days, increasing significantly to 9.37 mm/hr$^{0.5}$ at 90 days. This reflects the limited ability of LSP to improve water resistance, as it primarily acts as a filler without contributing to hydration or microstructural refinement. When

LSP is partially replaced with CWP, as in M5A (5% CWP) and M6A (7% CWP), the WSI values improve slightly. At 28 days, M5A records a WSI of 8.86 mm/hr$^{0.5}$, while M6A achieves 7.59 mm/hr$^{0.5}$. By 90 days, M5A decreases marginally to 9.35 mm/hr$^{0.5}$, while M6A increases slightly to 8.78 mm/hr$^{0.5}$. These results indicate that replacing LSP with CWP moderately enhances water resistance, especially for M6A, where the WSI values remain relatively lower compared to M4A.

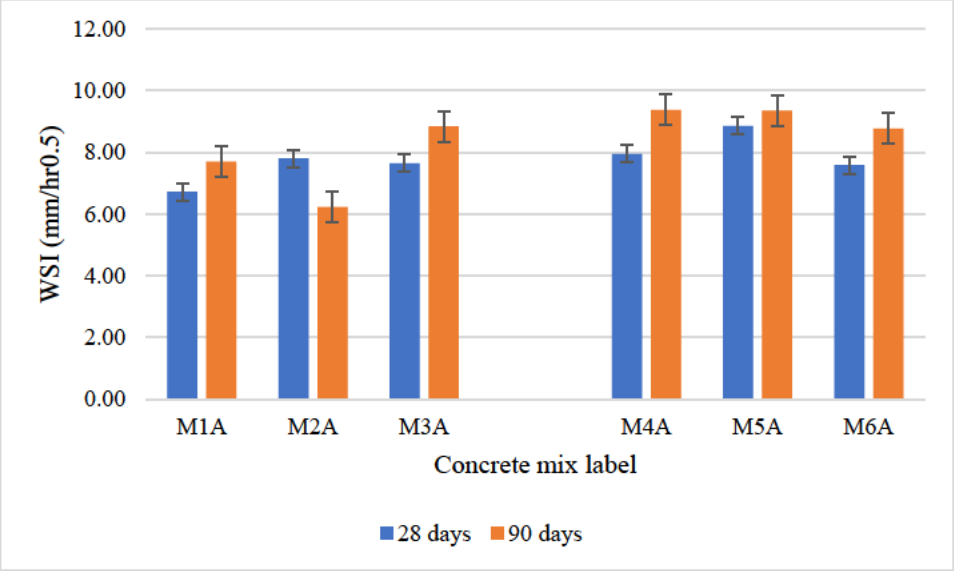

Figure 4.60: WSI of concrete at 0.45 w/b ratio

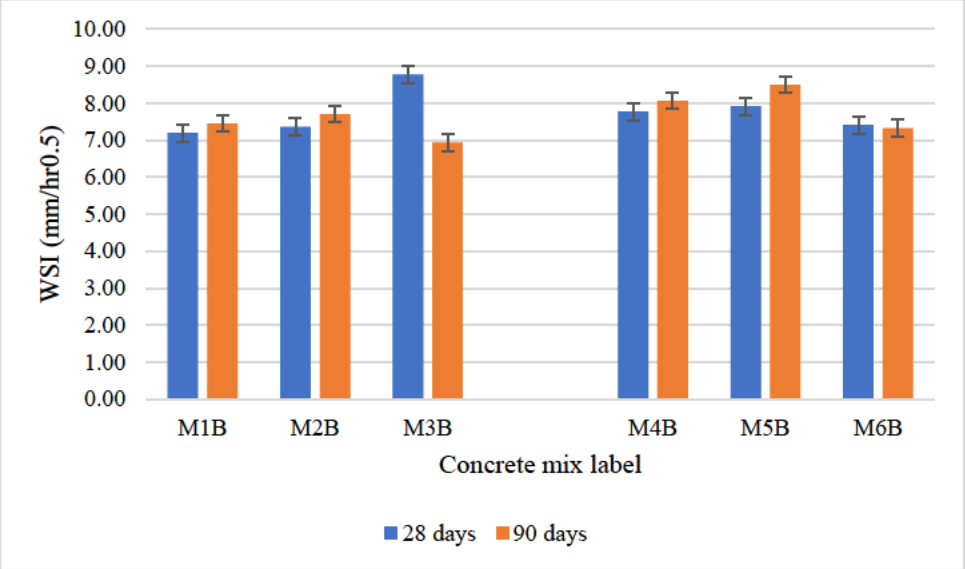

Figure 4.61: WSI of concrete at 0.50 w/b ratio

Figure 4.64 presents the WSI of CWP concrete at 0.50 w/b ratio. Mix M1B, reference GGBS-based mix, records a WSI of 7.20 mm/hr$^{0.5}$ at 28 days, increasing slightly to 7.45 mm/hr$^{0.5}$ at 90 days. When 10% and 20% of GGBS are replaced with CWP, as in M2B and M3B, the WSI

values show variations. At 28 days, M2B records a WSI of 7.37 mm/hr$^{0.5}$, slightly higher than M1B, while M3B shows a higher WSI of 8.77 mm/hr$^{0.5}$, indicating increased water absorption initially. By 90 days, the WSI for M2B increases marginally to 7.70 mm/hr$^{0.5}$, while M3B significantly improves to 6.94 mm/hr$^{0.5}$, demonstrating enhanced water resistance over time. These results indicate that replacing 20% of GGBS with CWP (M3B) yields significant long-term durability benefits, likely due to the gradual pozzolanic reaction of CWP improving the concrete matrix. Mix M4B, reference LSP-based mix, records a WSI of 7.78 mm/hr$^{0.5}$ at 28 days, increasing to 8.07 mm/hr$^{0.5}$ at 90 days. When 5% and 7% of LSP are replaced with CWP in M5B and M6B, the WSI values show noticeable improvements. At 28 days, M5B achieves a WSI of 7.92 mm/hr$^{0.5}$, while M6B records a lower WSI of 7.42 mm/hr$^{0.5}$. By 90 days, M5B shows a slight increase in WSI to 8.49 mm/hr$^{0.5}$, while M6B improves further to 7.33 mm/hr$^{0.5}$. These results suggest that replacing LSP with CWP enhances water resistance, particularly in M6B, where a higher percentage of CWP results in better durability.

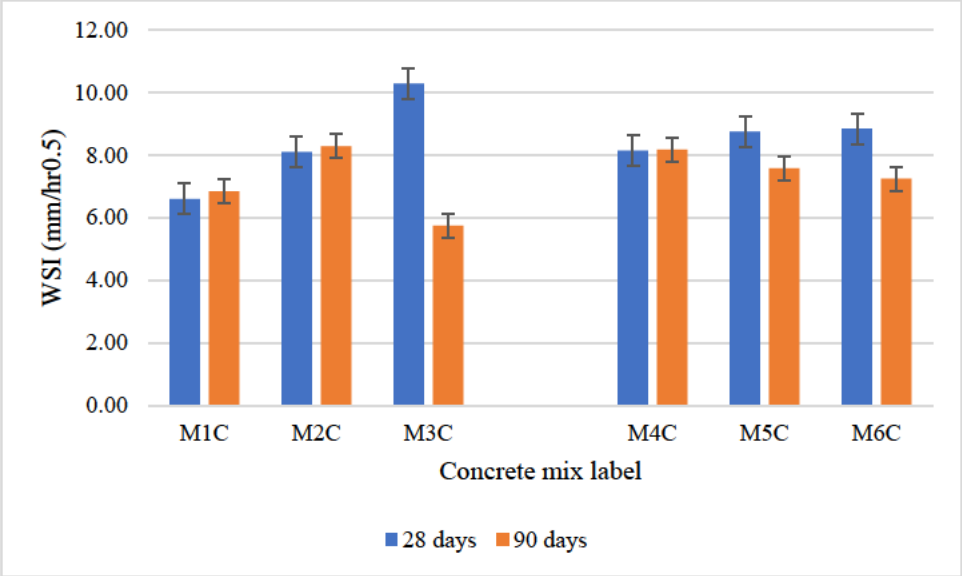

Figure 4.62: WSI of concrete at 0.55 w/b ratio

Figure 4.65 presents the WSI of CWP-based concrete at 0.55 w/b ratio. Mix M1C, containing 30% GGBS, records a WSI of 6.60 mm/hr$^{0.5}$ at 28 days, increasing slightly to 6.84 mm/hr$^{0.5}$ at 90 days. When GGBS is partially replaced with CWP, as in M2C and M3C, the WSI results vary. At 28 days, M2C has a WSI of 8.09 mm/hr$^{0.5}$, while M3C records a significantly higher WSI of 10.27 mm/hr$^{0.5}$, suggesting increased water absorption initially. However, at 90 days, M2C increases slightly to 8.28 mm/hr$^{0.5}$, while M3C shows a substantial improvement, decreasing to 5.75 mm/hr$^{0.5}$. This reflects the long-term pozzolanic activity of CWP in M3C,

significantly reducing water absorption over time and highlighting its potential to enhance durability when optimally used.

Mix M4C achieves a WSI of 8.14 mm/hr$^{0.5}$ at 28 days, increasing marginally to 8.17 mm/hr$^{0.5}$ at 90 days. When LSP is partially replaced with CWP, as in M5C (5% CWP) and M6C (7% CWP), the WSI values demonstrate notable improvements. At 28 days, M5C records a WSI of 8.74 mm/hr$^{0.5}$, while M6C achieves 8.84 mm/hr$^{0.5}$. By 90 days, M5C decreases to 7.58 mm/hr$^{0.5}$, and M6C decreases further to 7.24 mm/hr$^{0.5}$. These results show that incorporating CWP into LSP mixes significantly reduces water absorption, with hieving the best performance due to a higher CWP content.

The WSI results indicate that GGBS-based concrete mixes exhibit superior long-term resistance to water absorption compared to LSP-based mixes. The inclusion of CWP also significantly improves water resistance, particularly in M3B and M6C**,** which demonstrate the best performance within their respective groups. When used as a partial replacement for GGBS, CWP enhances microstructural refinement, reducing permeability and improving durability. Mix M2A and M3C showed the lowest WSI values at 90 days, confirming the effectiveness of CWP in reducing water absorption. Similarly, in LSP-based mixes, M6A and M6C achieved better performance compared to M4A, M5A, M4B, M5B, M4C, and M5C, suggesting that CWP improves water resistance across different binder systems. While GGBS-based mixes benefit more significantly from CWP incorporation, LSP-based mixes also experience moderate improvements. The findings suggest that CWP optimally refines the concrete matrix, improving durability by filling voids and reducing permeability. However, in some concrete mixes, higher water sorptivity indices (WSI) are observed at 90 days compared to 28 days. This increase is attributed to drying shrinkage and self-desiccation. As concrete ages, moisture loss induces shrinkage, leading to microcracks that form pathways for water ingress (Neville, 2011). Furthermore, Mehta and Monteiro (2006) explain that self-desiccation occurs in low w/b ratio concrete or mixes containing SCMs (such as GGBS) where ongoing hydration depletes internal moisture, creating tensile stresses and microcracking.

4.7.3 Chloride conductivity index (CCI)

The CCI evaluates the performance of CWP concrete mixes in terms of resistance to chloride ingress, comparing the effects of replacing GGBS and LSP with CWP.

Figure 4.66 presents the CCI of CWP concrete at 0.45 w/b ratio. Mix M1A records a CCI of 0.72 mS/cm at 28 days, which decreases significantly to 0.45 mS/cm at 90 days. When 10%

and 20% of GGBS are replaced with CWP, as in M2A and M3A, the CCI results show mixed trends. At 28 days, M2A records a slightly higher CCI of 0.81 mS/cm, and M3A shows a substantially higher value of 1.61 mS/cm, indicating reduced resistance to chloride ingress initially. However, at 90 days, the CCI values for M2A and M3A improve significantly, decreasing to 0.67 mS/cm and 0.58 mS/cm, respectively. These results indicate that while CWP initially reduces chloride resistance compared to GGBS, it also improves over time due to pozzolanic activity, particularly in M3A, where the long-term performance approaches that of the GGBS reference.

Mix M4A LSP reference mix records a CCI of 1.00 mS/cm at 28 days, decreasing to 0.62 mS/cm at 90 days. When LSP is partially replaced with CWP, the CCI values increase, as in M5A (5% CWP) and M6A (7% CWP). At 28 days, M5A records a CCI of 1.01 mS/cm, and M6A shows a slightly higher value of 1.13 mS/cm. By 90 days, the CCI values decrease to 0.58 mS/cm for M5A and 0.73 mS/cm for M6A, indicating enhanced chloride resistance over time. These results suggest that incorporating CWP into LSP mixes improves long-term resistance to chloride ingress, with M5A achieving the best performance due to its balanced mix design.

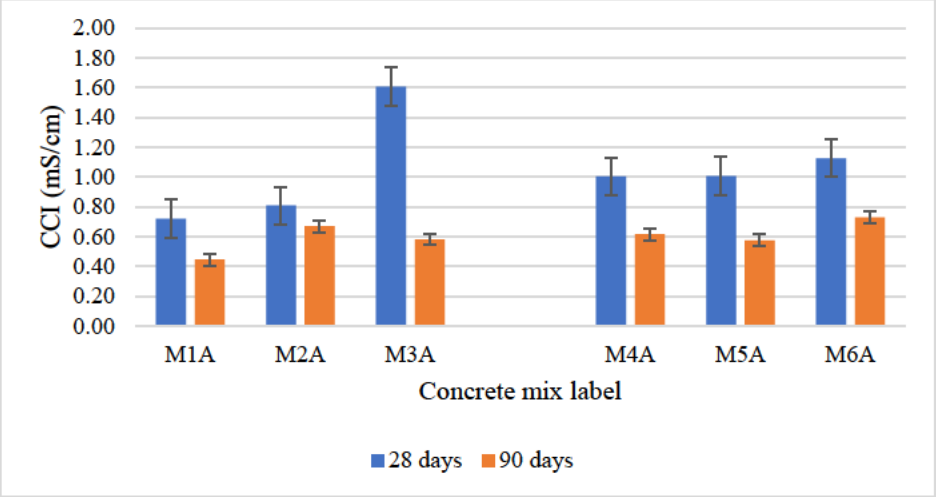

Figure 4.63: CCI of concrete at 0.45 w/b ratio

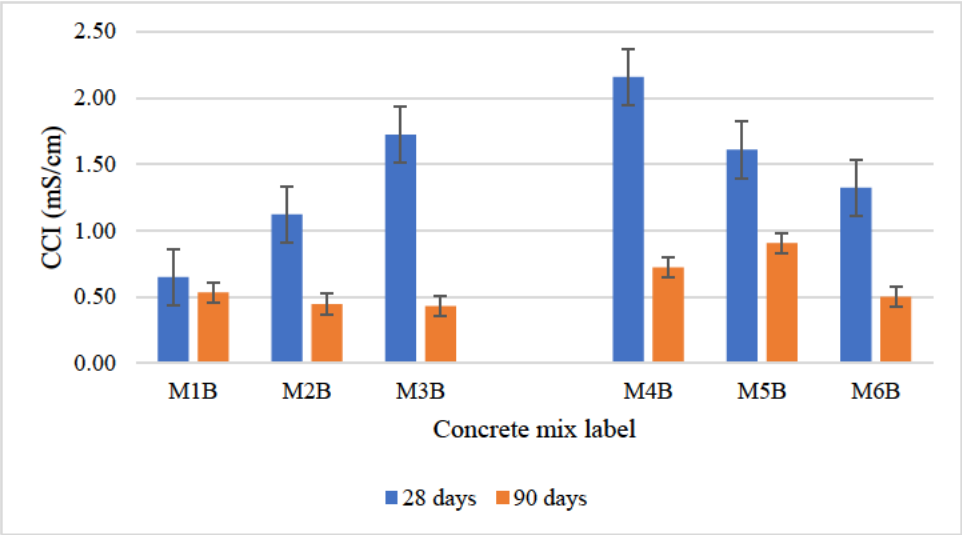

Figure 4.64: CCI of concrete at 0.50 w/b ratio

Figure 4.67 shows the CCI of concrete at 0.50 w/b ratio. Mix M1B achieves a CCI of 0.65 mS/cm at 28 days, which decreases to 0.53 mS/cm at 90 days. When GGBS is partially replaced with CWP, as in M2B and M3B, the CCI values show significant changes. At 28 days, M2B records a CCI of 1.12 mS/cm, while M3B shows a higher value of 1.72 mS/cm, indicating reduced resistance to chloride ingress initially. However, by 90 days, the CCI values for M2B and M3B improved markedly to 0.45 mS/cm and 0.43 mS/cm, respectively. These results demonstrate that CWP enhances chloride resistance over time, with M3B achieving the best performance at 90 days due to the long-term refinement of the concrete microstructure.

Mix M4B records a CCI of 2.16 mS/cm at 28 days, which decreases significantly to 0.72 mS/cm at 90 days. When LSP is partially replaced with CWP, as in M5B (5% CWP) and M6B (7% CWP), the CCI values improve substantially. At 28 days, M5B and M6B achieve CCIs of 1.61 mS/cm and 1.32 mS/cm, respectively. By 90 days, the CCI values decrease significantly to 0.91 mS/cm for M5B and 0.50 mS/cm for M6B. These results highlight the superior chloride resistance provided by CWP, with M6B demonstrating the most significant improvement due to its higher CWP content.

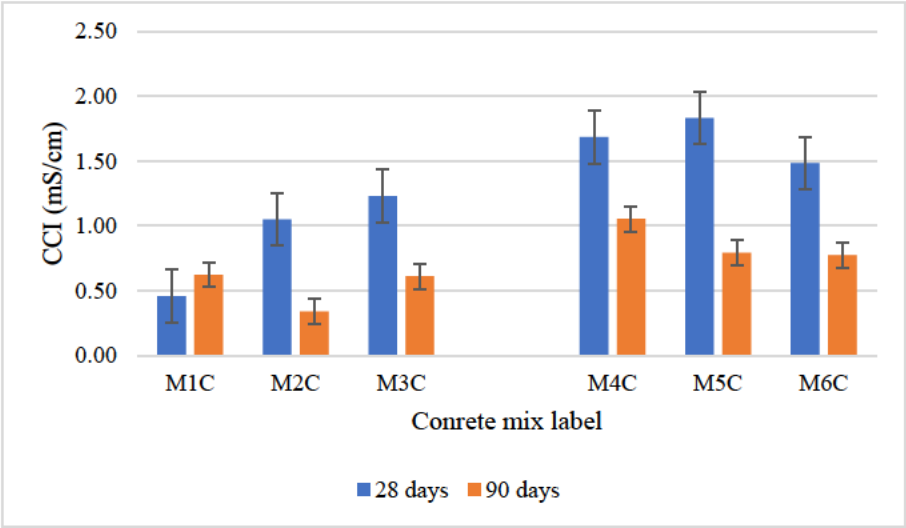

Figure 4.65: CCI of concrete at 0.55 w/b ratio

Figure 4.68 presents the CCI of CWP concrete at 0.55 w/b ratio. Mix M1C achieves a low CCI of 0.46 mS/cm at 28 days, increasing slightly to 0.62 mS/cm at 90 days. When GGBS is partially replaced with CWP, as in M2C and M3C, the results show varying effects. At 28 days, M2C records a higher CCI of 1.05 mS/cm, and M3C reaches 1.23 mS/cm, indicating reduced resistance to chloride ingress initially. However, at 90 days, the CCI values for M2C and M3C improve significantly, reducing to 0.34 mS/cm and 0.61 mS/cm, respectively. The substantial improvement in M2C demonstrates the optimal balance between GGBS and CWP in enhancing chloride resistance over time.

Mix M4C records a CCI of 1.69 mS/cm at 28 days, which decreases to 1.06 mS/cm at 90 days. While this indicates moderate improvement in chloride resistance, the limited pozzolanic activity of LSP restricts its ability to refine the concrete matrix. When LSP is partially replaced with CWP, as in M5C (5% CWP) and M6C (7% CWP), the CCI values improve notably. At 28 days, M5C achieves a CCI of 1.83 mS/cm, and M6C records 1.49 mS/cm, both initially higher than the limestone reference. However, by 90 days, M5C decreases to 0.79 mS/cm, and M6C reduces further to 0.77 mS/cm, highlighting the long-term benefits of incorporating CWP in improving chloride resistance. The better performance of M6C at 90 days suggests that a higher percentage of CWP in limestone mixes leads to enhanced durability.

The CCI values across all concrete mixes exhibit notable reductions between 28 and 90 days, highlighting the positive effects of extended curing and secondary hydration in enhancing durability. Generally, GGBS-based mixes (M1, M2, and M3) demonstrate superior long-term chloride resistance compared to LSP mixes (M4, M5, and M6). However, incorporating CWP into both GGBS and LSP mixes significantly enhances chloride resistance over time. For GGBS

replacements, CWP improves chloride resistance significantly, with M3 achieving a CCI comparable to the GGBS reference (M1) at 90 days. Similarly, in LSP mixes, CWP incorporation leads to lower CCI values, with M6 showing the best performance. At a 0.55 w/b ratio, M2 and M6 demonstrate optimal performance within their respective groups, effectively reducing chloride ingress and enhancing durability.

4.7.4 Porosity from WSI

The porosity derived from WSI evaluates the impact of replacing GGBS and LSP with CWP on the microstructure of concrete at a 0.45 w/b ratio. Porosity values are presented at 28 and 90 days to assess changes over time.

Figure 4.69 presents the porosity of concrete at 0.45 w/b ratio. Mix M1A exhibits a porosity of 8.70% at 28 days, which decreases significantly to 6.58% at 90 days. When GGBS is partially replaced with CWP, as in M2A and M3A, porosity values differ. At 28 days, M2A records a higher porosity of 10.02%, while M3A shows 9.83%, both indicating increased pore content initially. However, at 90 days, porosity decreases significantly to 8.15% for M2A and 7.07% for M3A. These results highlight the long-term benefits of CWP in reducing porosity, with M3A achieving the greatest reduction. This suggests that a higher CWP content (20%) contributes to more effective densification over time, enhancing the concrete's durability.

Mix M4A records a porosity of 9.61% at 28 days, which increases slightly to 9.90% at 90 days. This increase reflects the filler effect of LSP, which lacks pozzolanic activity and does not refine the pore structure over time. When LSP is partially replaced with CWP, as in M5A (5% CWP) and M6A (7% CWP), the porosity values improve. At 28 days, M5A achieves a lower porosity of 7.87%, while M6A records 9.40%. By 90 days, M5A experiences a slight increase in porosity to 9.61%, while M6A shows a significant reduction to 8.03%. These results indicate that CWP contributes to reducing porosity more effectively than LSP, with M6A showing the best performance due to a higher CWP content. The inclusion of CWP significantly reduces porosity in both replacement scenarios, demonstrating its effectiveness in improving durability by refining the concrete matrix.

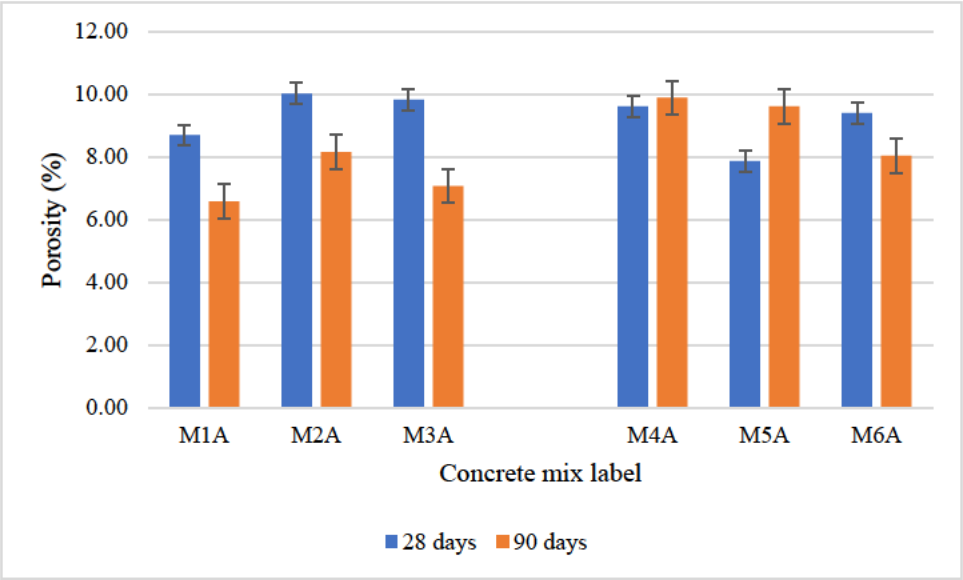

Figure 4.66: Porosity from sorptivity of concrete at 0.45 w/b ratio

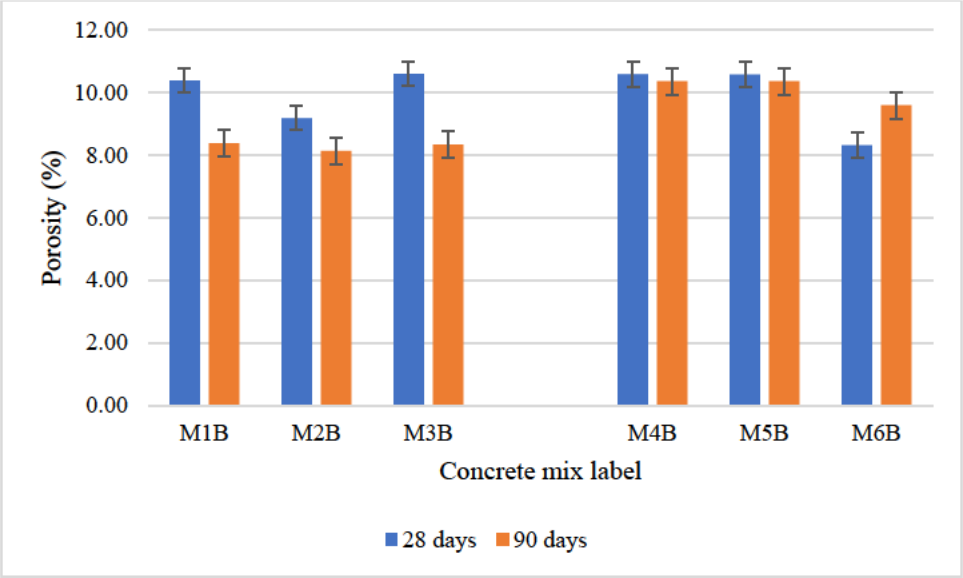

Figure 4.67:Porosity from sorptivity of concrete at 0.5 w/b ratio

Figure 4.70 presents the porosity of CWP concrete at 0.5 w/b ratio. Mix M1B records a porosity of 10.37% at 28 days, decreasing significantly to 8.38% at 90 days. When 10% and 20% of GGBS are replaced with CWP, as in M2B and M3B, the porosity values vary. At 28 days, M2B records a lower porosity of 9.18%, while M3B has a slightly higher value of 10.59%. By 90 days, the porosity reduces to 8.13% for M2B and 8.34% for M3B. These results indicate that replacing GGBS with CWP maintains or slightly reduces porosity over time, with M2B achieving the lowest porosity among the GGBS-CWP blends.

Mix M4B shows a porosity of 10.58% at 28 days, which decreases marginally to 10.35% at 90 days. This minimal change reflects the limited ability of LSP to refine the pore structure, as it primarily acts as a filler without significant pozzolanic activity. When 5% and 7% of LSP are replaced with CWP, as in M5B and M6B, the porosity improves. At 28 days, M5B records 10.57%, while M6B achieves a notably lower porosity of 8.31%. By 90 days, M5B reduces slightly to 10.36%, while M6B decreases further to 9.59%. These results demonstrate that incorporating CWP into LSP mixes significantly reduces porosity, with M6B exhibiting the most pronounced improvement due to its higher CWP content. These results affirm the ability of CWP to enhance concrete durability by reducing porosity, particularly when used to replace LSP.

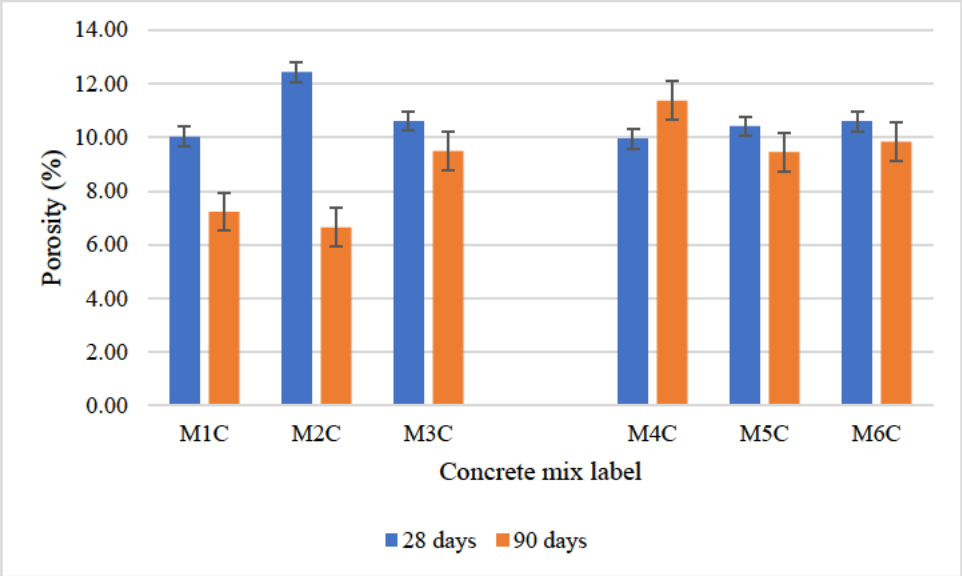

Figure 4.68: Porosity from sorptivity of concrete at 0.55 w/b ratio

Figure 4.71 presents the porosity of CWP concrete at 0.55 w/b. Mix M1C shows a porosity of 10.03% at 28 days, which decreases significantly to 7.23% at 90 days. When GGBS is partially replaced with CWP, as in M2C and M3C, the porosity results differ. At 28 days, M2C records the highest porosity of 12.43%, indicating higher initial pore content, while M3C records 10.61%, closer to M1C. By 90 days, M2C shows a dramatic reduction to 6.64%, the lowest among the GGBS-CWP mixes, while M3C decreases moderately to 9.49%. These results suggest that M2C achieves the best long-term microstructural refinement, highlighting the optimal role of a 10% CWP replacement in balancing pozzolanic activity and pore refinement.

Mix M4C achieves a porosity of 9.96% at 28 days, which increases to 11.36% at 90 days. This increase indicates a lack of refinement in the concrete matrix over time, as LSP primarily acts as a filler without contributing to hydration or pozzolanic reactions. When 5% and 7% of LSP

are replaced with CWP, as in M5C and M6C, the results improve. At 28 days, M5C records 10.41% porosity, while M6C has 10.60%. By 90 days, M5C reduces to 9.45%, and M6C decreases slightly to 9.83%. These results demonstrate that incorporating CWP enhances porosity reduction compared to LSP alone, with M5C achieving the best performance in the limestone-CWP group.

4.7.5 Porosity from conductivity

The porosity from CCI evaluates the effect of replacing GGBS and LSP with CWP on concrete microstructure at a 0.45 w/b ratio. Figure 4.72 presents the porosity of CWP concrete at 0.45 w/b ratio. Mix M1A exhibits exceptionally low porosity of 2.54% at 28 days, which increases to 5.43% at 90 days. This initially low porosity reflects the superior densification effects of GGBS. However, the increase over time suggests potential limitations in maintaining long-term microstructural refinement due to further microcracks caused by pozzolanic reactions. When GGBS is partially replaced with CWP, as in M2A and M3A, porosity values are higher initially. At 28 days, M2A records a porosity of 8.88%, and M3A records 8.60%. By 90 days, these values improve significantly, reducing to 6.33% for M2A and 6.67% for M3A. These results indicate that while CWP increases initial porosity, it contributes to long-term refinement due to its pozzolanic activity, with M2A achieving the most pronounced improvement.

Mix M4A records a porosity of 8.68% at 28 days, slightly decreasing to 7.80% at 90 days. When LSP is partially replaced with CWP, as in M5A (5% CWP) and M6A (7% CWP), porosity values improve. At 28 days, M5A achieves the lowest porosity of 7.03%, while M6A records 8.35%. By 90 days, M5A further reduces to 7.45%, while M6A slightly decreases to 8.11%. These findings highlight that incorporating CWP into LSP mixes enhances porosity reduction, with M5A demonstrating the most consistent improvement.

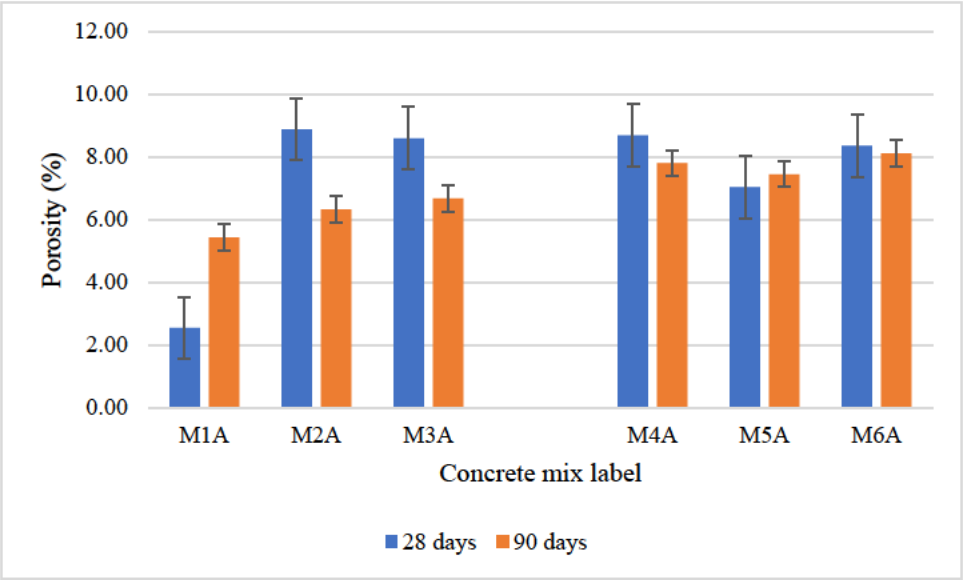

Figure 4.69: Porosity from conductivity of concrete at 0.45 w/b ratio

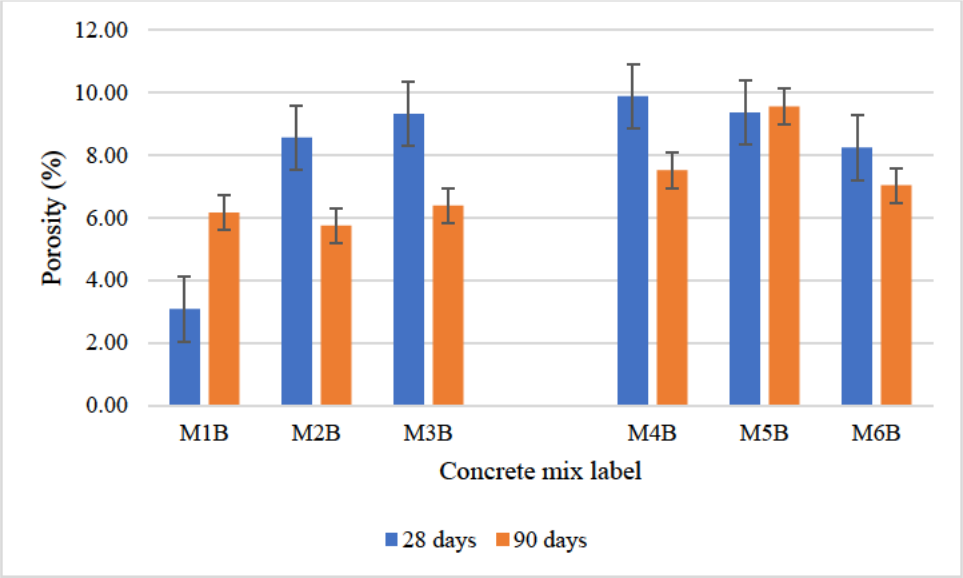

Figure 4.70: Porosity from conductivity of concrete at 0.50 w/b ratio

Figure 4.73 presents the porosity of CWP concrete at 0.50 w/b ratio. Mix M1B achieves an exceptionally low porosity of 3.08% at 28 days, increasing to 6.15% at 90 days. When GGBS is partially replaced with CWP, as in M2B and M3B, the porosity results vary. At 28 days, M2B records a porosity of 8.55%, and M3B records 9.32%, both significantly higher than M1B. However, by 90 days, M2B shows the most significant improvement, reducing to 5.74%, while M3B decreases to 6.38%. These results highlight the long-term benefits of incorporating CWP into GGBS blends, with M2B achieving the best performance due to the optimal balance of GGBS and CWP.

Mix M4B records a porosity of 9.88% at 28 days, reducing significantly to 7.51% at 90 days. When LSP is partially replaced with CWP, as in M5B (5% CWP) and M6B (7% CWP), the porosity results improve further. At 28 days, M5B achieves 9.36%, while M6B achieves the lowest porosity of 8.23%. By 90 days, M5B decreases slightly to 9.55%, and M6B improves significantly to 7.03%. These findings suggest that CWP enhances porosity reduction, particularly in M6B, where the higher CWP content leads to better microstructural refinement.

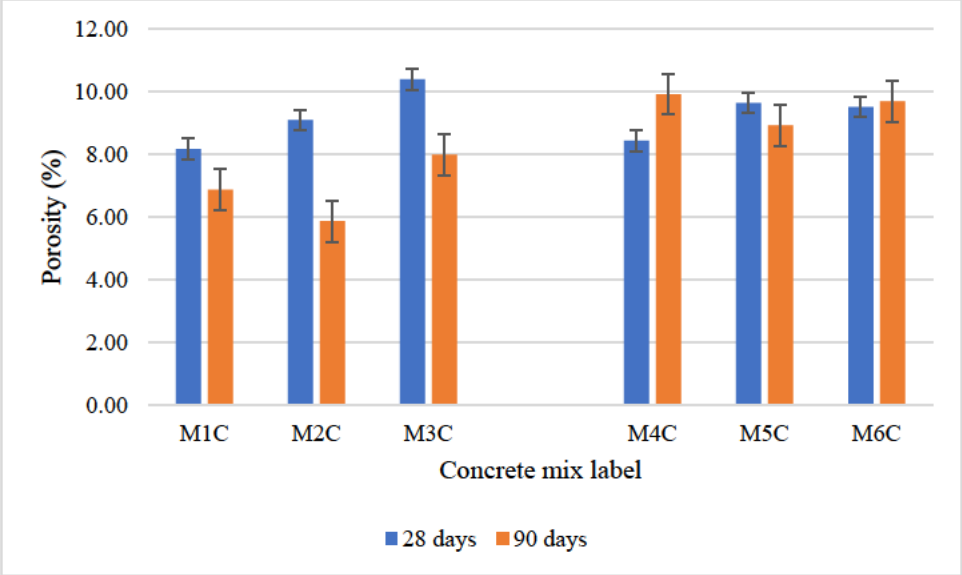

Figure 4.71: Porosity from conductivity of concrete at 0.55 w/b ratio

Figure 4.74 presents the porosity of CWP concrete at 0.55 w/b. Mix M1C, containing 30% GGBS, records a porosity of 8.17% at 28 days, which decreases to 6.87% at 90 days. This reduction highlights the contribution of GGBS in refining the pore structure over time. When GGBS is partially replaced with CWP, as in M2C and M3C, the porosity results show a higher initial value but significant reductions at 90 days. At 28 days, M2C and M3C record porosity values of 9.10% and 10.39%, respectively, but by 90 days, these reduce to 5.87% for M2C and 7.99% for M3C. The significant reduction in M2C demonstrates that the optimal replacement level of CWP in GGBS mixes enhances long-term microstructural refinement and durability.

Mix M4C records a porosity of 8.44% at 28 days, which increases to 9.92% at 90 days. This increase reflects the limited ability of LSP to refine the pore structure over time due to its lack of pozzolanic activity. When LSP is partially replaced with CWP, as in M5C (5% CWP) and M6C (7% CWP), the porosity results improve modestly. At 28 days, M5C records a higher porosity of 9.64%, while M6C records 9.52%. By 90 days, M5C reduces to 8.92%, while M6C achieves a modest reduction to 9.69%. These results suggest that incorporating CWP into LSP

mixes contributes to porosity reduction, with M5C demonstrating better performance in long-term refinement.

4.8 Microstructural Analysis of Concrete

This section presents the SEM of concrete mixtures containing reference mix M1A, M2A (10% CWP), and M3A (20% CWP) at 7 and 28 days (Figure 4.75 – 4.76). The microstructural observations include the presence of microcracks, C-S-H, and the interfacial transition zone (ITZ). A higher porosity was observed at 7 days compared to 28 days. At 7 days, microcracks in M1A were visible at 4,600× magnification. In M2A, the microstructure appeared denser at the same magnification, with well-formed C-S-H and noticeable ceramic powder grains at the ITZ. For M3A, microcracks were observed at 46,100× magnification, with a higher crack density compared to M1A and M2A. Additionally, a significant amount of ceramic powder grains was noted. At 28 days, microcracks were only observed in M1A at 10,000× magnification, with crack sizes approximately 1 µm or smaller. In M2A, the microstructure remained dense, though some cracks were visible at 2,000× magnification, along with ceramic powder grains. The M3A microstructure exhibited a denser matrix compared to its 7-day counterpart. The ITZ in M3A showed no visible cracks at 2,000× magnification.

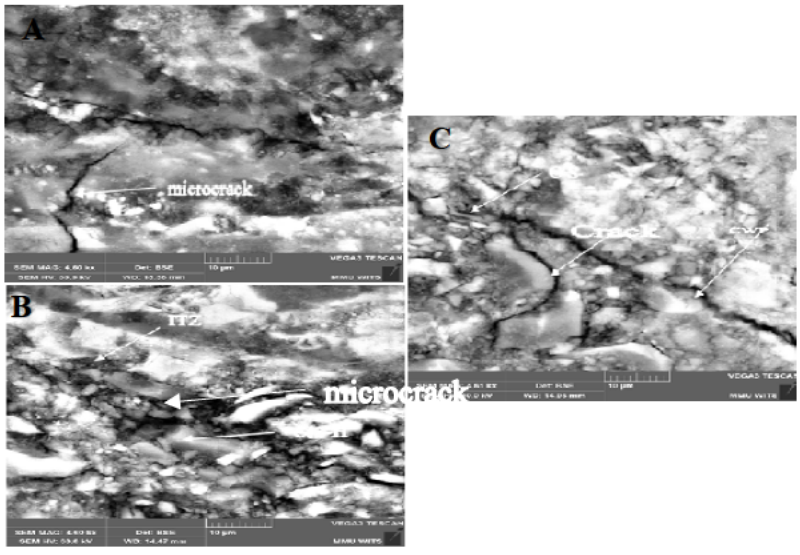

Figure 4.72: SEM images at 7days. A: SEM image of M1A at 7 days; B: SEM image of M2A at 7days; C: SEM image of M3A at 7 days

The SEM analysis at 7 days revealed distinct differences in the formation of C-S-H gel, pore structure, and the ITZ across the concrete mixes. M1A (70% PC + 30% GGBS) exhibited a moderately dense microstructure with visible capillary pores and partially hydrated slag

particles, indicating ongoing hydration. The ITZ appeared relatively weak with microcracks and loosely packed hydration products.

M2A (70% PC + 20% GGBS + 10% CWP) displayed a more refined microstructure than M1A, with a slightly denser C-S-H network and a noticeable reduction in pore size, suggesting early pozzolanic reactions facilitated by the CWP. The ITZ showed better particle packing and fewer microcracks. However, in M3A (70% PC + 10% GGBS + 20% CWP), a higher concentration of CWP led to a more porous structure, with a weaker ITZ and delayed C-S-H formation, likely due to a lower availability of calcium hydroxide for secondary hydration reactions.

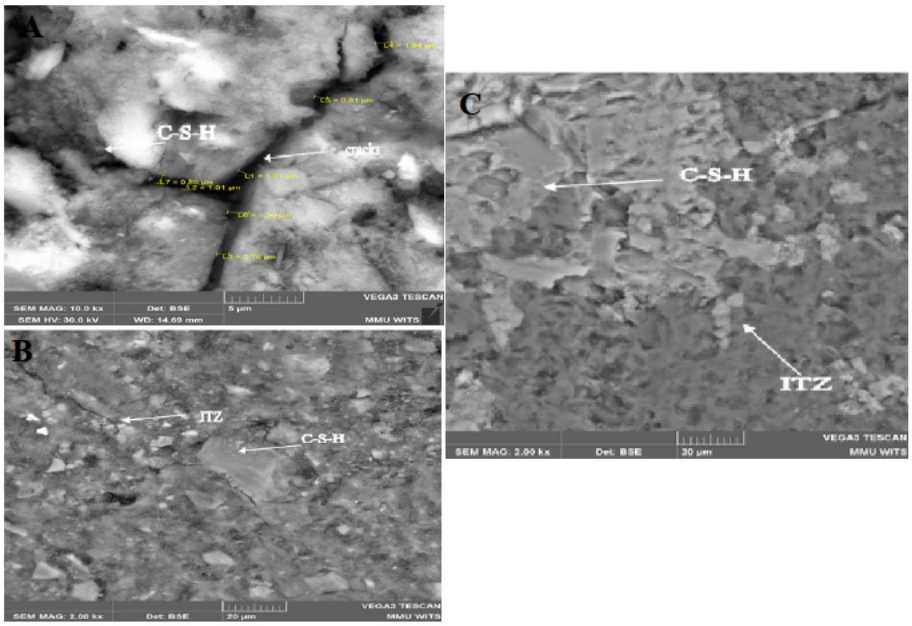

Figure 4.76: SEM images of concrete at 28 days. A: SEM image of M1A concrete at 28days; B: SEM image of M2A concrete at 28days; B: SEM image of M3A concrete at 28days

At 28 days, the SEM images demonstrated a more densified and refined microstructure in all samples, with a significant reduction in capillary pores and enhanced formation of C-S-H gel. M1A exhibited an improved microstructure, with better C-S-H connectivity, though some unreacted GGBS particles remained. The ITZ was denser compared to its 7-day counterpart but still contained microcracks (averagely 1 µm).

In M2A, the inclusion of 10% CWP led to a significantly denser microstructure, with a well-developed C-S-H network and minimal visible pores, indicating enhanced secondary hydration reactions. The ITZ in M2A appeared more compact, suggesting improved particle packing and reduced permeability. For M3A, while the microstructure showed noticeable densification compared to its 7-day state, it remained slightly more porous than M2A, with a less compact

ITZ. The higher CWP content may have contributed to a slower reaction rate, affecting the overall formation of hydration products.

Overall, the SEM analysis confirms that the inclusion of CWP enhances pore refinement and microstructural densification over time, with M2A (10% CWP) demonstrating the most optimized ITZ and C-S-H formation at 28 days.

4.9 Summary

The findings in this study largely affirm the usefulness of CWP as an alternative cement material in concrete. The results also indicate that while the pozzolanic reactivity of CWP is less than that of GGBS, it is higher than LSP, in addition to initial comparison of physical and chemical characteristics of CWP to the other binders. The results include the effects of CWP on concrete workability, compressive strength, splitting tensile strength, durability indices and microstructural analysis.

The workability of concrete varies depending on whether CWP replaces GGBS or LSP. In GGBS-based systems, increasing the CWP content led to an improvement in workability. For instance, the control mix (M1A) had a slump of 35 mm, while replacing 20% of GGBS with CWP (M3A) increased the slump to 72 mm. However, the improvement does not increase with an increase in the CWP content. Relative reduction is usually observed when the CWP is increased to 30%. Conversely, in LSP-based systems, increasing the CWP content results in reduced workability. For instance, the reference mix (M4A) without CWP had a higher initial slump of 30 mm, whereas M5A exhibited a significant decrease in slump (23 mm). To achieve the desired workability, higher dosages of superplasticizers were required, especially for LSP-based mixes. This suggests that CWP acts more like an inert filler when replacing LSP, increasing water demand and reducing slump. Overall, the slump test results show that increasing CWP content generally reduces workability, as evidenced by lower slump values with higher replacement levels, especially in the LSP-based mixes. This trend aligns with literature findings where researchers reported similar reductions in workability due to the higher surface area (Daniel & Raju, 2018; El-Dieb *et al.*, 2018; Li *et al.*, 2024). Previous studies also indicate the need for superplasticizers to mitigate this effect, restoring workability to acceptable levels (Sondarva et al. 2022b).

The compressive strength test was conducted to evaluate the influence of CWP on strength development at different curing ages. The results indicate that CWP affects compressive strength differently depending on whether it replaces GGBS or LSP. In GGBS-based systems,

increasing CWP content resulted in a decrease in early-age compressive strength. For instance, the reference mix (M1A) achieved the highest strength at 7 days (39.2 MPa), whereas the M3A mix (20% CWP replacement) had a lower strength (31.6 MPa). By 90 days, the strength gains improved, but it remained below that of the control mix. This indicates that CWP does not exhibit the same pozzolanic reactivity as GGBS, leading to slower strength development. However, in LSP-based systems, CWP improved both early and long-term compressive strength. For instance, at 7 days, M6C (7% CWP replacement) recorded the highest strength (42.4 MPa), surpassing the reference mix (M4C) with 41.3 MPa. By 90 days, M6C maintained superior strength (56.8 MPa), outperforming M4C (51.9 MPa). These indicate that CWP enhances long-term compressive strength when replacing LSP, possibly due to better particle packing and some later age pozzolanic activity. Also, the compressive strength results generally indicate a comparable strength at lower replacement levels (10–20%) but a decline beyond 20%. This pattern is consistent with literature findings, where the strength gain is attributed to the pozzolanic activity of CWP, which enhances secondary hydration (Heidari and Tavakoli, 2013b; Rani, 2016; Li *et al.*, 2024). At higher replacement levels, dilution effects and insufficient CaO content lead to a strength reduction in GGBS-based mixes, confirming similar trends observed in previous studies (Tahir & Kumar Poloju, 2017).

Splitting tensile strength follows a similar trend. For instance, at 7 days, M1A had the highest tensile strength (3.3 MPa), while M3A (20% CWP replacement) recorded the lowest (2.9 MPa). However, by 90 days, M3A improved to 4.2 MPa, showing a steady but delayed strength gain. For LSP-based systems, the results were more favourable. Higher CWP content led to improved tensile strength at later ages. The M6A mix (7% CWP replacement) achieved the highest tensile strength at 90 days (4.8 MPa), surpassing the reference mix (M4A). The rate of strength development was more pronounced in LSP-based mixes, indicating that CWP has a better pozzolanic reactivity than LSP.

The durability of CWP concrete was assessed using the South African durability indices, OPI, WSI and CCI. The OPI results showed that increasing CWP content slightly reduced permeability in GGBS-based mixes, although all values remained within the "good" to "excellent" durability range. In LSP-based mixes, CWP improved durability, particularly when used at 5–7% replacement levels. This confirms that CWP contributes to microstructural densification, reducing the permeability of the concrete.
The WSI results also indicated that higher CWP content reduced water absorption, particularly in LSP-based mixes. This improvement suggests that CWP enhances resistance to moisture

ingress, which is a key factor in concrete durability.
The CCI showed that CWP-modified concrete exhibited lower conductivity, indicating better resistance to chloride penetration. This is particularly important for structures exposed to aggressive environments, such as marine and coastal regions. The best performance was observed at 10% CWP replacement in GGBS-based mixes and 5% CWP in LSP-based mixes. These results confirm that CWP improves durability, especially in terms of permeability and chloride resistance.

The SEM images of M1A, M2A, and M3A concrete mixtures at 7 and 28 days revealed variations in microcracks, C-S-H formation, and ITZ characteristics. At 7 days, M1A showed microcracks at 4,600× magnification, while M2A had a denser microstructure with visible ceramic powder grains, and M3A exhibited higher crack density at 46,100× magnification. By 28 days, microcracks were minimal, with M3A showing the densest matrix and no visible ITZ cracks at 2,000× magnification. The results indicate that increasing the CWP content enhances microstructural densification over time, reducing microcracks and porosity, particularly in M3A. This suggests that CWP contributes to improved long-term durability by refining the ITZ and enhancing hydration products in concrete.

CHAPTER FIVE
CONCLUSIONS AND RECOMMENDATIONS

5.1 Preamble

This chapter presents the deductions based on the findings of this study. The research assessed the fresh, mechanical, durability, and microstructural properties of ceramic waste powder (CWP)-based concrete to determine whether CWP acts as a pozzolanic material or an inert filler. Key conclusions were drawn from experimental results, highlighting the role of CWP in improving durability but exhibiting limited pozzolanic reactivity. The chapter also discusses the practical implications of CWP in sustainable construction and provides recommendations for future research, industrial adoption, and optimization strategies.

5.2 Conclusions

The major objective of this study is to determine the role of CWP in concrete – whether as a pozzolanic material like ground granulated blast-furnace slag (GGBS) or inert cement filler like limestone powder (LSP). Hence, the following conclusions are made based on the results.

i. The particle size distribution analysis showed that the CWP has a slightly coarser grain structure than Portland cement (PC), LSP, and GGBS. This characteristic influenced the workability and strength of the concrete.

ii. The microstructural analyses confirmed that CWP is rich in silica (SiO_2) and alumina (Al_2O_3), which contribute to pozzolanic activity. However, its lower calcium oxide (CaO) content suggests a slower reaction rate compared to GGBS.

iii. The combined oxides (SiO_2, Al_2O_3, and Fe_2O_3) in CWP exceed 70%; therefore, it qualifies as a pozzolanic material according to SANS 50197-1 – 2013 and SANS 50450-1 & 2 – 2014. It also nearly meets ASTM C618 – 2019 Class F requirements; however, its SiO_2 content is slightly below the 70% threshold. Meanwhile, it does not meet ASTM C618 Class C specifications due to its low CaO content (<10%), meaning it lacks self-cementing properties and does not exhibit the high reactivity typical of Class C pozzolans.

iv. The slump test results indicated that CWP influenced the fresh properties of concrete differently in GGBS an LSP–based mixes. When replacing GGBS, CWP led to a decrease in slump, requiring higher dosages of superplasticizers to maintain standard consistency. However, in LSP-based mixes, CWP improved slump, reducing the need

for chemical admixtures. This behaviour can be attributed to the coarser nature of CWP in GGBS mixes, which increased water demand, while in limestone mixes, the improved packing effect contributed to better workability.

v. The replacement of GGBS with CWP showed a slight reduction in early-age strength, particularly at a higher CWP level (20%). However, at later curing ages (90 days), 10% CWP substitution (M2A, M2B, and M2C) exhibited strength comparable to the control mixes. However, in LSP-based concrete, incorporating CWP consistently enhanced compressive strength across all replacement levels. This indicates that while CWP outperforms LSP in strength, it does not reach the performance level of GGBS.

vi. The results of splitting tensile strength followed a similar trend to compressive strength. Lower CWP contents (5–10%) in GGBS mixes had minimal impact on tensile strength, but higher replacements led to strength reductions. Conversely, higher CWP levels (7%) in LSP-based mixes improved tensile strength, highlighting that CWP outperforms LSP in contributing to concrete strength.

vii. Regression analyses confirmed that GGBS-based mixes had a higher initial strength gain rate, but CWP substitution slowed the long-term hydration. LSP-based mixes, on the other hand, exhibited progressive strength development, with higher CWP levels yielding better long-term performance.

viii. Durability tests demonstrated that CWP had a positive impact on long-term durability, particularly in LSP-based systems. The following conclusions can be made:

    a. The OPI results indicate that replacing GGBS and LSP with CWP has a marginal to moderate impact on permeability, with most mixes maintaining values within the "good" to "excellent" classification. The incorporation of CWP contributes to densification, reducing capillary porosity and enhancing durability, particularly in mixes containing GGBS.

    b. The WSI results highlight that while CWP replacement initially increases water absorption, long-term hydration and pozzolanic activity reduce WSI values over time. The optimal performance is observed in mixes with 10–20% CWP replacement for GGBS and 5–7% replacement for LSP, where water ingress is significantly reduced, contributing to better resistance against moisture-related deterioration.

c. The CCI analysis reveals that CWP improves resistance to chloride ingress over time, particularly in GGBS-based mixes, where pozzolanic activity enhances microstructural refinement. While LSP-based mixes show moderate improvements, the addition of CWP leads to better performance, with higher replacement levels demonstrating greater chloride resistance.

d. The porosity analysis, derived from WSI and CCI, further supports the findings that CWP contributes to improved concrete durability by refining the microstructure and reducing permeability. Although initial porosity levels are sometimes higher with CWP incorporation, long-term hydration reactions result in notable reductions, enhancing the overall resistance to aggressive environmental conditions.

ix. The microstructural analysis of CWP concrete reveals significant densification over time, with noticeable improvements in calcium silicate hydrate (C-S-H) formation and reduced microcracking at 28 days. At 7 days, M1A exhibited visible microcracks, while M2A displayed a denser matrix with well-formed C-S-H and ceramic powder grains at the interfacial transition zone (ITZ). M3A showed higher crack density, but at 28 days, all mixes exhibited improved microstructure, with M3A demonstrating the most refined matrix and minimal visible cracks. These findings confirm that incorporating CWP enhances microstructural integrity, reducing porosity and improving overall durability as hydration progresses.

x. The CWP-based concrete shows only marginal strength gains at 10–15% replacement and does not meet the ASTM C618 Strength Activity Index (SAI) requirement of 75% at 28 days. Unlike reactive pozzolans, it lacks sustained strength development.

xi. The CWP behaves similarly to LSP in hydration, offering comparable early-age strength but lacking the delayed pozzolanic reaction observed in GGBS. Lower portlandite (CH) consumption further confirms its weak pozzolanic reactivity.

xii. The CWP concrete exhibits slightly better compressive and splitting tensile strength compared to LSP concrete. However, it falls short of matching the compressive and tensile strength of GGBS concrete at both early and later ages.

xiii. The CWP enhances durability through pore refinement rather than chemical reactions. While porosity decreases at 10–15% replacement, higher replacement levels increase

permeability, reinforcing its role as a filler rather than a reactive supplementary cementitious material (SCM).

xiv. The CWP mainly functions as an inert filler with minimal pozzolanic reactivity, enhancing microstructural densification rather than improving long – term strength development. Although it contains high levels of silica (SiO_2) and alumina (Al_2O_3), its pozzolanic activity is limited due to the crystalline nature of its silica, formed during high temperature sintering in ceramic production. Unlike GGBS, which has highly reactive silica, CWP reacts weakly with calcium hydroxide (CH), resulting in minimal formation of secondary Calcium Silicate Hydrate (C-S-H) and reducing its effectiveness as a pozzolanic material.

5.2.1 Practical applications of CWP in concrete

The incorporation of CWP in concrete presents significant environmental benefits, particularly in South Africa, where waste management and sustainability in the construction sector remain critical concerns. More than 2 million tonnes of ceramic waste are generated in South Africa annually (Department: Environmental Affairs 2018). These include rejected tiles and sanitary ware, which often end up in landfills, contributing to environmental degradation. Utilizing CWP as SCM provides an effective waste recycling strategy, reducing the environmental burden of ceramic waste while promoting sustainable construction practices.

Additionally, cement production is a major contributor to CO_2 emissions, accounting for nearly 8% of global greenhouse gas emissions (Abiodun et al. 2022). By partially replacing cement with CWP, the carbon footprint of concrete production can be significantly reduced. This aligns with South Africa's sustainability goals, including reducing construction waste, minimizing resource depletion, and promoting a circular economy. The use of CWP also mitigates the need for excessive quarrying of raw materials such as limestone, further contributing to environmental conservation and resource efficiency.

The use of CWP in concrete offers substantial environmental and technical benefits. From a sustainability perspective, CWP contributes to waste reduction, CO_2 emission mitigation, and circular economy practices in South Africa's construction industry. Technically, CWP enhances concrete durability and microstructural densification, particularly when used as a replacement for LSP rather than GGBS. To maximize its benefits, CWP should be limited to 10% in GGBS-based concrete to maintain strength, while higher levels (7%) can be effectively used in LSP-based concrete to improve durability. These findings underscore CWP's potential as a

sustainable alternative binder, supporting environmentally friendly and resource-efficient construction.

5.2.2 Contributions of the study to the body of knowledge

This study addresses the research gap regarding the pozzolanic reactivity and role of CWP in concrete. Despite numerous studies, there is no clear agreement on whether CWP functions as a pozzolanic material or an inert filler, making it difficult to explicitly define its role in concrete. The lack of agreement in previous research is due to conflicting findings on the chemical reactivity of CWP, its impact on strength development, and its effect on permeability. This study provides clarity by evaluating CWP as a partial replacement for both a pozzolanic material (GGBS) and an inert filler (LSP), thereby offering a comprehensive understanding of its performance in concrete.

This study confirms that CWP mainly functions as an inert filler with minimal pozzolanic reactivity, enhancing microstructural densification rather than improving long-term strength development. Although CWP contains high levels of silica (SiO_2) and alumina (Al_2O_3), its pozzolanic activity is restricted due to the crystalline nature of its silica, formed during high-temperature sintering in ceramic production. Unlike GGBS, which contains highly reactive silica, CWP reacts weakly with calcium hydroxide (CH), leading to minimal formation of secondary C-S-H. This limited reaction reduces its effectiveness as a pozzolanic material, explaining why it does not contribute significantly to strength gain over time.

The results demonstrate that CWP contributes to concrete densification, leading to enhanced durability rather than improved mechanical strength. Strength testing reveals that high CWP replacement levels (≥20%) negatively affect compressive strength, especially in GGBS-based concrete. In contrast, a 7% replacement in LSP-based concrete improves durability by refining the microstructure and reducing permeability. This finding resolves contradictions in previous research by confirming that CWP reduces permeability despite not significantly enhancing strength, positioning it closer to LSP rather than highly reactive SCMs like GGBS, fly ash, or silica fume.

concrete. Microstructural analysis shows that CWP primarily contributes to pore refinement, which lowers permeability and enhances resistance to aggressive environmental conditions. Results from WSI and OPI tests confirm that CWP improves concrete durability through physical densification rather than chemical reactivity.

This study also explains why some researchers previously observed C-S-H-like gel formation in CWP concrete. The presence of calcium-silicate-aluminate hydrates at specific replacement

levels suggests that CWP exhibits mild pozzolanic reactivity in certain conditions. Nevertheless, this reaction is not sufficient to classify CWP as a highly reactive pozzolanic material. Instead, the findings reaffirm that CWP behaves more like LSP, acting as a filler material with secondary durability benefits rather than as a fully reactive SCM. By resolving these conflicting interpretations, this study fills a critical research gap and provides practical recommendations for using CWP in concrete. It is recommended that CWP replacement be limited to ≤10% in GGBS-based concrete to maintain strength, while up to 7% can be used in LSP-based concrete to improve durability. These findings contribute valuable insights to the body of knowledge, offering a definitive classification of CWP's role in concrete and guiding its optimal application in sustainable construction.

5.3 Recommendations

Based on the findings of this study, the following recommendations are proposed:

1. Optimized blending of CWP with other pozzolanic materials: Given that CWP exhibits limited pozzolanic reactivity compared to GGBS, future research should explore its use in combination with other pozzolanic materials such as fly ash or silica fume to enhance its reactivity and improve long-term strength development.
2. Activation techniques for enhanced reactivity: Future research should explore activation techniques to enhance the pozzolanic reactivity of CWP for broader applications in sustainable construction. Methods such as thermal activation, mechanical grinding, or chemical activation could be investigated to improve its performance as a cementitious material.
3. Suitability for non-structural and supplementary applications: Since CWP outperformed LSP but did not match GGBS in strength development, it can be considered for applications where high pozzolanic activity is not critical, such as in non-structural concrete, masonry units, and plastering applications.
4. Further microstructural investigations: Advanced characterization techniques, such as thermogravimetric analysis (TGA) and scanning electron microscopy (SEM), should be conducted to gain deeper insights into the hydration mechanisms and long-term durability effects of CWP in concrete.
5. Durability-Based Performance Evaluation: While CWP demonstrated improved durability over LSP, more comprehensive long-term durability tests, including

resistance to sulphate attack, chloride ingress, and carbonation, should be conducted to establish its effectiveness in aggressive environments.

6. Industry adoption and sustainability considerations: Efforts should be made to promote the use of CWP in the construction industry as a sustainable alternative to traditional fillers. Policies and incentives could encourage industries to recycle ceramic

REFERENCES

Abiodun, YO, Olanrewaju, OA, Gbenebor, OP, Ochulor, EF, Obasa, DV & Adeosun, SO. 2022. Cutting Cement Industry CO2 Emissions through Metakaolin Use in Construction. Atmosphere. 13(9). doi.org/10.3390/atmos13091494.

Abou Rachied, T, Dbouk, F, Hamad, B & Assaad, JJ. 2023. Structural behavior of beams cast using normal and high strength concrete containing blends of ceramic waste powder and blast furnace slag. Cleaner Materials. 7. doi.org/10.1016/j.clema.2023.100179.

Abubakr, M, Khitab, A, Anwar, W, Tayyab, S, Sadiq, S & Tayyeb, S. 2019. Evaluation of Ordinary Concrete Having Ceramic Waste Powder as Partial Replacement of Cement. In: International Conference on Sustainable Development in Civil Engineering, MUET. Available from: https://www.researchgate.net/publication/339447452.

American Concrete Institute (ACI) (2019) *ACI 318-19: Building Code Requirements for Structural Concrete and Commentary.* Farmington Hills, MI: American Concrete Institute.

AfriSam (2018) *AfriSam Technical Reference Guide.* Johannesburg, South Africa: AfriSam (South Africa) (Pty) Ltd.

Ahmad, DH & Alhayani, AA. 2022. Investigation the influence of nano ceramic on the mechanical properties and shrinkage of lightweight concrete containing silica fume. Materials Today: Proceedings. 61:1140–1148. doi.org/10.1016/j.matpr.2021.11.540.

Alexander, MG, Mackechnie, JR & Ballim, Y. 1999. Guide to the use of durability indexes for achieving durability in concrete structures, Research Monograph No. 2. Department of Civil Engineering, University of Cape Town.

Alexander, MG, Ballim, Y & Stanish, K. 2008. A framework for use of durability indexes in performance-based design and specifications for reinforced concrete structures. Materials and Structures/Materiaux et Constructions. 41(5):921–936. doi.org/10.1617/s11527-007-9295-0.

Al-Ruqaishi, AAZM, Ali Allamki, MSH & Poloju, KK. 2019. The advancement of ceramic waste in concrete. International Journal of Advanced and Applied Sciences. 6(11):102–108. doi.org/10.21833/ijaas.2019.11.013.

Alsaif, A. (2021) 'Effect of ceramic waste powder on the mechanical and durability properties of concrete', *Construction and Building Materials*, 302, Article 124009. https://doi.org/10.1016/j.conbuildmat.2021.124009.

ASTM International (2018) ASTM C989/C989M-18: *Standard Specification for Ground Granulated Blast-Furnace Slag for Use in Concrete and Mortars.* West Conshohocken, PA: ASTM International.

ASTM International (2019) ASTM C618-19: *Standard Specification for Coal Fly Ash and Raw or Calcined Natural Pozzolan for Use in Concrete.* West Conshohocken, PA: ASTM International.

ASTM International (2020) ASTM C1012-20: *Standard Test Method for Length Change of Hydraulic-Cement Mortars Exposed to a Sulfate Solution.* West Conshohocken, PA: ASTM International.

ASTM International (2022) ASTM C618-22: *Standard Specification for Coal Fly Ash and Raw or Calcined Natural Pozzolan for Use in Concrete.* West Conshohocken, PA: ASTM International.

ASTM International (2016) *ASTM C33/C33M-16: Standard Specification for Concrete Aggregates.* West Conshohocken, PA: ASTM International. Available at: https://doi.org/10.1520/C0033_C0033M-16

Attaelmanan, M, Elhaj Mahgoub Kambal, M & Mansour, MI. 2021. Study the Effect of Using Ceramic Waste Powder as Partial Replacement for Cement on Concrete Properties. Journal of Karary University for Engineering and Science. (November, 21). doi.org/10.54388/jkues.v1i1.125.

Barbhuiya, S, Das, BB, Qureshi, T & Adak, D. 2024. Cement-based solidification of nuclear waste: Mechanisms, formulations and regulatory considerations. Journal of Environmental Management. 356:120712. doi.org/10.1016/J.JENVMAN.2024.120712.

British Standards Institution. 2009. Admixture for concrete, mortar and grout. Concrete admixtures. Definitions, requirement, conformity, making and labelling BS EN 934-2:2009 (2009).

British Standards Institution. 2013. BS EN 206:2013 – Concrete – Specification, performance, production, and conformity.

British Standards Institution (2013) BS EN 206:2013 – Concrete — Specification, Performance, Production and Conformity. London: BSI Standards Limited.

European Committee for Standardization (CEN) (2011) EN 197-1:2011 – Cement — Part 1: Composition, Specifications and Conformity Criteria for Common Cements. Brussels: CEN.

Ceramic Materials. 2007. New York, NY: Springer New York. doi.org/10.1007/978-0-387-46271-4.

Chen, MC, Fang, W, Xu, KC & Xie, L. 2017. Research on Durability of Recycled Ceramic Powder Concrete. In: IOP Conference Series: Materials Science and Engineering. V. 216. Institute of Physics Publishing. doi.org/10.1088/1757-899X/216/1/012018.

Chen, X, Zhang, D, Cheng, S, Xu, X, Zhao, C, Wang, X, Wu, Q & Bai, X. 2022a. Sustainable reuse of ceramic waste powder as a supplementary cementitious material in recycled aggregate concrete: Mechanical properties, durability and microstructure assessment. Journal of Building Engineering. 52. doi.org/10.1016/j.jobe.2022.104418.

Daniel, S & Raju, AA. 2018. A Study of Properties of Concrete Making Partial Replacement of Cement by Ceramic waste Powder. International Research Journal of Engineering and Technology. Available from: www.irjet.net.

Department: Environmental Affairs. 2018. South Africa-State of Waste Report II. Available from: www.environment.gov.za.

Department: Mineral Resources. 2010. Ceramic Industry in South Africa, 2010. Available from: http://www.dmr.gov.za.

Department of Environmental Affairs (2011) *National Waste Management Strategy.* Pretoria, South Africa: Department of Environmental Affairs, Republic of South Africa.

Diamond, S. 2004. The microstructure of cement paste and concrete - A visual primer. Cement and Concrete Composites. 26(8):919–933. doi.org/10.1016/j.cemconcomp.2004.02.028.

European Federation of National Associations Representing Producers and Applicators of Specialist Building Products for Concrete (EFNARC) (2002) Specification and Guidelines for Self-Compacting Concrete (SCC). Surrey, UK: EFNARC.

El-Dieb, AS & Kanaan, DM. 2018. Ceramic waste powder an alternative cement replacement – Characterization and evaluation. Sustainable Materials and Technologies. 17. doi.org/10.1016/j.susmat.2018.e00063.

El-Dieb, AS, Taha, MR, Kanaan, D & Aly, ST. 2018. Ceramic waste powder: From landfill to sustainable concretes. Proceedings of Institution of Civil Engineers: Construction Materials. 171(3):109–116. doi.org/10.1680/jcoma.17.00019.

El-Hawary, M & Nouh, K. 2018. Properties and sustainability of concrete containing fillers*. Australian Journal of Civil Engineering. 16(2):96–105. doi.org/10.1080/14488353.2018.1453968.

Fayomi, GU, Mini, SE, Fayomi, OSI & Ayoola, AA. 2019. Perspectives on environmental CO2 emission and energy factor in Cement Industry. In: IOP Conference Series: Earth and Environmental Science. V. 331. Institute of Physics Publishing. doi.org/10.1088/1755-1315/331/1/012035.

Gol, F, Kacar, E, Saritas, ZG, Cibuk, S, Ture, C, Arslan, M & Sen, F. 2023. The use of boron based materials on efficiency of environmentally friendly porous ceramics. Environmental Research. 216:114454. doi.org/10.1016/j.envres.2022.114454.

Govindarajalu, E & Ganapathy, GP. 2024. Reuse of ceramic waste in concrete production for a sustainable ecosystem. Revista Materia. 29(3). doi.org/10.1590/1517-7076-RMAT-2024-0325.

Hampshire, S & Pomeroy, M. 2021. Overview: Oxide Ceramics and Non-oxide Ceramics. In: Encyclopedia of Materials: Technical Ceramics and Glasses. Elsevier. 1–2. doi.org/10.1016/B978-0-12-818542-1.00104-1.

Heidari, A & Tavakoli, D. 2013. A study of the mechanical properties of ground ceramic powder concrete incorporating nano-SiO2 particles. Construction and Building Materials. 38:255–264. doi.org/10.1016/j.conbuildmat.2012.07.110.

Hilal, AA. 2016. Microstructure of Concrete. In: High Performance Concrete Technology and Applications. InTech. doi.org/10.5772/64574.

Howe, PD. 1998. A review of boron effects in the environment. Biological Trace Element Research. 66(1–3):153–166. doi.org/10.1007/BF02783135.

Huseien, GF, Sam, ARM, Shah, KW & Mirza, J. 2020. Effects of ceramic tile powder waste on properties of self-compacted alkali-activated concrete. Construction and Building Materials. 236. doi.org/10.1016/j.conbuildmat.2019.117574.

Hussain Ali Assistant Professor, A, Abbas Al-Attar, D, Emad Kasm, Z, Author, C, Hussain Ali, A & Abbas Al-Attar, A. 2019. Effect of solid ceramic waste powder in partial replacement of cement on mechanical properties and sorptivity of CEMENT MORTAR. International Journal of Civil Engineering and Technology (IJCIET). 10(3):3055–3066.

Ige, OE, Olanrewaju, OA, Duffy, KJ & Collins, OC. 2022. Environmental Impact Analysis of Portland Cement (CEM1) Using the Midpoint Method. Energies. 15(7). doi.org/10.3390/en15072708.

Ikotun, J, Adedeji, P, Babafemi, A & Otieno, M. 2025. Use of Ceramic Waste Powder as a Partial Cement Replacement in Concrete—A Review of Microstructure and Durability Properties. In: Proceedings of the 7th International Conference on Concrete Repair, Rehabilitation and Retrofitting. ICCRRR 2024. H. Beushausen, J. Ndawula, M. Alexander, F. Dehn, & P. Moyo, Eds. RILEM Bookseries, vol 59. Springer, Cham. 505–519. doi.org/https://doi.org/10.1007/978-3-031-75507-1_49.

International Organization for Standardization (ISO) (2020) *ISO 13320:2020. Particle Size Analysis — Laser Diffraction Methods.* Geneva: ISO.

Jamal, MA, Mohammed, AS & Ali, JA. 2025. Innovative assessment of cement chemistry and the impact of additives on compressive strength across various specimen sizes and extended curing conditions. Multiscale and Multidisciplinary Modeling, Experiments and Design. 8(1):106. doi.org/10.1007/s41939-024-00691-1.

John, VM, Damineli, BL, Quattrone, M & Pileggi, RG. 2018. doi.org/10.1016/j.cemconres.2017.09.013.

Kannan, DM, Aboubakr, SH, EL-Dieb, AS & Reda Taha, MM. 2017. High performance concrete incorporating ceramic waste powder as large partial replacement of Portland cement. Construction and Building Materials. 144:35–41. doi.org/10.1016/j.conbuildmat.2017.03.115.

Kulovaná, T, Vejmelková, E, Keppert, M, Rovnaníková, P, Keršner, Z & Černý, R. 2016a. Mechanical, durability and hygrothermal properties of concrete produced using Portland cement-ceramic powder blends. Structural Concrete. 17(1):105–115. doi.org/10.1002/suco.201500029.

Kumar, VP & Reddy, KC. 2017. Durability Aspects of Concrete By Partial Replacement of Cement By Ceramic Waste. International Journal of Civil Engineering and Technology. 8(4):22–30.

Lai, M, Hanzic, L & Ho, JCM. 2019. Fillers to improve passing ability of concrete. Structural Concrete. 20(1):185–197. doi.org/10.1002/suco.201800047.

Lasseuguette, E, Burns, S, Simmons, D, Francis, E, Chai, HK, Koutsos, V & Huang, Y. 2019. Chemical, microstructural and mechanical properties of ceramic waste blended cementitious

systems. Journal of Cleaner Production. 211:1228–1238. doi.org/10.1016/j.jclepro.2018.11.240.

Lee, JH, Choi, SM, Lee, JH, Hong, J, Kim, H, Yoon, KJ & Kim, BK. 2014. Effect of sintering atmosphere on phase stability, and electrical conductivity of proton-conducting Ba(Zr0.84Y0.15Cu 0.01)O3-δ. International Journal of Hydrogen Energy. 39(13):7100–7108. doi.org/10.1016/j.ijhydene.2014.02.072.

Li, L, Liu, W, You, Q, Chen, M & Zeng, Q. 2020. Waste ceramic powder as a pozzolanic supplementary filler of cement for developing sustainable building materials. Journal of Cleaner Production. 259. doi.org/10.1016/j.jclepro.2020.120853.

Li, L, Joseph, P, Zhang, X & Zhang, L. 2024. A study of some relevant properties of concrete incorporating waste ceramic powder as a cement replacement agent. Journal of Building Engineering. 87. doi.org/10.1016/j.jobe.2024.109106.

Li, W, Lin, X, Bao, DW & Min Xie, Y. 2022. A review of formwork systems for modern concrete construction. Structures. 38:52–63. doi.org/10.1016/J.ISTRUC.2022.01.089.

Ling, T-C & Poon, C-S. 2014. Use of recycled CRT funnel glass as fine aggregate in dry-mixed concrete paving blocks. Journal of Cleaner Production. 68:209–215. doi.org/10.1016/j.jclepro.2013.12.084.

Luhar, S, Cheng, TW, Nicolaides, D, Luhar, I, Panias, D & Sakkas, K. 2019. doi.org/10.1016/j.conbuildmat.2019.06.169.

Madadi, A & Wei, J. 2022. Characterization of Calcium Silicate Hydrate Gels with Different Calcium to Silica Ratios and Polymer Modifications. Gels. 8(2). doi.org/10.3390/gels8020075.

Magbool, H.M. (2022) 'Recycling ceramic waste powder as a supplementary cementitious material: effects on strength and durability of concrete', *Journal of Building Engineering*, 46, Article 103815. https://doi.org/10.1016/j.jobe.2021.103815.

Malhotra, VM & Mehta, PK. 2004. Pozzolanic and Cementitious Materials. CRC Press. doi.org/10.1201/9781482296761.

Medina, C, Frías, M & Sánchez de Rojas, MI. 2014. Leaching in concretes containing recycled ceramic aggregate from the sanitary ware industry. Journal of Cleaner Production. 66:85–91. doi.org/10.1016/j.jclepro.2013.10.029.

Medina, C, Sánchez De Rojas, MI, Thomas, C, Polanco, JA & Frías, M. 2016. Durability of recycled concrete made with recycled ceramic sanitary ware aggregate. Inter-indicator

relationships. Construction and Building Materials. 105:480–486. doi.org/10.1016/j.conbuildmat.2015.12.176.

Mehta, P.K. and Monteiro, P.J.M. (2001) *Concrete: Microstructure, Properties and Materials.* 3rd edn. New York: McGraw-Hill.

Mezidi, A, Merabti, S, Benyamina, S & Sadouki, M. 2023. Effect of Substituting White Cement with Ceramic Waste Powders (CWP) on the Performance of a Mortar Based on Crushed Sand. Advances in Materials Science. 23(4):123–133. doi.org/10.2478/adms-2023-0026.

Mindess, S, Young, JF & Darwin, D. 2003. Concrete . 2nd ed. ed. Prentice Hall. ISBN: 9780130646323.

Rahaman, M.N. (2007) *Sintering of Ceramics.* 2nd edn. Boca Raton, FL: CRC Press.

Mohammadhosseini, H, Lim, NHAS, Tahir, MM, Alyousef, R, Samadi, M, Alabduljabbar, H & Mohamed, AM. 2020. Effects of Waste Ceramic as Cement and Fine Aggregate on Durability Performance of Sustainable Mortar. Arabian Journal for Science and Engineering. 45(5):3623–3634. doi.org/10.1007/s13369-019-04198-7.

Mohit, M, Haftbaradaran, H & Riahi, HT. 2023. Investigating the ternary cement containing Portland cement, ceramic waste powder, and limestone. Construction and Building Materials. 369. doi.org/10.1016/j.conbuildmat.2023.130596.

Moosberg-Bustnes, H, Lagerblad, B & Forssberg, E. 2004a. The function of fillers in concrete.

Moosberg-Bustnes, H, Lagerblad, B & Forssberg, E. 2004b. The function of fillers in concrete. Materials and Structures. 37:74–81.

Mouiya, M, Bouazizi, A, Abourriche, A, El Khessaimi, Y, Benhammou, A, El hafiane, Y, Taha, Y, Oumam, M, et al. 2019. Effect of sintering temperature on the microstructure and mechanical behavior of porous ceramics made from clay and banana peel powder. Results in Materials. 4. doi.org/10.1016/j.rinma.2019.100028.

Najm, HM & Ahmad, S. 2022. The Use of Waste Ceramic Concrete for a Cleaner and Sustainable Environment-A Comprehensive Study of Mechanical and Microstructural Properties. doi.org/10.21203/rs.3.rs-1616616/v1.

Neville, A.M. (2011) *Properties of Concrete.* 5th edn. Harlow, England: Pearson Education Limited.

Nikodemski, S, Tong, J & O'Hayre, R. 2013. Solid-state reactive sintering mechanism for proton conducting ceramics. Solid State Ionics. 253:201–210. doi.org/10.1016/j.ssi.2013.09.025.

Pacheco-Torgal, F & Jalali, S. 2010. Reusing ceramic wastes in concrete. Construction and Building Materials. 24(5):832–838. doi.org/10.1016/j.conbuildmat.2009.10.023.

Paiva, H, Silva, AS, Velosa, A, Cachim, P & Ferreira, VM. 2017. Microstructure and hardened state properties on pozzolan-containing concrete. Construction and Building Materials. 140:374–384. doi.org/10.1016/j.conbuildmat.2017.02.120.

Parashar, AK, Sharma, P & Sharma, N. 2022. An investigation on Properties of Concrete with the adding of Waste of Ceramic and micro silica. Materials Today: Proceedings. 62:4036–4040. doi.org/10.1016/j.matpr.2022.04.603.

Patel, H, Arora, NK & Vaniya, SR. 2015. Use of Ceramic Waste Powder in Cement Concrete. IJIRST-International Journal for Innovative Research in Science & Technology|. 2(1). Available from: www.ijirst.org.

Rahaman, MN. 2017. Ceramic Processing and Sintering. CRC Press. doi.org/10.1201/9781315274126.

Rani, SM. 2016. A Study on Ceramic Waste Powder. SSRG International Journal of Civil Engineering (SSRG-IJCE). 3. Available from: www.internationaljournalssrg.org.

Raval, AD, Patel, N & Pitroda, J. 2013. Ceramic Waste : Effective Replacement Of Cement For Establishing Sustainable Concrete. International Journal of Engineering Trends and Technology (IJETT). Available from: http://www.ijettjournal.org.

Rawarkar, K & Ambadkar, S. 2018. A Review on Factors Affecting Workability of Concrete. International Journal of Innovative Research in Science. 7. doi.org/10.15680/IJIRSET.2018.0708024.

Richerson, DW & Lee, WE. 2018. Modern Ceramic Engineering. CRC Press. doi.org/10.1201/9780429488245.

Salvi, D, Gupta, T & Sharma, RK. 2021a. A Review on Hardened Properties of Eco-Friendly Concrete Containing Ceramic Waste Powder. Journal of Scientific Research and Reports. (June, 28):87–103. doi.org/10.9734/jsrr/2021/v27i530392.

South African Bureau of Standards (2006a) SANS 5845:2006 – Aggregate Tests: Bulk Density of Aggregates. Pretoria: SABS Standards Division.

South African Bureau of Standards (2006b) SANS 5862-1:2006 – Concrete Tests – Part 1: Consistence of Freshly Mixed Concrete (Slump Test). Pretoria: SABS Standards Division.

South African Bureau of Standards (2006c) SANS 5861-1:2006 – Concrete Tests – Part 1: Mixing Fresh Concrete in the Laboratory. Pretoria: SABS Standards Division.

South African Bureau of Standards (2006d) SANS 5860:2006 – Concrete Mould Preparation. Pretoria: SABS Standards Division.

South African Bureau of Standards (2006e) SANS 5863:2006 – Concrete Tests: Compressive Strength of Hardened Concrete. Pretoria: SABS Standards Division.

South African Bureau of Standards (2006f) SANS 6253:2006 – Concrete Tests: Tensile Splitting Strength of Concrete. Pretoria: SABS Standards Division.

South African Bureau of Standards (2013) SANS 50197:2013 – Common Cements. Pretoria: SABS Standards Division.

South African Bureau of Standards (2014a) SANS 1083:2014 – Aggregates from Natural Sources: Aggregate for Concrete. Pretoria: SABS Standards Division.

South African Bureau of Standards (2014b) SANS 10100-2:2014 – The Structural Use of Concrete – Part 2: Materials and Execution of Work. Pretoria: SABS Standards Division.

South African Bureau of Standards (2014c) SANS 51008:2014 – Mixing Water for Concrete: Specification for Sampling, Testing and Assessing the Suitability of Water, Including Water Recovered from Processes in the Concrete Industry as Mixing Water for Concrete. Pretoria: SABS Standards Division.

South African Bureau of Standards (2014d) SANS 50450-1:2014 – Portland Cement Extenders – Part 1: Fly Ash. Pretoria: SABS Standards Division.

South African Bureau of Standards (2015) SANS 3001-CO3-1:2015 – Civil Engineering Test Methods – Part CO3-1: Concrete Durability Index Testing – Preparation of Test Specimens. Pretoria: SABS Standards Division.

Scrivener, KL, John, VM & Gartner, EM. 2018. Eco-efficient cements: Potential economically viable solutions for a low-CO2 cement-based materials industry. Cement and Concrete Research. 114:2–26. doi.org/10.1016/j.cemconres.2018.03.015.

Siddique, R. 2014. Utilization of industrial by-products in concrete. In: Procedia Engineering. V. 95. Elsevier Ltd. 335–347. doi.org/10.1016/j.proeng.2014.12.192.

Silva, R V., De Brito, J & Dhir, RK. 2014. Properties and composition of recycled aggregates from construction and demolition waste suitable for concrete production. Construction and Building Materials. 65:201–217. doi.org/10.1016/j.conbuildmat.2014.04.117.

Sondarva, PR, Pitroda, JR, Gujar, R & Soni, J. 2022a. An Experimental Investigation on the Strength Properties of Ceramic Tiles Waste Powder based Bacterial Concrete. Materials Today: Proceedings. 62(P13):7062–7067. doi.org/10.1016/j.matpr.2022.01.140.

Subaşı, S, Öztürk, H & Emiroğlu, M. 2017a. Utilizing of waste ceramic powders as filler material in self-consolidating concrete. Construction and Building Materials. 149:567–574. doi.org/10.1016/j.conbuildmat.2017.05.180.

Taher, MJ, Abed, EH & Hashim, MS. 2023. Using ceramic waste tile powder as a sustainable and eco-friendly partial cement replacement in concrete production. Materials Today: Proceedings. doi.org/10.1016/j.matpr.2023.04.060.

Tahir, A & Kumar Poloju, K. 2017. Use of Ceramic Powder in Concrete-Strength & Durability Properties. Journal of Student Research. Available from: www.jofsr.com.

Tawfik, TA, Sičáková, A, Kuzielová, E, Kušnír, Š, Eštoková, A, Bálintová, M & Junáková, N. 2024. Sustainable reuse of waste ceramic tiles powder and waste brick powder as a replacement for cement on green high strength concrete properties. Innovative Infrastructure Solutions. 9(5). doi.org/10.1007/s41062-024-01498-2.

Taylor, HFW (Harry FW). 1997. Cement chemistry. T. Telford.

Umar, T, Tahir, A, Egbu, C, Honnurvali, MS, Saidani, M & Al-Bayati, AJ. 2021. Developing a Sustainable Concrete Using Ceramic Waste Powder. Advances in Science, Technology and Innovation. 157–162. doi.org/10.1007/978-3-030-48465-1_27.

Wang, Y, Zhu, S, Zhou, X & Zhang, T. 2022. Effect Of Sintering Process On Micro-structure And Properties Of Mullite Porous Ceramics Containing magnesium oxide. Journal of Physics: Conference Series. 2206(1). doi.org/10.1088/1742-6596/2206/1/012037.

Zhang, GY, Ahn, YH, Lin, RS & Wang, XY. 2021. Effect of waste ceramic powder on properties of alkali-activated blast furnace slag paste and mortar. Polymers. 13(16). doi.org/10.3390/polym13162817.

Zhang, Z., Qian, S., Zhang, Q. and Li, L. (2022) ‘Effects of ceramic waste powder on concrete properties: A comprehensive review’, *Advances in Materials Science and Engineering*, 2022, Article ID 9781273. Available at: https://doi.org/10.1155/2022/9781273

Appendix A
Data from SEM-EDS of CWP

Table A. 1: Chemical composition of CWP from SEM-EDS for all spectrums

Spectrum Label	Spectrum 61	Spectrum 62	Spectrum 63	Spectrum 64	Spectrum 65	Spectrum 66	Spectrum 67	Spectrum 68	Spectrum 69	Spectrum 70	Spectrum 71
O	53,07	53,24	54,16	53,84	54,17	56,35	46,58	54,93	51,23	55,73	53,49
Na	1,22	1,36	1,06	1,11	1,29	0,65	1,32	1,14	0,29	1,04	1,00
Mg	0,57	0,24	0,04	0,00	0,09	0,49	0,00	0,03	0,79	0,41	0,34
Al	13,54	14,99	13,38	13,42	13,07	12,72	17,84	15,05	13,37	12,15	13,53
Si	28,73	28,93	29,98	28,95	28,86	28,34	30,26	27,39	31,96	28,03	30,15
S	0,00	0,00	0,00	0,11	0,18	0,00	0,00	0,00	0,00	0,00	0,00
Ca	0,62	0,06	0,19	0,62	0,38	0,13	0,00	0,00	0,16	0,64	0,51
Ti	0,92	0,58	0,72	0,69	0,53	0,21	2,44	0,38	0,81	0,60	0,00
Fe	1,33	0,60	0,46	1,26	1,43	1,12	1,56	1,07	1,38	1,40	0,99
Total	100	100	100	100	100	100	100	100	100	100	100

Table A. 2: Summary of the chemical composition of CWP

Statistics	O	Na	Mg	Al	Si	S	Ca	Ti	Fe
Max	56,35	1,36	0,79	17,84	31,96	0,18	0,64	2,44	1,56
Min	46,58	0,29	0	12,15	27,39	0	0	0	0,46
Average	53,34	1,04	0,27	13,91	29,23	0,03	0,30	0,72	1,15
Standard Deviation	2,63	0,32	0,27	1,56	1,27	0,06	0,26	0,63	0,35

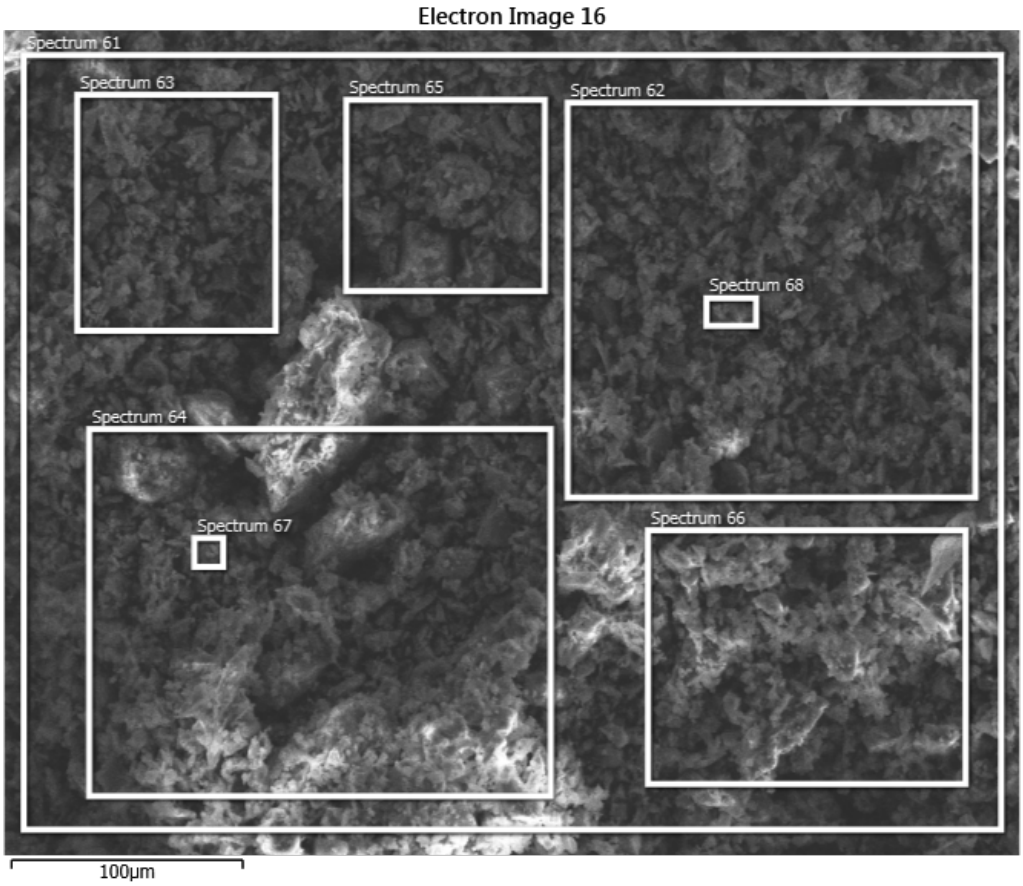

Figure A. 1: electron image 16

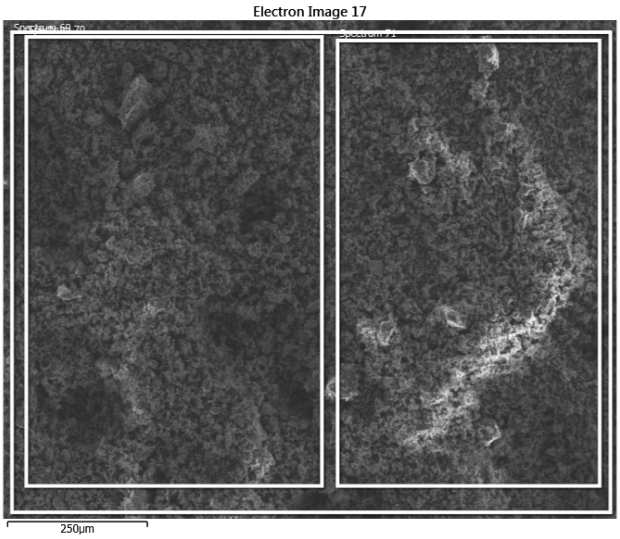

Figure A. 2: electron image 17

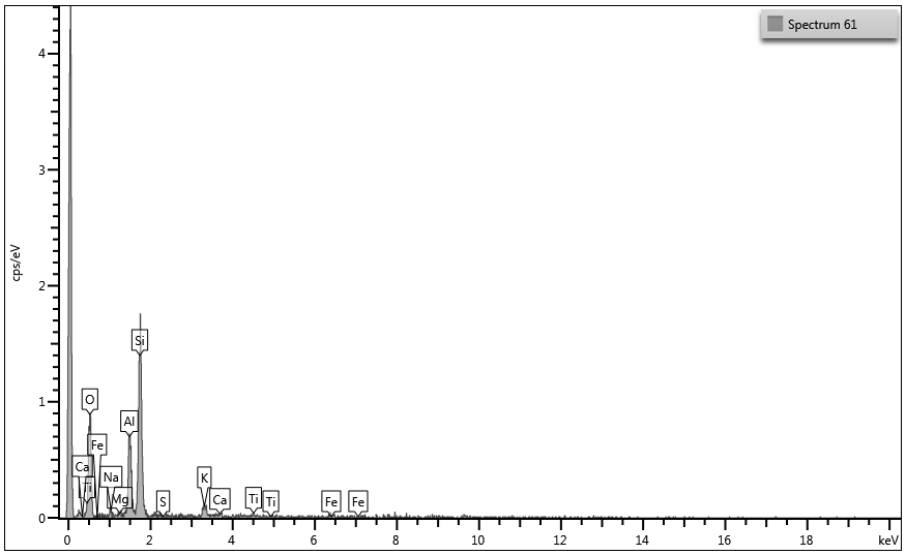

Figure A. 3: SEM-EDS of CWP spectrum 61

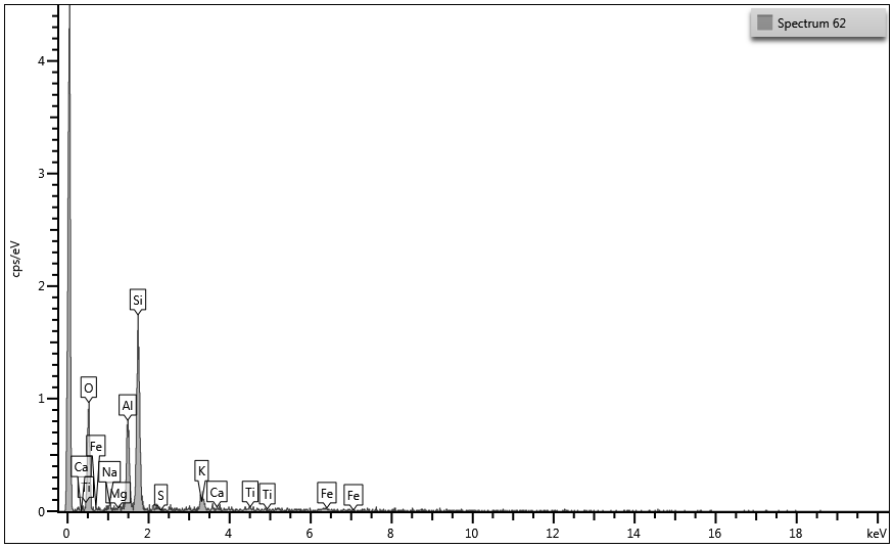

Figure A. 4: SEM-EDS of CWP spectrum 62

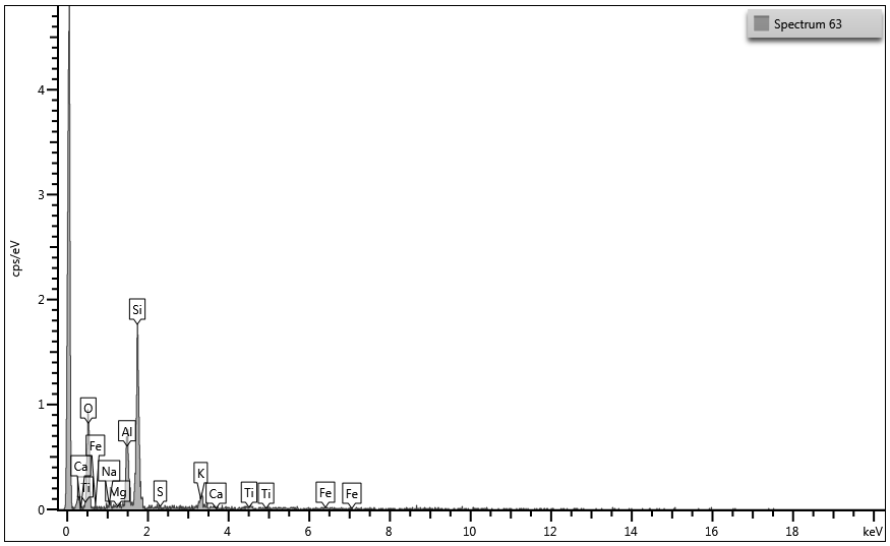

Figure A. 5: SEM-EDS of CWP spectrum 63

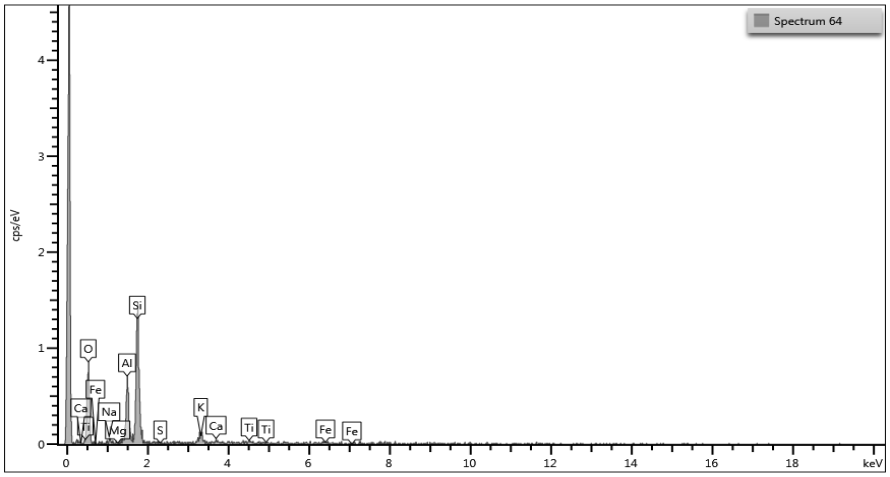

Figure A. 6: SEM-EDS of CWP spectrum 64

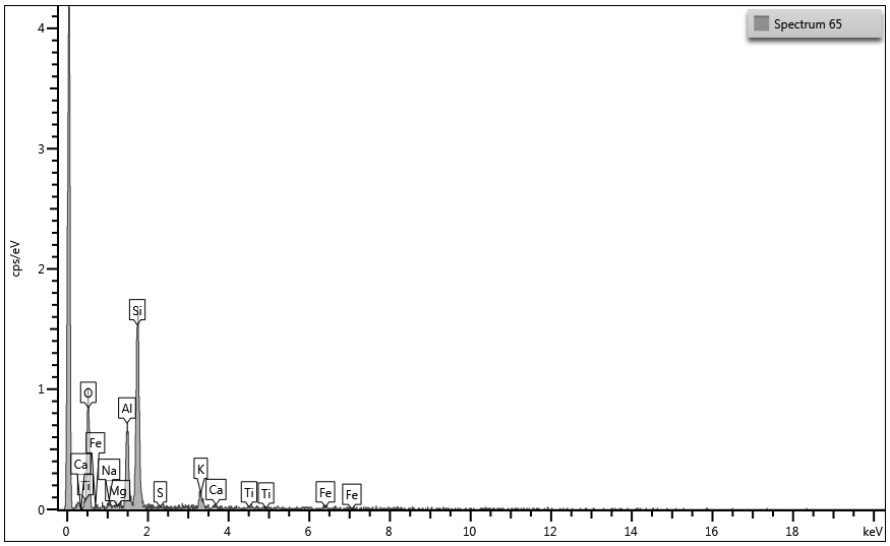

Figure A. 7: SEM-EDS of CWP spectrum 65

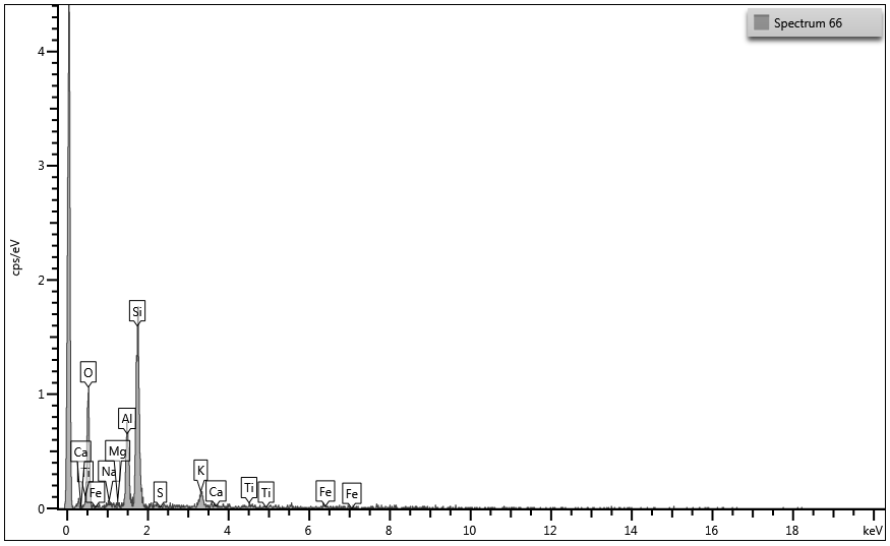

Figure A. 8: SEM-EDS of CWP spectrum 66

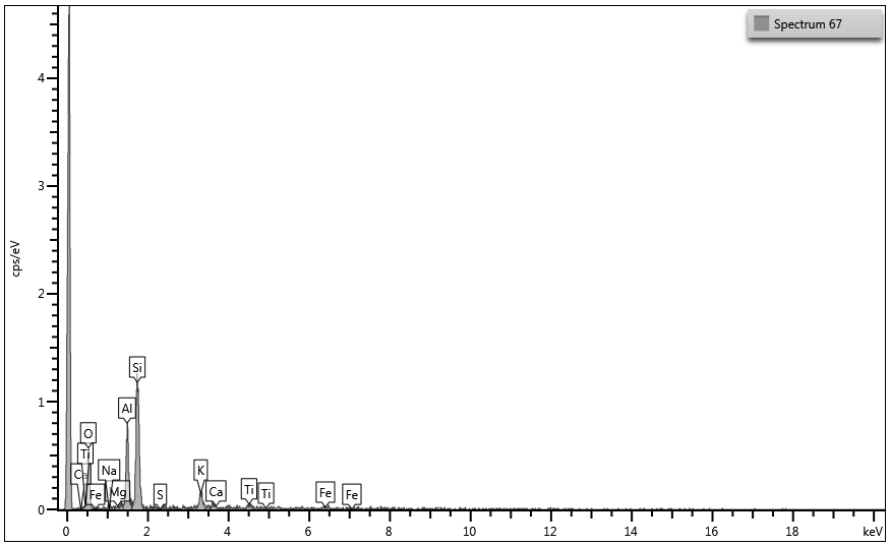

Figure A. 9: SEM-EDS of CWP spectrum 67

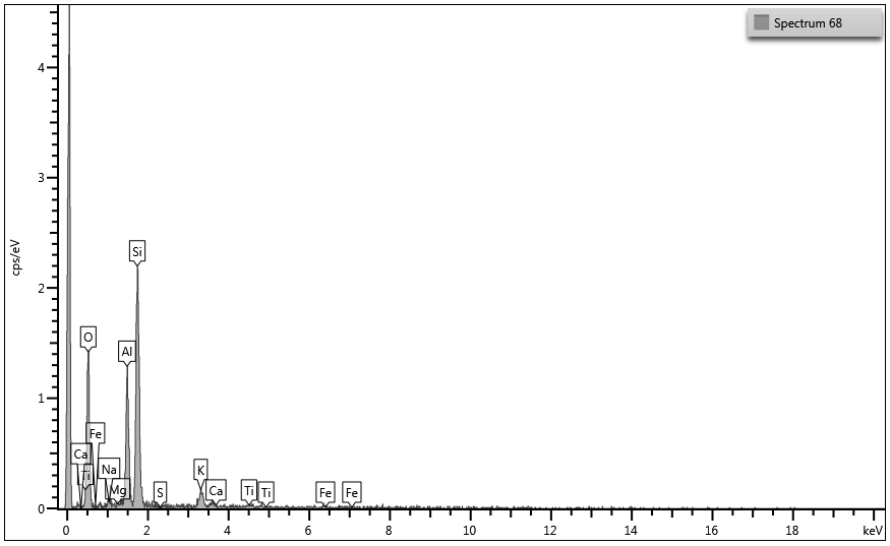

Figure A. 10: SEM-EDS of CWP spectrum 68

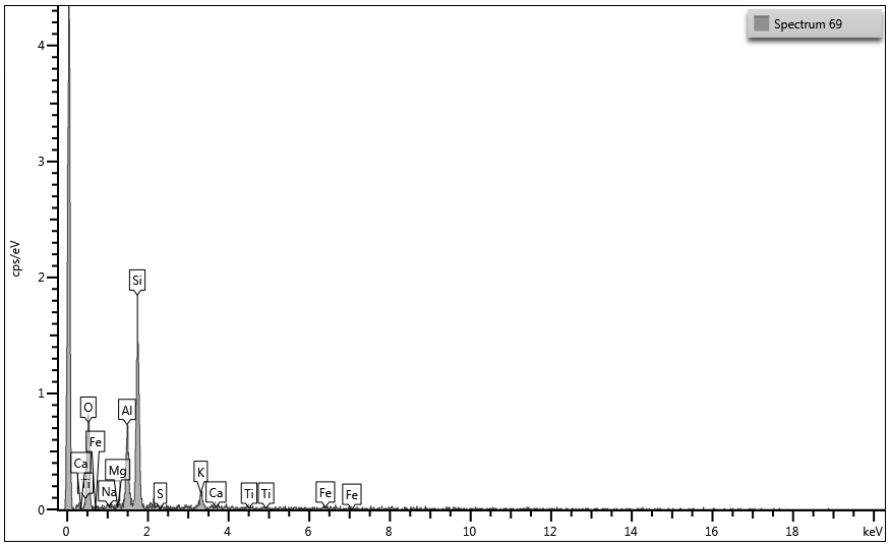

Figure A. 11: SEM-EDS of CWP spectrum 69

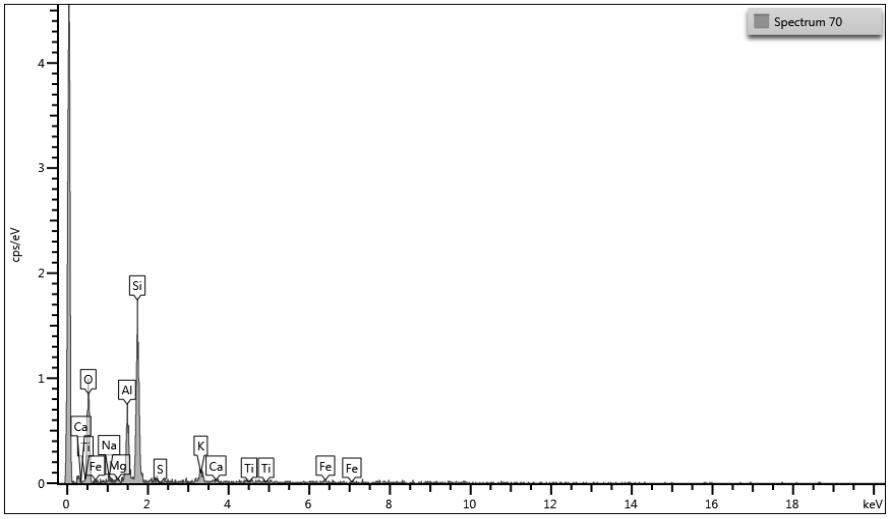

Figure A. 12: SEM-EDS of CWP spectrum 70

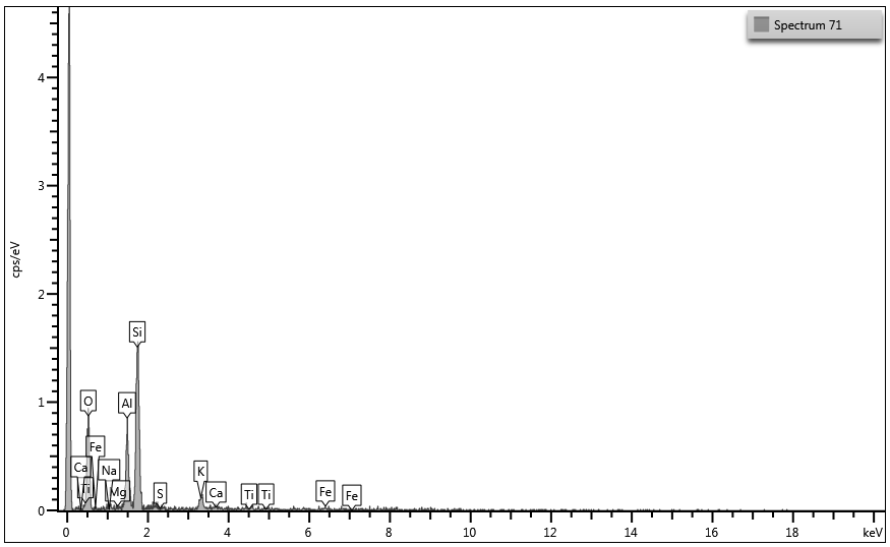

Figure A. 13: SEM-EDS of CWP spectrum 71

Appendix B

Supplementary data on material characterization

Table A. 3: Physical characteristics of coarse aggregates

S/N	Characteristics	Value
1.	Type	Andesite Crusher sand
2.	Specific gravity	2.79
3.	Fineness Modulus	2.90
4.	Density	2021.57kg/m^3

Table A. 4: Sieve Analysis of Fine Aggregates

ASTM C136: Sieve Analysis of Fine Aggregates

Sieve size (mm)	ASTM C33 Finer Limit (ASTM C 33 2016)		Mass of Sample A retained (g)	Mass of Sample B retained (g)	Mass of Sample C retained (g)	Av. Sample retained (g)	Percentage Retained (%)	Cumulative percentage retrained (%)	Percentage Passing (%)
9.5	100	100	0,00	0,00	0,00	0,00	0	0	100
4,75	100	95	20,34	12,39	18,91	17,21	3,44	3,44	96,56
2,36	100	80	89,38	75,42	84,13	82,98	16,60	20,04	79,96
1,18	85	50	123,61	122,29	115,12	120,34	24,07	44,11	55,89
0,6	60	25	65,92	76,59	71,55	71,35	14,27	58,38	41,62
0,3	30	5	85,85	90,39	61,45	79,23	15,85	74,22	25,78
0,15	10	0	83,44	72,06	70,71	75,40	15,08	89,30	10,70
PAN			30,66	50,30	77,72	52,89	10,58	99,88	
Total			**499,20**	**499,43**	**499,58**	**499,40**	**99,88**		

Mass of Dry Sample A, B and C = 500g

Fineness Modulus = $\frac{\sum Cummulative\ \%\ Retained}{100}$

= 289.49/100 = 2.90

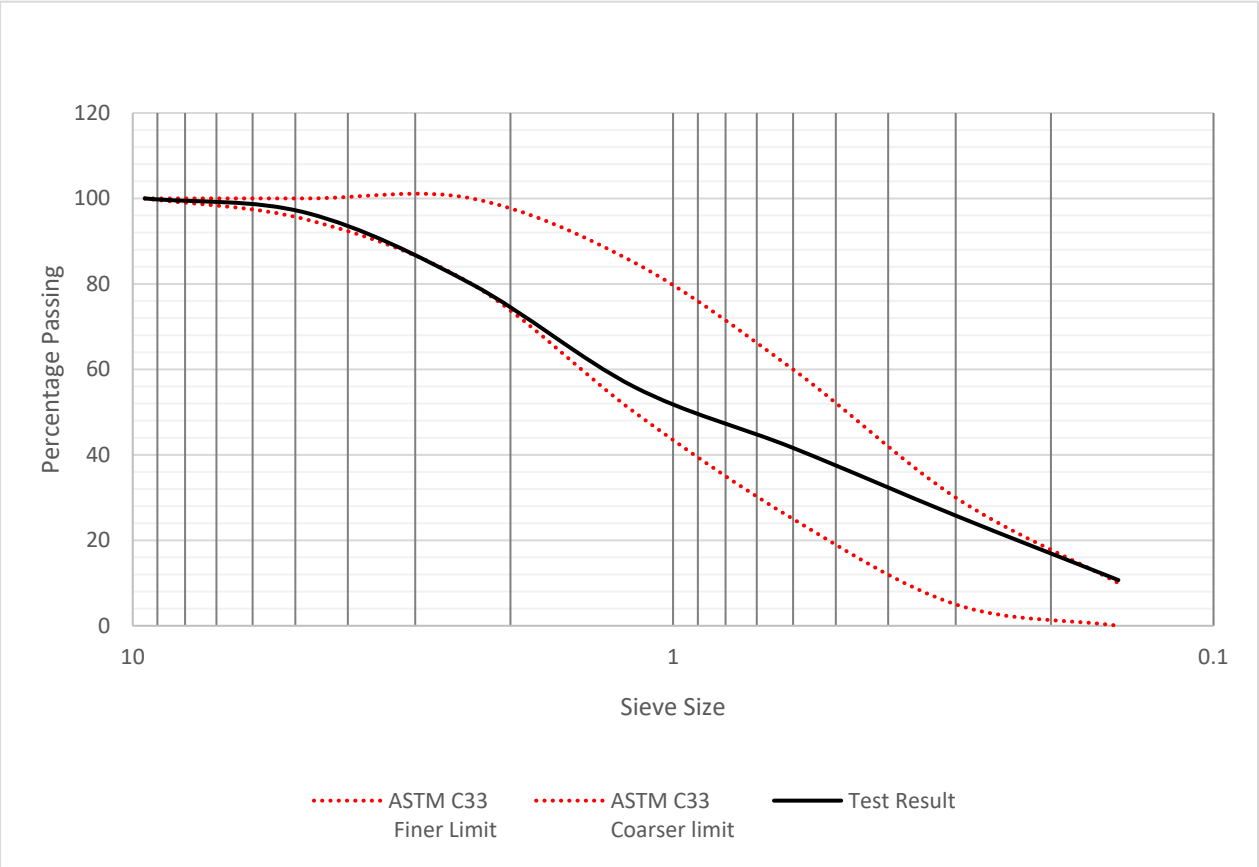

Figure A. 14: Sieve Analysis of Fine Aggregates

Table A. 5: Properties of Coarse Aggregates

S/N	Characteristics	Value
1.	Type	Andesite stones
2.	Specific gravity	2.88
3.	Density	1636.90kg/m^3

Table A. 6: Sieve Analysis of Coarse Aggregates

ASTM C136: Sieve Analysis of Fine Aggregates								
Sieve size (mm)	**ASTM C33 Finer Limit** (ASTM C 33 2016)	**SAMPLE A Retained weight (g)**	**SAMPLE B Retained weight (g)**	**SAMPLE C Retained weight (g)**	**Average retained (g)**	**Percentage Retained (%)**	**Cumulative % retrained**	**Percentage Passing**

25. 0	100	100	0,00	0,0	0,0	0,0	0,00	0,00	100,00
19,00	100	90	0,00	0,0	0,0	0,0	0,00	0,00	100,00
12.5	55	20	596,66	637,9	586,9	607,2	60,72	60,72	39,28
9,50	15	0	358,68	313,3	349,4	340,5	34,05	94,76	5,24
4,75	5	0	42,38	48,0	62,8	51,1	5,11	99,87	0,13
Pan			1,70	0,6	0,3	0,9	0,09	99,96	
Total			**999,42**	**999,8**	**999,5**	**999,6**	**99,96**		

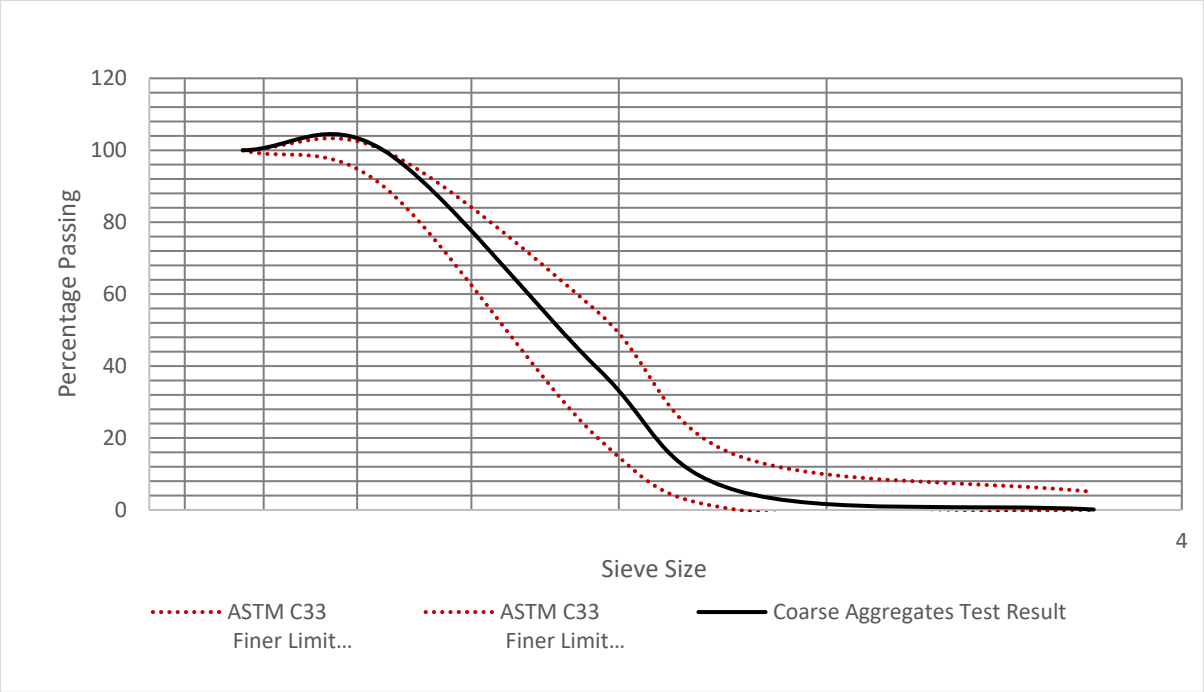

Figure A. 15: Coarse Aggregates Grading

Appendix C
Tables of mechanical properties of concrete

Table A. 7: compressive strength data

COMPRESSIVE STRENGTH AT 0.45 W/B						
Concrete mix label	**Binder**	**Percentage replacement (%)**	**7 days**	**28 days**	**56 days**	**90 days**
Replacement of GGBS with CWP						
M1A	CR1	0	40.32	58.3	64.45	73.67
M2A	CR1-C1	10	39.18	55.41	64.63	66.26
M3A	CR1-C2	20	35.09	48.52	56.07	61.17
Replacement of LSP with CWP						
M4A	CR2	0	51.29	60.19	67.83	69.01
M5A	CR2-C1	5	54.82	58.95	67.89	67.96
M6A	CR2-C2	7	52.4	61.85	70.01	70.05
COMPRESSIVE STRENGTH SUMMARY AT 0.50 W/B						
Concrete mix label	**Binder**	**Percentage replacement (%)**	**7 days**	**28 days**	**56 days**	**90 days**
Replacement of GGBS with CWP						
M1B	CR1	0	31.73	49.89	60.69	64.43
M2B	CR1-C1	10	30.47	41.75	53.66	54.01
M3B	CR1-C2	20	33.23	43.49	55.33	56.95
Replacement of LSP with CWP						
M4B	CR2	0	44.47	51.35	58.99	59.43
M5B	CR2-C1	5	45.19	54.91	59.62	60.56
M6B	CR2-C2	7	47.63	55.46	61.01	63.65
COMPRESSIVE STRENGTH SUMMARY AT 0.55 W/B						
Concrete mix label	**Binder**	**Percentage replacement (%)**	**7 days**	**28 days**	**56 days**	**90 days**
Replacement of GGBS with CWP						
M1C	CR1	0	29.79	43.96	52.67	59.84
M2C	CR1-C1	10	28.43	46.93	50.89	55.44
M3C	CR1-C2	20	27.41	37.34	46.11	51.05
Replacement of LSP with CWP						
M4C	CR2	0	41.35	48.98	50.95	51.9
M5C	CR2-C1	5	40.55	49.94	52.40	53.17
M6C	CR2-C2	7	42.45	52.41	56.21	56.78

Table A. 8: Splitting tensile strength data

SPLITTING TENSILE STRENGTH 0.45 W/B						
Concrete mix label	**Binder**	**Percentage replacement (%)**	**7 days**	**28 days**	**56 days**	**90 days**
Replacement of GGBS with CWP						
M1A	CR1	0	3.35	3.97	4.10	5.01
M2A	CR1-C1	10	3.01	3.89	3.94	3.95
M3A	CR1-C2	20	2.89	3.26	4.03	4.24
Replacement of LSP with CWP						
M4A	CR2	0	2.92	3.73	3.93	4.22
M5A	CR2-C1	5	3.33	3.74	4.04	4.52
M6A	CR2-C2	7	3.08	3.77	4.14	4.79
SPLITTING TENSILE STRENGTH AT 0.50 W/B						
Concrete mix label	**Binder**	**Percentage replacement (%)**	**7 days**	**28 days**	**56 days**	**90 days**
Replacement of GGBS with CWP						
M1B	CR1	0	3.09	3.68	3.80	4.75
M2B	CR1-C1	10	2.66	3.41	3.66	3.85
M3B	CR1-C2	20	2.7	2.96	3.88	4.39
Replacement of LSP with CWP						
M4B	CR2	0	2.69	2.92	3.31	3.93
M5B	CR2-C1	5	2.61	3.54	3.73	3.74
M6B	CR2-C2	7	3.17	3.29	4.88	4.91
SPLITTING TENSILE STRENGTH AT 0.55 W/B						
Concrete mix label	**Binder**	**Percentage replacement (%)**	**7 days**	**28 days**	**56 days**	**90 days**
Replacement of GGBS with CWP						
M1C	CR1	0	2.83	3.85	3.99	4.01
M2C	CR1-C1	10	2.46	2.46	3.44	4.16
M3C	CR1-C2	20	2.3	2.31	2.41	4.11
Replacement of LSP with CWP						
M4C	CR2	0	2.76	2.86	2.87	3.53
M5C	CR2-C1	5	3.05	3.19	3.50	3.64
M6C	CR2-C2	7	3.19	3.57	3.60	3.81

Table A. 9: Hard concrete density

HARD CONCRETE DENSITY SUMMARY 0.45 W/B						
Concrete mix label	**Binder**	**Percentage replacement (%)**	**7 days**	**28 days**	**56 days**	**90 days**
Replacement of GGBS with CWP						
M1A	CR1	0	2493.3	2493.3	2520.00	2546.7
M2A	CR1-C1	10	2503.3	2503.3	2516.67	2503.3
M3A	CR1-C2	20	2483.3	2483.3	2496.67	2513.3
Replacement of LSP with CWP						
M4A	CR2	0	2516.7	2516.7	2553.67	2510
M5A	CR2-C1	5	2506.7	2506.7	2503.33	2513.3
M6A	CR2-C2	7	2483.3	2483.3	2496.67	2480
HARD CONCRETE DENSITY SUMMARY 0.50 W/B						
Concrete mix label	**Binder**	**Percentage replacement (%)**	**7 days**	**28 days**	**56 days**	**90 days**
Replacement of GGBS with CWP						
M1B	CR1	0	2510	2500	2540.00	2543.3
M2B	CR1-C1	10	2486.7	2463.3	2510.00	2476.7
M3B	CR1-C2	20	2506.7	2480	2473.33	2466.7
Replacement of LSP with CWP						
M4B	CR2	0	2500	2506.7	2533.33	2520
M5B	CR2-C1	5	2500	2503.3	2506.67	2480
M6B	CR2-C2	7	2510	2500	2490.00	2506.7
HARD CONCRETE DENSITY SUMMARY 0.45 W/B						
Concrete mix label	**Binder**	**Percentage replacement (%)**	**7 days**	**28 days**	**56 days**	**90 days**
Replacement of GGBS with CWP						
M1C	CR1	0	2510	2510	2483.33	2500
M2C	CR1-C1	10	2473.3	2513.3	2476.67	2490
M3C	CR1-C2	20	2493.3	2490	2510.00	2520
Replacement of LSP with CWP						
M4C	CR2	0	2503	2473.3	2503.33	2480
M5C	CR2-C1	5	2500	2523.3	2500.00	2490
M6C	CR2-C2	7	2510	2523.3	2526.67	2513.3

Appendix E
Durability index results

Table A. 10: Durability Index results at 0.45 W/B ratio

VALUES OF K (m/s) for OPI								
Replacement of GGBS with CWP					**Replacement of Limestone with CWP**			
	M1A	**M2A**	**M3A**			**M4A**	**M5A**	**M6A**
28 days	2.18E-10	2.24E-11	2.86E-11		**28 days**	2.29E-11	2.58E-10	5.99E-11
90 days	1.02E-10	4.41E-11	3.43E-11		**90 days**	4.51E-11	4.26E-11	4.50E-11
OXYGEN PERMEABILITY INDEX (OPI)								
Replacement of GGBS with CWP					**Replacement of Limestone with CWP**			
	M1A	**M2A**	**M3A**			**M4A**	**M5A**	**M6A**
28 days	9.99	10.66	10.55		**28 days**	10.65	9.67	10.26
90 days	10.18	10.36	10.48		**90 days**	10.36	10.38	10.40
WATER SORPTVITY INDEX (mm/hr0.5)								
Replacement of GGBS with CWP					**Replacement of Limestone with CWP**			
	M1A	**M2A**	**M3A**			**M4A**	**M5A**	**M6A**
28 days	6.73	7.80	7.65		**28 days**	7.95	8.86	7.59
90 days	7.70	6.23	8.84		**90 days**	9.37	9.35	8.78
POROSITY (%) (from sorptivity)								
Replacement of GGBS with CWP					**Replacement of Limestone with CWP**			
	M1A	**M2A**	**M3A**			**M4A**	**M5A**	**M6A**
28 days	8.70	10.02	9.83		**28 days**	9.61	7.87	9.40
90 days	6.58	8.15	7.07		**90 days**	9.90	9.61	8.03
CHLORIDE CONDUCTIVITY INDEX (mS/cm)								
Replacement of GGBS with CWP					**Replacement of Limestone with CWP**			
	M1A	**M2A**	**M3A**			**M4A**	**M5A**	**M6A**
28 days	0.72	0.81	1.61		**28 days**	1.00	1.01	1.13
90 days	0.45	0.67	0.58		**90 days**	0.62	0.58	0.73
POROSITY (%) (from conductivity)								
Replacement of GGBS with CWP					**Replacement of Limestone with CWP**			
	M1A	**M2A**	**M3A**			**M4A**	**M5A**	**M6A**
28 days	2.54	8.88	8.60		**28 days**	8.68	7.03	8.35
90 days	5.43	6.33	6.67		**90 days**	7.80	7.45	8.11

Table A. 11: Durability index results at 0.50 W/B ratio

VALUES OF K (m/s) for OPI								
Replacement of GGBS with CWP					**Replacement of Limestone with CWP**			
	M1B	**M2B**	**M3B**			**M4B**	**M5B**	**M6B**
28 days	3.95E-11	1.77E-10	1.60E-11		**28 days**	8.10E-11	2.11E-11	6.48E-11
90 days	4.08E-11	3.95E-11	2.09E-11		**90 days**	8.07E+00	4.31E-11	3.07E-11
OXYGEN PERMEABILITY INDEX (OPI)								
Replacement of GGBS with CWP					**Replacement of Limestone with CWP**			
	M1B	**M2B**	**M3B**			**M4B**	**M5B**	**M6B**
28 days	10.47	10.08	10.85		**28 days**	10.12	10.68	10.24
90 days	10.46	10.42	10.68		**90 days**	10.35	10.38	10.53
WATER SORPTVITY INDEX (mm/hr0.5)								
Replacement of GGBS with CWP					**Replacement of Limestone with CWP**			
	M1B	**M2B**	**M3B**			**M4B**	**M5B**	**M6B**
28 days	7.20	7.37	8.77		**28 days**	7.78	7.92	7.42
90 days	7.45	7.70	6.94		**90 days**	8.07	8.49	7.33
POROSITY (%) (from sorptivity)								
Replacement of GGBS with CWP					**Replacement of Limestone with CWP**			
	M1A	**M2A**	**M3A**			**M4A**	**M5A**	**M6A**
28 days	10.37	9.18	10.59		**28 days**	10.58	10.57	8.31
90 days	8.38	8.13	8.34		**90 days**	10.35	10.36	9.59
CHLORIDE CONDUCTIVITY INDEX (mS/cm)								
Replacement of GGBS with CWP					**Replacement of Limestone with CWP**			
	M1B	**M2B**	**M3B**			**M4B**	**M5B**	**M6B**
28 days	0.65	1.12	1.72		**28 days**	2.16	1.61	1.32
90 days	0.53	0.45	0.43		**90 days**	0.72	0.91	0.50
POROSITY (%) (from conductivity)								
Replacement of GGBS with CWP					**Replacement of Limestone with CWP**			
	M1B	**M2B**	**M3B**			**M4B**	**M5B**	**M6B**
28 days	3.08	8.55	9.32		**28 days**	9.88	9.36	8.23
90 days	6.15	5.74	6.38		**90 days**	7.51	9.55	7.03

Table A. 12: Durability index result at 0.55 W/B ratio

VALUES OF K (m/s) for OPI								
Replacement of GGBS with CWP					**Replacement of Limestone with CWP**			
	M1C	**M2C**	**M3C**			**M4C**	**M5C**	**M6C**
28 days	8.33E-11	8.95E-11	9.00E-11		**28 days**	1.87E-11	3.51E-11	1.29E-10
90 days	3.01E-11	1.84E-11	4.75E-11		**90 days**	4.17E-11	4.26E-11	4.47E-11
OXYGEN PERMEABILITY INDEX (OPI)								
Replacement of GGBS with CWP					**Replacement of Limestone with CWP**			
	M1B	**M2B**	**M3B**			**M4B**	**M5B**	**M6B**
28 days	10.08	10.05	10.10		**28 days**	10.73	10.46	9.94
90 days	10.55	10.77	10.37		**90 days**	10.42	10.39	10.39
WATER SORPTVITY INDEX (mm/hr0.5)								
Replacement of GGBS with CWP					**Replacement of Limestone with CWP**			
	M1B	**M2B**	**M3B**			**M4B**	**M5B**	**M6B**
28 days	6.60	8.09	10.27		**28 days**	8.14	8.74	8.84
90 days	6.84	8.28	5.75		**90 days**	8.17	7.58	7.24
POROSITY (%) (from sorptivity)								
Replacement of GGBS with CWP					**Replacement of Limestone with CWP**			
	M1A	**M2A**	**M3A**			**M4A**	**M5A**	**M6A**
28 days	10.03	12.43	10.61		**28 days**	9.96	10.41	10.60
90 days	7.23	6.64	9.49		**90 days**	11.36	9.45	9.83
CHLORIDE CONDUCTIVITY INDEX (mS/cm)								
Replacement of GGBS with CWP					**Replacement of Limestone with CWP**			
	M1B	**M2B**	**M3B**			**M4B**	**M5B**	**M6B**
28 days	0.46	1.05	1.23		**28 days**	1.69	1.83	1.49
90 days	0.62	0.34	0.61		**90 days**	1.06	0.79	0.77
POROSITY (%) (from conductivity)								
Replacement of GGBS with CWP					**Replacement of Limestone with CWP**			
	M1B	**M2B**	**M3B**			**M4B**	**M5B**	**M6B**
28 days	8.17	9.10	10.39		**28 days**	8.44	9.64	9.52
90 days	6.87	5.87	7.99		**90 days**	9.92	8.92	9.69

Appendix F
Detailed result of durability index

Table A. 13: Detailed OPI result at 0.45 W/B ratio

Specimen		28 days		90 days	
Replacement of GGBS with CWP					
	Disk Number	**k (m/s)**	**OPI**	**k (m/s)**	**OPI**
M1A	1	1.8568E-11	10.73123	2.35064E-11	10.628814
	2	9.3147E-11	10.03083	1.38066E-10	9.8599144
	3	6.6808E-10	9.175169	2.53267E-11	10.596422
	4	9.0623E-11	10.04276	2.22448E-10	9.6527723
	Mean	**2.1761E-10**	**9.994998**	**1.02337E-10**	**10.184481**
	S.D.	3.023E-10	0.63711	9.63465E-11	0.5017252
	COV (%)	138.922434	6.374286	94.14669411	4.9263705
M2A	1	2.933E-11	10.53269	3.18096E-11	10.497442
	2	1.7683E-11	10.75245	4.97693E-11	10.303038
	3	2.0845E-11	10.681	4.72034E-11	10.326027
	4	2.1569E-11	10.66617	4.76406E-11	10.322023
	Mean	**2.2357E-11**	**10.65808**	**4.41057E-11**	**10.362133**
	S.D.	4.9455E-12	0.091684	8.27369E-12	0.0907619
	COV (%)	22.1208927	0.860232	18.7587847	0.8759002
M3A	1	3.3142E-11	10.47962	1.94799E-11	10.710413
	2	2.2385E-11	10.65004	4.20497E-11	10.376237
	3	3.5369E-11	10.45137	4.28436E-11	10.368114
	4	2.3343E-11	10.63185	3.28163E-11	10.483911
	Mean	**2.856E-11**	**10.55322**	**3.42974E-11**	**10.484669**
	S.D.	6.6512E-12	0.10222	1.08764E-11	0.1594819
	COV (%)	23.2884992	0.968616	31.71201171	1.5210966
Replacement of LSP with CWP					
M4A	1	3.3355E-11	10.47683	3.34953E-11	10.475017
	2	1.8864E-11	10.72436	3.62758E-11	10.440383
	3	1.8955E-11	10.72227	5.50123E-11	10.25954
	4	2.0363E-11	10.69115	5.5517E-11	10.255574
	Mean	**2.2885E-11**	**10.65365**	**4.50751E-11**	**10.357629**
	S.D.	7.0143E-12	0.118855	1.18223E-11	0.1164255
	COV (%)	30.6506565	1.115628	26.22805416	1.124056
M5A	1	5.0877E-10	9.293477	3.16463E-11	10.499677
	2	2.295E-10	9.639216	3.68534E-11	10.433523
	3	1.9997E-10	9.699025	5.05012E-11	10.296699
	4	9.2852E-11	10.03221	5.12051E-11	10.290686
	Mean	**2.5777E-10**	**9.665982**	**4.25515E-11**	**10.380146**
	S.D.	1.7733E-10	0.302594	9.823E-12	0.1034459

	COV (%)	68.7931558	3.130508	23.08497328	0.9965744
M6A	1	5.4622E-11	10.26263	6.3791E-11	10.195241
	2	8.3819E-11	10.07666	6.12621E-11	10.212808
	3	7.3542E-11	10.13347	1.79312E-11	10.74639
	4	2.7725E-11	10.55713	3.69025E-11	10.432945
	Mean	**5.9927E-11**	**10.25747**	**4.49717E-11**	**10.396846**
	S.D.	2.4639E-11	0.214392	2.17244E-11	0.256904
	COV (%)	41.1156923	2.090109	48.30674985	2.4709798

Table A. 14: Detailed OPI result at 0.50 W/B ratio

Specimen		**28 days**		**90 days**	
Replacement of GGBS with CWP					
	Disk Number	**k (m/s)**	**OPI**	**k (m/s)**	**OPI**
M1B	1	2.8139E-11	10.55069	6.7827E-11	10.168597
	2	1.5718E-11	10.80359	1.4396E-11	10.8417531
	3	7.6176E-11	10.11818	5.4244E-11	10.2656518
	4	3.7839E-11	10.42206	2.6711E-11	10.5733146
	Mean	**3.9468E-11**	**10.47363**	**4.0794E-11**	**10.4623291**
	S.D.	2.6093E-11	0.285083	2.4542E-11	0.30618125
	COV (%)	66.1116211	2.721907	60.1591325	2.92651136
M2B	1	3.614E-11	10.44201	2.2349E-11	10.6507458
	2	2.3299E-11	10.63266	4.4304E-11	10.3535525
	3	1.0476E-10	9.9798	4.6043E-11	10.3368409
	4	5.4253E-10	9.265577	4.5228E-11	10.3445932
	Mean	**1.7668E-10**	**10.08001**	**3.9481E-11**	**10.4214331**
	S.D.	2.4651E-10	0.608225	1.1443E-11	0.15302759
	COV (%)	139.519232	6.033974	28.9848068	1.46839301
M3B	1	2.2803E-11	10.64201	2.2429E-11	10.6491967
	2	8.8372E-12	11.05368	2.0526E-11	10.6876974
	3	8.8401E-12	11.05354	1.7524E-11	10.7563665
	4	2.3394E-11	10.6309	2.2997E-11	10.6383207
	Mean	**1.5969E-11**	**10.84503**	**2.0869E-11**	**10.6828953**
	S.D.	8.2364E-12	0.240891	2.4678E-12	0.05336528
	COV (%)	51.5790487	2.221208	11.8249611	0.49953953
Replacement of LSP with CWP					
M4B	1	5.563E-11	10.25469	6.80334805	10.834258
	2	5.0349E-11	10.29801	7.9678353	10.057518
	3	1.0641E-10	9.973029	9.33704847	9.56134406
	4	1.115E-10	9.952719	8.15823865	10.9622923
	Mean	**8.0972E-11**	**10.11961**	**8.06661762**	**10.3538531**
	S.D.	3.245E-11	0.182037	1.0373037	0.66253858
	COV (%)	40.0755587	1.798849	12.859215	6.39895678

M5B	1	2.4869E-11	10.60433	3.1246E-11	10.5051992
	2	1.9796E-11	10.70342	3.1653E-11	10.499588
	3	1.6116E-11	10.79275	5.8857E-11	10.2302022
	4	2.3617E-11	10.62677	5.0761E-11	10.2944669
	Mean	**2.11E-11**	**10.68182**	**4.3129E-11**	**10.3823641**
	S.D.	3.9618E-12	0.085258	1.3887E-11	0.14107806
	COV (%)	18.7768375	0.798156	32.1977145	1.35882407
M6B	1	4.8443E-11	10.31477	2.6243E-11	10.5809885
	2	1.0865E-10	9.963987	3.6605E-11	10.4364597
	3	7.4781E-11	10.12621	1.8631E-11	10.729758
	4	2.7311E-11	10.56366	4.1263E-11	10.3844406
	Mean	**6.4795E-11**	**10.24215**	**3.0685E-11**	**10.5329117**
	S.D.	3.5095E-11	0.257848	1.0197E-11	0.15535606
	COV (%)	54.1630722	2.517513	33.232092	1.4749583

Table A. 15: Detailed OPI result at 0.55 W/B ratio

Specimen		**28 days**		**90 days**	
Replacement of GGBS with CWP					
	Disk Number	**k (m/s)**	**OPI**	**k (m/s)**	**OPI**
M1C	1	7.9364E-11	10.10037	2.306E-11	10.637221
	2	8.6504E-11	10.06297	5.218E-11	10.282462
	3	8.1595E-11	10.08834	2.252E-11	10.647368
	4	8.5874E-11	10.06614	2.258E-11	10.646258
	Mean	**8.3334E-11**	**10.07945**	**3.009E-11**	**10.553327**
	S.D.	3.4295E-12	0.017943	1.473E-11	0.1806342
	COV (%)	4.11532	0.178013	48.972899	1.7116328
M2C	1	8.9929E-11	10.0461	1.273E-11	10.895272
	2	8.4299E-11	10.07418	2.268E-11	10.644267
	3	9.0773E-11	10.04204	1.031E-11	10.986952
	4	9.3179E-11	10.03068	2.769E-11	10.557622
	Mean	**8.9545E-11**	**10.04825**	**1.835E-11**	**10.771028**
	S.D.	3.7585E-12	0.018474	8.214E-12	0.2030354
	COV (%)	4.197278	0.183858	44.758978	1.8850142
M3C	1	4.6467E-11	10.33286	2.117E-11	10.674185
	2	1.3E-10	9.88605	4.417E-11	10.354865
	3	1.3582E-10	9.867031	4.342E-11	10.362299
	4	4.7655E-11	10.32189	8.119E-11	10.090491
	Mean	**8.9986E-11**	**10.10196**	**4.749E-11**	**10.37046**
	S.D.	4.9625E-11	0.260443	2.487E-11	0.2387059
	COV (%)	55.147573	2.578144	52.373756	2.3017873
Replacement of LSP with CWP					
	1	2.2006E-11	10.65746	2.582E-11	10.588026

M4C	2	1.6409E-11	10.78492	2.34E-11	10.630723
	3	1.753E-11	10.75622	6.473E-11	10.188917
	4	1.8845E-11	10.72481	5.281E-11	10.277267
	Mean	**1.8697E-11**	**10.73085**	**4.169E-11**	**10.421233**
	S.D.	2.42E-12	0.054742	2.034E-11	0.2209095
	COV (%)	12.9429125	0.510141	48.7773	2.1198016
M5C	1	4.5095E-11	10.34587	3.02E-11	10.520035
	2	2.763E-11	10.55862	2.92E-11	10.534544
	3	3.2618E-11	10.48654	6.194E-11	10.208057
	4	3.4981E-11	10.45617	4.918E-11	10.308204
	Mean	**3.5081E-11**	**10.4618**	**4.263E-11**	**10.39271**
	S.D.	7.3456E-12	0.088426	1.582E-11	0.1607965
	COV (%)	20.9390608	0.845224	37.101087	1.5472049
M6C	1	7.3089E-11	10.13615	2.863E-11	10.543135
	2	2.0406E-10	9.690245	2.712E-11	10.566632
	3	6.5025E-11	10.18692	7.478E-11	10.126189
	4	1.7375E-10	9.760073	4.816E-11	10.317281
	Mean	**1.2898E-10**	**9.943347**	**4.468E-11**	**10.388309**
	S.D.	7.0369E-11	0.254395	2.224E-11	0.2077836
	COV (%)	54.5575498	2.558442	49.78435	2.0001679

Table A. 16: Detailed WSI result at 0.45 W/B ratio

Specimen		**28 days**		**90 days**	
Replacement of GGBS with CWP					
	Disk Number	**Sorptivity (mm/hr0.5)**	**Porosity (%)**	**Sorptivity (mm/hr0.5)**	**Porosity (%)**
M1A	1	5.46045236	8.519567	6.961951481	6.7297008
	2	6.51823266	8.94509	7.012574419	6.8266994
	3	6.12638416	8.774919	9.581291125	6.2711029
	4	8.79813529	8.545273	7.229215642	6.4818515
	Mean	**6.72580112**	**8.696212**	**7.696258167**	**6.5773387**
	S.D.	1.44891474	0.20176	1.26202321	0.2505282
	COV (%)	21.5426343	2.320088	16.39788041	3.8089601
M2A	1	8.32999724	10.17404	5.972011447	8.2658521
	2	8.40776019	10.27602	6.878851289	7.8961079
	3	6.83993401	10.0374	5.109923369	7.2517234
	4	7.64166283	9.600578	6.960341976	9.205211
	Mean	**7.80483857**	**10.02201**	**6.23028202**	**8.1547236**
	S.D.	0.72960565	0.297475	0.870926103	0.8161219
	COV (%)	9.34811974	2.968221	13.97891942	10.007965
	1	7.82032129	10.06977	9.742608368	6.8179594
	2	7.44416221	9.658894	7.50015597	6.5591808
	3	8.73824845	10.29471	9.25494464	7.0054308

M3A	4	6.59097749	9.282063	8.876853789	7.9007622
	Mean	**7.64842736**	**9.826359**	**8.843640692**	**7.0708333**
	S.D.	0.89016516	0.448295	0.963218239	0.5827501
	COV (%)	11.6385384	4.562166	10.89164828	8.2416039
Replacement of LSP with CWP					
M4A	1	8.5412167	10.23139	9.325793049	9.5568228
	2	6.89051101	9.584608	8.561066261	10.459946
	3	8.59383266	9.118511	10.57354246	10.225016
	4	7.77856101	9.521326	9.037208787	9.3458746
	Mean	**7.95103034**	**9.613958**	**9.374402639**	**9.8969148**
	S.D.	0.79915824	0.460482	0.859363129	0.5303968
	COV (%)	10.0510023	4.789724	9.167124154	5.3592136
M5A	1	9.52979215	7.933622	8.821373592	11.495583
	2	8.81126878	7.445395	9.195806653	11.148826
	3	9.53703369	8.360504	8.309486384	7.6904008
	4	7.54843847	7.724627	11.07930702	8.1200599
	Mean	**8.85663327**	**7.866037**	**9.351493413**	**9.6137175**
	S.D.	0.9362192	0.385574	1.207805712	1.9856264
	COV (%)	10.570825	4.901757	12.91564522	20.654096
M6A	1	7.83260303	9.305824	10.07706981	7.3477964
	2	7.1852505	8.691582	7.993893332	10.498034
	3	8.42879209	9.526739	8.413273277	7.1161839
	4	6.93116007	10.08613	8.617047721	7.1740561
	Mean	**7.59445142**	**9.402568**	**8.775321034**	**8.0340177**
	S.D.	0.67336007	0.576637	0.905779248	1.6456236
	COV (%)	8.86647412	6.132759	10.32189301	20.483195

Table A. 17: Detailed WSI results at 0.50 W/B ratio

Specimen		**28 days**		**90 days**	
Replacement of GGBS with CWP					
	Disk Number	**Sorptivity (mm/hr0.5)**	**Porosity (%)**	**Sorptivity (mm/hr0.5)**	**Porosity (%)**
M1B	1	7.31451218	10.63575	6.97112322	9.31225595
	2	7.33858293	9.700702	9.17653113	8.11989373
	3	7.06542638	10.97277	7.35535886	7.75356303
	4	7.08113739	10.18807	6.3126827	8.34186843
	Mean	**7.19991472**	**10.37432**	**7.45392398**	**8.38189528**
	S.D.	0.14669313	0.552251	1.22646086	0.66598783
	COV (%)	2.03742866	5.32325	16.4538955	7.94555173
M2B	1	7.876231	9.462735	7.93910639	8.16126795
	2	7.10472707	8.128752	8.58948885	9.24775253
	3	7.39366344	9.722902	6.9026324	7.15927535
	4	7.09208615	9.40828	7.38671623	7.94534074

	Mean	**7.36667692**	**9.180668**	**7.70448597**	**8.12840914**
	S.D.	0.36714731	0.714589	0.72622852	0.8615381
	COV (%)	4.98389324	7.783632	9.42604771	10.5990986
M3B	1	8.13831984	11.30248	7.04559281	8.24398308
	2	7.95552568	10.22368	7.50633107	8.03354413
	3	9.4087154	10.41179	6.37325377	7.75394293
	4	9.59463996	10.4165	6.83646499	9.31411838
	Mean	**8.77430022**	**10.58861**	**6.94041066**	**8.33639713**
	S.D.	0.84662126	0.484311	0.47039021	0.68201956
	COV (%)	9.64887505	4.573888	6.77755583	8.18122684
Replacement of LSP with CWP					
M4B	1	7.84928492	10.16441	6.80334805	10.834258
	2	7.25886814	10.09844	7.9678353	10.057518
	3	8.0754478	11.1407	9.33704847	9.56134406
	4	7.93043414	10.9114	8.15823865	10.9622923
	Mean	**7.77850875**	**10.57874**	**8.06661762**	**10.3538531**
	S.D.	0.35883597	0.525616	1.0373037	0.66253858
	COV (%)	4.61317175	4.968611	12.859215	6.39895678
M5B	1	8.74976345	9.869656	8.63769714	10.9729606
	2	7.76139212	10.02951	8.53809454	9.76664535
	3	7.1571996	10.82939	8.63173584	10.4928301
	4	8.00677926	11.57007	8.17101681	10.2054057
	Mean	**7.91878361**	**10.57466**	**8.49463608**	**10.3594604**
	S.D.	0.65905311	0.78527	0.22051521	0.50640317
	COV (%)	8.32265595	7.425961	2.59593479	4.88831604
M6B	1	7.47850503	8.54193	7.87720229	10.5979723
	2	8.16234232	8.225457	5.99602614	8.9737921
	3	7.03924572	7.562091	8.91079708	9.46464396
	4	6.98427643	8.923254	6.52727727	9.32048802
	Mean	**7.41609237**	**8.313183**	**7.3278257**	**9.58922411**
	S.D.	0.54444551	0.576295	1.31936612	0.70334175
	COV (%)	7.3414068	6.932301	18.0048786	7.33470972

Table A. 18: Detailed WSI results at 0.55 W/B ratio

Specimen	**28 days**			**90 days**	
Replacement of GGBS with CWP					
	Disk Number	**Sorptivity (mm/hr0.5)**	**Porosity (%)**	**Sorptivity (mm/hr0.5)**	**Porosity (%)**
M1C	1	5.40442681	8.836139	6.763622	7.3491251
	2	5.91619386	11.52421	6.7787913	7.9922378
	3	6.68537746	8.741413	7.3126779	6.5451035
	4	8.38432726	10.99926	6.4904716	7.0373144
	Mean	**6.59758135**	**10.02526**	**6.8363907**	**7.2309452**

	S.D.	1.30231535	1.444275	0.3440555	0.6059166
	COV (%)	19.7392844	14.40637	5.0327063	8.3794934
M2C	1	10.4444602	11.07412	7.1535827	6.8985512
	2	9.41388119	10.26241	9.2830628	6.3058261
	3	4.25174577	17.27977	9.8941448	6.0657136
	4	8.25183321	11.11445	6.7706528	7.2913747
	Mean	**8.0904801**	**12.43269**	**8.2753608**	**6.6403664**
	S.D.	2.71136675	3.25514	1.5447176	0.5575584
	COV (%)	33.5130513	26.18211	18.666468	8.3965009
M3C	1	9.73751826	11.04632	5.4028194	9.1027557
	2	9.2687106	9.611276	6.5054011	10.408407
	3	10.4872872	9.2828	4.9378025	9.9600067
	4	11.6011639	12.49785	6.1421887	8.4855895
	Mean	**10.27367**	**10.60956**	**5.7470529**	**9.4891896**
	S.D.	1.01739446	1.47346	0.7081919	0.8608471
	COV (%)	9.90293104	13.88804	12.322696	9.0718713
Replacement of LSP with CWP					
M4C	1	8.35218593	9.280971	8.2837664	11.382255
	2	8.9050417	10.54858	8.2649215	11.024311
	3	8.14505059	10.04821	8.5672132	11.093324
	4	7.15567933	9.94269	7.5800307	11.945862
	Mean	**8.13948939**	**9.955111**	**8.173983**	**11.361438**
	S.D.	0.73011947	0.521373	0.4194169	0.4193348
	COV (%)	8.9700893	5.237235	5.1311203	3.6908601
M5C	1	9.09941075	10.6142	8.7902705	10.018065
	2	8.20131285	10.283	6.0688544	8.8661037
	3	9.09587328	10.44752	9.2400373	9.1274006
	4	8.57509068	10.31002	6.2060946	9.8028492
	Mean	**8.74292189**	**10.41369**	7.5763142	**9.4536048**
	S.D.	0.43709902	0.151853	1.6724833	0.54533
	COV (%)	4.99946155	1.458209	22.075158	5.7684869
M6C	1	8.65312805	11.14851	6.2388373	9.0985547
	2	8.64957296	10.6078	7.8189947	10.084608
	3	9.16760649	10.60773	7.0656845	9.9339529
	4	8.88183998	10.04359	7.849599	10.203964
	Mean	**8.83803687**	**10.60191**	**7.2432788**	**9.8302699**
	S.D.	0.24511546	0.451135	0.7614713	0.5001641
	COV (%)	2.7734152	4.25522	10.512798	5.0879994

Table A. 19: Detailed CCI results at 0.45 W/B ratio

Specimen		28 days		90 days	
Replacement of GGBS with CWP					
	Disk Number	**Conductivity (mS/cm)**	**Porosity (%)**	**Conductivity (mS/cm)**	**Porosity (%)**
M1A	1	0.70798174	2.585483	0.548380201	5.4954457
	2	0.67833196	2.656238	0.357978705	5.3777358
	3	0.78708082	2.659446	0.455873902	5.3549841
	4	0.71341505	2.241395	0.425407772	5.4962279
	Mean	**0.72170239**	**2.53564**	**0.446910145**	**5.4310984**
	S.D.	0.04623227	0.046232	0.079052038	0.079052
	COV (%)	6.40600266	7.852525	17.68857549	1.386994
M2A	1	0.85481622	9.623173	0.549889205	5.9447438
	2	0.89041762	9.357633	0.984815921	6.9046639
	3	0.83972128	8.460868	0.566828834	6.5186162
	4	0.65146796	8.090968	0.581009574	5.9426766
	Mean	**0.80910577**	**8.883161**	**0.670635883**	**6.3276751**
	S.D.	0.10721948	0.107219	0.209839332	0.2098393
	COV (%)	13.2516024	8.166083	31.28960695	7.4362846
M3A	1	1.53909082	8.525598	0.574176778	6.8729609
	2	1.66177012	8.469708	0.575232703	6.5619564
	3	1.58973396	8.785428	0.673719652	6.691962
	4	1.64030646	8.609311	0.508369012	6.5624109
	Mean	**1.60772534**	**8.597511**	**0.582874536**	**6.6723225**
	S.D.	0.05482321	0.054823	0.068161467	0.0681615
	COV (%)	3.40998628	1.602661	11.69402038	2.2044172
Replacement of LSP with CWP					
M4A	1	0.90975713	8.788421	0.617109352	8.031948
	2	1.04060519	8.600174	0.653287257	7.6633829
	3	0.93750035	8.094639	0.646772178	7.8304293
	4	1.12867702	9.246532	0.550210643	7.6596082
	Mean	**1.00413492**	**8.682441**	**0.616844858**	**7.7963421**
	S.D.	0.10031309	0.100313	0.047130604	0.0471306
	COV (%)	9.99000125	5.490316	7.640592839	2.2589065
M5A	1	1.07686796	7.083378	0.417647641	5.8566975
	2	1.02155269	7.330509	0.75805218	8.669301
	3	0.93704934	6.881563	0.615656063	8.750252
	4	0.99171778	6.840102	0.511868728	6.5092896
	Mean	**1.00679694**	**7.033888**	**0.575806153**	**7.446385**
	S.D.	0.05836605	0.058366	0.145949465	0.1459495
	COV (%)	5.79720221	3.191567	25.34697906	19.920201
	1	1.15380505	8.469823	0.623254015	7.3901439
	2	0.98017032	7.753056	1.0843796	9.9577644
	3	1.21725462	8.594488	0.560719779	7.9682875

M6A	4	1.15720933	8.595589	0.646325013	7.1275925
	Mean	**1.12710983**	**8.353239**	**0.728669602**	**8.1109471**
	S.D.	0.10220228	0.102202	0.239881793	0.2398818
	COV (%)	9.06764122	4.84187	32.92051598	15.785041

Table A. 20: Detailed CCI results at 0.50 W/B ratio

Specimen	**28 days**			**90 days**	
Replacement of GGBS with CWP					
	Disk Number	**Conductivity (mS/cm)**	**Porosity (%)**	**Conductivity (mS/cm)**	**Porosity (%)**
M1B	1	0.59504212	3.56156	0.55814426	6.31156394
	2	0.73443747	2.744844	0.42214501	6.08022831
	3	0.5822271	2.744844	0.65001343	6.52179165
	4	0.68845566	3.26021	0.5038932	5.70526716
	Mean	**0.65004059**	**3.077865**	**0.53354898**	**6.15471276**
	S.D.	0.07353469	0.073535	0.09567167	0.09567167
	COV (%)	11.3123231	13.11752	17.9311882	5.68204333
M2B	1	0.93212088	8.737136	0.39390944	5.97209601
	2	1.08117086	7.890682	0.5141497	5.65010036
	3	1.26791672	9.124723	0.46913369	5.52630951
	4	1.20409254	8.463547	0.40813375	5.81979836
	Mean	**1.12132525**	**8.554022**	**0.44633165**	**5.74207606**
	S.D.	0.14804296	0.148043	0.05575658	0.05575658
	COV (%)	13.2024992	6.064893	12.492186	3.39434152
M3B	1	1.78562579	9.752	0.39581699	5.95195406
	2	1.81828643	9.376153	0.43069394	5.94117794
	3	1.72610327	8.831315	0.43911281	6.87158951
	4	1.55760539	9.305032	0.45834569	6.75273305
	Mean	**1.72190522**	**9.316125**	**0.43099236**	**6.37936364**
	S.D.	0.11599096	0.115991	0.02615047	0.02615047
	COV (%)	6.73619873	4.057966	6.06750305	7.87102116
Replacement of LSP with CWP					
M4B	1	2.27105934	9.539341	0.66870587	7.50944142
	2	2.06905486	10.38974	0.63853397	7.61130534
	3	2.21800619	9.925327	0.80298479	7.86922687
	4	2.07573586	9.649067	0.77328119	7.05932474
	Mean	**2.15846406**	**9.875868**	0.72087645	**7.51232459**
	S.D.	0.10175284	0.101753	0.07956149	0.07956149
	COV (%)	4.71413179	3.838861	11.0367717	4.4970514
M5B	1	1.71717714	9.567445	0.86480535	9.67803253
	2	1.31903685	9.086225	1.16343852	9.3286294
	3	1.73167482	9.520729	0.71743679	9.54998957
	4	1.67309023	9.255154	0.87674576	9.65771422

	Mean	**1.61024476**	**9.357388**	**0.9056066**	**9.55359143**
	S.D.	0.19573059	0.195731	0.18653227	0.18653227
	COV (%)	12.1553317	2.427448	20.5974945	1.67637612
M6B	1	1.17241179	7.402268	0.49607125	7.00560577
	2	1.38973036	8.446788	0.54743438	7.12489515
	3	1.35115215	8.248754	0.46236484	6.99667051
	4	1.37894994	8.830654	0.49598156	6.99045432
	Mean	**1.32306106**	**8.232116**	**0.50046301**	**7.02940643**
	S.D.	0.10173933	0.101739	0.03510532	0.03510532
	COV (%)	7.68969286	7.333125	7.01456904	0.90992264

Table A. 21: Detailed CCI results at 0.55 W/B ratio

Specimen		**28 days**		**90 days**	
Replacement of GGBS with CWP					
	Disk Number	**Conductivity (mS/cm)**	**Porosity (%)**	**Conductivity (mS/cm)**	**Porosity (%)**
M1C	1	0.38504779	8.577068	0.4426575	6.9518257
	2	0.47439913	7.863058	0.6313031	6.7251627
	3	0.50776752	8.466772	0.5498637	7.0181672
	4	0.46547473	7.772931	0.8705524	6.7974821
	Mean	**0.4581723**	**8.169957**	**0.6235942**	**6.8731594**
	S.D.	0.05203689	0.052037	0.1818626	0.1818626
	COV (%)	11.3574948	5.025123	29.163621	1.967226
M2C	1	1.10504776	9.099675	0.3943559	5.956444
	2	1.04511269	9.101234	0.2677838	6.1534785
	3	1.0067818	8.758385	0.3475774	5.7517334
	4	1.04514421	9.423043	0.3410951	5.604796
	Mean	**1.05052161**	**9.095584**	**0.337703**	**5.866613**
	S.D.	0.04059739	0.040597	0.0523044	0.0523044
	COV (%)	3.86449861	2.983917	15.488291	4.0827334
M3C	1	1.28201306	9.425921	0.4266921	7.4955865
	2	1.1561461	11.52798	0.4166531	7.1011592
	3	1.12698527	10.26613	0.9443179	8.7359154
	4	1.35141602	10.35438	0.659783	8.6164517
	Mean	**1.22914011**	**10.3936**	**0.6118615**	**7.9872782**
	S.D.	0.1056893	0.105689	0.2484738	0.2484738
	COV (%)	8.59863748	8.315617	40.609484	10.179655
Replacement of LSP with CWP					
M4C	1	1.7580515	8.586721	1.1083511	9.8901492
	2	1.46520096	8.018831	0.9018569	9.8468328
	3	2.02402	8.820489	1.172401	9.6015098
	4	1.49537182	8.34591	1.0388229	10.345341

	Mean	**1.68566107**	**8.442988**	**1.055358**	**9.9209583**
	S.D.	0.26111288	0.261113	0.1159646	0.1159646
	COV (%)	15.4902359	4.059968	10.988174	3.1262813
M5C	1	1.97972751	10.08568	0.8164456	8.454235
	2	2.05404997	9.26108	0.8164514	9.3369869
	3	1.75098347	9.949353	0.8114679	9.090037
	4	1.55060028	9.283529	0.725451	8.8109353
	Mean	**1.83384031**	**9.644911**	**0.792454**	**8.9230486**
	S.D.	0.22866682	0.228667	0.0447303	0.0447303
	COV (%)	12.4692873	4.499059	5.6445292	4.2506915
M6C	1	1.45310052	9.424001	0.9871206	9.5330237
	2	1.47131988	9.306224	0.778777	9.8513312
	3	1.51106943	9.247563	0.6771037	9.3390679
	4	1.50565008	10.08386	0.650951	10.028636
	Mean	**1.48528498**	**9.515412**	**0.773488**	**9.6880147**
	S.D.	0.02775151	0.027752	0.1527221	0.1527221
	COV (%)	1.86842995	4.056591	19.744595	3.2008361